# Metabolic Engineering of *Saccharomyces cerevisiae* towards the Biotransformation of D-Galacturonic acid to L-Galactonate

Dissertation zur Erlangung
des Doktorgrades der Naturwissenschaften

vorgelegt beim Fachbereich Biowissenschaften
der Johann Wolfgang Goethe
Universität
in Frankfurt am Main

von
**Simon Harth**
aus Bremen

Frankfurt, 2022
(D30)

vom Fachbereich Biowissenschaften
der Johann Wolfgang Goethe-Universität
als Dissertation angenommen.

| | |
|---|---|
| Dekan: | Prof. Dr. Sven Klimpel |
| 1. Gutachter: | Dr. Mislav Oreb |
| 2. Gutachter: | Prof. Dr. Jörg Soppa |

Datum der Disputation: 26.10.2022

## Table of Contents

# 1 Introduction

## 1.1 Synthetic Biology as a Powerful Tool of Todays Biotechnology

The field of biotechnology is widely understood as the application of biology in useful processes for humankind. Although rather unconscious, biotechnology became part of human's life since first humans started to brew beer, bake bread and conserve foods already in ancient ages (Katz and Maytag, 1991). As the time proceeded, microbes were discovered to catalyze these beneficial processes. Today, biotechnological products range from foods to pharmaceuticals, biofuels, chemicals and more. So far, these production processes were limited by the intrinsic metabolic activity of only few fermenting microbes like yeasts (beer and bread), lactobacilli (yoghurt) and filamentous fungi (eatable molds on cheeses). However, the work of Cohen et al., in 1973 describing the first recombinant plasmid (DNA vectors), enabled gene transfer even beyond species borders and thus broke ground for a surge of genetic methods in various microbes. This given as a tool, biotechnology experienced a fundamental revolution leading to the term 'synthetic biology'. This term first was coined by the use of recombinant DNA-molecules transformed across species borders, but, until today, this term was complemented by engineering microbes to fulfill new tasks (Andrianantoandro et al., 2006).

While biotechnologists understand microbes and the variety of their enzymes as microscopic cell factories harboring biological machines of molecular assembly lines, synthetic biologists, moreover, even tear down species borders and enable artificial recombinations of these molecular assembly lines by using the growing set of versatile genomic tools (reviewed by Keasling, 2008). Thereby, the complexity of nature's enzymatic networks is broken into fundamental bricks of freely interchangeable modules. Furthermore, optimizing and complementing metabolic networks towards higher flux through streamlined metabolic pathways is referred to as 'metabolic engineering', which facilitates the production even of hardly accessible compounds in a cost-efficient manner (reviewed by Keasling, 2010). Especially the substance classes isoprenoids (McCaskill and Croteau, 1997), polyketides (Pfeifer and Khosla, 2001), lipids (Yu et al., 2018) and carbohydrates (Protzko et al., 2018) are prominent targets approached by metabolic engineering. The outstanding diversity of nature itself bears manifold applications of natural compounds for diverse aspects of human life. Thereby, the most powerful and industrially interesting aspect in harnessing the metabolic power of biology is based also on the ability of microbes to grow on cheap substrates, while producing valuable compounds. Furthermore, biotechnological processes are performed at mild conditions and are known to produce less toxic or environmentally harmful waste products compared to standard processes in chemical industry. These characteristics of biotechnological processes could enable an ecological revolution in the sector of compound production.

Until today, synthetic biology and metabolic engineering strongly boosted the range of biotechnological products available and thus exceed the imagination of our ancestors by far.

## 1.2 The Potent Production Host *Saccharomyces cerevisiae*

In 1858, the microbiologist Louis Pasteur observed the capability of microbes to produce ethanol from sugar and thus discovered the fundamental biochemical reaction of brewing. Not least because of this fermentative capability used in the brewing process, the Ascomycota fungus *S. cerevisiae* ranks high among the microbes employed by humankind. Due to its low cultivation requirements, this yeast embarked on a journey of biological research ever since and asserted itself as one of the best understood model organisms and most employed microbial work horses in industry (reviewed by Kavšček et al., 2015).

Many physiological and genetic phenomena have been elucidated due to extensive research in this yeast. The characteristic asymmetrical type of cell fission gave *S. cerevisiae* its alias "budding yeast", since the daughter cell starts off from the body of the mother cell as a small bud (Figure 1-1).

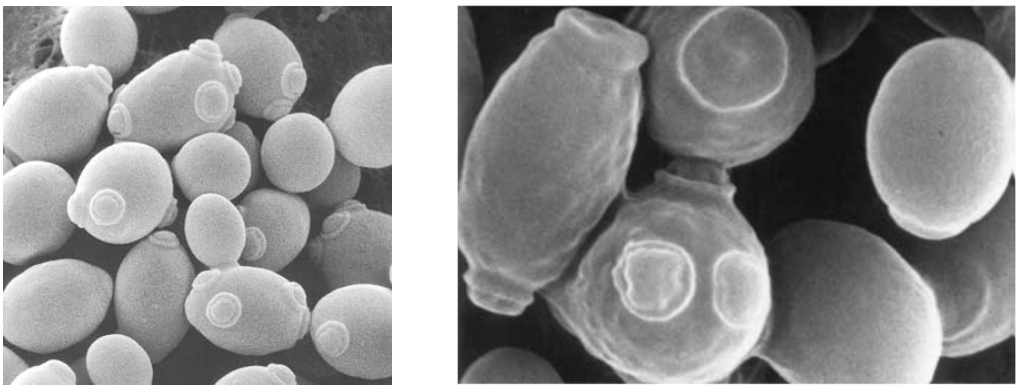

**Figure 1-1: Scanning electron microscopy of *S. cerevisiae* cells.**
The scanning electron microscope image shows the oval cell shape of *S. cerevisiae* and depicts the daughter cells emerging from the body of the mother cell. After successful cell fission, a scar remains on the surface of the mother cell. This type of cell fission gave *S. cerevisiae* the alias "budding yeast" (pictures taken from chemistryland.com and Bennis et al., 2004).

While most other organisms produce ethanol only under anaerobic conditions *S. cerevisiae* became prominent due to its outstanding capability to produce considerable amounts of ethanol from glucose under aerobic conditions. This effect was called Crabtree effect and describes an overflow metabolism in which anaerobic fermentation pathways contribute to the utilization of excess glucose even under aerobic conditions. After the glucose is consumed, the cells metabolism switches to ethanol as carbon source resulting in a diauxic growth profile (De Deken, 1966; Piškur et al., 2006).

Besides its metabolic characteristics, *S. cerevisiae* also is known for its convenient genomic accessibility, which is predominantly shaped by its preferential use of homologous recombination over the non-homologous end joining mechanism (NHEJ) to repair DNA strand breaks. Namely, this repair mechanism requires homologous sequences on both sides of the DNA-lesion (reviewed by Dudáš and Chovanec, 2004). In applied sciences, this repair mechanism can be easily exploited to integrate recombinant gene cassettes into the genome, to delete genes and to replace genetic regulatory elements, such as promoters and terminators (Apel et al., 2017). The implementation of the CRISPR-Cas9 method further boosted the toolbox for genome editing in yeast (Dicarlo et al., 2013; Jinek et al., 2012). Taken together, the well characterized physiology complemented with the efficient set of genetic methods showcases the yeast *S. cerevisiae* as highly potential industrial production host, which even qualifies as GRAS (generally regarded as safe). Consequently, this yeast serves as industrial host for various products throughout all biochemical classes like the human peptide hormone insulin (reviewed by Baeshen et al., 2014), the isoprenoid artemisinin (Paddon et al., 2013) and the polyketide olivetolic acid, which is precursor of the cannabinoids tetrahydro cannabinol (THC) and cannabidiol (CBD) (Luo et al., 2019). Beyond these, many more synthetic products of yeast fermentations have been reported, which hold promise to ease the life of humankind (Keasling, 2010; Nevoigt, 2008).

The study of van Dijken et al. in 2000 classified physiological and genetic properties of the *S. cerevisiae* strain CEN.PK122 as very suitable among several other industrially relevant yeast strains for further metabolic engineering approaches. This was confirmed by the success to engineer artemisinin and cannabinoid production in haploid descendants of the CEN.PK122 (Luo et al., 2019; Paddon et al., 2013). Such metabolic engineering approaches often not only require the heterologous expression of genes, but also the modification of the endogenous metabolism of the host to ensure cofactor and precursor supply. Already harnessed in many biotechnological processes, the well understood physiology and the easily accessible genetics of the yeast *S. cerevisiae* pave the way in many progressive biotechnological approaches even towards a more ecologically friendly industry of the future.

## 1.3 The Core Metabolism in *Saccharomyces cerevisiae* Strongly Relies on the Redox Cofactors NAD(P)$^+$ and NAD(P)H

The metabolism is understood to be the entirety of biochemical reactions taking place in living biological cells, which commonly is grouped into catabolism and anabolism. While the catabolism describes the energy releasing breakdown of mainly big organic molecules often sourced from the

environment and the anabolism is the energy demanding construction of organic molecules from smaller assembly units. For example, the sugar catabolism follows this principle, as glucose undergoes several metabolic steps, which, among other metabolites, result in acetate (oxidative process, catabolism), when fused to the coenzyme A is a building block for the fatty acid synthesis (reductive process, anabolism). Fatty acids for example are essential constituents in the cell membrane or function as building blocks for higher molecular compounds (Figure 1-2).

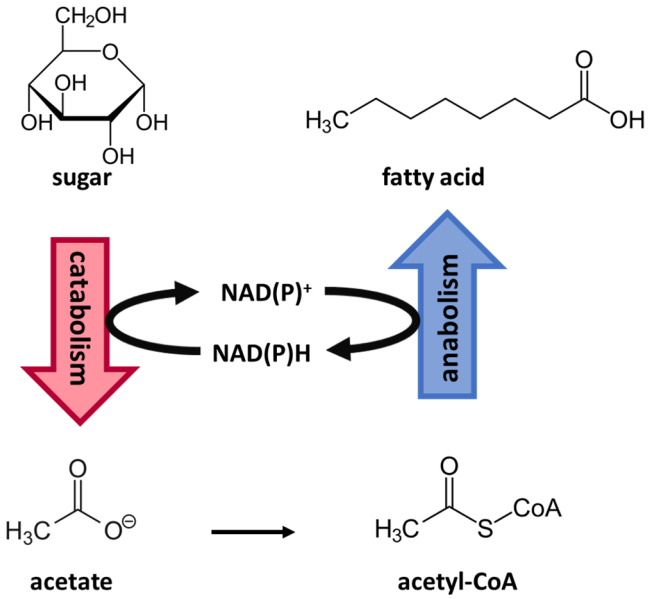


**Figure 1-2: The metabolism of a living cell is divided into catabolism and anabolism.**
Living cells make the energy of organic molecules accessible through biochemical reactions, which are grouped to metabolic pathways. Biochemical reactions that release energy, usually oxidations, make up the catabolism of a cell, while the biochemical reactions, that require energy, usually reductions, make up the anabolism. As an example, the degradation of glucose to acetate and the construction of fatty acids from acetate-CoA is shown. The cofactors $NAD(P)^+$ and NAD(P)H fuel catabolism and anabolism as electron acceptor or donor, to drive respective reactions. In general, the catabolism is of dissimilatory character, so the complexity of the metabolites decreases along the catabolism, while the oxidative state increases. In contrast, anabolic reactions as part of the assimilation follow the opposite principle.

The oxidative and reductive reactions of the metabolism mainly are linked by nicotinamide adenine dinucleotide (phosphate) species, $NAD(P)^+$ and NAD(P)H, these cofactors function as an intracellular currency for oxidative and reductive power and thus drive respective reactions.

The metabolism of cells is based on freely transferrable electrons between metabolites (redox reactions), therefore the cofactor pairs $NAD(P)^+$ and NAD(P)H have evolved. These cofactors own a nicotinamide molecule as functional moiety, as it is capable to accept and donate hydride ions ($H^+$+2$e^-$). The uptake of a hydride ion causes a reorganization of the electron configuration in the nicotinamide ring, which stabilizes the additional electron at the positively charged nitrogen in the heterocycle. The donation of the hydride ion to a suitable substrate restores the aromatic ring within the heterocycle. In this system, uptake and donation of hydride ions is reversible, which constitutes the indispensable role of this cofactor for cellular reactions. A common reaction where

these redox cofactors find application are the reduction of carbonyl-groups and the oxidation of alcohol groups resulting in the respective other. Given the example of a ketone reduction, where the carbonyl carbon becomes more electrophilic, as the electron density is drawn towards the oxygen. The hydride from the NAD(P)H attacks this electrophilic carbon and ties a new atom bond, while the ketone oxygen accepts a proton and thereby forms an alcohol group. In this reaction a ketone and a NAD(P)H react to an alcohol and a $NAD(P)^+$, whereby the ketone is reduced and the nicotinamide cofactor is oxidized (Figure 1-3).

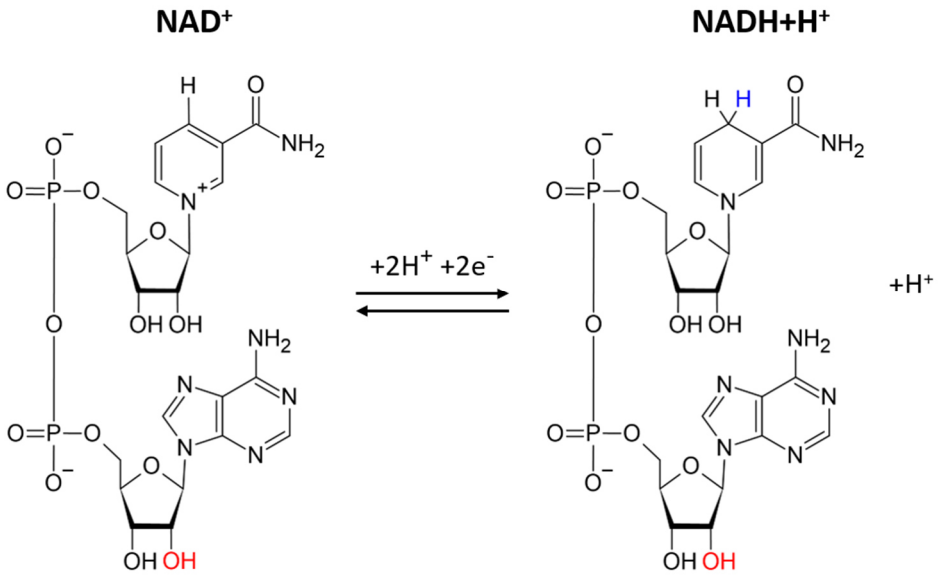


**Figure 1-3: The function of the redox-cofactor pairs NAD(H) and NADP(H).**
The function of nicotinamide adenine dinucleotide (phosphate) as a redox cofactor is based on the ability to accept and donate hydrides, which are stored in the heterocycle of the nicotinamide moiety. These reactions usually take place at carbonyl or alcohol groups of molecules. Thereby, the oxidized form $NAD(P)^+$ accepts a hydride to then result in the reduced form NAD(P)H (shown in blue). At a spatial distance from the reactive nicotinamide, at the adenine ribose the cofactor NAD(H), can be phosphorylated to NADP(H), which has strong effect on the enzyme cofactor interaction (phosphorylation site is marked in red).

Besides the nicotinamide ring these cofactors contain an adenine dinucleotide, which fulfills structural functions by playing a major role during the enzyme interaction (Figure 1-3). The enzyme interaction is decisively influenced by a phosphorylation, which makes up the cofactor pair $NADP^+$ and NADPH. In *S. cerevisiae*, this phosphorylation is performed by two cytosolic NADH-kinases, Utr1 and Yef1, as well as the mitochondrial NADH-kinase, Pos5 (Kawai et al., 2001; Shi et al., 2005). Differently to other organisms like *E. coli* (Anderlund et al., 1999), no transhydrogenase was identified in *S. cerevisiae* which could transfer electrons between unphosphorylated and phosphorylated cofactor species. Therefore, the phosphorylation divides the cofactors into two rather separated cofactor currencies in this organism, which only rarely overlap and thus take over different roles in metabolic reactions. For example, the sources of these cofactors vary, while NADH mainly is generated in the glycolysis and the tricarboxylic acid cycle (TCA-cycle), NADPH is generated mainly in the

pentose phosphate pathway. Moreover, the $NADP^+$-dependent acetaldehyde dehydrogenase, Ald6, (Bruinenberg et al., 1983) contributes to the cytosolic pool of NADPH. Furthermore, the reduced cofactor species find application in different pathways, e.g., NADH is used by the respiratory chain at the mitochondria and the formation of glycerol and ethanol and NADPH is used in anabolic reactions like fatty acid synthesis and biomass generation as well as protection against oxidative stress. Due to their different roles in the metabolism, it was found that the equilibrium within the pairs is different, while the ratio of the cofactor pair $NAD^+$/NADH is 100 to 1 (Canelas et al., 2008) and in contrast the ratio of $NADP^+$/NADPH is 1 to 100 (Murray et al., 2011). Overall, the ratios within the cofactor pairs stay rather constant. Overall, $NAD^+$ acts as an oxidizing agent in the catabolism, whereas NADPH is used as a reducing agent in the anabolism and in detoxification reactions (van Dijken and Scheffers, 1986).

Besides their predominant function as redox-cofactor the nicotinamide adenine dinucleotides, unphosphorylated or phosphorylated, are also involved in further biological processes like ageing and cell death often as signaling molecule (Ying, 2008). Furthermore, the cofactors itself can function as signaling molecules (Pollak et al., 2007).

## 1.4 The Core Metabolism of Glucose in the Prominent Yeast *Saccharomyces cerevisiae* is Based on the Glycolysis

The yeast *S. cerevisiae* is very proficient in metabolizing glucose. After taken up through one of several sugar transporters, glucose is phosphorylated to glucose-6-phosphate (G6P) the starting point of the glycolysis (also known as the Embden-Meyerhof-Parnas-pathway). The fate of the G6P is further determined by two competing key enzymes the phosphoglucose isomerase (Pgi1) and the glucose-6-phosphate dehydrogenase (Zwf1). While the isomerization results in fructose-6-phosphate (F6P) which further follows the glycolytic degradation, the dehydrogenation by the Zwf1 generates one molecule NADPH and determines the G6P to branch into the pentose phosphate pathway (PPP). Furthermore, the F6P is the entry point of the sorbitol metabolism into the core metabolism of yeast from which fructose-1-6-bisphosphate (FBP) is generated by phosphofructokinases (Pfk1 and Pfk2) under consumption of one molecule ATP. FBP then is cleaved by an aldolase reaction to dihydroxyacetone phosphate (DHAP, also known as glycerone phosphate) and D-glyceraldehyde-3-phosphate (GAP), which also represents the re-entry point of the previously branched off PPP. These two metabolites are interconvertible by the triose phosphate isomerase (Tpi1) and thereby act as another metabolic branch point. DHAP can be reduced to later result in glycerol, while GAP undergoes several oxidation steps to form pyruvate, the end product of the glycolysis.

During these oxidative steps the glyceraldehyde-3-phosphate dehydrogenases (GAP-DH: Tdh1 but mainly Tdh2 and Tdh3 (McAlister and Holland, 1985)) generate one molecule NADH and the phosphoglycerate kinase (Pgk1) as well as the pyruvate kinases (Pyk2 and Cdc19) generate one molecule ATP each. In summary, only the glycolysis generates 4 ATP, of which two will be expended for another round of glycolysis, 2 molecules NADH and 2 molecules pyruvate. Pyruvate can flux into three different metabolic pathways, i) by carboxylation the molecule is converted into oxaloacetate, ii) by dehydrogenation the molecule fluxes into the TCA-cycle and iii) by decarboxylation the molecule is converted into acetaldehyde, which can further be oxidized or reduced to acetate and ethanol, respectively. An overview of the yeast metabolism based on glucose is depicted in Figure 1-4.

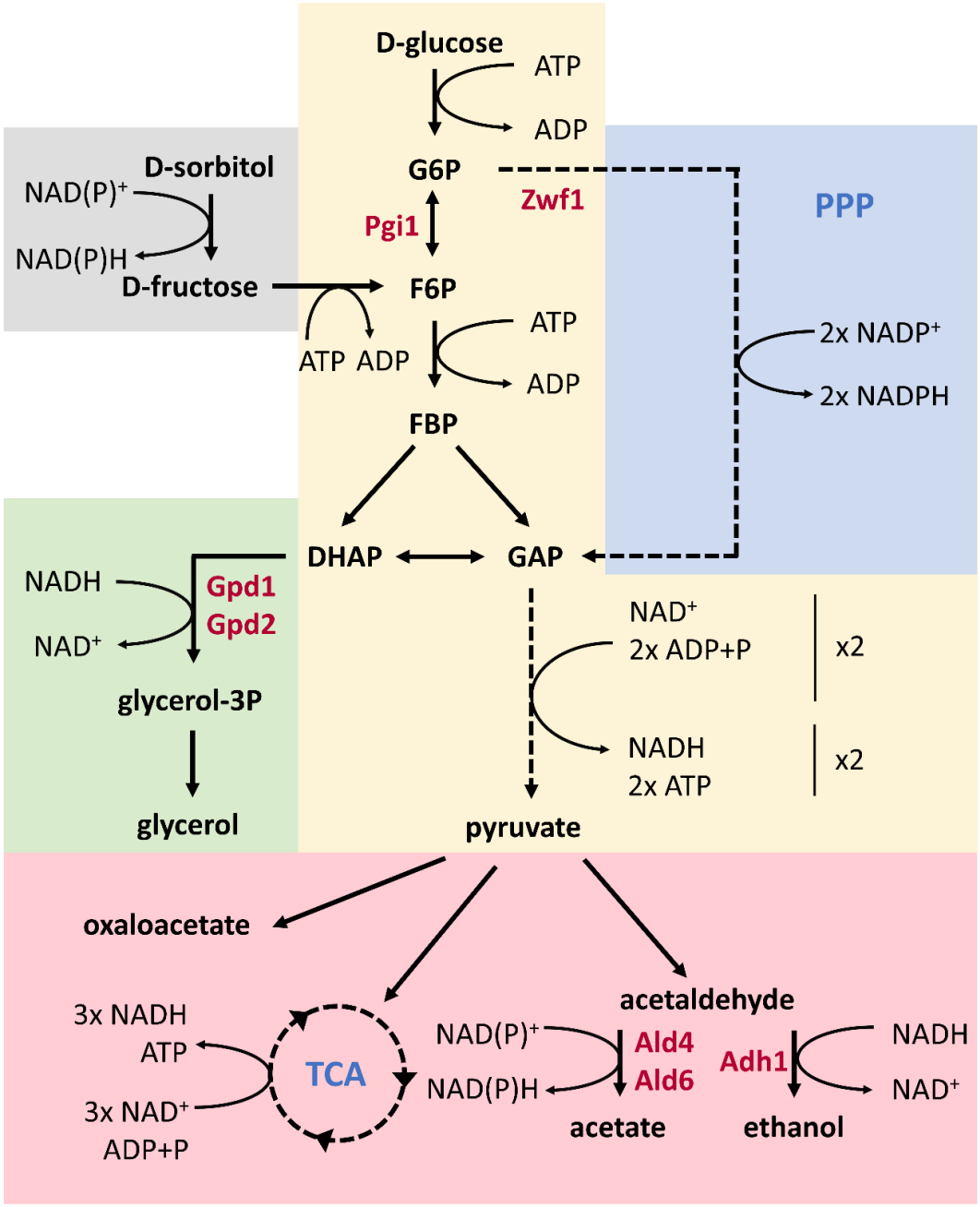


**Figure 1-4: Overview of the core metabolism in *S. cerevisiae*.**
Shown is a simplified overview of the core metabolism of the yeast *S. cerevisiae* based on the hexose sugar glucose. The different parts and branches of the metabolism are illustrated, glycolysis (yellow), pentose phosphate pathway (blue), sorbitol metabolism (grey), glycerol formation (green) and pyruvate metabolism (red). This scheme laid focus on the generation and consumption of nicotinamide adenine dinucleotide (phosphate) ($NAD(P)^+$ and NAD(P)H) and adenosine triphosphate (ATP) and their descendants. Single reaction steps are illustrated by a singular arrow, while multiple reaction steps are illustrated by a dashed lined arrow. Blue letters indicate branches of the pathway (tricarboxylic acid cycle, TCA-cycle; pentose phosphate pathway, PPP) and red letters indicate a selection of enzymes, which are of higher interest. Certain metabolites were abbreviated, D-glucose-6-phosphate (G6P), D-fructose-6-phosphate(F6P), D-furctose-1,6-bisphosphate (FBP), dihydroxyacetone phosphate (DHAP), D-glyceraldehyde 3-phosphate (GAP).

### 1.4.1 Pentose Phosphate Pathway

This pathway branches off from the glycolysis where the Pgi1 and the Zwf1 compete over G6P (Figure 1-4). In *S. cerevisiae* the ratio between glycolysis and PPP lays strongly on glycolytic side, as only about 4% of the flux through this metabolic key point goes via the Zwf1 when grown in glucose batch culture (Fiaux et al., 2003). Zwf1 funnels the carbon body into the oxidative branch of the PPP (oxPPP) via a dehydrogenation reaction which generates NADPH and causes a lactonization to 6-phospho-D-glucono-δ-lactone. After addition of $H_20$ to the lactone by a 6-phosphogluconolactonase the resulting D-gluconate-6-phosphate undergoes a dehydrogenation, which generates NADPH and $CO_2$. This decarboxylation results in D-ribulose-5-phosphate from which the non-oxidative branch of the PPP embarks.

While the oxidative branch mainly serves the function of NADPH-generation for central biosynthetic purposes of the cell, the non-oxidative branch mainly generates essential building blocks of a variety of sugars of 3, 5 and 6 carbons. The reversible interconversion of these carbon bodies ensures the supply of building blocks for purine and pyrimidine nucleotides and the amino acids tryptophane, histidine and the aromatic amino acids. Furthermore, the non-oxidative branch of the PPP is the entry point of pentoses into the catabolism of *S. cerevisiae*, as this branch results into glyceraldehyde-3-phosphate, which is an intermediate of the glycolysis and is further oxidized to pyruvate. The connection between glycolysis and the non-oxidative PPP is reversible, as it was found, that in a *Δzwf1* strain, GAP from glycolytic descent can contribute to the pool of carbon building blocks generated in the non-oxidative PPP (Blank et al., 2005).

Due to the essential role of strong NADPH-regeneration in many biotechnological applications, several engineering approaches have been conducted to increase the rather low flux through the PPP in wildtype *S. cerevisiae*. These approaches included the overexpression of the *ZWF1*, which turned out to be beneficial in NADPH-consuming pathways (Reshamwala and Lali, 2020; Wernig et al., 2021; Zhao et al., 2015). However, the deletion of the *PGI1* is of fatal impact on the cells fitness (Aguilera, 1986) due to NADPH-accumulation indicating the sensitive balance between $NADP^+$ and NADPH in *S. cerevisiae* (Boles et al., 1993). In contrast, Yu et al. in 2018 demonstrated the beneficial effect of replacing the *PGI1* promoter with a relatively weak promoter on the NADPH-supply without severely perturbing the growth performance.

### 1.4.2 Sorbitol Metabolism

Polyols or hexitols often are found in plants and algae. These reduced species of sugars stand out by their multiple hydroxylations (Loeschner and Everard, 2000; Wargacki et al., 2012). In this group of sugars, the keto group is reduced to an alcohol group, which perturbs the cyclization of the molecule. In nature the hexitols mannitol and sorbitol are very common in plants. Due to the ubiquitous occurrence of these polyols many phyla of life own genes, which code for polyol degrading enzymes and polyol transporters. The polyol dehydrogenases convert sorbitol to fructose (Jordan et al., 2016; Napora et al., 2013), which is funneled into the glycolysis by phosphorylation. The yeast *S. cerevisiae* is able to use polyols as carbon source, which, however, requires an adaptation phase for many strains (Enquist-Newman et al., 2014; Quain and Boulton, 1987; Sarthy et al., 1993). Furthermore, the yeast hexose transporters Hxt13, Hxt15, Hxt16 and Hxt17 were found capable to transport the polyols sorbitol and mannitol (Jordan et al., 2016), which intracellularly are degraded by the dehydrogenases Sor1, Sor2, Dsf1 and Man2. These polyol dehydrogenases rely on $NAD^+$ as electron acceptor. The yeast *Yarrowia lipolytica* owns a gene for a short chain dehydrogenase/reductase called *YlSDR*, which accepts sorbitol and mannitol and interestingly was reported to be $NADP^+$-dependent (Napora et al., 2013). Due to the highly reduced state of polyols, the metabolism of these means an additionally generated NADH or NADPH for the cell compared to the valorization of the common hexoses fructose or glucose.

### 1.4.3 Glycerol Formation and its Role in Yeast Cell Physiology

Glycerol is formed by reduction of DHAP, an intermediate of the glycolysis, to glycerol-3-phosphate (G3P). In *S. cerevisiae*, this reaction step is catalyzed by the G3P dehydrogenases Gpd1 (Albertyn et al., 1994; Larsson et al., 1993) and Gpd2 (Eriksson et al., 1995). Consecutively, the G3P is dephosphorylated by one of the glycerol-3-phosphate phosphatases Gpp1 and Gpp2 to result in glycerol (Norbeck et al., 1996).

The pathway for glycerol production was unveiled when the cellular mechanisms of osmoregulation was studied. Thereby the essential role of the glycerol production to maintain growth under osmolar stress was found (Albertyn et al., 1994). A specific signal transduction pathway was investigated which senses the osmotic situation of the medium and also induces the cell to react physiologically. This regulation mechanism is based on the two regulators Hog1 and Pbs2 (Brewster et al., 1993;

Schüller et al., 1994), which trigger the glycerol production under high osmolarity conditions, therefore the name 'high osmolarity glycerol response pathway' (*HOG1*-pathway). By producing glycerol, the cell is able to increase the intracellular osmolarity to defy fatal cell shrinkage.

Besides the essential role in the osmoregulation, the NADH-dependent glycerol formation functions as a redox sink to maintain the intracellular redox balance (Bakker et al., 2001; Overkamp et al., 2002; van Dijken and Scheffers, 1986). While under aerobic conditions the NADH can also be reoxidized in the respiratory chain at the mitochondrial membrane, this function is especially important under anaerobic conditions, when mitochondrial respiration is not possible due to the lack of oxygen. Moreover, being a redox-neutral process ethanol production via the alcohol dehydrogenases cannot serve this function.

### 1.4.4 Pyruvate Metabolism as a Metabolic Branchpoint

Pyruvate is the end product of the glycolysis, where two moles of pyruvate are formed from one mole of glucose. This highly oxidized metabolite undergoes one of three metabolic routes, which are initiated by i) carboxylation, ii) dehydrogenation or iii) decarboxylation (Figure 1-5).

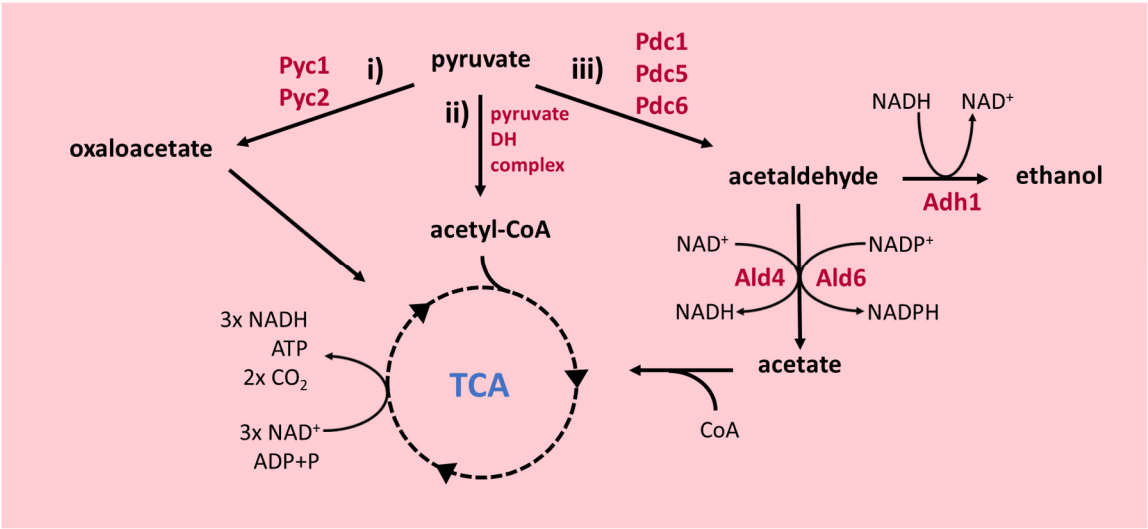


**Figure 1-5: The pyruvate metabolism.**
Starting off from pyruvate, the end product of the glycolysis, the three different chemical reactions i) carboxylation, ii) dehydrogenation and iii) decarboxylation determine the fate of the molecule by leading it into different metabolic pathways. Especially the decarboxylation is strong in *S. cerevisiae* when grown in high glucose medium. Enzymes are abbreviated and colored in red, while the tricarboxylic acid cycle (TCA-cycle) as a multi-step pathway is shown in dashed lines.

**i)** Accepted by the pyruvate carboxylases Pyc1 and Pyc2 the pyruvate is converted to oxaloacetate under consumption of one molecule of ATP:

$$pyruvate + HCO_3^- + ATP \xrightarrow{Pyc1,\ Pyc2} oxaloacetate + ADP + P$$

The oxaloacetate is an important building block for the synthesis of amino acids like aspartate, which arises directly from transamination. Furthermore, oxaloacetate being the acceptor molecule of the TCA-cycle, makes the pyruvate carboxylation hold the role of an anaplerotic reaction for the TCA-cycle. Suitably, the Pyc1 and Pyc2 are inhibited by NADH, which intracellularly indicate a functional TCA-cycle and thus make the anaplerotic role unnecessary (Cazzulo and Stoppani, 1968).

**ii)** After being transported into the mitochondrion, the pyruvate dehydrogenase a large multi-component enzyme complex accepts the pyruvate and converts it into acetyl-CoA (Kresze and Ronft, 1981a; Reed and Yeaman, 1987):

$$pyruvate + coenzyme\ A + NAD^+ \xrightarrow{pyruvate\ DH\ complex} acetyl - CoA + CO_2 + NADH$$

The acetyl-CoA is guided into the TCA-cycle by fusion to oxaloacetate. The TCA-cycle generates important building blocks for the anabolism of the cell, among these α-ketoglutarate, which, for instance, is the direct precursors of the amino acid glutamate. Furthermore, ii) sources the NADH-regeneration, which is an important part of the energy metabolism at the mitochondrial membrane. In the TCA-cycle, the acetyl-CoA is fused to oxaloacetate and undergoes multiple reaction steps, which generate one molecule of ATP, 2 molecules of $CO_2$ and 3 molecules of NADH per pyruvate. Whilst the fully oxidized $CO_2$ leaves the cell, the NADH plays a major role in the energy metabolism of the cell by being oxidized in the oxygen-dependent respiration chain located at the mitochondrial membrane, which fuels the proton gradient across the inner mitochondrial membrane the necessary driving force of the ATP generation. Similar to the pyruvate carboxylase, the activity of the pyruvate dehydrogenase complex is inhibited by NADH as well, but also by acetyl-CoA. This demonstrates a regulatory function of the cofactor and a feedback inhibition of acetyl-CoA itself (Kresze and Ronft, 1981b; Pronk et al., 1996).

**iii)** However, when grown in high glucose medium the decarboxylation is the predominant metabolic path of pyruvate in *S. cerevisiae*. The effect that under these conditions the pyruvate decarboxylation performed by the Pdc-complex consisting of Pdc1, Pdc5 and Pdc6 is strong and the TCA-cycle even is suppressed forms the biochemical mechanism behind the already mentioned Crabtree-effect (De Deken, 1966; Piškur et al., 2006). The product of the pyruvate decarboxylation reaction, acetaldehyde, can be oxidized to acetate or reduced to ethanol. As a consequence, these two compounds are common products of *S. cerevisiae* when grown in high-glucose medium. The

ethanol formation is reversible, which qualifies ethanol as carbon source. When used as a carbon source, ethanol is oxidized to acetaldehyde, which is further converted to acetate by acetaldehyde dehydrogenases, mainly the cytosolic Ald2 and Ald6. Thereby, the Ald2 generates NADH from $NAD^+$ and the Ald6 uses the phosphorylated cofactor $NADP^+$ and thus contributes to NADPH-regeneration (Meaden et al., 1997; Navarro-Aviño et al., 1999). The Pdc-complex as well as the alcohol and acetate formation were localized in the cytosol (van Urk et al., 1989).

### 1.4.5 Implementing Heterologous Reactions into the Core Metabolism of *Saccharomyces cerevisiae*

Already mentioned above, *S. cerevisiae* serves as an excellent production host for biotechnological products, sometimes these products are natively produced by heterologous organisms. However, to successfully implement heterologous metabolic pathways into this yeast, the requirements of the biochemical reaction (or metabolic pathway) and the endogenous host metabolism must be considered. Different organisms rely on different cofactors for certain biochemical reactions, which unfortunately often diverge in the preferred cofactor utilization. Consequently, the supply of reducing equivalents can face limitations and thus hamper the efficiency of the heterologous pathway. In this context two strategies emerge, **i)** the modification of the host metabolism itself to suit the requirements of the to be implemented pathway and **ii**) adjusting the to be implemented pathway or biochemical reaction to align the requirements present in the host metabolism.

**i)** To overcome such limitations various approaches to increase the NADH- or the NADPH-level in yeast have been conducted. Streamlining the yeast metabolism often includes the knockout or overexpression of certain genes to redirect the metabolic flux towards tailored cofactor replenishment or perturbation of endogenous competitor reactions (Wess et al., 2019; Yu et al., 2018; Zhao et al., 2015). Such metabolic engineering approach was successfully conducted by Wess et al., in 2019, when the NADH-dependent metabolic pathway for isobutanol production was aligned with the redox-cofactor recycling system of the core metabolism in the yeast *S. cerevisiae*. Therefore, the ethanol and glycerol formation were perturbed (Δ*adh1*, Δ*gpd1* and Δ*gpd2*) to defy the competition of the desired pathway over the cofactor NADH. Furthermore, the acetate formation via the NADH-generating Ald2 was enhanced by deleting the gene of the NADPH-generating Ald6 (Δ*ald6*). Together, the modifications in the ethanol, glycerol and acetate formation strongly increased the isopropanol production of the yeast strain (Wess et al., 2019). In the literature, not only the NADH-recycling system was subject to metabolic engineering approaches, the benefit of a tailored metabolism was also demonstrated for pathways dependent on NADPH like the fatty acid or carotenoid

synthesis. Therefore, the interplay between the enzymes Pgi1 and Zwf1 regarding the flux of glucose either into the glycolysis (NADH-generation) or the PPP (NADPH-generation) has been described as suitable target to boost the NADPH-generation of the yeast cell. To redirect the flux more towards the PPP, the strong expression of the *PGI1* must be decreased end the relatively low expression of the *ZWF1* has to be increased. Thereby, it was demonstrated that an overexpression of the *ZWF1* had a beneficial effect on the efficiency of the NADPH-dependent pathway (Zhao et al., 2015), while the *PGI1* deletion is to be handled carefully. If no reaction is provided to reoxidized the NADPH, Δ*pgi1* strains often result in a crucial growth defect of the yeast (Boles et al., 1993). In respect of both findings it was shown, that even the downregulation of the *PGI1* by replacing the native promoter with a relatively weak promoter was sufficient to further increase the beneficial effect of an overexpressed *ZWF1* on the NADPH-accessibility in the cell (Wernig et al., 2021; Yu et al., 2018). A further strategy to improve the NADPH-supply for (heterologous) reactions was demonstrated by overexpression of the NADH-kinase gene *POS5* (Gao et al., 2018; Zhao et al., 2015). However, this approach seems to not be fully understood, as it was reported in a different study that the overexpression of the *POS5* severely hampered the cell growth (Kim et al., 2018). This further illustrates the sensitive ratio between the reduced and oxidized species of this cofactor pair ($NADP^+$/NADPH).

**ii)** Since major modifications in the cofactor utilization in the host can severely perturb the fitness of the cell, another strategy aims to switch the cofactor preference of an (heterologous) enzyme to rather suit the redox conditions found in the host. In the literature this approach was described for various NADPH-dependent enzymes from different classes. Among these an imine reductase (Borlinghaus and Nestl, 2018), dehydrogenases for phosphite and formate (Seelbach et al., 1996; Woodyer et al., 2003) as well as a Baeyer-Villiger monooxygenase (Beier et al., 2016) have been engineered. In addition, also NADH-dependent enzymes were engineered to rather accept NADPH, shown for a xylose reductase (Khoury et al., 2009). These approaches were guided by structure analysis and computational design to predict the amino acids which had to be exchanged to achieve the cofactor switch.

Especially a combination of both strategies **i**) and **ii**) might be of great impact for streamlining the implementation of heterologous enzymes and pathways towards efficient biotechnological processes.

## 1.5 The Potential of the Widely Underused Sugar Beet Residues from Sugar Industry

With fruits being part of the human diet, the sweet flavor of sugars delighted humankind already for centuries. In early medieval ages (~600 AD), this intensified with the first processes to refine sugars from the plant sugar cane, which, however, requires warmer climates to grow and thus became a costly good in Europe. Only the discovery to refine sugars from sugar beets in 1747 by Andreas Sigismund Marggraf in former Prussia (Germany) revolutionized the sugar refinery industry. Concomitantly to further optimizations of the Marggraf-process, refined sugars became an inexpensive additive in food industry. Consequently, many products of the everyday life contain refined sugars for preserving and especially for sweetening purposes. To meet the high demand of sugars for the food industry, the sugar beet became a prominent crop plant on the fields of today's agricultural sector. However, the increased cultivation of sugar beets and the consecutive sugar refinery entails vast production of sugar beet debris. This debris mainly consists of the polymer pectin (up to 20% in the dry total solids) (Grohmann and Bothast, 1994), which is one of the major constituents of the plant cell wall. Implemented into the cell wall, pectin fulfills a number of different tasks in the matrix between the cells, where it contributes to the cell-cell-adhesion, the water holding capacity and the structure of the cell wall itself (reviewed by Mohnen, 2008). Pectin rich waste streams are not unique to sugar refinery from sugar beets, for instance they are also accumulated in citrus fruit processing industry (Kuivanen et al., 2014).

The structure of pectin is complex, based on a backbone of mainly O-1 and O-4 linked D-galacturonic acid units (GalA) it also contains various other sugar monomers predominantly L-arabinose, D-galactose, L-rhamnose and D-xylose. Among these sugars, the GalA moiety makes up to 70% (reviewed by Mohnen, 2008). Different subtypes of pectin have been described, which mainly differ by the sugar composition of their backbone and sidechains (Figure 1-6).

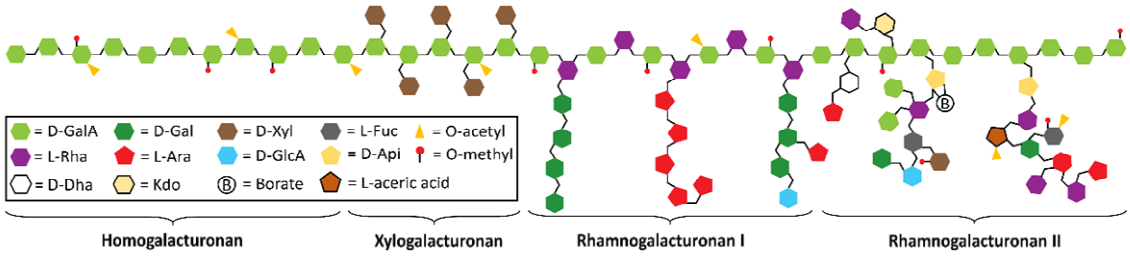


**Figure 1-6: Structure of the polymer pectin.**
Shown are the structures of the four different subtypes of pectin: Homogalacturonan, Xylogalacturonan, Rhamnogalacturonan I and Rhamnogalacturonan II. These subtypes differ in the composition of their backbone and sidechains. Possible sugar subunits are GalA, D-galactose (D-Gal), D-xylose (D-Xyl), L-fucose (L-Fuc), L-rhamnose (L-Rha), L-arabinose (L-Ara), D-glucuronic acid (D-GlcA), D-apiose (D-Api), 3-deoxy-D-lyxo-2-heptulosaric acid (D-Dha), 3-deoxy-D-manno-2-octulosonic acid (Kdo). Furthermore, these monosaccharide units can carry O-acetylations and O-methylations as well as borate groups. The figure was taken with permission from Schmitz et al., 2019, who adapted it from Harholt et al., 2010.

While in nature many microbes have evolved pathways to degrade pectin and to catabolize the released monomers, this feature is mainly underutilized in industry, as pectin is only fed to cattle or simply burnt. However, pectin classifies as second-generation feedstock, since its generation does not interfere with the farming of eatable foods (Tilmann et al., 2009). Therefore, establishing pectin-rich biomass streams as feedstock for industry bears great potential to build a chemical industry based on renewable resources, which already was exemplarily shown for ethanol production (Edwards and Doran-Peterson, 2012; Grohmann et al., 1994).

### 1.5.1 Microbial Catabolism of the Major Pectin Monomer GalA

Various microbes are capable to break down pectin and to utilize the sugar monomers released in this process, among these are filamentous fungi like *Hypocrea jecorina* (also known as *Trichoderma reesei*) and *Aspergillus niger* as well as different bacteria. The very first step of the GalA-catabolism is the depolymerization of the pectin, which is catalyzed by pectinases. Pectinases are a heterogenous group of enzymes, which perform hydrolase, lyase and esterase reactions to cope with the heterogeneity of pectin (Sharma et al., 2013). Due to the size of the pectin polymer, it cannot directly be taken up by microbes, therefore the pectinase activity is required outside of the cell. Microbes had to evolve transporter systems to take up the degradation products, especially the GalA-monomers. Therefore, GalA-transporters have been described (Benz et al., 2014; Protzko et al., 2019, 2018; San Francisco and Keenan, 1993). The intracellular catabolism of GalA follows different metabolic routes in fungi and bacteria. While the fungal pathway is of reductive nature, in bacteria the pathway can also follow an oxidative strategy (Figure 1-7 and 1-8).

The fungal catabolism of GalA starts off with the reduction to L-galactonate (GalOA) by a GalA-reductase. In a second step, a water molecule is cleaved off irreversibly of the molecule's body by

a dehydratase (Kuorelahti et al., 2006), which is split into pyruvate and L-glyceraldehyde in a following third step (Hilditch et al., 2007). While pyruvate directly fluxes into the core metabolism, the L-glyceraldehyde is converted to glycerol by a suitable reductase (Liepins et al., 2006) (Figure 1-7). The fungal GalA-reductases especially of *H. jecorina* and *A. niger* were extensively studied, so in *H. jecorina* it is called TrGar1 and mainly utilizes NADPH (Kuorelahti et al., 2005), while the variant in *A. niger* (AnGaaA) utilizes NADPH and also to a lower extent NADH (Martens-Uzunova and Schaap, 2008). In addition, another rather NADPH-accepting GalA-reductase was proposed in *A. niger,* which, compared with TrGar1, shows an amino acid sequence identity of 61% (Hilditch, 2010).

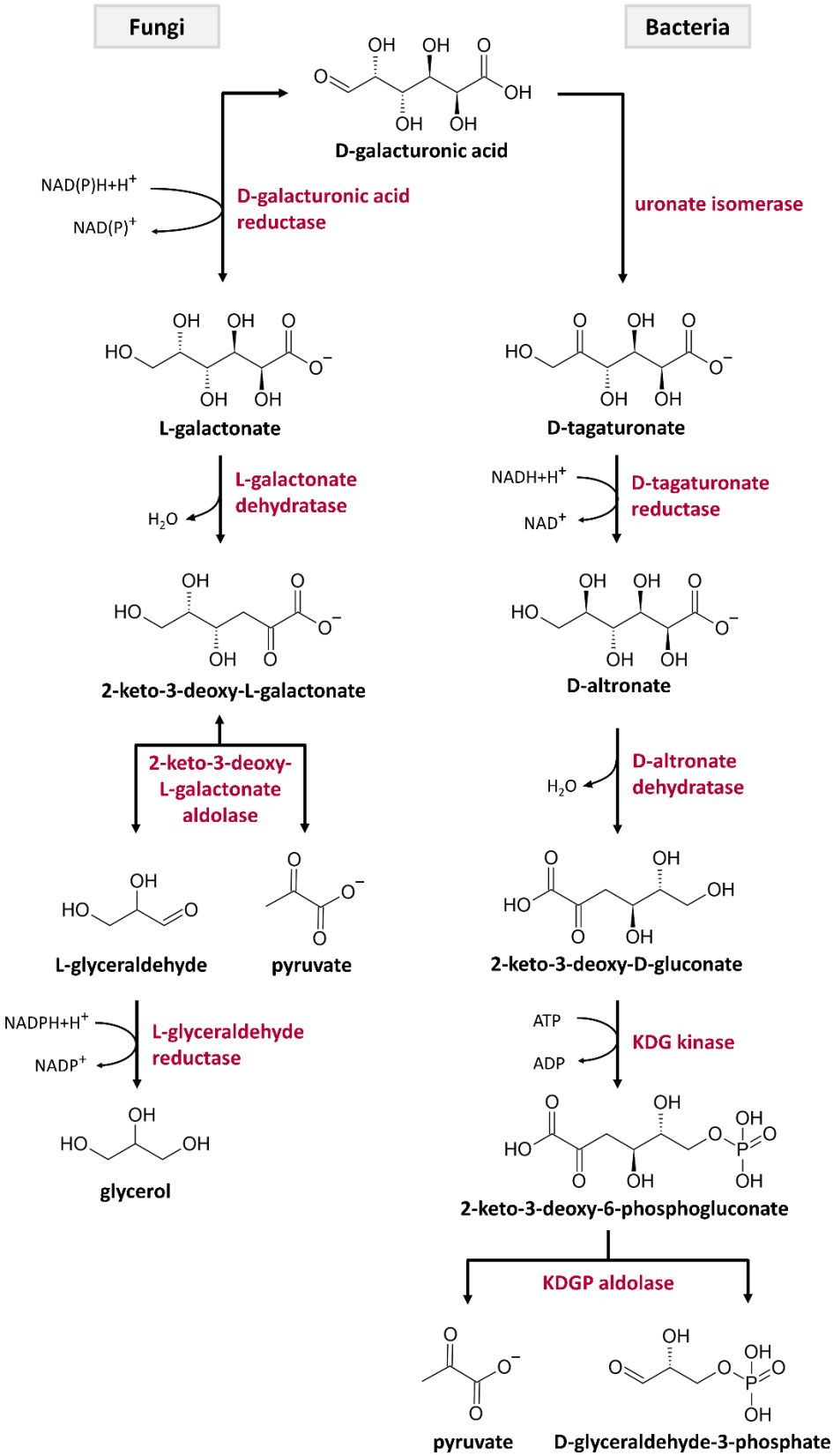


**Figure 1-7: Overview of the reductive GalA-catabolism in Fungi and Bacteria.**
Reductive metabolic routes have been described for fungal and bacterial GalA-catabolism. The fungal pathway consists of reduction, dehydratase and aldolase steps, while the bacterial pathway is initiated by an isomerase step. The end products of these pathways flux into the respective core metabolism of the organisms. The enzymes are highlighted in red and the 2-keto-3-deoxy-D-gluconate kinase and the 2-keto-3-deoxy-6-phosphogluconate aldolase are abbreviated by KDG kinase and KDGP aldolase, respectively. The figure was adapted from Schmitz et al., 2019 and Richard and Hilditch, 2009.

Besides the described reductive isomerase pathway for GalA-catabolism, oxidative pathways as well have been found in bacteria like *Agrobacterium tumefaciens* (Richard and Hilditch, 2009), which start with the oxidation of GalA to *meso*-galactarate by an uronate dehydrogenase using $NAD^+$ (Boer et al., 2010; Chang and Feingold, 1969). By undergoing a dehydratase reaction *meso*-galactarate is converted into 5-dehydro-4-deoxy-L-glucarate (Chang and Feingold, 1970). Catalyzed by only one enzyme, this compound undergoes dehydration and decarboxylation to result in α-ketoglutarate semialdehyde (Jeffcoat, 1975), which is converted to α-ketoglutarate by a $NAD^+$-dependent dehydrogenase reaction (Chang and Feingold, 1970). α-Ketoglutarate is a native intermediate of the tricarboxylic acid cycle and thus is further funneled into the core metabolism of the bacterial cell (Figure 1-8).

In *E coli*, the intermediate 5-dehydro-4-deoxy-L-glucarate, however, is substrate to an aldolase, which produces L-tartronate semialdehyde and pyruvate, of which first is reduced to D-glycerate by an NADH-dependent reductase. A glycerate kinase phosphorylates the D-glycerate to 2-phosphoglycerate and thus funnels it into the glycolysis, where it is oxidized to pyruvate and further metabolized in the core metabolism of the bacterial cell (Figure 1-8) (Hubbard et al., 1998).

To be mentioned, the bacterial degradation of pectin can also result in 4-Deoxy-5-keto-L-threo-hexarate from a lyase reaction. This compound can be metabolized by the bacterial cell as well, but will not be further described in this work (Richard and Hilditch, 2009).

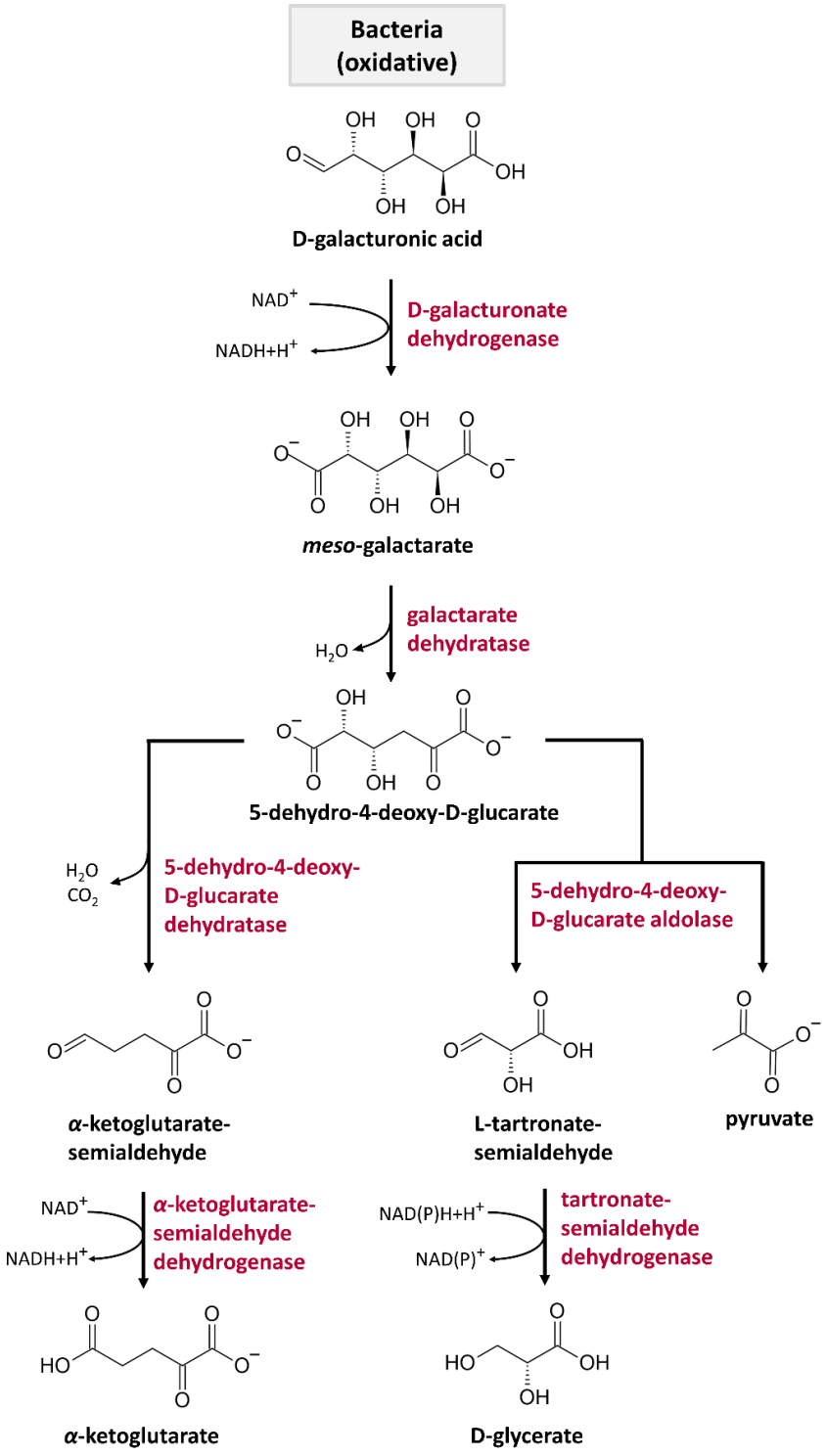


**Figure 1-8: The oxidative GalA-catabolism in Bacteria.**
Besides the reductive GalA-catabolism, also oxidative pathways exist in Bacteria. These pathways follow oxidative steps including dehydrogenases and dehydratases to form 5-dehydro-4-deoxy-D-glucarate, which is a metabolic branch point. This compound can be further converted to eventually result in α-ketoglutarate, which can be used as an intermediate of the tricarboxylic acid pathway. Alternatively, this compound can undergo an aldolase reaction to eventually result in pyruvate and D-glycerate, which can be utilized in the glycolysis after phosphorylation to also form pyruvate. Pyruvate is part of the core metabolism and thus is further processed. Enzymes are highlighted in red. The figure was adapted from Richard and Hilditch, 2009.

### 1.5.2 Engineering Microbes for GalA-Utilization and the Production of GalA-Derivatives towards Industrial Application

Harnessing the GalA-catabolism can be of great potential for industrial processes. Being an abundant side product of the sugar refinery industry, pectin rich waste streams might serve as cheap carbon sources for biorefinery processes. Therefore, certain approaches have been conducted to transfer GalA-catabolism to one of the well-known production hosts in biotechnology, *S. cerevisiae,* which does not naturally grow on GalA but was demonstrated to be a powerful host for synthetic biology approaches and robust to acidic fermentation conditions (Abbott et al., 2009; Benz et al., 2014; Keasling, 2008). So far, it was not possible to transfer the bacterial isomerase pathway for GalA-catabolism to *S. cerevisiae*, as only the first two steps were found functional in this yeast (Huisjes et al., 2012b). In contrast, the expression of the analog metabolic route which was found in Fungi could successfully be transferred to this yeast, however, the efficiency was low and vast amounts of co-substrates were necessary (Biz et al., 2016; Jeong et al., 2020; Protzko et al., 2018). This was proposed to be based on the reductive character of the GalA-catabolism, which requires the reductive equivalents NADH and NADPH for GalA-reduction from the core metabolism of the cell, even in one of the native hosts *A. niger* (Alazi et al., 2017). Thereby, in a yeast strain expressing the fungal pathway, it was found that a rather NADH-dependent GalA-reductase (AnGaaA) could lead to a more efficient GalA-consumption compared to a NADPH-dependent variant (TrGar1) (Protzko et al., 2018). This finding was further supported by the study of Perpelea et al. in 2022, which showed that glycerol could be exploited to deliver reductive equivalents for GalA-reduction, considering that the glycerol metabolism is NADH-dependent in this yeast. A yeast strain capable of growing on GalA could be further engineered to also produce compounds relevant for biorefinery industry like fine chemicals and ethanol.

However, potential applications of the GalA-catabolism emerge not only from the degradation of the pectin wastes to form biomass, but also from intermediates of respective pathways (Figure 1-9). For instance, the first intermediate of the fungal pathway, GalOA, shows high structural similarity to L-gluconate, which is widely used in food and cosmetic industry as complexing agent and slow acidifier. This property is due to the fact that L-gluconate, just like GalOA, is a polyhydroxy acid, which is capable of complexing metal ions (Sawyer, 1964). GalOA can spontaneously lactonize to L-galactono-γ-lactone, which shares strong structure similarity with D-glucono-δ-lactone the lactonization product of L-gluconate, which is commonly used in food industry as slow-release acidifier. Moreover, L-galactono-γ-lactone is a precursor for L-ascorbic acid, better known as vitamin C (Figure 1-9). The conversion to vitamin C can be performed using biological (Onofri et al., 1997; Roland et al., 1986) or chemical catalysts (Csiba et al., 1993).

In metabolic opposite direction to the reductive GalA-catabolism, GalA can also be oxidized via an uronate dehydrogenase (Udh) resulting in *meso*-galactaric acid (Boer et al., 2010). This dicarboxylic sugar acid qualifies as an attractive platform chemical especially for polymer technology, as it can be reduced to adipic acid a precursor for Nylon (Li et al., 2014) and to 2,5-furandicarboxylic acid, which holds potential to replace plastics based on fossil fuels (De Jong et al., 2012; Lewkowski, 2001; Yoichi et al., 2008). The biotechnological production of *meso*-galactaric acid via the Udh has been demonstrated for various microbes like *A. niger* (Kuivanen et al., 2016), *T. reesei* (Paasikallio et al., 2017), *S. cerevisiae* (Protzko et al., 2018) and *E. coli* (Zhang et al., 2016).

The described applications for GalA utilization by microbial fermentations underline the biotechnological relevance and the great potential inherent in pectin-rich waste streams from the fruit and sugar industries.

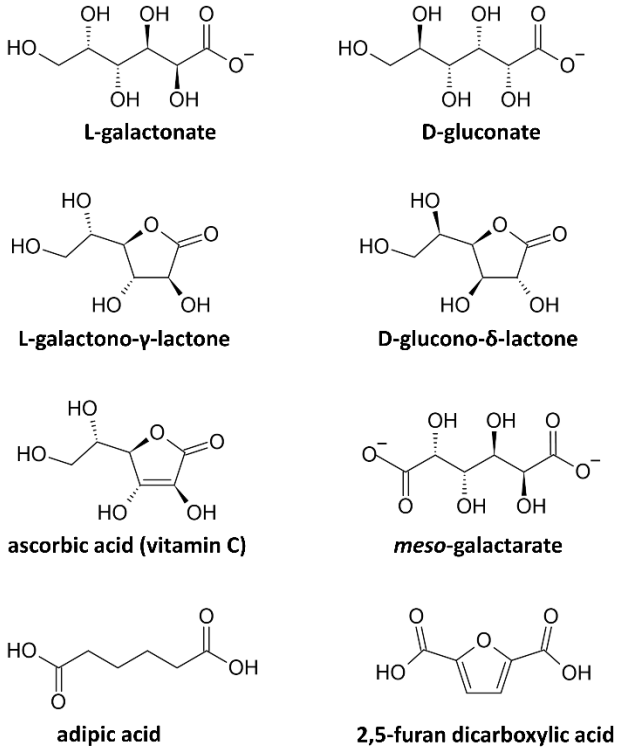


**Figure 1-9: Examples of GalA derivatives of biotechnological relevance.**
Metabolic pathways emerging from GalA result in compounds, which are of interest for biotechnology. The intermediates L-galactonate and L-galactono-γ-lactone resemble the respective counterparts D-gluconate and D-glucono-δ-lactone, which already found application in industry. Furthermore, L-galactono-γ-lactone can serve as precursor for ascorbic acid production. After undergoing one oxidative step, galacturonic acid converts to *meso*-galactarate a platform chemical for various applications, e.g., for adipic acid and 2,5-furan dicarboxylic acid, which are used for polymer production independent of fossil-fuels.

## 1.6 Aim of this Study

The sugar industry produces vast amounts of pectin rich waste streams of which GalA forms a great moiety. Despite its high abundance, the potential of GalA to serve as a precursor or as carbon source, however, is widely underused. The product of GalA-reduction, L-galactonate, might find application as cosmetic and food additive. Even though filamentous fungi are endogenous hosts of the GalA-catabolism, this class of organisms remains challenging in terms of bioreactor cultivation and genetic accessibility. Therefore, the versatile biotechnological production host *S. cerevisiae* for which manifold genetic tools and fermentation related knowledge is accessible will be harnessed. So far, first approaches have already been conducted in this organism, however these approaches indicated limitations regarding GalA-uptake and cofactor replenishment due to the high oxidative state of GalA (Biz et al., 2016; Matsubara et al., 2016; Protzko et al., 2018).

The polyol sorbitol has a lower oxidation state than GalA and therefore could serve as a donor of reductive equivalents to meet the large demand for the very same by the GalA-reductases. However, *S. cerevisiae* does not efficiently utilize sorbitol as carbon source, so to establish the sorbitol metabolism in this yeast, suitable transporter and sorbitol dehydrogenases must be implemented. However, sorbitol itself does not qualify as reasonable carbon source for cost efficient industrial processes. Instead, sorbitol fermenting strains could serve as platform to screen engineered GalA-reductases in regard of efficient cofactor utilization, since sorbitol dehydrogenases were described to generate both NADH or NADPH (Jordan et al., 2016; Napora et al., 2013). By potentially switching the cofactor preference of these GalA-reductases via protein engineering, it appears plausible that the GalA-reduction reaction might be more successfully implemented into the core metabolism of *S. cerevisiae* when grown on industrially feasible carbon sources like glucose.

To further align the demand of the GalA-reduction and the metabolic conditions of the expression host, further modifications might have to be introduced into its redox-cofactor recycling system. Therefore, the role of the ethanol, glycerol and acetate formation as major participants in the intracellular redox-cycle are to be investigated in terms of their effect on the GalA-reduction. Furthermore, variations in the flux ratio between the NADH-generating glycolysis and the NADPH-generating pentose phosphate pathway, might be of great interest towards optimized cofactor supply for the GalA-reductases.

Aiming to establish pectin rich waste streams as a second-generation feedstock, this work aims to overcome the challenging metabolic character of GalA itself by aligning the GalA-conversion to the endogenous cofactor recycling system and suitable rerouting of metabolic fluxes. Successfully established GalA-utilization could transform *S. cerevisiae* into a biorefinery platform of high industrial value based on the utilization of abundant production residues of the sugar refinery.

# 2 Material and Methods

## 2.1 Devices and Chemicals

### 2.1.1 Devices

Devices, which are beyond the standard equipment, but used in this work are listed in Table 2.1.

**Table 2-1: Used devices stating the producers.**

| Device | Producer |
|---|---|
| Agarose gel-electrophoresis chambers | Neolab |
| Cell electroporator, Gene Pulser | Bio-Rad |
| Cell growth quantifier | Aquila Biolabs |
| Fluorescence spectrophotometer, *CLARIOstar Plus* | BMG LABTECH |
| Incubator | Multitron Standard, Infors HT |
| Nanodrop 1000 spectrophotometer | Thermo Fisher Scientific |
| PCR Cycler, labcylcler triple block | SensoQuest |
| PCR Cycler, Piko thermal cycler | Finnzymes |
| pH-meter 765 Calimatic | Knick |
| Pipette, 0.1-2.5 µL | starlab |
| Pipette, 0.5-10 µL | starlab |
| Pipette, 10-100 µL | starlab |
| Pipette, 100-1000 µL | starlab |
| Shaker | Infors HT |
| Spectrophotometer Ultrospec 2100 pro | Amersham Bioscience |
| Thermomixer comfort | eppendorf |
| Vibrax VXR basic | IKA |
| | |
| **HPLC systems:** | |
| BioLC: | |
| Autosampler | AS50, Thermo Scientific |
| Column oven | TCC-100, Thermo Scientific |
| Gradient pump | GS50, Thermo Scientific |
| Degasser | Ultimate3000, Thermo Scientific |
| RI-detector | RI-101, Shodex |
| Wave length detector | VWD-3100, Dionex |
| | |
| Ultimate3000: | |
| Autosampler | WPS300SL, Thermo Scientific |
| Column oven | TCC-300SD, Thermo Scientific |
| Pump system | ISO-3100SD, Thermo Scientific |
| Degasser | Ultimate3000, Thermo Scientific |
| RI-detector | RI-101, Shodex |
| | |
| Columns: | |
| HPLC column, VA 300/7.8 NUCLEOGEL Sugar 810 H | Macherey Nagel |
| HPLC column, ICSep 801 FA, HPLC-column 250x4.0mm | Concise Separations |
| HPLC column, ICSep ICE-Coregel 87H3 9µm, 300x7.8mm | Concise Separations |

### 2.1.2 Chemicals and Reagents

Chemicals, reagents and kits used in this work are listed in Table 2.2.

**Table 2-2: Used chemicals and preparation kits including producer.**

| Product | Producer |
|---|---|
| Bacterial trypton | Difco |
| Bacteriological peptone | Oxoid |
| Carbenicillin | Roth |
| Chloramphenicol | Roth |
| ClonNAT (Nourseothricin) | WERNER BioAgents |
| DNA loading dye | NEB, Fermentas |
| dNTPs | NEB |
| DreamTaq, incl. buffer | NEB |
| DTT | Roth |
| Fructose-6-phosphate | Roth |
| G418-sulfate, Geneticin | Calbiochem |
| Geneticin (G418) | Merck |
| Glass beads (0.45 mm) | Roth |
| Glucose-6-phosphate | Roth |
| Glucose-6-phosphate dehydrogenase | Sigma |
| Hygromycin B | Roth |
| Kanamycin sulfate | Roth |
| Maltose | Difco |
| $MgCl_2$ | Roth |
| β-Nicotinamide-adenine-dinucleotide hydrate ($NAD^+$) | Roche |
| β-Nicotinamide-adenine-dinucleotide reduced disodium salt hydrate (NADH) | Roche |
| β-Nicotinamide-adenine-dinucleotide phosphate disodium hydrate ($NADP^+$) | Roche |
| β-Nicotinamide-adenine-dinucleotide 2’ phosphate reduced tetrasodium salt hydrate (NADPH) | Roche |
| PEG-4000 | Roth |
| PEG-8000 | Roth |
| Phusion DNA polymerase, incl. buffer | NEB |
| Q5 DNA polymerase, incl. buffer | NEB |
| Restriction enzymes, incl. buffer | NEB |
| Roti-Quant | Roth |
| Sheared salmon sperm DNA | Ambion |
| Synthetic oligonucleotides | biomers, microsynth |
| T4 DNA ligase | NEB |
| T7 DNA ligase | NEB |
| Taq DNA ligase | NEB |
| Tris-HCl | Roth |
| Yeast extract | Difco |
| Yeast nitrogen base (YNB) w/o amino acids and w/o ammonium sulfate | Difco |
| | |
| **Kits:** | |
| GeneJET Plasmid Miniprep kit | Thermo Scientific |
| NucleoSpin Gel and PCR clean up | Macherey-Nagel |

If not stated differently, all other chemicals were bought from Roth.

## 2.2 Microbial Strains and Plasmids

### 2.2.1 Microbial Strains

Different laboratory strains of *E. coli* and *S. cerevisiae* were used in this work (Table 2-3).

**Table 2-3: Microbial strains used in this work.**

| Strain | Description | Reference |
|---|---|---|
| ***E. coli*** | | |
| DH10B | F⁻ *mcr*A Δ(*mrr-hsd*RMS-*mcr*BC) ϕ80*lac*ZΔM15 Δ*lac*X74 *rec*A1 *end*A1 *ara*D139 Δ(*ara-leu*)7697 *gal*U *gal*K λ⁻ *rps*L(Str$^R$) *nup*G | Thermo Fisher Scientific |
| ***S. cerevisiae*** | | |
| CEN.PK2-1C | *MATa leu2-3,112 ura3-52 trp1-289 his3-Δ1 MAL2-8c SUC2* | EUROSCARF, Frankfurt |
| EBY.VW4000 | *MATa leu2-3,112 ura3-52 trp1-289 his3-Δ1 MAL2-8c SUC2 Δhxt1-17 gal2Δ::loxP stl1Δ::loxP agt1Δ::loxP mph2Δ::loxP mph3Δ::loxP* | Wieczorke et al., 1999 |
| JWY019 | *MATa; MAL2-8c; SUC2; Δilv2; Δbdh1; Δbdh2; Δleu4; Δleu9; Δecm31; Δilv1; Δadh1; Δgpd1; Δgpd2* | Wess et al., 2019 |
| JWY023 | *MATa; MAL2-8c; SUC2; Δilv2; Δbdh1; Δbdh2; Δleu4; Δleu9; Δecm31; Δilv1; Δadh1; Δgpd1; Δgpd2, Δald6* | Wess et al., 2019 |
| SiHY001 | The strain was constructed by integration of the NotI-linearized plasmid SiHV040 into the *URA3*-locus of EBY.VW4000.<br><br>*URA3::pCCW12-AnGATA_CO-tPGK1-pPGK1-AnGAR1_CO-tENO1-pTDH3-HXT13-tSSA1-pTEF2-YlSDR-tADH1-KanMX* | this study |
| SiHY002 | The strain was constructed by integration of the NotI-linearized plasmid SiHV041 into the *URA3*-locus of EBY.VW4000.<br><br>*URA3::pCCW12-AnGATA_CO-tPGK1-pPGK1-TrGAR1_CO-tENO1-pTDH3-HXT13-tSSA1-pTEF2-YlSDR-tADH1-KanMX* | this study |
| SiHY003 | The strain was constructed by integration of the NotI-linearized plasmid SiHV042 into the *URA3*-locus of EBY.VW4000.<br><br>*URA3::pCCW12-AnGATA_CO-tPGK1-pPGK1-AnGAR1_CO-tENO1-pTDH3-HXT13-tSSA1-pTEF2-SOR2-tADH1-KanMX* | this study |
| SiHY004 | The strain was constructed by integration of the NotI-linearized plasmid SiHV043 into the *URA3*-locus of EBY.VW4000.<br><br>*URA3::pCCW12-AnGATA_CO-tPGK1-pPGK1-TrGAR1_CO-tENO1-pTDH3-HXT13-tSSA1-pTEF2-SOR2-tADH1-KanMX* | this study |
| SiHY007 | The strain was constructed by integration of the NotI-linearized plasmid SiHV046 into the *URA3*-locus of EBY.VW4000.<br><br>URA3::*pCCW12-AnGATA_CO-tPGK1-pTDH3-HXT13-tSSA1-pTEF2-YlSDR-tADH1-KanMX* | this study |
| SiHY008 | The strain was constructed by integration of the NotI-linearized plasmid SiHV047 into the *URA3*-locus of EBY.VW4000.<br><br>*URA3::pCCW12-AnGATA_CO-tPGK1-pTDH3-HXT13-tSSA1-pTEF2-SOR2-tADH1-KanMX* | this study |

| | | |
|---|---|---|
| SiHY018 | The strain was constructed by integration of the NotI-linearized plasmid SiHV041 into the *URA3*-locus of CEN.PK2-1C.<br><br>*URA3::pCCW12-AnGATA_CO-tPGK1-pPGK1-TrGAR1_CO-tENO1-pTDH3-HXT13-tSSA1-pTEF2-YlSDR-tADH1-KanMX* | this study |
| SiHY019 | The strain was constructed by integration of the NotI-linearized plasmid SiHV043 into the *URA3*-locus of CEN.PK2-1C.<br><br>*URA3::*pCCW12-AnGATA_CO-tPGK1-pPGK1-TrGAR1_CO-tENO1-pTDH3-HXT13-tSSA1-pTEF2-SOR2-tADH1-KanMX-URA3 | this study |
| SiHY023 | The strain was constructed by integration of the NotI-linearized plasmid SiHV090 into the *URA3*-locus of EBY.VW4000.<br><br>*URA3::pRNR1-AnGATA_CO-tPGK1-pPGK1-TrGAR1_CO-tENO1-pTDH3-HXT13-tSSA1-pTEF2-YlSDR-tADH1-KanMX* | this study |
| SiHY024 | The strain was constructed by integration of the NotI-linearized plasmid SiHV091 into the *URA3*-locus of EBY.VW4000.<br><br>*URA3::pCCW12-AnGATA_CO-pRNR1-TrGAR1_CO-tENO1-pTDH3-HXT13-tSSA1-pTEF2-YlSDR-tADH1-KanMX* | this study |
| SiHY025 | The strain was constructed by integration of the NotI-linearized plasmid SiHV092 into the *URA3*-locus of EBY.VW4000.<br><br>*URA3::pCCW12-AnGATA_CO-tPGK1-pPGK1-TrGAR1_CO-tENO1-pRNR1-HXT13-tSSA1-pTEF2-YlSDR-tADH1-KanMX* | this study |
| SiHY026 | The strain was constructed by integration of the NotI-linearized plasmid SiHV093 into the *URA3*-locus of EBY.VW4000.<br><br>*URA3::pCCW12-AnGATA_CO-tPGK1-pPGK1-TrGAR1_CO-tENO1-pTDH3-HXT13-tSSA1-pRNR1-YlSDR-tADH1-KanMX* | this study |
| SiHY033 | The strain was constructed by Crispr-Cas9 mediated deletion of the *ADH1* gene in CEN.PK2-1C. Therefore, the plasmid FWV100 and the annealed DNA oligomers SiHP370 and SiHP371 were used.<br><br>*Δadh1* | this study |
| SiHY036 | The strain was constructed by integration of the NotI-linearized plasmid SiHV136 into the *URA3*-locus of SiHY033.<br><br>*Δadh1*<br>*URA3::pCCW12-AnGATA_CO-tPGK1-pPGK1-AnGAR1 [R267L]_CO-tENO1-KanMX* | this study |
| SiHY037 | The strain was constructed by integration of the NotI-linearized plasmid SiHV137 into the *URA3*-locus of SiHY033.<br><br>*Δadh1*<br>*URA3::pCCW12-AnGATA_CO-tPGK1-pPGK1-AnGAR1 [K261M, R267L]_CO-tENO1-KanMX* | this study |

| | | |
|---|---|---|
| SiHY040 | The strain was constructed by integration of the NotI-linearized plasmid SiHV136 into the *URA3*-locus of CENPK2-1C.<br><br>*URA3::pCCW12-AnGATA_CO-tPGK1-pPGK1-AnGAR1 [R267L]_CO-tENO1-KanMX* | this study |
| SiHY041 | The strain was constructed by integration of the NotI-linearized plasmid SiHV137 into the *URA3*-locus of CEN.PK2-1C.<br><br>*URA3::pCCW12-AnGATA_CO-tPGK1-pPGK1-AnGAR1 [K261M, R267L]_CO-tENO1-KanMX* | this study |
| SiHY057 | The strain was constructed by integration of the NotI-linearized plasmid SiHV158 into the *URA3*-locus of CEN.PK2-1C.<br><br>*URA3::pCCW12-AnGATA_CO-pPGK1-AnGAR1_CO--KanMX* | this study |
| SiHY062 | The strain was constructed by integration of the NotI-linearized plasmid SiHV136 into the *URA3*-locus of JWY019.<br><br>MATa; MAL2-8c; SUC2; Δilv2; Δbdh1; Δbdh2; Δleu4; Δleu9; Δecm31; Δilv1; Δadh1; Δgpd1; Δgpd2<br>*URA3::pCCW12-AnGATA_CO-tPGK1-pPGK1-AnGAR1 [R267L]_CO-tENO1-KanMX* | this study |
| SiHY063 | The strain was constructed by integration of the NotI-linearized plasmid SiHV137 into the *URA3*-locus of JWY019.<br><br>MATa; MAL2-8c; SUC2; Δilv2; Δbdh1; Δbdh2; Δleu4; Δleu9; Δecm31; Δilv1; Δadh1; Δgpd1; Δgpd2<br>*URA3::pCCW12-AnGATA_CO-tPGK1-pPGK1-AnGAR1 [K261M, R267L]_CO-tENO1-KanMX* | this study |
| SiHY064 | The strain was constructed by integration of the NotI-linearized plasmid SiHV136 into the *URA3*-locus of JWY023.<br><br>MATa; MAL2-8c; SUC2; Δilv2; Δbdh1; Δbdh2; Δleu4; Δleu9; Δecm31; Δilv1; Δadh1; Δgpd1; Δgpd2, Δald6<br>*URA3::pCCW12-AnGATA_CO-tPGK1-pPGK1-AnGAR1 [R267L]_CO-tENO1-KanMX* | this study |
| SiHY065 | The strain was constructed by integration of the NotI-linearized plasmid SiHV137 into the *URA3*-locus of JWY023.<br><br>MATa; MAL2-8c; SUC2; Δilv2; Δbdh1; Δbdh2; Δleu4; Δleu9; Δecm31; Δilv1; Δadh1; Δgpd1; Δgpd2, Δald6<br>*URA3::pCCW12-AnGATA_CO-tPGK1-pPGK1-AnGAR1 [K261M, R267L]_CO-tENO1-KanMX* | this study |
| SiHY072 | The strain was constructed by integration of the NotI-linearized plasmid SiHV158 into the *URA3*-locus of JWY019.<br><br>MATa; MAL2-8c; SUC2; Δilv2; Δbdh1; Δbdh2; Δleu4; Δleu9; Δecm31; Δilv1; Δadh1; Δgpd1; Δgpd2<br>*URA3::pCCW12-AnGATA_CO-pPGK1-AnGAR1_CO-KanMX* | this study |

| | | |
|---|---|---|
| SiHY073 | The strain was constructed by integration of the NotI-linearized plasmid SiHV158 into the *URA3*-locus of JWY023.<br><br>MATa; MAL2-8c; SUC2; Δilv2; Δbdh1; Δbdh2; Δleu4; Δleu9; Δecm31; Δilv1; Δadh1; Δgpd1; Δgpd2, Δald6<br>*URA3::pCCW12-AnGATA_CO-pPGK1-AnGAR1_CO-KanMX* | this study |
| SiHY077 | The strain was constructed by exchanging the native *pZWF1* promoter with the truncated *pHXT7t* promoter (Hauf et al., 2000) in CEN.PK2-1C based on the Crispr-Cas9 plasmid FWV157. The *pHXT7t* promoter was PCR amplified from the plasmid p426HXT7 using the primers FWP327 and SiHP434.<br><br>*pHXT7t-ZWF1* | this study |
| SiHY078 | The strain was constructed by exchanging the native *pPGI1* promoter with the endogenous *pCOX9* promoter in SiHY077 based on the Crispr-Cas9 plasmid FWV156. The *pCOX9* promoter was amplified via PCR from genomic yeast DNA using the primers FWP322 and FWP323.<br><br>*pHXT7t-ZWF1*<br>*pCOX9-PGI1* | this study |
| SiHY079 | The strain was constructed by Crispr-Cas9 mediated deletion of the *ALD6* gene in CEN.PK2-1C. Therefore, the plasmid VSV111 and the annealed DNA oligomers VSP370 and JWP092 were used.<br><br>*Δald6* | this study |
| SiHY080 | The strain was constructed by integration of the NotI-linearized plasmid SiHV158 into the *URA3*-locus of SiHY079.<br><br>Δald6<br>*URA3::pCCW12-AnGATA_CO-pPGK1-AnGAR1_CO-KanMX* | this study |
| SiHY081 | The strain was constructed by integration of the NotI-linearized plasmid SiHV201 into the *LEU2*-locus of SiHY001.<br><br>*hxt0*<br>*URA3::pCCW12-AnGATA_CO-tPGK1-pPGK1-AnGAR1_CO-tENO1-pTDH3-HXT13-tSSA1-pTEF2-YlSDR-tADH1-KanMX*<br>*LEU2::pTDH3-AnGAR1_CO-tENO1, ClonNAT* | this study |
| SiHY082 | The strain was constructed by integration of the NotI-linearized plasmid SiHV202 into the *LEU2*-locus of SiHY001.<br><br>*hxt0*<br>*URA3::pCCW12-AnGATA_CO-tPGK1-pPGK1-AnGAR1_CO-tENO1-pTDH3-HXT13-tSSA1-pTEF2-YlSDR-tADH1-KanMX*<br>*LEU2::pTDH3-HXT13-tENO1, ClonNAT* | this study |

| | | |
|---|---|---|
| SiHY083 | The strain was constructed by integration of the NotI-linearized plasmid SiHV203 into the *LEU2*-locus of SiHY001.<br><br>*hxt0*<br>*URA3::pCCW12-AnGATA_CO-tPGK1-pPGK1-AnGAR1_CO-tENO1-pTDH3-HXT13-tSSA1-pTEF2-YlSDR-tADH1-KanMX*<br>*LEU2::pTDH3-YlSDR-tENO1, ClonNAT* | this study |
| SiHY084 | The strain was constructed by integration of the NotI-linearized plasmid SiHV204 into the *LEU2*-locus of SiHY001.<br><br>*hxt0*<br>*URA3::pCCW12-AnGATA_CO-tPGK1-pPGK1-AnGAR1_CO-tENO1-pTDH3-HXT13-tSSA1-pTEF2-YlSDR-tADH1-KanMX*<br>*LEU2::pTDH3-AnGATA_CO-tENO1, ClonNAT* | this study |
| SiHY085 | The strain was constructed by exchanging the native *pZWF1* promoter with the truncated *pHXT7t* promoter (Hauf et al., 2000) in SiHY079 based on the Crispr-Cas9 plasmid FWV157. The *pHXT7t* promoter was PCR amplified from the plasmid p426HXT7 using the primers FWP327 and SiHP434.<br><br>*Δald6, pHXT7t-ZWF1* | this study |
| SiHY088 | The strain was constructed by Crispr-Cas9 mediated deletion of the *GPD2* gene in SiHY079. Therefore, the plasmid pRCC-K_GD01 and the annealed DNA oligomers GPD200 and GPD201 were used.<br><br>*Δald6, Δgpd2* | this study |
| SiHY094 | The strain was constructed by exchanging the native *pPGI1* promoter with the endogenous *pCOX9* promoter in CEN.PK2-1C based on the Crispr-Cas9 plasmid FWV156. The *pCOX9* promoter was amplified via PCR from genomic yeast DNA using the primers FWP322 and FWP323.<br><br>*pCOX9-PGI1* | this study |
| SiHY095 | The strain was constructed by integration of the NotI-linearized plasmid SiHV158 into the *URA3*-locus of SiHY085.<br><br>*Δald6, pHXT7t-ZWF1*<br>*URA3::pCCW12-AnGATA_CO-pPGK1-AnGAR1_CO-KanMX* | this study |
| SiHY097 | The strain was constructed by integration of the NotI-linearized plasmid SiHV158 into the *URA3*-locus of SiHY094.<br><br>*pCOX9-PGI1*<br>*URA3::pCCW12-AnGATA_CO-pPGK1-AnGAR1_CO-KanMX* | this study |
| SiHY098 | The strain was constructed by integration of the NotI-linearized plasmid SiHV158 into the *URA3*-locus of SiHY077.<br><br>*pHXT7t-ZWF1*<br>*URA3::pCCW12-AnGATA_CO-pPGK1-AnGAR1_CO-KanMX* | this study |

| | | |
|---|---|---|
| SiHY099 | The strain was constructed by integration of the NotI-linearized plasmid SiHV158 into the *URA3*-locus of SiHY078.<br><br>*pCOX9-PGI1; pHXT7t-ZWF1*<br>*URA3::pCCW12-AnGATA_CO-pPGK1-AnGAR1_CO-KanMX* | this study |
| SiHY104 | The strain was constructed by Crispr-Cas9 mediated deletion of the *ADH1* gene in SiHY088. Therefore, the plasmid FWV100 and the annealed DNA oligomers SiHP370 and SiHP371 were used.<br><br>*Δald6, Δgpd2, Δadh1* | this study |
| SiHY105 | The strain was constructed by integration of the NotI-linearized plasmid SiHV158 into the *URA3*-locus of SiHY104.<br><br>*Δald6, Δgpd2, Δadh1*<br>*URA3::pCCW12-AnGATA_CO-pPGK1-AnGAR1_CO-KanMX* | this study |
| SiHY115 | The strain was constructed by Crispr-Cas9 mediated deletion of the *ECM31* gene in SiHY105. Therefore, the plasmid JWV03 and the annealed DNA oligomers WGP518 and JWP005 were used.<br><br>*Δald6, Δgpd2, Δadh1, Δecm31*<br>*URA3::pCCW12-AnGATA_CO-pPGK1-AnGAR1_CO-KanMX* | this study |

Strain verification:
Integrations into the *URA3*-locus were verified in a control PCR using the DNA oligomer pairs SiHP060 and SiHP061 as well as SiHP062 and SiHP063. In an agarose gel electrophoresis, positive clones showed PCR products of the length 538 bp or 546 bp, respectively. Furthermore, integrations into the *LEU2*-locus were verified with the DNA oligomer pairs SiHP175 and SiHP176 as well as SiHP177 and SiHP178. Here, positive clones showed PCR fragments of the length of 553 bp or 540 bp, respectively.

### 2.2.2 Plasmids

Various plasmids were used in this work, most of them are shuttle vectors and contain genetic elements for cloning and DNA-amplification in *E. coli* and protein expression in *S. cerevisiae* (Table 2-4). Following abbreviations were used in the description section of the table 2-4: CamR (chloramphenicol resistance cassette: chloramphenicol acetyltransferase gene), AmpR (ampicillin resistance cassette: β-lactamase gene), KanR (kanamycin resistance cassette: neomycin phosphotransferase II gene), KanMX (Geneticin/G418 resistance cassette: aminoglycoside phosphotransferase gene), ClonNAT (nourseothricin resistance cassette), hygR (hygromycin resistance cassette: hygromycin B phosphotransferase gene), ORF (open reading frame), ColE1 (origin of replication in *E. coli*), 2µ (origin of replication in *S. cerevisiae*) and _CO (respective gene was codon optimized). For codon optimization the online platform JCat was used (Grote et al., 2005). Further, promoters are indicated with a lowercase p and terminators are indicated with a lowercase t. In case heterologous genes were cloned the initials of genus and species of the origin are indicated: An (*Aspergillus niger)* and Tr (*Hypocrea jecorina,* formerly: *Trichoderma reesei).*

**Table 2-4: Used plasmids mentioning description and reference.**

| Plasmid | Description | Reference |
|---|---|---|
| FWV156 | Crispr-Cas9-plasmid, which is descendant of pRCC-K targeting the *PGI1.*<br><br>*[pROX3-CAS9-tCYC1, pSNP52-gPGI1-tSUP4, KanMX, 2µ, AmpR, ColE1]* | Prof. Boles group, Frankfurt |
| FWV157 | Crispr-Cas9-plasmid, which is descendant of pRCC-K targeting the *ZWF1.*<br><br>*[pROX3-CAS9-tCYC1, pSNP52-gZWF1-tSUP4, KanMX, 2µ, AmpR, ColE1]* | Prof. Boles group, Frankfurt |
| JWV03 | Crispr-Cas9-plasmid, which is descendant of pRCC-N targeting the ECM31. The annealed pair of DNA oligomers WGP518 and JWV005 served as repair fragment for the Cas9-induced double strand break via homologous recombination.<br><br>*[pROX3-CAS9-tCYC1, pSNP52-gECM31-tSUP4, ClonNATR, 2µ, AmpR, ColE1]* | Wess et al., 2019 |
| p426HXT7 | Descendant of YEplac195, contains truncated *pHXT7t* promoter and *tCYC1* terminator for gene expression and 2µ-yeast origin and URA3-marker for plasmid maintenance, as well as the *E. coli* elements AmpR and pBR322 origin. | Becker and Boles, 2003 |
| p426MET25 | Descendant of YEplac195, contains inducible pMet25 promoter and *tCYC1* terminator for gene expression and 2µ-yeast origin and URA3-marker for plasmid maintenance, as well as the *E. coli* elements AmpR and pBR322 origin. | Prof. Boles group, Frankfurt |
| pGG3.2 *(HXT13)* | Golden Gate part 3 plasmid containing the ORF of the endogenous *HXT13;* plasmid is derived from pYTK001 and contains overhangs to part 2 and part 4 Golden Gate plasmids. | this study |
| pGG3.3 (*YlSDR)* | Golden Gate part 3 plasmid containing the ORF of the *YlSDR* from *Y. lipolytica* (Napora et al., 2013)*;* plasmid is derived from pYTK001 and contains overhangs to part 2 and part 4 Golden Gate plasmids. | this study |
| pGG3.4 (*SOR2)* | Golden Gate part 3 plasmid containing the ORF of the endogenous *SOR2;* plasmid is derived from pYTK001 and contains overhangs to part 2 and part 4 Golden Gate plasmids. | this study |
| pGG3.6 (*AnGAR1)* | Golden Gate part 3 plasmid containing the ORF of the *AnGAR1_CO* from *A. niger;* plasmid is derived from pYTK001 and contains overhangs to part 2 and part 4 Golden Gate plasmids. | this study |
| pGG3.7 *(TrGAR1)* | Golden Gate part 3 plasmid containing the ORF of the *TrGAR1_CO* from *H. jecorina;* plasmid is derived from pYTK001 and contains overhangs to part 2 and part 4 Golden Gate plasmids. | this study |
| pGG3.9 *(AnGATA)* | Golden Gate part 3 plasmid containing the ORF of the *AnGATA* from *A. niger;* plasmid is derived from pYTK001 and contains overhangs to part 2 and part 4 Golden Gate plasmids. | this study |
| pGG3.18 *(AnGAAA)* | Golden Gate part 3 plasmid containing the ORF of the *AnGAAA* from *A. niger* (Biz et al., 2016)*;* plasmid is derived from pYTK001 and contains overhangs to part 2 and part 4 Golden Gate plasmids. | this study |

| | | |
|---|---|---|
| pGG-L2-R3 | This plasmid codes for spacer element with overhangs to the elements of L2 and R3. | this study |
| pGG-L2-RE | This plasmid codes for spacer element with overhangs to the elements of L2 and RE. | this study |
| pRCC-K | Crispr-Cas9-plasmid to induce targeted double strand breaks. [pROX3-CAS9-tCYC1, pSNP52-gRNA-tSUP4, KanMX, 2µ, AmpR, ColE1] | Generoso et al., 2016 |
| pRCC-K _GD01 | Crispr-Cas9-plasmid, which is descendant of pRCC-K targeting the *GPD2*. The annealed pair of DNA oligomers JWP061 and JWP062 served as repair fragment for the Cas9-induced double strand break via homologous recombination. *[pROX3-CAS9-tCYC1, pSNP52-gGPD2-tSUP4, KanMX, 2µ, AmpR, ColE1]* | Prof. Boles group, Frankfurt |
| pRCC-N | Crispr-Cas9-plasmid to induce targeted double strand breaks. [pROX3-CAS9-tCYC1, pSNP52-gRNA-tSUP4, *ClonNAT*, 2µ, AmpR, ColE1] | Generoso et al., 2016 |
| pRS62N | Contains truncated *pHXT7t* promoter and *tCYC1* terminator for gene expression and 2µ-yeast origin and ClonNAT-marker for plasmid maintenance, as well as the *E. coli* elements AmpR and pBR322 origin. | Prof. Boles group, Frankfurt |
| pYTK001 | Golden Gate entry plasmid containing: CamR, ColE1, Esp3I *GFP*-drop out-cassette. This plasmid was used to expand the set of genetic elements available for Golden Gate Cloning. | Lee et al., 2015 |
| pYTK002 | Golden Gate part 1 plasmid containing: ConLS (connector), CamR, ColE1, BsaI recognition sites. | Lee et al., 2015 |
| pYTK003 | Golden Gate part 1 plasmid containing: ConL1 (connector), CamR, ColE1, BsaI recognition sites. | Lee et al., 2015 |
| pYTK004 | Golden Gate part 1 plasmid containing: ConL2 (connector), CamR, ColE1, BsaI recognition sites. | Lee et al., 2015 |
| pYTK005 | Golden Gate part 1 plasmid containing: ConL3 (connector), CamR, ColE1, BsaI recognition sites. | Lee et al., 2015 |
| pYTK008 | Golden Gate part 1 plasmid containing: ConLS' (connector), CamR, ColE1, BsaI recognition sites. | Lee et al., 2015 |
| pYTK009 | Golden Gate part 2 plasmid containing: *pTDH3,* CamR, ColE1, BsaI and Esp3I recognition sites. | Lee et al., 2015 |
| pYTK010 | Golden Gate part 2 plasmid containing: *pCCW12,* CamR, ColE1, BsaI and Esp3I recognition sites. | Lee et al., 2015 |
| pYTK011 | Golden Gate part 2 plasmid containing: *pPGK1,* CamR, ColE1, BsaI and Esp3I recognition sites. | Lee et al., 2015 |
| pYTK013 | Golden Gate part 2 plasmid containing: *pTEF1,* CamR, ColE1, BsaI and Esp3I recognition sites. | Lee et al., 2015 |
| pYTK014 | Golden Gate part 2 plasmid containing: *pTEF2,* CamR, ColE1, BsaI and Esp3I recognition sites. | Lee et al., 2015 |
| pYTK021 | Golden Gate part 2 plasmid containing: *pRNR1,* CamR, ColE1, BsaI and Esp3I recognition sites. | Lee et al., 2015 |

| | | |
|---|---|---|
| pYTK038 | Golden Gate part 3a plasmid containing: *VENUS,* CamR*,* ColE1, BsaI and Esp3I recognition sites. | Lee et al., 2015 |
| pYTK047 | Golden Gate part 234r plasmid containing: *GFP*-dropout cassette, CamR*,* ColE1, BsaI recognition sites. | Lee et al., 2015 |
| pYTK051 | Golden Gate part 4 plasmid containing: *tENO1,* CamR*,* ColE1, BsaI and Esp3I recognition sites. | Lee et al., 2015 |
| pYTK052 | Golden Gate part 4 plasmid containing: *tSSA1,* CamR*,* ColE1, BsaI and Esp3I recognition sites. | Lee et al., 2015 |
| pYTK053 | Golden Gate part 4 plasmid containing: *tADH1,* CamR*,* ColE1, BsaI and Esp3I recognition sites. | Lee et al., 2015 |
| pYTK054 | Golden Gate part 4 plasmid containing: *tPGK1,* CamR*,* ColE1, BsaI and Esp3I recognition sites. | Lee et al., 2015 |
| pYTK056 | Golden Gate part 4 plasmid containing: *tTDH1,* CamR*,* ColE1, BsaI and Esp3I recognition sites. | Lee et al., 2015 |
| pYTK067 | Golden Gate part 5 plasmid containing: ConR1 (connector), CamR, ColE1, BsaI recognition sites. | Lee et al., 2015 |
| pYTK068 | Golden Gate part 5 plasmid containing: ConR2 (connector), CamR, ColE1, BsaI recognition sites. | Lee et al., 2015 |
| pYTK069 | Golden Gate part 5 plasmid containing: ConR3 (connector), CamR, ColE1, BsaI recognition sites. | Lee et al., 2015 |
| pYTK072 | Golden Gate part 5 plasmid containing: ConRE (connector), CamR, ColE1, BsaI recognition sites. | Lee et al., 2015 |
| pYTK073 | Golden Gate part 5 plasmid containing: ConRE' (connector), CamR, ColE1, BsaI recognition sites. | Lee et al., 2015 |
| pYTK074 | Golden Gate part 6 plasmid containing: *pURA3-URA3-tURA3,* CamR, ColE1, BsaI recognition sites. | Lee et al., 2015 |
| pYTK075 | Golden Gate part 6 plasmid containing: *pLEU2-LEU2-tLEU2*, CamR, ColE1, BsaI recognition sites. | Lee et al., 2015 |
| pYTK077 | Golden Gate part 6 plasmid containing: KanMX *(pAgTEF1, tAgTEF)*, CamR, ColE1, BsaI recognition sites. | Lee et al., 2015 |
| pYTK078 | Golden Gate part 6 plasmid containing: *ClonNAT (pAgTEF1, tAgTEF)*, CamR, ColE1, BsaI recognition sites. | Lee et al., 2015 |
| pYTK082 | Golden Gate part 7 plasmid containing: 2µ element, CamR, ColE1, BsaI recognition sites. | Lee et al., 2015 |
| pYTK083 | Golden Gate part 8 plasmid containing: AmpR, CamR, ColE1, BsaI recognition sites. | Lee et al., 2015 |
| pYTK084 | Golden Gate part 8 plasmid containing: KanR, CamR, ColE1, BsaI recognition sites. | Lee et al., 2015 |
| pYTK086 | Golden Gate part 7 plasmid containing: *URA3* 3' Homology region, CamR, ColE1, BsaI recognition sites. | Lee et al., 2015 |
| pYTK087 | Golden Gate part 7 plasmid containing: *LEU2* 3' Homology region, CamR, ColE1, BsaI recognition sites. | Lee et al., 2015 |
| pYTK090 | Golden Gate part 8a plasmid containing: KanR, CamR, ColE1, BsaI recognition sites. | Lee et al., 2015 |
| pYTK092 | Golden Gate part 8b plasmid containing: *URA3* 5' Homology region, CamR, ColE1, BsaI recognition sites. | Lee et al., 2015 |

| | | |
|---|---|---|
| pYTK093 | Golden Gate part 8b plasmid containing: *LEU2* 5' Homology region, CamR, ColE1, BsaI recognition sites. | Lee et al., 2015 |
| pYTK095 | Golden Gate assembly vector for subcloning containing: AmpR, ColE1, Esp3I-restriction sites. | Lee et al., 2015 |
| SiHV005 | Golden Gate backbone vector containing Esp3I- and BsaI-restriction sites, the yeast elements *pURA3-URA3-tURA3* and 2µ, as well as the *E. coli* elements KanR and ColE1.<br><br>*[ConLS'-GFP-dropout-ConRE'-URA3-2µ-KanR-ColE1]* | this study |
| SiHV009 | Golden Gate backbone vector containing Esp3I- and BsaI-restriction sites, the yeast elements ClonNAT and 2µ, as well as the *E. coli* elements KanR and ColE1. | this study |
| SiHV015 | Golden Gate cassette-plasmid, which was assembled from the Golden Gate part plasmids pYTK002, pYTK010, pYTK054, pYTK067, pYTK095 and pGG3.9 via BsaI-digest.<br><br>*[ConLS-pCCW12-AnGATA_CO-tPGK1-ConR1-AmpR-ColE1]* | this study |
| SiHV016 | Golden Gate cassette-plasmid, which was assembled from the Golden Gate part plasmids pYTK003, pYTK011, pYTK051, pYTK068, pYTK095 and pGG3.6 via BsaI-digest.<br><br>*[ConL1-pPGK1-AnGAR1_CO-tENO1-ConR2-AmpR-ColE1]* | this study |
| SiHV017 | Golden Gate cassette-plasmid, which was assembled from the Golden Gate part plasmids pYTK003, pYTK011, pYTK051, pYTK068, pYTK095 and pGG3.7 via BsaI-digest.<br><br>*[ConL1-pPGK1-TrGAR1_CO-tENO1-ConR2-AmpR-ColE1]* | this study |
| SiHV018 | Golden Gate cassette-plasmid, which was assembled from the Golden Gate part plasmids pYTK004, pYTK009, pYTK052, pYTK069, pYTK095 and pGG3.2 via BsaI-digest.<br><br>*[ConL2-pTDH3-HXT13-tSSA1-ConR3-AmpR-ColE1]* | this study |
| SiHV019 | Golden Gate cassette-plasmid, which was assembled from the Golden Gate part plasmids pYTK005, pYTK014, pYTK053, pYTK072, pYTK095 and pGG3.3 via BsaI-digest.<br><br>*[ConL3-pTEF2-YlSDR-tADH1-ConRE-AmpR-ColE1]* | this study |
| SiHV020 | Golden Gate cassette-plasmid, which was assembled from the Golden Gate part plasmids pYTK005, pYTK014, pYTK053, pYTK072, pYTK095 and pGG3.4 via BsaI-digest.<br><br>*[ConL3-pTEF2-SOR2-tADH1-ConRE-AmpR-ColE1]* | this study |
| SiHV033 | Golden Gate backbone vector containing Esp3I- and BsaI-restriction sites, the yeast elements for integration into the *URA3*-locus and a KanMX-cassette, as well as the *E. coli* elements KanR and ColE1.<br><br>*[ConLS'-GFP-dropout-ConRE'-KanMX-URA3 3'Hom-KanR-ColE1-URA3 5'Hom]* | this study |
| SiHV034 | pGG3.7 descendant carrying the ORF version *TrGAR1 [K254M*], product of site directed mutagenesis using the primer pair SiHP046 and SiHP047, constructed via Gibson isothermal assembly. | this study |

| | | |
|---|---|---|
| SiHV035 | pGG3.7 descendant carrying the ORF version *TrGAR1 [R260L]*, product of site directed mutagenesis using the primer pair SiHP048 and SiHP049, constructed via Gibson isothermal assembly. | this study |
| SiHV036 | pGG3.7 descendant carrying the ORF version *TrGAR1 [K254M, R260L]*, product of site directed mutagenesis using the primer pair SiHP048 and SiHP050, constructed via Gibson isothermal assembly. | this study |
| SiHV037 | pGG3.6 descendant carrying the ORF version *AnGAR1 [K261M]*, product of site directed mutagenesis using the primer pair SiHP051 and SiHP052, constructed via Gibson isothermal assembly. | this study |
| SiHV038 | pGG3.6 descendant carrying the ORF version *AnGAR1 [R267L]*, product of site directed mutagenesis using the primer pair SiHP053 and SiHP054, constructed via Gibson isothermal assembly. | this study |
| SiHV039 | pGG3.6 descendant carrying the ORF version *AnGAR1 [K261M, R267L]*, product of site directed mutagenesis using the primer pair SiHP053 and SiHP055, constructed via Gibson isothermal assembly. | this study |
| SiHV040 | Golden Gate expression plasmid for genome integration into the *URA3-locus* which was assembled from the Golden Gate part plasmids SiHV015, SiHV016, SiHV018, SiHV019, SiHV033 via Esp3I-digest.<br><br>[URA3 5'-Hom-pCCW12-*AnGATA_CO-tPGK1*-pPGK1-*AnGAR1_CO-tENO1*-pTDH3-*HXT13-tSSA1*-pTEF2-*YlSDR-tADH1*-KanMX-URA3 3'-Hom] | this study |
| SiHV041 | Golden Gate expression plasmid for genome integration into the *URA3-locus,* which was assembled from the Golden Gate part plasmids SiHV015, SiHV017, SiHV018, SiHV019, SiHV033 via Esp3I-digest.<br><br>*[URA3 5'-Hom-pCCW12-AnGATA_CO-tPGK1-pPGK1-TrGAR1_CO-tENO1-pTDH3-HXT13-tSSA1-pTEF2-YlSDR-tADH1-KanMX-URA3 3'-Hom]* | this study |
| SiHV042 | Golden Gate expression plasmid for genome integration into the *URA3-locus,* which was assembled from the Golden Gate part plasmids SiHV015, SiHV016, SiHV018, SiHV020, SiHV033 via Esp3I-digest.<br><br>*[URA3 5'-Hom-pCCW12-AnGATA_CO-tPGK1-pPGK1-AnGAR1_CO-tENO1-pTDH3-HXT13-tSSA1-pTEF2-SOR2-tADH1-KanMX-URA3 3'-Hom]* | this study |
| SiHV043 | Golden Gate expression plasmid for genome integration into the *URA3-locus,* which was assembled from the Golden Gate part plasmids SiHV015, SiHV017, SiHV018, SiHV020, SiHV033 via Esp3I-digest.<br><br>*[URA3 5'-Hom-pCCW12-AnGATA_CO-tPGK1-pPGK1-TrGAR1_CO-tENO1-pTDH3-HXT13-tSSA1-pTEF2-SOR2-tADH1-KanMX-URA3 3'-Hom]* | this study |

| | | |
|---|---|---|
| SiHV046 | Golden Gate expression plasmid for genome integration into the *URA3-locus,* which was assembled from the Golden Gate part plasmids SiHV023, SiHV018, SiHV019, SiHV033 via Esp3I-digest.<br><br>*[URA3 5'-Hom-pCCW12-AnGATA_CO-tPGK1-pTDH3-HXT13-tSSA1-pTEF2-YlSDR-tADH1-KanMX-URA3 3'-Hom]* | this study |
| SiHV047 | Golden Gate expression plasmid for genome integration into the *URA3-locus,* which was assembled from the Golden Gate part plasmids SiHV023, SiHV018, SiHV020, SiHV033 via Esp3I-digest.<br><br>*[URA3 5'-Hom-pCCW12-AnGATA_CO-tPGK1-pTDH3-HXT13-tSSA1-pTEF2-SOR2-tADH1-KanMX-URA3 3'-Hom]* | this study |
| SiHV053 | Golden Gate cassette plasmid, which was assembled from the Golden Gate part plasmids pYTK002, pYTK011, pYTK051, pYTK072, pYTK095 and pGG3.18 via BsaI-digest.<br><br>*[ConLS-pPGK1-AnGAAA_CO-tENO1-ConRE-AmpR-ColE1]* | this study |
| SiHV054 | Golden Gate cassette plasmid, which was assembled from the Golden Gate part plasmids pYTK002, pYTK011, pYTK051, pYTK072, pYTK095 and SiHV034 via BsaI-digest.<br><br>*[ConLS-pPGK1-TrGAR1 [K254M]_CO-tENO1-ConRE-AmpR-ColE1]* | this study |
| SiHV055 | Golden Gate cassette plasmid, which was assembled from the Golden Gate part plasmids pYTK002, pYTK011, pYTK051, pYTK072, pYTK095 and SiHV035 via BsaI-digest.<br><br>*[ConLS-pPGK1-TrGAR1 [R260L]_CO-tENO1-ConRE-AmpR-ColE1]* | this study |
| SiHV056 | Golden Gate cassette plasmid, which was assembled from the Golden Gate part plasmids pYTK002, pYTK011, pYTK051, pYTK072, pYTK095 and SiHV036 via BsaI-digest.<br><br>*[ConLS-pPGK1-TrGAR1 [K254M, R260L]_CO-tENO1-ConRE-AmpR-ColE1]* | this study |
| SiHV057 | Golden Gate expression plasmid, which was assembled from the Golden Gate part plasmids SiHV005 and SiHV053 via BsaI-digest.<br><br>*[pPGK1-AnGAAA_CO-tENO1, URA3, 2µ]* | this study |
| SiHV058 | Golden Gate expression plasmid, which was assembled from the Golden Gate part plasmids SiHV005 and SiHV054 via BsaI-digest.<br><br>*[pPGK1-TrGAR1[K254M]_CO-tENO1, URA3, 2µ]* | this study |
| SiHV059 | Golden Gate expression plasmid, which was assembled from the Golden Gate part plasmids SiHV005 and SiHV055 via BsaI-digest.<br><br>*[pPGK1-TrGAR1[R260L]_CO-tENO1, URA3, 2µ]* | this study |
| SiHV060 | Golden Gate expression plasmid, which was assembled from the Golden Gate part plasmids SiHV005 and SiHV056 via BsaI-digest.<br><br>*[pPGK1-TrGAR1[K254M, R260L]_CO-tENO1, URA3, 2µ]* | this study |

| | | |
|---|---|---|
| SiHV067 | Golden Gate cassette plasmid, which was assembled from the Golden Gate part plasmids pYTK002, pYTK011, pYTK051, pYTK072, pYTK095 and pGG3.7 via BsaI-digest.<br><br>*[ConLS-pPGK1-TrGAR1_CO-tENO1-ConRE-AmpR-ColE1]* | this study |
| SiHV074 | Golden Gate expression plasmid, which was assembled from the Golden Gate part plasmids SiHV005 and SiHV067 via BsaI-digest.<br><br>*[pPGK1-TrGAR1_CO-tENO1, URA3, 2µ]* | this study |
| SiHV078 | Golden Gate cassette plasmid, which was assembled from the Golden Gate part plasmids pYTK002, pYTK011, pYTK051, pYTK072, pYTK095 and pGG3.6 via BsaI-digest.<br><br>*[ConLS-pPGK1-AnGAR1_CO-tENO1-ConRE-AmpR-ColE1]* | this study |
| SiHV079 | Golden Gate expression plasmid, which was assembled from the Golden Gate part plasmids SiHV005 and SiHV078 via BsaI-digest.<br><br>*[pPGK1-AnGAR1_CO-tENO1, URA3, 2µ, KanR-ColE1]* | this study |
| SiHV084 | Golden Gate cassette plasmid, which was assembled from the Golden Gate part plasmids pYTK002, pYTK021, pYTK054, pYTK067, pYTK095 and pGG3.9 via BsaI-digest.<br><br>*[ConLS-pRNR1-AnGATA_CO-tPGK1-ConR1-AmpR-ColE1]* | this study |
| SiHV085 | Golden Gate cassette plasmid, which was assembled from the Golden Gate part plasmids pYTK003, pYTK021, pYTK051, pYTK068, pYTK095 and pGG3.7 via BsaI-digest.<br><br>*[ConL1-pRNR1-TrGAR1_CO-tENO1-ConR2-AmpR-ColE1]* | this study |
| SiHV086 | Golden Gate cassette plasmid, which was assembled from the Golden Gate part plasmids pYTK004, pYTK021, pYTK052, pYTK069, pYTK095 and pGG3.2 via BsaI-digest.<br><br>*[ConL2-pRNR1-HXT13-tSSA1-ConR3-AmpR-ColE1]* | this study |
| SiHV087 | Golden Gate cassette plasmid, which was assembled from the Golden Gate part plasmids pYTK005, pYTK021, pYTK053, pYTK072, pYTK095 and pGG3.3 via BsaI-digest.<br><br>*[ConL3-pRNR1-YlSDR-tADH1-ConRE-AmpR-ColE1]* | this study |
| SiHV090 | Golden Gate expression plasmid for genome integration into the *URA3-locus,* which was assembled from the Golden Gate part plasmids SiHV017, SiHV018, SiHV019, SiHV033 and SiHV084 via Esp3I-digest.<br><br>*[URA3-5'-Hom-pRNR1-AnGATA_CO-tPGK1-pPGK1-TrGAR1_CO-tENO1-pTDH3-HXT13-tSSA1-pTEF2-YlSDR-tADH1-KanMX-URA3-3'-Hom]* | this study |

| | | |
|---|---|---|
| SiHV091 | Golden Gate expression plasmid for genome integration into the *URA3-locus,* which was assembled from the Golden Gate part plasmids SiHV015, SiHV018, SiHV019, SiHV033 and SiHV085 via Esp3I-digest.<br><br>*[URA3-5'-Hom-pCCW12-AnGATA_CO-pRNR1-TrGAR1_CO-tENO1-pTDH3-HXT13-tSSA1-pTEF2-YlSDR-tADH1-KanMX-URA3-3'-Hom]* | this study |
| SiHV092 | Golden Gate expression plasmid for genome integration into the *URA3-locus,* which was assembled from the Golden Gate part plasmids SiHV015, SiHV017, SiHV019, SiHV033 and SiHV086 via Esp3I-digest.<br><br>*[URA3-5'-Hom-pCCW12-AnGATA_CO-tPGK1-pPGK1-TrGAR1_CO-tENO1-pRNR1-HXT13-tSSA1-pTEF2-YlSDR-tADH1-KanMX-URA3-3'-Hom]* | this study |
| SiHV093 | Golden Gate expression plasmid for genome integration into the *URA3-locus*, which was assembled from the Golden Gate part plasmids SiHV015, SiHV017, SiHV018, SiHV033 and SiHV087 via Esp3I-digest.<br><br>*[URA3-5'-Hom-pCCW12-AnGATA_CO-tPGK1-pPGK1-TrGAR1_CO-tENO1-pTDH3-HXT13-tSSA1-pRNR1-YlSDR-tADH1-KanMX-URA3-3'-Hom]* | this study |
| SiHV100 | Golden Gate expression plasmid, which was assembled from the Golden Gate part plasmids pYTK002, pYTK011, pYTK051, pYTK072, pYTK074, pYTK082 and SiHV037 via BsaI-digest.<br><br>*[pPGK1-AnGAR1_CO [K261M]-tENO1, URA3, 2µ, KanR-ColE1]* | this study |
| SiHV101 | Golden Gate expression plasmid, which was assembled from the Golden Gate part plasmids pYTK002, pYTK011, pYTK051, pYTK072, pYTK074, pYTK082 and SiHV038 via BsaI-digest.<br><br>*[pPGK1-AnGAR1_CO [R267L]-tENO1, URA3, 2µ, KanR-ColE1]* | this study |
| SiHV102 | Golden Gate expression plasmid, which was assembled from the Golden Gate part plasmids pYTK002, pYTK011, pYTK051, pYTK072, pYTK074, pYTK082 and SiHV039 via BsaI-digest.<br><br>*[pPGK1-AnGAR1_CO [K261M, R267L]-tENO1, URA3, 2µ, KanR-ColE1]* | this study |
| SiHV110 | Golden Gate backbone vector containing Esp3I- and BsaI-restriction sites, the yeast elements for integration into the *LEU2*-locus and a ClonNAT-cassette, as well as the *E. coli* elements KanR and ColE1.<br><br>*[ConLS'-GFP-dropout-ConRE'-ClonNAT-LEU2 3'Hom-KanR-ColE1-LEU2 5'Hom]* | this study |
| SiHV112 | Golden Gate expression plasmid, which was assembled from the Golden Gate part plasmids pYTK013, pYTK056, pGG3.9 and SiHV005 via BsaI-digest.<br><br>*[pTEF1-AnGATA_CO-tTDH1, URA3, 2µ, KanR-ColE1]* | this study |

| | | |
|---|---|---|
| SiHV114 | Golden Gate expression plasmid, which was assembled from the Golden Gate part plasmids pYTK013, pYTK056, pGG3.6 and SiHV005 via BsaI-digest.<br><br>*[pTEF1-AnGAR1_CO-tTDH1, URA3, 2µ, KanR-ColE1]* | this study |
| SiHV117 | Golden Gate expression plasmid, which was assembled from the Golden Gate part plasmids pYTK013, pYTK056, pGG3.3 and SiHV005 via BsaI-digest.<br><br>*[pTEF1-YlSDR-tTDH1, URA3, 2µ, KanR-ColE1]* | this study |
| SiHV122 | Golden Gate expression plasmid, which was assembled from the Golden Gate part plasmids pYTK013, pYTK056, pGG3.2 and SiHV005 via BsaI-digest.<br><br>*[pTEF1-HXT13-tTDH1, URA3, 2µ, KanR-ColE1]* | this study |
| SiHV123 | Golden Gate expression plasmid for genome integration into the URA3-locus, which was assembled from the Golden Gate part plasmids SiHV015, SiHV016, SiHV018, SiHV019, SiHV033 via Esp3I-digest.<br><br>*[pCCW12-AnGATA_CO-tPGK1-pPGK1-AnGAR1_CO-tENO1-pTDH3-HXT13-tSSA1-pTEF2-YlSDR-tADH1, URA3, 2µ, KanR-ColE1]* | this study |
| SiHV132 | Golden Gate cassette plasmid, which was assembled from the Golden Gate part plasmids pYTK003, pYTK011, pYTK051, pYTK072, pYTK095 and SiHV038 via BsaI-digest.<br><br>*[ConL1-pPGK1-AnGAR1 [R267L]_CO-tENO1-ConRE-AmpR-ColE1]* | this study |
| SiHV133 | Golden Gate cassette plasmid, which was assembled from the Golden Gate part plasmids pYTK003, pYTK011, pYTK051, pYTK072, pYTK095 and SiHV039 via BsaI-digest.<br><br>*[ConL1-pPGK1-AnGAR1 [K261M, R267L]_CO-tENO1-ConRE-AmpR-ColE1]* | this study |
| SiHV136 | Golden Gate expression plasmid for genome integration into the *URA3*-locus, which was assembled from the Golden Gate part plasmids SiHV015, SiHV132, SiHV033 via Esp3I-digest.<br><br>*[URA3 5'-Hom-pCCW12-AnGATA_CO-tPGK1-pPGK1-AnGAR1 [R267L]_CO-tENO1-KanMX-URA3 3'-Hom]* | this study |
| SiHV137 | Golden Gate expression plasmid for genome integration into the *URA3*-locus, which was assembled from the Golden Gate part plasmids SiHV015, SiHV133, SiHV033 via Esp3I-digest.<br><br>*[URA3 5'-Hom-pCCW12-AnGATA_CO-tPGK1-pPGK1-AnGAR1 [K261M, R267L]_CO-tENO1-KanMX-URA3 3'-Hom]* | this study |
| SiHV150 | Golden Gate cassette plasmid, which was assembled from the Golden Gate part plasmids pYTK003, pYTK011, pYTK051, pYTK072, pYTK095 and pGG3.6 via BsaI-digest.<br><br>*[ConL1-pPGK1-AnGAR1_CO-tENO1-ConRE-AmpR-ColE1]* | this study |

| | | |
|---|---|---|
| SiHV158 | Golden Gate expression plasmid for genome integration into the *URA3*-locus, which was assembled from the Golden Gate part plasmids SiHV015, SiHV150, SiHV033 via Esp3I-digest.<br><br>*URA3 5'-Hom-pCCW12-AnGATA_CO-pPGK1-AnGAR1_CO-KanMX-URA3 3'-Hom]* | this study |
| SiHV201 | Golden Gate expression plasmid for genome integration into the *LEU2*-locus, which was assembled from the Golden Gate part plasmids pYTK009, pYTK051, pGG3.6 SiHV110 via Esp3I-digest.<br><br>*[LEU2 5'-Hom-pTDH3-AnGAR1_CO-tENO1, ClonNAT-LEU2 3'-Hom]* | this study |
| SiHV202 | Golden Gate expression plasmid for genome integration into the *LEU2*-locus, which was assembled from the Golden Gate part plasmids pYTK009, pYTK051, pGG3.2 SiHV110 via Esp3I-digest.<br><br>*[LEU2 5'-Hom-pTDH3-HXT13-tENO1, ClonNAT-LEU2 3'-Hom]* | this study |
| SiHV203 | Golden Gate expression plasmid for genome integration into the *LEU2*-locus, which was assembled from the Golden Gate part plasmids pYTK009, pYTK051, pGG3.3 SiHV110 via Esp3I-digest.<br><br>*[LEU2 5'-Hom-pTDH3-YlSDR-tENO1, ClonNAT-LEU2 3'-Hom]* | this study |
| SiHV204 | Golden Gate expression plasmid for genome integration into the *LEU2*-locus, which was assembled from the Golden Gate part plasmids pYTK009, pYTK051, pGG3.9 SiHV110 via Esp3I-digest.<br><br>*[LEU2 5'-Hom-pTDH3-AnGATA-tENO1, ClonNAT-LEU2 3'-Hom]* | this study |
| SiHV221 | Expression plasmid, which was constructed from PCR fragment generated with primers SiHP426 and SiHP427 from plasmid p426HXT7 as well as the PCR fragment generated from pGG3.6 (*AnGAR1_WT*) using primers SiHP424 and SiHP425.<br><br>*[pHXT7t-AnGAR1-tCYC1, URA3, AmpR-ColE1]* | this study |
| SiHV222 | Expression plasmid, which was constructed from PCR fragment generated with primers SiHP426 and SiHP427 from plasmid p426HXT7 as well as the PCR fragment generated from SiHV037 (*AnGAR1 [K261M]_CO*) using primers SiHP424 and SiHP425.<br><br>*[pHXT7t-AnGAR1 [K261M]_CO-tCYC1, URA3, AmpR-ColE1]* | this study |
| SiHV223 | Expression plasmid, which was constructed from PCR fragment generated with primers SiHP426 and SiHP427 from plasmid p426HXT7 as well as the PCR fragment generated from SiHV039 (*AnGAR1 [K261M, R267L]_CO*) using primers SiHP424 and SiHP425.<br><br>*[pHXT7t-AnGAR1 [K261M, R267L]_CO-tCYC1, URA3, AmplE1]* | this study |
| VSV111 | Crispr-Cas9-plasmid, which is descendant of pRCC-K targetting the *ALD6.* The annealed pair of DNA oligomers VSP390 and JWP092 served as repair fragment for the Cas9-induced double strand break via homologous recombination.<br><br>*[pROX3-CAS9-tCYC1, pSNP52-gALD6-tSUP4, KanMX, 2µ, AmpR, ColE1]* | Prof. Boles group, Frankfurt |

| | | |
|---|---|---|
| YEplac195 | Yeast expression plasmid containing 2µ-plasmid, *URA3*-marker, as well as *E. coli* elements AmpR and pBR322-origin. | Prof. Boles group, Frankfurt |

Plasmid verification:
Overall, assembled plasmids were verified using suitable restriction enzymes. The pattern of the DNA fragments in the agarose gel electrophoresis confirmed the correct assembly. Only if the plasmid assembly involved PCR amplifications, sequencing was necessary for plasmid verification.

### 2.2.3 DNA Oligomers

Throughout this study, DNA oligomers were used for various applications. Used DNA oligomers are listed in following table (Table 2-5).

**Table 2-5: DNA-oligomers used in this work.**

| Name | Sequence | Annealing locus, Application |
|---|---|---|
| FWP327 | ACCCGTGTACATAAGCGTGAAATCACCACAAACTGTGTGTAGCT CGTAGGAACAATTTCG | *pHXT7t+ZWF1*-overhang_fw |
| JWP005 | AAAGTTTTTTTCCCTATGCAGTGATTTTTATCTATATATTATTGTG AGTAAAAATTTCCCTAATTTTATGGCAAGCTAAT | donor DNA for *Δecm31* |
| JWP092 | TATTTTGTGTATATGACGGAAAGAAATGCAGGTTGGTACATGTA TTCTGATAGTATGTGTTTGTGTATGTTAAAGATGTT | donor DNA for *Δald6* |
| SiHP011 | CGTCTCGTCGGTCTCATATGTCTAGTGCGCAATCCTCTA | *HXT13*_fw |
| SiHP012 | CGTCTCAGGTCGGTCTCAGGATTCAATCAGAATTCTTTGAGAAC TTC | *HXT13*_rev |
| SiHP013 | CGTCTCGTCGGTCTCATATGCCTGCACCAGCAAC | *YlSDR*_fw |
| SiHP014 | CGTCTCAGGTCGGTCTCAGGATTCAAGGACAACAGTAGCCGC | *YlSDR*_rev |
| SiHP015 | CGTCTCGTCGGTCTCATATGTCTCAAAATAGTAACCCTGCAGT | *SOR2*_fw |
| SiHP016 | CGTCTCAGGTCGGTCTCAGGATTCATTCAGGACCAAAGATAATA GTCTT | *SOR2*_rev |
| SiHP046 | GGTTCTACTGTTTTGGCTATGTCTGTTACTCCAGCT | *AnGAR1*: K254M_fw |
| SiHP047 | GCTGGAGTAACAGACATAGCCAAAACAGTAGAACCTCTG | *AnGAR1*: K254M_rev |
| SiHP048 | TACTCCAGCTCTGATCAAGGCTAACTTGGAAATCGTTGACTT GGA | *AnGAR1*: R260L_fw |
| SiHP049 | AGTTAGCCTTGATCAGAGCTGGAG-TAACAGACTTAGCCAAAACAGTAGAACC | *AnGAR1*: R260L_rev |
| SiHP050 | AGTTAGCCTTGATCAGAGCTGGAGTAACAGACATAGCCAAAA CAGTAGAACCTCTGTTAACGTGG | *AnGAR1*: K254M, R260L_rev |
| SiHP051 | CTGTTTTGGCTATGTCTGTTAACCCATCTAGAATCGAAGG | *TrGAR1*: K261M_fw |
| SiHP052 | GATGGGTTAACAGACATAGCCAAAACAGAAGAACCTCTAGAGA TGTGC | *TrGAR1*: K261M_rev |
| SiHP053 | GTCTGTTAACCCATCTCTGATCGAAGGTAACAGAAACTTGGTTG CTTTGG | *TrGAR1*: R267L_fw |
| SiHP054 | CCAAGTTTCTGTTACCTTCGATCAGAGATGGGTTAACAGACTTA GCCAAAACAGAAGAAC | *TrGAR1*: R267L_rev |

| | | |
|---|---|---|
| SiHP055 | CCAAGTTTCTGTTACCTTCGATCAGAGATGGGTTAACAGACATA GCCAAAACAGAAGAACCTCTAGAGATGTGC | *TrGAR1*: K261M, R267L_rev |
| SiHP060 | GGGCGGATTACTACCGTT | integration verif. *URA3*_UP_fw |
| SiHP061 | GTAATGTTATCCATGTGGGC | integration verif. *URA3*_UP_rev |
| SiHP062 | AGAGCACTTGAATCCACTGC | integration verif. *URA3*_DN_fw |
| SiHP063 | GATTTGGTTAGATTAGATATGGTTTC | integration verif. *URA3*_DN_rev |
| SiHP175 | GAAAGAATTTAAGGGCATAAATACCTTTCA | integration verif. LEU2_UP_fw |
| SiHP176 | TACAATCCTTGCCCGTGATG | integration verif. LEU2_UP_rev |
| SiHP177 | ACTCGTATCGCATGTCGGTG | integration verif. LEU2_DN_fw |
| SiHP178 | CTTCCCTAGAACCTTCTTATGTTTTACATG | integration verif. LEU2_DN_rev |
| SiHP370 | TCAAGCTATACCAAGCATACAATCAACTATCTCATATACAGCGAA TTTCTTATGATTTATGATTTTTATTATTAAATAAG | donor DNA for *Δadh1* |
| SiHP371 | CTTATTTAATAATAAAAATCATAAATCATAAGAAATTCGCTGTAT ATGAGATAGTTGATTGTATGCTTGGTATAGCTTGA | donor DNA for *Δadh1* |
| SiHP424 | TAAGCGTGACATAACTAATTACATGAAACTCTACCGATCTTGTC TGGG | amplific. *AnGAR1 (WT/ [R267L]/ [K261M, R267L])*_rev |
| SiHP425 | CAAAAAGTTTTTTTAATTTTAATCAAAAAATGGGTTCTACTTCTA CTGTTGC | amplific. *AnGAR1 (WT/ [R267L]/ [K261M, R267L])*_fw |
| SiHP426 | GTTTCCCAGACAAGATCGGTAGAGTTTCATGTAATTAGTTATGTC ACGCTTACATT | amplific. p426HXT7 back-bone_fw |
| SiHP427 | TCAGCAACAGTAGAAGTAGAACCCATTTTTTGATTAAAATTAAA AAAACTTTTTGTTTTTGTGT | amplific. p426HXT7 back-bone_rev |
| SiHP434 | TTGACGGGGCCTTCACTCATTTTTTGATTAAAATTAAAAAAACTT TTTGT | *pHXT7t*+*ZWF1*-overhang_rev |
| SiHSeq001 | TCCTGGCCTTTTGCTGG | Sequence verification of pYTK001 insertions, ColE1 |
| SiHSeq002 | GGACTCCTGTTGATAGATC | Sequence verification of pYTK001 insertions, CamR |
| VSP390 | AACATCTTTAACATACACAAACACATACTATCAGAATACATGTAC CAACCTGCATTTCTTTCCGTCATATACACAAAATA | donor DNA for *Δald6* |
| WGP518 | ATTAGCTTGCCATAAAATTAGGGAAATTTTTACTCACAATAATAT ATAGATAAAAATCACTGCATAGGGAAAAAAACTTT | donor DNA for *Δecm31* |

## 2.3 Culture Media and Medium Supplements

### 2.3.1 General Growth Medium for *Escherichia coli*

Luria-Bertani Broth (LB-medium) is rich in nutrients and therefore was used for general cultivations of *E. coli*. For LB-plate preparation 15 g $L^{-1}$ agar was added to the medium before autoclaving.

**Table 2-6: Composition of LB-medium.**

| | | |
|---|---|---|
| Tryptone | 10 | g $L^{-1}$ |
| Yeast extract | 5 | g $L^{-1}$ |
| NaCl | 5 | g $L^{-1}$ |

pH was adjusted to 7.5 with NaOH

### 2.3.2 General Growth Medium for *Saccharomyces cerevisiae*

The nutrient-rich medium YP-medium was used for general cultivations of yeast cells. While sterile autoclaved sugars were added after autoclaving, 15 g $L^{-1}$ agar was added to the medium before autoclaving, if needed.

**Table 2-7: Composition of YP-medium.**

| | | |
|---|---|---|
| Bacto peptone | 20 | g $L^{-1}$ |
| Bacto yeast extract | 10 | g $L^{-1}$ |
| Carbon source | 20 | g $L^{-1}$ |

carbon source was added after autoclaving

### 2.3.3 SC-Minimal Medium for *Saccharomyces cerevisiae* Cultivations

The semi defined medium SC was supplemented with a carbon source and used for fermentations. This medium is suitable for the application of auxotrophic markers, as the essential compounds histidine, leucine, tryptophan and uracil are excluded from the amino acid mix and were added regarding the needed auxotrophy used. If solid plates were needed, 15 g $L^{-1}$ agar was added to the medium before autoclaving.

**Table 2-8: Composition SC-minimal medium.**

| | | |
|---|---|---|
| Yeast nitrogen base w/o amino acids and ammonium sulfate | 1.7 | g $L^{-1}$ |
| Ammonium sulfate | 5 | g $L^{-1}$ |
| 20X Amino acid mix | 50 | mL $L^{-1}$ |
| Carbon source | 10-20 | g $L^{-1}$ |

was adjusted to 6.3 with KOH
carbon source was added after autoclaving

**Table 2-9: Composition of 20X-amino acid mix without histidine, leucine, tryptophan and uracil.**

| Compound | Stock solution mg $L^{-1}$ $H_2O$ | Stock solution [mM] | Final concentration [mM] |
|---|---|---|---|
| Adenine | 224 | 1.66 | 0.083 |
| Arginine | 768 | 4.41 | 0.221 |
| Isoleucine | 1152 | 8.78 | 0.439 |
| Lysine | 1152 | 7.88 | 0.394 |
| Methionine | 768 | 5.15 | 0.258 |
| Phenylalanine | 960 | 5.81 | 0.291 |
| Threonine | 1152 | 9.67 | 0.484 |
| Tyrosine | 288 | 1.59 | 0.080 |
| Valine | 1152 | 9.83 | 0.492 |

autoclaved and stored at 4°C

**Table 2-10: Supplementing the drop out compounds histidine, leucine, tryptophan and uracil.**

| Compound | Stock solution g $L^{-1}$ $H_2O$ | Stock solution [mM] | mL used per liter of medium | Final concentration [mM] |
|---|---|---|---|---|
| Histidine | 2.4 | 15.47 | 8 | 0.124 |
| Leucine | 3.6 | 27.44 | 16 | 0.439 |
| Tryptophan | 2.4 | 11.57 | 8 | 0.093 |
| Uracil* | 1.2 | 10.71 | 16 | 0.171 |

autoclaved and stored at 4°C
*stored at room temperature

### 2.3.4 Medium Supplements

Certain cultivations required special additives. Stock solutions of these were prepared, sterile filtered and added to the medium after autoclaving. Following list provides information about concentrations and preparations (Table 2-11).

**Table 2-11: Medium additives for growth and selection of bacterial and yeast strains.**

| Medium supplement | Stock solution | Final concentration |
|---|---|---|
| Carbenicillin | 100 mg/mL in $ddH_2O$ | 100 µg $mL^{-1}$ |
| Chloramphenicol | 34 mg/mL in 70% (v/v) ethanol | 34 µg $mL^{-1}L$ |
| ClonNAT (Nourseothricin) | 100 mg/mL | 100 µg $mL^{-1}$ |
| Geneticin (G418) | 200 mg/mL | 200 µg $mL^{-1}L$ |
| Hygromycin B | 200 mg/mL | 200 µg $mL^{-1}L$ |
| Kanamycin sulfate | 50 mg/mL in $ddH_2O$ | 50 µg $mL^{-1}L$ |

## 2.4 Microbiological Techniques

### 2.4.1 Sterilization Techniques

Heat stable substances, solutions and glassware were sterilized using an autoclave running for 30-45 min at 120°C and 1 bar overpressure. Substances sensitive to heat were sterile filtered using a filter with a pore diameter of 0.2 µm.

### 2.4.2 Cultivation and Storage of Microorganisms

#### 2.4.2.1 Cultivation on Solid Medium

Both bacterial and yeast strains were either streaked out on agar plates from glycerol stock or re-streaked from single colonies. Regarding medium and supplements are described and listed in chapter 2.3. The strains were cultivated at 30 to 37°C for 1-4 days regarding the organism and growth speed. Solid cultures were stored either at 4°C for up to 4 weeks or at room temperature for a few days.

#### 2.4.2.2 Long term storage of Microorganisms

For long term storage of microbial strains, 500 µL overnight culture was thoroughly mixed with 50% (w/V) sterile glycerol and stored at -80°C.

#### 2.4.2.3 Cultivation in Liquid Medium

*E. coli* cells were grown in 5 mL LB-medium supplemented with appropriate antibiotic at 37°C and 180 $min^{-1}$ overnight. Yeast strains were cultivated in 5-50 mL medium at 30°C and 180 $min^{-1}$ up to 4 days. YP-medium or SC-medium supplemented with regarding carbon source and appropriate addition of antibiotic or essential compound (histidine, tryptophan, leucine and uracil) for auxotrophic selection was used. Media compositions and tables of supplements are listed in chapter 2.3.

#### 2.4.2.4 Measurement of Cell Density

The growth of microbes can be monitored by the optical density (OD) of the cultures. The $OD_{600}$ is measured in a photometer using light of the wavelength λ=600 nm. The measured $OD_{600}$ stands in linear relation with the cell density up to 0.5, samples exceeding this number were diluted accordingly.

## 2.5 Molecular Biological Techniques

### 2.5.1 Polymerase Chain Reaction for DNA-Amplification

Many methods in molecular biology especially cloning and diagnostics involve DNA-amplification. To amplify DNA the polymerase chain reaction (PCR) was performed. Since different applications bear specific requirements, different engineered DNA-polymerases were used in this work. For cloning applications, which demand precise amplification of DNA-templates, the DNA polymerases *Phusion High-Fidelity DNA Polymerase* (2.5.1.1) and *Q5 High-Fidelity DNA Polymerase* (2.5.1.2) from *New England Biolabs* were chosen. Since diagnostics rather focus on amplification speed and the correct length of fragments than the flawless sequence the DNA-polymerase *DreamTaq DNA Polymerase* (2.5.1.3) from *Thermo Fisher Scientific* was used.

#### 2.5.1.1 Phusion High-Fidelity DNA Polymerase PCR Procedure:

The *Phusion High-Fidelity DNA Polymerase* was used for DNA amplifications involved in cloning and DNA sequencing. After the run, the PCR reaction was mixed with the *Gel Loading Dye, Purple (6X)* from *New England Biolabs* and analyzed via agarose gel electrophoresis in a 1% (w/v) agarose gel.

**Table 2-12: Reaction mix for Phusion DNA polymerase.**

| Component | Stock solution | Concentration in mix | Volume used |
|---|---|---|---|
| Phusion HF buffer | 5X | 1X | 10 µL |
| dNTPs | 10 mM | 200 µM | 1 µL |
| Primer mix | 10 µM each | 0.5 µM each | 2.5 µL |
| DMSO | 100 % | 3% | 1.5 µL |
| Phusion DNA polymerase | 2000 U $mL^{-1}$ | 1 U | 0.5 µL |
| Template | - | 20 ng | variable |

volume was added up to 50 µL with $ddH_2O$

**Table 2-13: PCR conditions for standard PCR protocol using Phusion DNA polymerase.**

| Step | Temperature | Duration | Function |
|---|---|---|---|
| 1 | 98°C | 30 s | Denaturation of DNA |
| 2 | 98°C | 10 s | Denaturation of DNA |
| | 45-72°C | 20 s | Primer annealing |
| | 72°C | 30 s per kb | DNA extension |
| 3 | 72°C | 5 min | Final extension |

preheated lid of the thermocycler to 96°C, step 2 was repeated 30 times and stored at 10°C

The online tool *NEB Tm Calculator* of *New England Biolabs* was used to calculate the annealing temperature of the primer pair used. In general, primers were designed to melt at 61°C to accumulate a highly versatile set of primers which can be individually combined throughout this study.

### 2.5.1.2 Q5 High-Fidelity DNA Polymerase PCR Procedure:

The *Q5 High-Fidelity DNA Polymerase* was used for DNA amplifications involved in cloning and DNA sequencing. After the run, the PCR reaction was mixed with the *Gel Laoding Dye, Purple (6X)* from *New England Biolabs* and analyzed via agarose gel electrophoresis in a 1% agarose gel.

**Table 2-14: Reaction mix for Phusion DNA polymerase.**

| Component | Stock solution | Concentration in mix | Volume used |
|---|---|---|---|
| Q5 Reaction Buffer | 5X | 1X | 10 µL |
| dNTPs | 10 mM | 200 µM | 1 µL |
| Primer Mix | 10 µM each | 0.5 µM each | 2.5 µL |
| Q5 DNA Polymerase | 2000 U $mL^{-1}$ | 1 U | 0.5 µL |
| Template | - | 20 ng | variable |

volume was added up to 50 µL with $ddH_2O$

**Table 2-15: PCR conditions for standard PCR protocol using Phusion DNA polymerase.**

| Step | Temperature | Duration | Function |
|---|---|---|---|
| 1 | 98°C | 30 s | Denaturation of DNA |
| 2 | 98°C | 10 s | Denaturation of DNA |
| | 50-72°C | 20 s | Primer annealing |
| | 72°C | 30 s per kb | DNA extension |
| 3 | 72°C | 2 min | Final Extension |

preheated lid of the thermocycler to 96°C, step 2 was repeated 30 times and stored at 10°C

The online tool *NEB Tm Calculator* of *New England Biolabs* was used to calculate the annealing temperature of the primer pair used. In general, primers were designed to melt at 61°C to accumulate a highly versatile set of primers which could be individually combined throughout this study.

### 2.5.1.3 DreamTaq DNA Polymerase PCR Procedure:

The *DreamTaq DNA Polymerase* was used for diagnostic purposes. The readily made *10X DreamTaq Green Buffer* already contains loading dye for later analysis via agarose gel electrophoresis in a 1% agarose gel.

**Table 2-16: Reaction mix for Phusion DNA polymerase.**

| Component | Stock solution | Concentration in mix | Volume used |
|---|---|---|---|
| 10X DreamTaq green buffer | 10X | 1X | 1.25 µL |
| dNTPs | 2 mM of each | 200 µM of each | 1.25 µL |
| Primer Mix | 10 µM of each | 0.5 µM of each | 0.625 µL |
| DreamTaq DNA Polymerase | 5 U $\mu L^{-1}$ | 1.75 U | 0.35 µL |
| Template | - | variable | variable |

volume was added up to 12.5 µL with $ddH_2O$

**Table 2-17: PCR conditions for standard PCR protocol using Phusion DNA polymerase.**

| Step | Temperature | Duration | Function |
|---|---|---|---|
| 1 | 95°C | 30 s | Denaturation of DNA |
| 2 | 95°C | 10 s | Denaturation of DNA |
| | Tm-5°C | 20 s | Primer annealing |
| | 72°C | 1 min per kb | DNA extension |
| 3 | 72°C | 5 min | Final extension |

preheated lid of the thermocycler to 96°C, step 2 was repeated 35 times and stored at 10°C

The online tool *Tm Calculator* of *Thermo Fisher Scientific* was used to calculate the annealing temperature of the primer pair used.

## 2.5.2 Agarose Gel Electrophoresis for DNA-Analysis

The identity of DNA fragments can be characterized by their molecular weight; therefore, agarose gel electrophoresis was used. Due to the negative charge of its phosphate backbone, DNA fragments of different size can be separated, when exposed to an electric field.
The DNA samples were mixed with *Gel Loading Dye, Purple (6X)* from *New England Biolabs* and applied to a 1% (w/v) agarose gel in 1X TAE-buffer. The electric field is created by electrical tension of 120-150 V. For size estimation the DNA ladder *Gene Ruler 1kb Plus DNA Ladder* from *Thermo Fisher Scientific* was applied next to the DNA samples.

**Table 2-18**: **1x TAE-buffer.**

| | | |
|---|---|---|
| TRIS | 40 | mM |
| EDTA | 1 | mM |

pH was adjusted to 8 with acetic acid

### 2.5.3 Plasmid Assembly

In biotechnology, especially in metabolic engineering, enzymes of various organisms are combined to construct novel and powerful pathways. Therefore, plasmids have proven themselves to be an outstanding tool in transferring enzyme expression cassettes upon species borders, hence they are often referred as so-called vectors. Because of the importance of plasmids in biotechnology, diverse methods have been developed and some of them were used in this study. The used methods were restriction ligation cloning, Golden Gate assembly, Gibson isothermal assembly, splicing by overhang PCR and yeast homologous recombination cloning.

#### 2.5.3.1 Restriction Ligation Cloning

Restriction enzymes recognize specific DNA sequences. Dependent on the endonuclease the cleavage process often leaves DNA overhangs of different length. Compatible overhangs of two DNA fragments can be connected by a ligase. Before DNA-fragments were ligated, they were gel purified using the gel purification kit *NucleoSpin Gel and PCR clean up* from Macherey and Nagel.

**Table 2-19: Restriction digest.**

| | | |
|---|---|---|
| DNA | 500-1000 | ng |
| CutSmart buffer | 1 | µL |
| Restriction enzyme | 0,5 | µL |
| volume was added up to 10 µL and incubated at 37°C for 45 min | | |

**Table 2-20: Ligation reaction.**

| | | |
|---|---|---|
| DNA (each piece) | 100-500 | ng |
| T4 Ligase buffer | 1 | µL |
| T7 DNA ligase | 0,5 | µL |
| volume was added up to 10 µL and incubate at room temperature for 45 min or overnight | | |

#### 2.5.3.2 Golden Gate Assembly

The Golden Gate Cloning is similar to classical restriction ligation cloning, which is based on the ability of restriction enzymes, endonucleases, to cut DNA fragments at a certain sequence, the recognition site. Often, the restriction unveils specific overhangs, which can be ligated by DNA ligases. The overhangs determine the order in which fragments are ligated. Golden Gate Cloning is based on this strategy, but uses type IIS endonucleases, which cleave the DNA outside of their asymmetric recognition site. Due to this, the cleavage site becomes independent of the recognition site, so that arbitrarily designed overhangs are unveiled by an enzyme. Once ligated, the fragments lose the recognition site of the endonuclease and such cannot be cleaved anymore, enabling a one pot reaction approach of alternating steps of restriction and ligation.
These characteristics are exploited by the highly characterized yeast toolkit for modular multipart assembly. The cloning was performed following the instructions described in the regarding paper of (Lee et al., 2015).
Deviating from the described procedure, the enzyme Esp3I was used instead of BsmBI because these enzymes are isoschizomeres, which temperature optima, however, range from 37°C to 55°C. In this study the optimized enzyme BsaI-HFv2 was used. The enzymes and the T4 ligase buffer from *New England Biolabs* were used. The plasmids used in this study were cloned using this cloning method, if not stated differently.

**Table 2-21: Golden Gate assembly mix.**

| Component | Stock Solution | Concentration in Mix | Volume used |
|---|---|---|---|
| T4 ligase buffer | 10X | 1X | 1 µL |
| Type IIS endonuc. (BsaI/Esp3I) | 10000- 20000 U $mL^{-1}$ | 5-10 U | 0.5 µL |
| T7 DNA ligase | 3000000 U $mL^{-1}$ | 1500 U | 0.5 µL |
| DNA (each piece) | variable | 50 ng | variable |

volume was added up to 10 µL with $ddH_2O$

**Table 2-22: Conditions of Golden Gate assembly.**

| Repeats | Temperature | Duration | Function |
|---|---|---|---|
| 1x | 37°C | 10 min | Initial digestion |
| 25x/15x | 37°C | 1.5 min | Digestion |
| | 16°C | 3 min | Annealing and ligation |
| 1x | 37°C | 5 min | Digestion |
| 1x | 50°C | 5 min | Digestion and ligase inactivation |
| 1x | 80°C | 10 min | Inactivation |

preheated lid of the thermocycler to 96°C, stored at 10°C

The assembly step was repeated 15 times for reactions up to 5 parts, while reactions of 6 and more parts were repeated 25 times.
In case the parts to be assembled contain additional recognition sites of BsaI or Esp3I, the assembly was performed using following Golden Gate protocol for trouble shooting. In this protocol, the digestion temperature is reduced to 34°C and the final digestion step is skipped.

**Table 2-23: Conditions of Golden Gate assembly, troubleshooting protocol.**

| Repeats | Temperature | Duration | Function |
|---|---|---|---|
| 1x | 37°C | 10 min | Initial digestion |
| 15x | 34°C | 1.5 min | Digestion |
| | 16°C | 3 min | Annealing and ligation |
| 1x | 50°C | 5 min | Ligase inactivation |
| 1x | 80°C | 10 min | Restriction enzyme inactivation |

preheated lid of the thermocycler to 96°C, stored at 10°C

### 2.5.3.3 Gibson Isothermal Assembly

*Gibson Isothermal Assembly* is a sequence independent cloning method of up to six overlapping DNA fragments. The fragments overlap by 20-25 bp. The method is based on complementary single-stranded (ss) DNA which is unveiled from double-stranded DNA through exonuclease digest. The complementary ssDNA anneals and occurring gaps are filled in by a DNA polymerase to then be ligated by a DNA ligase. This cloning method was used for directed mutagenesis approaches and to clone plasmids.

For plasmid assembly 50 ng backbone DNA (biggest fragment) was mixed with up to 5 DNA fragments in a molar ratio of up to 1:3. The DNA mixture was given to the 2X Gibson isothermal assembly master mix and added up with $ddH_2O$. The reaction mix was incubated at 50°C for 1 h and transformed into the *E. coli* strain DH10b. After selection on appropriate plates, the correct assembly was verified by suitable restriction digest and sequencing.

**Table 2-24: 5X Isothermal reaction buffer.**

| | | |
|---|---|---|
| PEG-8000 | 25 | % |
| Tris-HCl, pH 7.5 | 500 | mM |
| $MgCl_2$ | 50 | mM |
| DTT | 50 | mM |
| dNTP | 1 | mM |
| NAD | 5 | mM |
| | store at -20°C | |

**Table 2-25: 2X Gibson isothermal assembly master mix.**

| | | |
|---|---|---|
| Isothermal reaction buffer | 1 | X |
| T5 exonuclease | 10 | U $\mu L^{-1}$ |
| Taq DNA ligase | 40 | U $\mu L^{-1}$ |
| Phusion DNA polymerase | 2 | U $\mu L^{-1}$ |
| | store 5 µL aliquots at -20°C | |

### 2.5.3.4 Splicing by overlap PCR (SOE-PCR)

Especially, in *Gibson Isothermal Cloning* described in 2.5.3.3 the efficiency of the assembly decreases drastically with increasing number of DNA fragments to be assembled. To overcome this problem *Splicing by Overlap PCR* was used. This method is suitable if the fragments to be merged contain overlapping DNA sequences. To splice these fragments a PCR was run using the forward primer of the first fragment and the reverse primer of the second fragment. Throughout the PCR, the fragments 5'-ends prime the DNA synthesis on the other fragment. Successfully, fused fragments then are PCR amplified by the two primers added to the PCR reaction.

### 2.5.3.5 Yeast Homologous Recombination Cloning

Homologous recombination is the most pronounced DNA repair mechanism in yeast. This feature can be exploited in plasmid assembly or exchanging of plasmid elements. Therefore, regarding fragments with homologous overhangs of 20-40 bp were transformed into yeast following the protocol below, (chapter 2.5.10). The yeast cells were spread on selection plates. Grown colonies were inoculated in appropriate medium, the DNA was prepared and transformed into electrocompetent *E. coli* (2.5.5).

## 2.5.4 Preparation and Transformation of $CaCl_2$-Competent *Escherichia coli* Cells

Preparation:

To prepare $CaCl_2$-competent *E. coli* cells, 400 mL LB-medium were inoculated from a 5 mL overnight preculture, which was inoculated from a single colony of a DH10b plate and incubated at 37°C and 180 $rpm^{-1}$. The main culture was incubated at 30°C and 180 $rpm^{-1}$ until an $OD_{600}$ of 0.6-0.8 was reached. The cells were distributed to 50 mL tubes and cooled on ice for 10 min, then centrifuged for 10 min at 4°C and 4000 $min^{-1}$ for harvesting. The supernatant was removed and the sedimented cells were resuspended in 10 mL resuspension buffer. The resuspended cells were incubated on ice for 15 min and centrifuged for 10 min at 4°C and 4000 $min^{-1}$. After the supernatant was removed, the cells were resuspended in 1 mL, which then were aliquoted to 50-100 µL and frozen at -80°C immediately.

**Table 2-26: Resuspension buffer $CaCl_2$-competent *E. coli*-cells.**

| | | |
|---|---|---|
| $CaCl_2$ | 100 | mM |
| Glycerol | 10 | % (w/v) |

autoclaved and stored at 4°C

Transformation:
For the transformation 50-100 µL of the frozen competent cells were thawed on ice. 1-5 µL plasmid assembly mix or 20 ng of plasmid DNA were added to the cells and incubated on ice for 30 min (optional). The cell-DNA-mix was incubated at 42°C for 45 s (heat shock) and cooled in ice for the next 2 min. For recovery, the cells were mixed with 500 µL LB-medium and incubated under shaking conditions at 37°C for 30-60 min. Successful transformants were incubated at 37°C over night on selection plates supplemented with antibiotic.

### 2.5.5 Preparation and Transformation of Electro-Competent *Escherichia coli* Cells

Preparation:
To prepare electrocompetent *E. coli* cells, 5 mL preculture of LB-medium was inoculated with a single colony of *E. coli* DH10b from a plate. The preculture was incubated at 37°C and 180 $rpm^{-1}$. From the preculture a prewarmed 1L baffled shake flask containing 400 mL LB medium was inoculated and incubated at 30°C until an $OD_{600}$ of 0.6-0.7 was reached. After, the culture was transferred to precooled 50 mL-tubes, the culture was cooled in ice for 30 min. The cells were centrifuged at 4000xg and 4°C for 15 min. To wash the cells, the cells were resuspended in 25 mL ice cold $ddH_2O$ and pooled to 50 mL suspensions, which were centrifuged at 4000xg and 4°C for 15 min. The washing step was repeated until the culture was condensed in one 50 mL tube. The cell pellet was washed in 4 mL 10% (w/v) ice cold sterile glycerol and centrifuged at 4000xg and 4°C for 15 min. The cells were resuspended in 4 mL 10% (w/v) ice cold sterile glycerol aliquoted to 50 µL each and frozen at -80°C directly.

Transformation:
The purified DNA was given to the frozen cell aliquot and incubated for 10 min. The cell-DNA-mixture was transferred to electroporation cuvettes and an electric pulse of 2.5 kV applied to the *Gene Pulser* from *BioRad* (settings: electrical resistance 200 Ω, capacity 25 µF). The electroporated cells were incubated at 37°C for 1 h to recover the electrical stress and to express the genetic marker.

### 2.5.6 Preparation of Plasmid DNA from *Escherichia coli* Cells

The *GeneJET Plasmid Miniprep Kit* from *Thermo Scientific* was used to isolate plasmidic DNA from *E. coli* cells. The procedure was performed according to the protocol supplied with the kit.

### 2.5.7 Preparation of Genomic DNA from *Saccharomyces cerevisiae* Cells

For DNA-extraction a 5 mL culture was inoculated in appropriate medium and grown over night at 30°C and 180 rpm. The grown culture was centrifuged at 3000xg for 2 min. After discarding the supernatant, the cells were resuspended in 1 mL sterile $ddH_2O$ in a 2 mL test tube and centrifuged again. The supernatant was discarded and the sedimented cells were resuspended in 400 µL buffer 1. To the resuspended cells, 400 µL of buffer 2 was added and mixed. To disrupt the cells approximately two thirds of the tube was filled with glass beads (diameter 0.45 mm) and shaken in the *Vibrax VXR basic* at maximal speed for 8 min at 4°C. After brief centrifugation for 30 s at room temperature, 650 µL of the supernatant was transferred into a fresh 1.5 mL test tube. 325 µL or

half the transferred volume of cold buffer 3 was added and gently mixed. A precipitate forms after 10 min incubation on ice and is sedimented by centrifugation for 15 min at max speed and 4°C. 700 µL of the supernatant were mixed with the same amount of isopropanol (room temperature) and thoroughly mixed, then incubated for 10 min at room temperature. The precipitated DNA was centrifuged at max speed for 15 min. After discarding the supernatant, the sediment was washed with 500 µL cold (-20°C) 70% (v/v, analytical grade) ethanol by thorough mixing and centrifugation for 5 min at maximal speed and 4°C. The wash step was repeated. Remaining supernatant was discarded completely and the pellet was dried for 15-30 min at room temperature until the ethanol has evaporated. For full dissolution of the prepared DNA 30 µL $ddH_2O$ were added and incubated for 30 min at room temperature.

**Table 2-27: Composition of buffer 1.**

| | | |
|---|---|---|
| EDTA (Titriplex III) | 10 | mM |
| Tris-HCl, pH 8 | 25 | mM |
| RNase A* | 100 | µg $mL^{-1}$ |

autoclaved and stored at 4°C
*added after autoclaving

**Table 2-28: Composition of buffer 2.**

| | | |
|---|---|---|
| NaOH | 0.2 | M |
| SDS | 1 | % (w/v) |

stored at room temperature

**Table 2-29: Composition of buffer 3.**

| | | |
|---|---|---|
| Potassium acetate | 3 | M |

pH adjusted to 5.5 and stored at 4°C

### 2.5.8 Quick Preparation of Genomic DNA from *Saccharomyces cerevisiae* Cells for PCR-Based Applications

For DNA-extraction, 100 µL yeast culture ($OD_{600}$ ≥ 0.4) were mixed with 100 µL of the extraction solution consisting of 200 mM lithium acetate and 1% SDS (w/V). Also, a suspension of yeast colonies scraped of a plate can be used. The extraction mix was thoroughly mixed and incubated for more than 5 min at 70°C or more than 10 min at room temperature. To precipitate the DNA 300 µL 96% (V/V) ethanol was added, thoroughly mixed and centrifuged at 15000 g for 3 min. The supernatant was removed and 500 µL 70% (V/V) ethanol was added. The mixture was centrifuged at 15000 g for 3 min and the supernatant was discarded. The sediment was suspended in 100 µL $ddH_2O$ and centrifuged at 15000 g for 1 min, to transfer the DNA-containing supernatant into a new reaction tube. For general use, 1 µL was used for a 25 µL PCR (2.5.1). This protocol was developed by Lõoke et al., 2011.

### 2.5.9 DNA Sequencing

Whenever DNA sequencing was necessary samples were sequenced using the service of the company Microsynth Seqlab, which uses the Sanger chain-termination method. In 15 µL total volume, 500-800 ng DNA were mixed with 2 µM primers.

## 2.5.10 Yeast Cell Transformation

For general yeast transformation, an overnight preculture was started from a single colony in YP-medium supplemented with a suitable carbon source at 30°C and 200 $min^{-1}$. From this preculture a main culture of 50 mL was started and grown at the same conditions to an $OD_{600}$ over 0.8. Once the appropriate $OD_{600}$ was reached the cells were sedimented at 3000 g for 3 min, washed with $ddH_2O$ and centrifuged again. The yeast cells were resuspended in 1 mL $ddH_2O$ and distributed to aliquots of 5 $OD_{600}$ equivalents of cells. The aliquots were centrifuged at 5000 g for 1 min and the supernatant was discarded. For the transformation, 240 µL 50% (w/V) $PEG_{4000}$, 36 µL 1M lithium acetate, 10 µL ssDNA (salmon sperm) and 500-1000 ng DNA in 64 µL $ddH_2O$ were added to the cells and mixed thoroughly by vertically oriented oscillation in a vortex mixer. Further, a heat shock was performed at 42°C for 25-35 min. For recovery, the reaction mix was transferred to 5 mL of YP-medium supplemented with a suitable carbon source. In case of an auxotrophic selection marker the cells were incubated for 1 h, while dominant selection markers required recovery of 3 h to up to overnight. After recovery, the cells were spread on appropriate selection plates.

## 2.5.11 Enzyme Activity Assays

To measure the activity of certain NADH/NADPH-dependent enzymes, the chemical characteristic of the cofactors NADH and NADPH to absorb light of the wavelength 340 nm only in their reduced form was exploited. Therefore, the decrease or increase of the absorption at this wavelength is the measure of the enzyme activity.

Preparation of cell extracts:

Inoculated from a suitable preculture, a 25-50 mL yeast culture was grown to an $OD_{600}$ of 1-2. The cells were harvested at 3000 g for 10 min at room temperature. The cells were washed with $ddH_2O$ and sedimented. If needed the cells were stored at -80°C for up to one week.

In approximately the same volume of the sedimented cells, assay buffer and glass beads were added to the cells. Disruption of the cells was performed in the *Vibrax VXR basic* for 10 min at 4°C and maximum speed. The disrupted cells were sedimented for 5 min at 4°C and 13000 g and the supernatant was transferred to a fresh tube. The cell extract was stored on ice continuously. The protein concentration was estimated in a Bradford assay using the *ROTI-Quant* solution obtained from *Roth*. The Bradford assay was performed as described in the product instructions.

Procedure of the enzyme assay to screen **GalA-reductases**:

The enzyme assay was performed in 10 mM potassium phosphate buffer, pH 7.2 and measured at 340 nm. 100 mM of the substrate, 160 µM nicotinamide adenine dinucleotide cofactor (reduced (NADH), oxidized ($NAD^+$) or phosphorylated ($NADP^+$, NADPH)) and approximately 10 µg protein extract were used in a total volume of 200 µL. The procedure was adapted from Martens-Uzunova and Schaap, 2008.

Procedure of the enzyme assay to measure **Zwf1 and Pgi1 activity**:

The enzyme assay to measure Zwf1 activity was performed in imidazole buffer and measured at 340 nm. 0.25 mM glucose-6-phosphate, 500 µM $NADP^+$ and 10 µg protein extract were used in a total volume of 1 mL. Compared to the direction of the glycolysis, the Pgi1-activity was measured in reversed direction. Therefore, 0.25 mM fructose-6-phosphate, 500 µM $NADP^+$, 40 U glucose-6-

phosphate-dehydrogenase from *S. cerevisiae* (Merck) and 10 µg protein extract were used in a total volume of 1 mL.

**Table 2-30: Imidazole buffer.**

| | | |
|---|---|---|
| Imidazole | 50 | mM |
| $MgCl_2$ | 10 | mM |
| KCl | 100 | mM |
| EDTA | 0.1 | mM |

pH was adjusted to 7

Analysis of the enzyme assays:

As the change in absorption is non-linear, the slope of the first 45-200 s were used for further analysis. The slope $m$ was normalized to the protein concentration $c_{Protein}$ used in the reaction. Considering the dilution factors and the extinction factors $\varepsilon_{NAD(P)H}$= 6220 $mol^{-1}$ $cm^{-1}$, the maximal enzyme velocity $v_{max}$ in U follows from following formula (1):

$$v_{max} = \frac{m \cdot \varepsilon_{NAD(P)H}}{c_{Protein}} \quad (1)$$

## 2.6 Analytic Methods

### 2.6.1 Online Cell Growth Monitoring and Calculation of Growth Rate

The Cell Growth Quantifier from Aquila Biolabs was used for online Cell Growth Monitoring. The specific growth rate µ as a measure of the growth speed is defined as the mathematical derivation of the growth curve normalized by the cell density of the start (2). Here, the mathematical derivation was approximated as the change of cell density $\Delta x$ over the change of time $\Delta t$, hence formula (3) was used:

$$\mu\,(t) = \frac{dx}{dt} \cdot \frac{1}{x} \quad (2)$$

$$\mu = \frac{x_2 - x_1}{t_2 - t_1} \cdot \frac{1}{x_1} \quad (3)$$

### 2.6.2 High Performance Liquid Chromatography

To monitor the metabolism of the *S. cerevisiae* strains cultured, samples were taken and analyzed via HPLC.

The samples were prepared by centrifugation at 5000 g for 3 min, acidification with 1/9 volume 0.5 M $H_2SO_4$ and incubation at 65°C for 1.5 h. The thermal treatment favored the lactonization of GalOA to the galactono-γ-lactone, which results in a more isolated peak in the later HPLC-spectrum. The HPLC+ focused system *Dionex UltiMate 3000* from *Thermo Scientific* connected with the refractive index detector *RI-101* from *Shodex* was used for analysis. The HPLC-system was equipped with the *Coregel™ 87H3* from Concise Separation or the *NucleoGel Sugar 810 H* from *Macherey and Nagel* if samples contained sorbitol. Glucose containing samples were analyzed by equipping the *Coregel 801 FA* from Concise Separation. Suitable standards were prepared with concentrations ranging from 1 to 20 g $L^{-1}$. The separation was performed at a column temperature of 35°C and a flow rate of 0.4 mL $min^{-1}$ of 0.5 mM $H_2SO_4$. To operate the HPLC-system and to perform the analysis, the *Chromeleon* software from *Thermo Scientific* was used.

# 3 Results

## 3.1 Establishing GalA-Reduction in Yeast

In nature the pectin degradation product GalA is consumed by microbes, which degrade complex biomatter. The filamentous fungus *A. niger* is capable to secrete pectinases to degrade the pectin polymer. GalA enters the cell via the proton symporter AnGatA (Benz et al., 2014) and is reduced by the reductase AnGar1, which was described to use the cofactor NADPH prioritized over NADH (Martens-Uzunova and Schaap, 2008). Heterologous expression of respective genes could confer the ability to reduce GalA to GalOA in yeast. However, the toxicity of involved compounds is to be tested prior to any engineering approaches.

### 3.1.1 Testing the Toxicity of GalA and GalOA on the Wildtype Yeast Strain CEN.PK2-1C

Prior to the engineering approaches of transforming yeast strains into hosts for GalOA-production from GalA-reduction, involved compounds were tested towards their toxicity on the yeast cell. Unlike GalA, the compound GalOA (L-galactonate), unfortunately, is commercially not available, therefore its lactonized form, galactono-y-lactone, was used for the toxicity study. The lactonization of GalOA occurs spontaneously, which is favored by heat or in low pH medium. Given the fact that yeasts tend to strongly acidify the culture medium, it is very likely that galactono-y-lactone is formed in later fermentation phases as well.

To test potential toxicity of GalA and galactono-y-lactone on yeast cells, yeast cells were grown in unbuffered SC-glucose medium of pH 6.3 containing a series of different concentrations of the compounds. Inoculated from a suitable preculture of the strain CEN.PK2-1C in SC-glucose medium, this toxicity assay was performed in 500 µL total volume in 24-well plate format. $OD_{600}$, as a proxy of cell growth, was measured in the *CLARIOstar Plus* plate reader (BMG LABTECH). Four samples per concentration were distributed randomly on the plate to avoid the effect of uneven liquid vaporization. The growth measured after 24 h at 30°C was normalized to the growth of the yeast strain grown without substance supplementation (Figure 3-1).

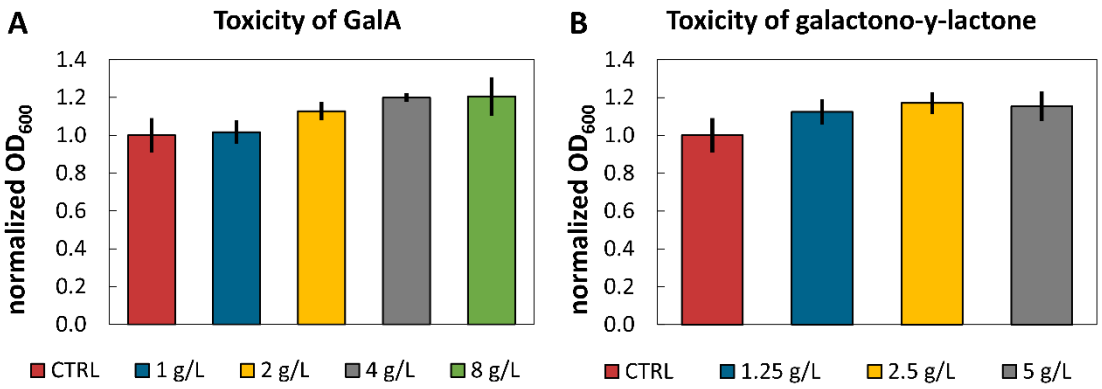


**Figure 3-1: Testing the toxicity of GalA and galactono-y-lactone on yeasts in a growth-based assay.** (**A**) The effect of the compounds GalA and (**B**) galactono-y-lactone on the growth of CEN.PK2-1C cells were tested in a growth-based assay. The $OD_{600}$ after 24h was normalized to the cell density of the control, the yeast strain cultivated without the addition of the tested compounds. The mean values and standard deviations were calculated from biological quadruplicates.

The normalized cell densities of the samples containing 1 g $L^{-1}$, 2 g $L^{-1}$, 4 g $L^{-1}$ and 8 g $L^{-1}$ GalA ranged between 1 and 1.2, thus slightly increasing $OD_{600}$ values were observed towards the higher GalA concentrations tested (Figure 3-1, A). Similarly, the results for the tested galactono-y-lactone concentrations ranging from 1.25 g $L^{-1}$ to 5 g $L^{-1}$ resulted in normalized $OD_{600}$ ratios of 1 to 1.2 compared to the control strain (Figure 3-1, B).

Overall, the growth of the strain CEN.PK2-1C was not or even positively affected by the addition of the tested compounds.

### 3.1.2 Demonstration of GalOA-Production on Glucose Illustrates the Importance of a Closed Redox-Cycle

To confer the ability of GalA-reduction to yeasts, the ORFs (open reading frames) of *AnGATA* and *AnGAR1* were cloned under the control of the constitutive yeast promoters and terminators *pCCW12* and *tPGK1*, as *pPGK1* and *tENO1*, respectively. The resulting plasmid SiHV158 was linearized and genome integrated into the *URA3*-locus of the auxotrophic yeast strain CEN.PK2-1C to construct the yeast strain SiHY057. The preculture was performed in phosphate buffered SC medium supplemented with 20 g $L^{-1}$ glucose, while the main culture was inoculated to $OD_{600}$ of 0.1 and performed in phosphate buffered SC medium supplemented with 20 g $L^{-1}$ glucose and 5 g $L^{-1}$ GalA. The cell growth was monitored photometrically ($OD_{600}$) and the metabolites were monitored via HPLC throughout the cultivation time of 5 days (Figure 3-2).

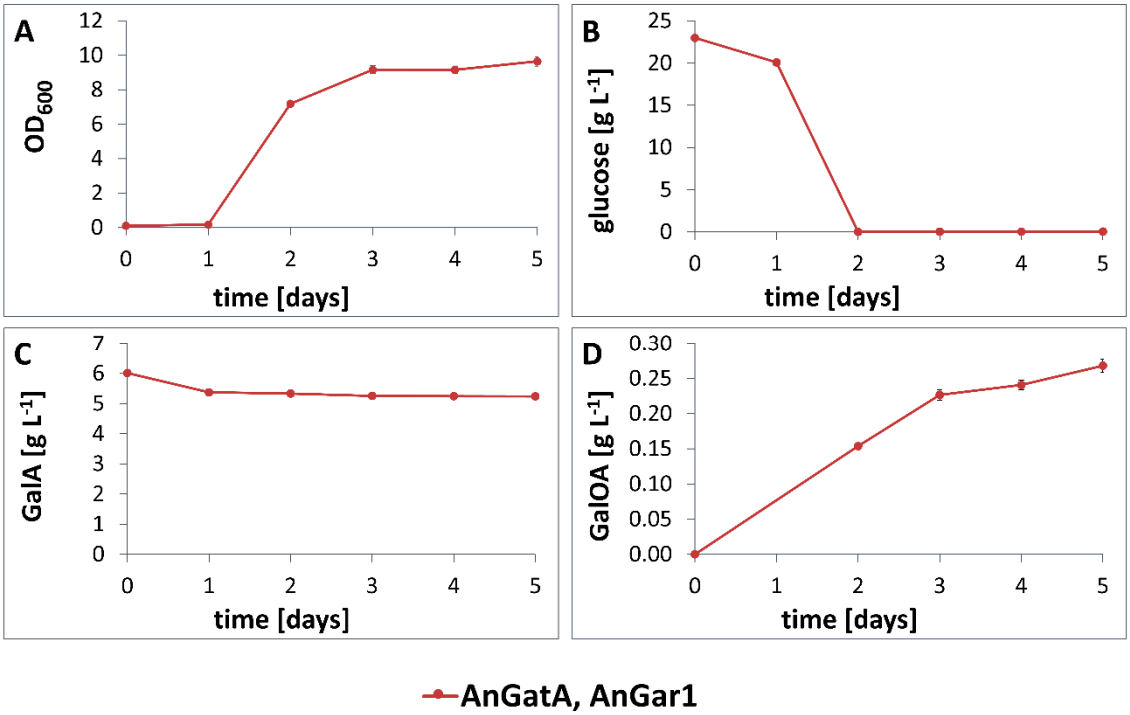


**Figure 3-2: Co-fermentation of GalA and glucose in the yeast strain SiHY057.**
The yeast strain SiHY057 expressing the heterologous genes *AnGATA* and *AnGAR1* from *A. niger* was cultured in shake flasks in phosphate buffered SC-medium supplemented with glucose as carbon source and GalA. (**A**) The cell growth was monitored via $OD_{600}$-measurement and (**B-D**) the metabolites were monitored via HPLC-analysis. Due to superposition with an unknown substance, the analytics of GalOA in the samples of day one can only hardly be measured, hence the GalOA-sample is omitted at this time point. The unknown substance degrades over time. The mean value and the standard deviation of biological triplicates are depicted, error bars may be smaller than the symbols.

Exponential cell growth started after the first day of cultivation. While strong growth was observed until day three of the cultivation, the glucose was fully consumed after the second day. Major product formation was observed within the first three days of cultivation to a concentration of 0.23 g $L^{-1}$, which slightly increased to a titer of 0.27 g $L^{-1}$ after 5 days of cultivation. Roughly 5 g $L^{-1}$ of GalA remained in the shake flasks. The GalA-conversion of only 4% illustrates the vast room for optimization.

Already Matsubara et al. in 2016 emphasized the crucial importance of a closed redox cycle, therefore, a source to replenish the redox cofactor has to be found.

### 3.1.3 Strengthening the Pentose Phosphate Pathway via Modulation of *ZWF1* and *PGI1* Expression Affects GalOA-Biotransformation Efficiency

The reductase AnGar1 was deployed to confer the biotransformation of GalA to GalOA in yeast. Since this enzyme mainly uses NADPH as cofactor (Harth et al., 2020), its regeneration is essential for the success of the process. One of the major sources of NADPH in yeasts, is the pentose phosphate pathway (PPP), where it is generated in the Zwf1 and Gnd1/2 catalyzed steps. The PPP branches off from the NADH generating glycolysis right after the formation of glucose-6-phophate, which is substrate to both the phosphoglucoisomerase Pgi1 and the glucose-6-phosphate-dehydrogenase Zwf1 (elaborated in chapter 1.4.1 and depicted in Figure 1-4). The interplay of these two enzymes was described to bear strong impact on the ratio between glycolysis and PPP and thus on the levels of NADH and NADPH in the cell. Increasing the flux through the PPP can increase the accessibility of NADPH for endogenous but also heterologous pathways in *S. cerevisiae* (Wernig et al., 2021; Yu et al., 2018; Zhao et al., 2015). The flux through the PPP can be improved by downregulation of the *PGI1* expression and the upregulation of the *ZWF1* expression, hence Yu et al., 2018 demonstrated the beneficial effect of the promoter exchange of the native *pPGI1* with the weak promoter *pCOX9*, which has a relative activity of 15% compared to the promoter of the *PGI1*. The expression of the *ZWF1* could be increased by exchanging the native promoter with the stronger promoter *pHXT7t*, as described from Wernig et al. in 2021.

To test the effect of the strengthened PPP on the GalOA-production novel strains were constructed according to Yu et al. in 2018 and Wernig et al. in 2021. The promoters of *ZWF1* and *PGI1* were replaced using the Crispr/Cas9-method in the CEN.PK2-1C wildtype strain. In the consecutive strains SiHY077 (*pHXT71-ZWF1*), SiHY078 (*pHXT71-ZWF1, pCOX9-PGI1*) and SiHY094 (*pCOX9-PGI1*) the linearized plasmid SiHV158 (*AnGATA, AnGAR1*) was genome integrated to confer the ability of GalA reduction and GalA transport. The GalOA-production of the novel strains was investigated in fermentations. The preculture was grown in SC-glucose medium and the main culture was performed in phosphate buffered SC-glucose medium supplemented with GalA. The cultivation was monitored via photometric measurements and HPLC-analysis (Figure 3-3).

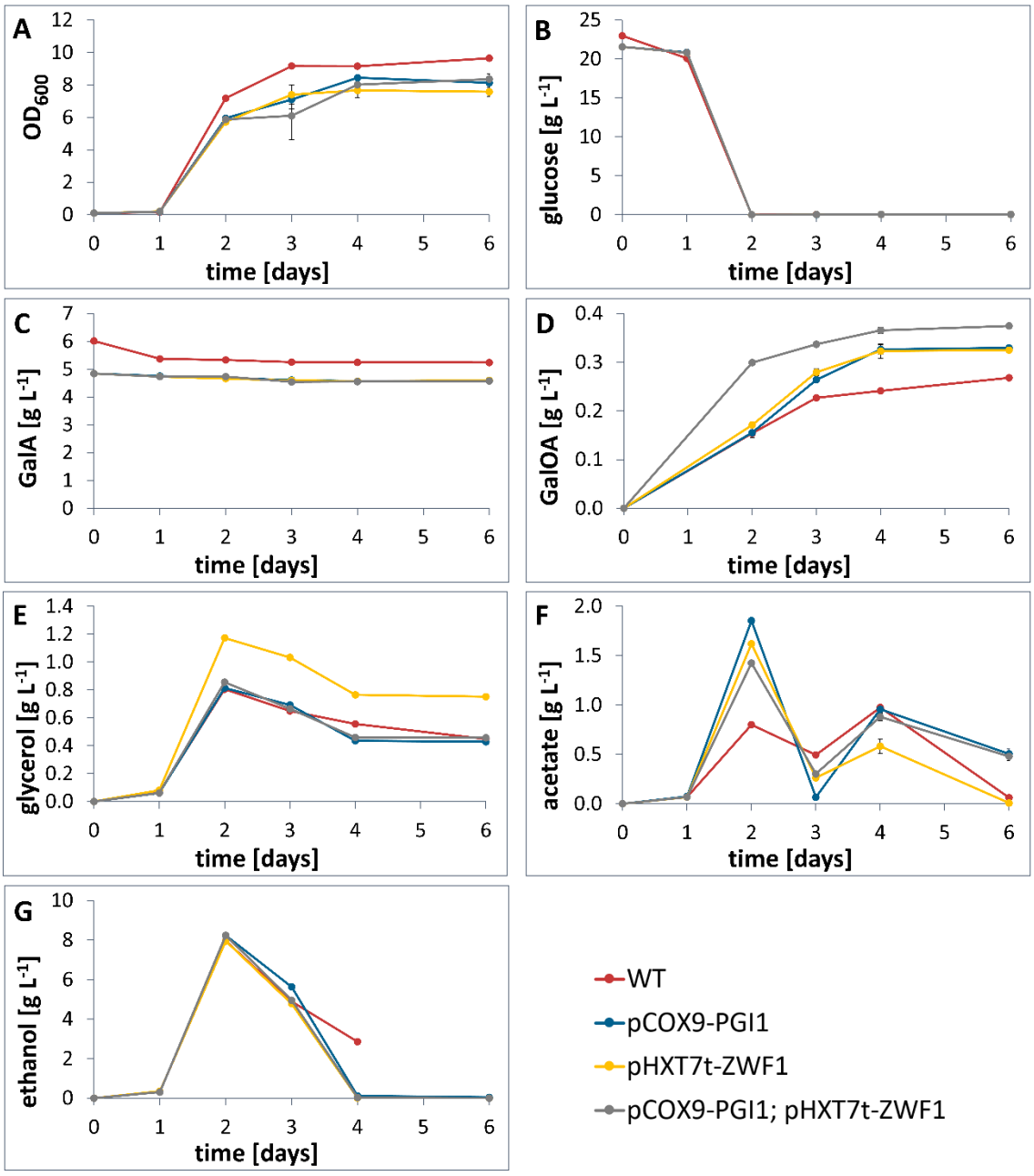


**Figure 3-3: Boosting the pentose phosphate pathway to promote the NADPH-accessibility for the GalOA-formation.**
The expression levels of the genes *PGI1* and *ZWF1* encoding for the gatekeeper enzymes of the pentose phosphate pathway were modulated by replacing respective promoters. The *PGI1* expression was decreased by replacing the native promoter with the weaker promoter *pCOX9* (Keren et al., 2013) and the *ZWF1* expression was increased by replacing the native promoter with the constitutive promoter *pHXT7t* (Hauf et al., 2000). The modifications were tested individually and in combination. (**A**) The growth was monitored photometrically ($OD_{600}$) and (**B**) glucose, (**C**) GalA, (**D**) GalOA, (**E**) glycerol, (**F**) acetate and (**G**) ethanol were measured in the HPLC. For comparative reasons the result for the wildtype strain from Figure 3-2 is shown again. Depicted are the mean values and standard deviations of biological triplicates of the respective measurements, the error bars may be smaller than the symbols.

In comparison with the performance of the strain SiHY057 (from chapter 3.1.2), the effect of the modified *PGI1* and *ZWF1* expressions were tested individually and in combination. The resulting three modified strains grew up to slightly lower final cell densities of around $OD_{600}$=8 compared to the wildtype strain, which grew up to an $OD_{600}$ of 10. However, the growth profile remained the

same as cells entered exponential growth phase between day 1 and 2 and reached stationary phase between day 3 and 4 (Figure 3-3, A). The glucose was consumed within the first two days of the cultivation in all samples (Figure 3-3, B). The effect of the modified pentose phosphate pathway flux was observed in the GalOA-production, as both modifications individually (SiHY097 *pCOX9-PGI1*; SiHY098 *pHXT7t-ZWF1*) led to increased GalOA-production of 0.33 g $L^{-1}$ and the strain with both modifications combined (SiHY099 *pCOX9-PGI1*, *pHXT7t-ZWF1*) resulted in an even higher GalOA-titer of 0.38 g $L^{-1}$ compared to the wildtype result of 0.27 g $L^{-1}$ GalOA, even though the wildtype started with a slightly higher GalA concentration. Thus, the GalOA-production increased by 40% (Figure 3-3, D). In accordance, the GalA concentration in the medium decreased only slightly, revealing an inefficient GalA-biotransformation (Figure 3-3, C). Also, the glycerol concentrations were measured throughout the cultivation, resulting in very similar glycerol accumulation of around 0.8 g $L^{-1}$ glycerol by day 2 for all strains except the strain with increased *ZWF1* expression, this strain accumulated 1.2 g $L^{-1}$ glycerol (Figure 3-3, E). The production of acetate was increased in the strains with modified pentose phosphate pathway, as these strains produced acetate ranging from 1.4 g $L^{-1}$ to 1.9 g $L^{-1}$, while only 0.8 g $L^{-1}$ acetate was measured in the culture of the wildtype strain background. In all fermentations the measured acetate dropped by day 3 to peak again on day 4 (Figure 3-3, F). This behavior is due to the diauxic shift from glucose to ethanol metabolism, which both have acetate as an intermediate. The analysis of the ethanol formation showed strong production of 8 g $L^{-1}$ by day 2 of the cultivation for all four strains. The accumulated ethanol was entirely consumed by day 4 or 5 (Figure 3-3, G).

Overall, the beneficial effect of the upregulation of the pentose phosphate pathway on a NADPH-consuming pathway like the GalA-biotransformation could be demonstrated in this experimental set up. The effect was shown in a stepwise manner, which emphasized the additivity of the individual effects of the modulated *PGI1* and *ZWF1* expression.
Strain construction, cultivation and probing of the samples were conducted by Leonie Harth (bachelor student) under supervision of the author.

## 3.2 Deploying the Highly Reduced Sugar Alcohol Sorbitol to Close the Redox Cycle

The metabolism of yeasts is highly optimized on the utilization of glucose, one of the most prominent carbon sources in nature. Glucose fluxes either through the glycolysis, which generates NADH or, to a much smaller moiety of 4% (Fiaux et al., 2003), through the pentose phosphate pathway, which generates NADPH. However, major pathways like the ethanol formation consume reducing

equivalents (NADH) in a stoichiometric manner to glucose degradation and thus constitute a major competitor on reducing equivalents for the GalA-reduction. In contrast, the sugar alcohol sorbitol, which exhibits a higher state of reduction, must be oxidized to fructose before entering the carbon metabolism of yeast. The oxidation of sorbitol to fructose is catalyzed by a sorbitol dehydrogenase and, per molecule, generates an additional reducing equivalent to the equivalents generated in the glycolysis, resulting in a surplus (Figure 3-4).

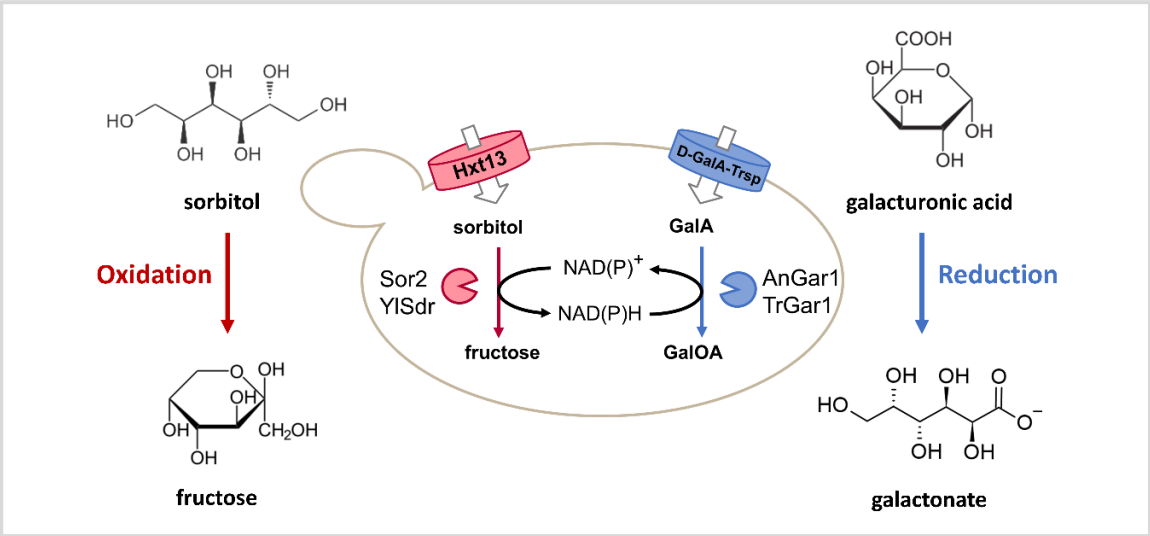


**Figure 3-4: Scheme of GalOA-production based on sorbitol as carbon source.**
The sugar alcohol sorbitol, due to its high reduced state, bears great potential to supply reducing equivalents. The reducing power from sorbitol could be conferred to GalA, resulting in a driving force for GalOA-production. Sorbitol enters the cell through the transporter Hxt13, where it is accepted by a sorbitol dehydrogenase (SDH), here the $NAD^+$-dependent Sor2 and $NADP^+$-dependent YlSdr. The SDH reaction converts sorbitol to fructose, which is funneled into glycolysis, and concomitantly generates reducing equivalents. The generated reducing equivalents fuel the GalA-reduction catalyzed by AnGar1 and TrGar1. The GalA is imported into the cell by the transporter AnGatA.

### 3.2.1 Establishing Efficient GalOA-Production Using Sorbitol as a Redox-Donor

As outlined above, sorbitol bears a potential to generate a surplus of reducing equivalents. Two sorbitol dehydrogenases were chosen, since the endogenous sorbitol dehydrogenase Sor2 (Jordan et al., 2016) generates NADH and the heterologous enzyme YlSdr from *Y. lipolytica* generates NADPH (Napora et al., 2013). Combined with the overexpression of the endogenous *HXT13*-transporter gene for sorbitol uptake (Jordan et al., 2016), the overexpression of the sorbitol dehydrogenases is sufficient to enable *S. cerevisiae* to consume sorbitol as a carbon source. In the literature, TrGar1 from *H. jecorina* (UniProtKB—Q3ZFI7, Kuorelahti et al., 2005) is described to be the most prominent GalA-reductase, for which a homolog, AnGar1 (encoded by gene An16g04770; UniProt Acc. Number A2R7U3, Hilditch, 2010), was identified in *A. niger*. From both enzymes, at least TrGar1

was described to strongly prefer NADPH over NADH. Hence, a surplus of NADPH is necessary to fuel the GalOA-production.

To establish GalOA-production based on the sorbitol metabolism, the GalA-reductases TrGar1 and AnGar1 were individually combined with the sorbitol dehydrogenases Sor2 (NADH) and YlSdr (NADPH) and the transporters AnGatA and Hxt13 for GalA and sorbitol uptake, respectively. Respective gene combinations were cloned into the plasmids SiHV040 to SiHV043 under the control of yeast regulatory elements. From these plasmids the strains SiHY001 (*AnGATA, AnGAR1, HXT13* and *YlSDR*), SiHY002 (*AnGATA, TrGAR1, HXT13* and *YlSDR*), SiHY003 (*AnGATA, AnGAR1, HXT13* and *SOR2*) and SiHY004 (*AnGATA, TrGAR1, HXT13* and *SOR2*) were constructed in the parent strain EBY.VW4000 (hxt0). The hxt0 strain was chosen since it carries deletions of all known hexose transporters and therefore its outer membrane is less likely to be over saturated with heterologously expressed transporters. That a saturated outer membrane can affect the transport capacity was recently reported by Tamayo Rojas et al., 2021. The novel constructed strains were tested in aerobic fermentations in phosphate buffered SC sorbitol medium supplemented with and without GalA. The preculture of this fermentation was performed in SC-maltose medium due to the inability of the strain to take up glucose (Figure 3-5).

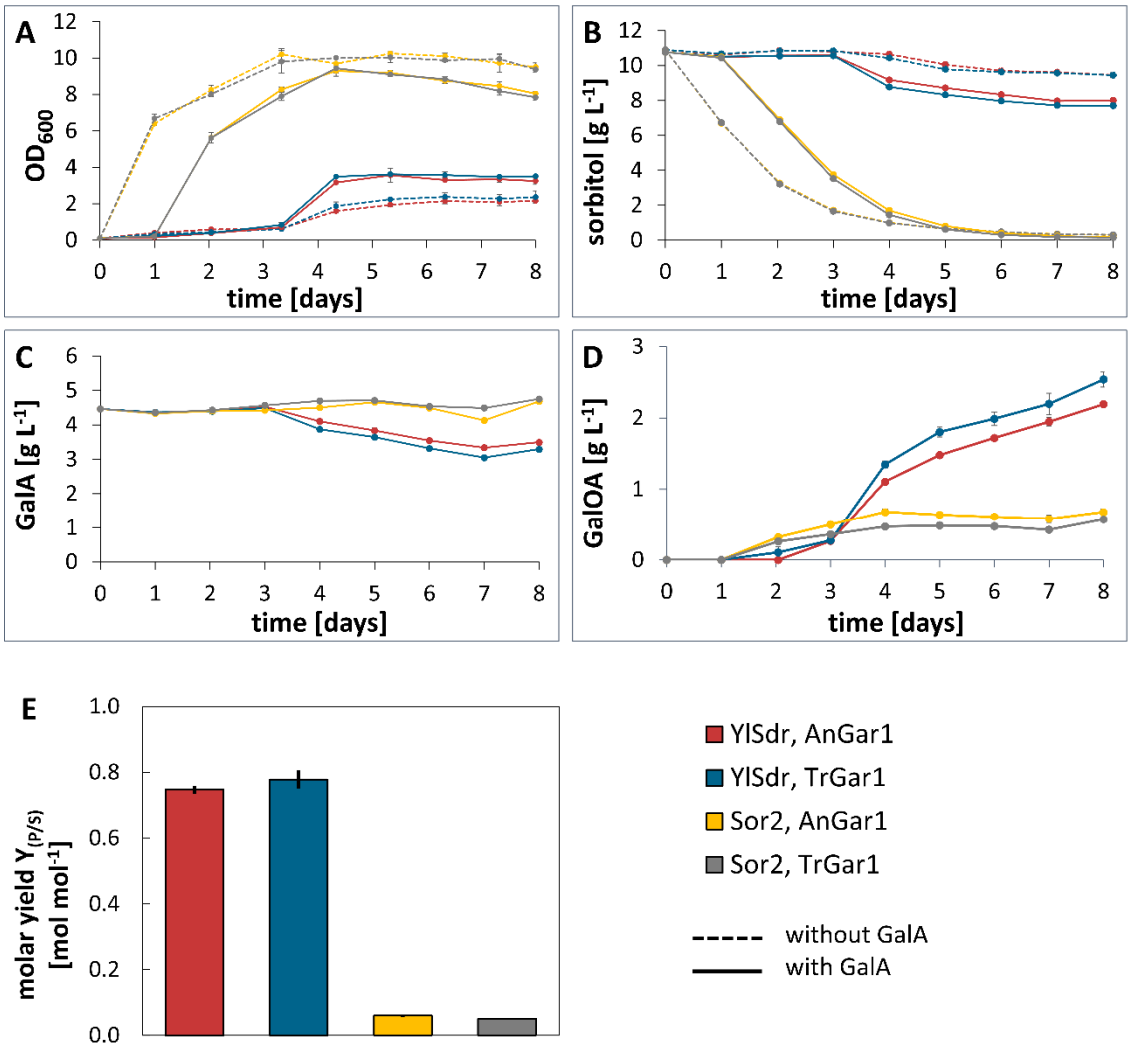


**Figure 3-5: Establishing co-cultivation of GalA and sorbitol.**
Recombinant yeast strains expressing the transporters *AnGATA* and *HXT13* from constitutive promoters with a combination of the indicated GalA-reductases, *TrGAR1* or *AnGAR1*, and the sorbitol dehydrogenases, *SOR2* (NADH) or *YlSDR* (NADPH) were cultured. (**A**) Cell growth was monitored photometrically. (**B**) Sorbitol consumption, (**C**) GalA-consumption and (**D**) GalOA-production were monitored via HPLC-analysis. (**E**) The ratio between produced GalOA per consumed sorbitol is illustrated as the molar yield. Cultures with and without GalA-supplementation are depicted in solid lines or dashed lines, respectively. The mean value and the standard deviation of biological triplicates are depicted, error bars may be smaller than the symbols.

Cell growth on sorbitol was observed in all cultures, however cell growth was affected by the addition of GalA (Figure 3-5, A). The strains expressing *SOR2* showed strong growth up to an $OD_{600}$ of approximately 10 and fast sugar consumption regardless of the expressed GalA-reductase (Figure 3-5, B). With both TrGar1 and AnGar1, the production results in GalOA-titers of approximately 0.7 g $L^{-1}$ after a process time of 4 days (Figure 3-5, D). In contrast, the strains expressing YlSdr showed weak growth, a delayed growth start and low sorbitol consumption. Furthermore, the negative effect of GalA on the growth, observed for the Sor2-strains (Figure 3-5, A, grey and yellow lines), was not reproduced in YlSdr-strains as GalA-supplemented cultures grew better (Figure 3-5, A, red and blue lines). Further difference was found in the GalOA-production, as the expression of

*YlSDR* enabled production titers of up to 2.5 g $L^{-1}$ GalOA after 8 days of cultivation, mainly independent of the employed GalA-reductases TrGar1 and AnGar1 (Figure 3-5, D). Thus, the production on sorbitol increased by a factor of 3.5 by deploying the heterologous NADPH-generating YlSdr instead of the endogenous Sor2, which generates NADH. Interestingly, major GalOA-production was observed during the exponential growth phase, which refers to a growth dependent characteristic of the production. From the sorbitol consumption and the GalOA-production of the Sor2- and YlSdr-strains, the molar yield was calculated from produced GalOA per consumed sorbitol (Figure 3-5, E). The comparison of the values showed a drastic difference from a molar yield of around 0.8 mol $mol^{-1}$ in the YlSdr-strains to 0.06 mol $mol^{-1}$ in the strains based on Sor2, representing a difference of a factor 12. These findings underpin the crucial role of suitable cofactor replenishment for an efficient biotransformation.

After the functionality of the *Y. lipolytica* enzyme YlSdr in *S. cerevisiae* was demonstrated and thus GalOA-production based on sorbitol was established, the unfavorable growth behavior of the producing strains is to be further investigated in the following chapters.

### 3.2.2 Characterization of the Sorbitol Dehydrogenases Sor2 and YlSdr in an Enzyme Assay

In previous chapter GalOA-production on sorbitol was established and concomitantly the functionality of the enzymes Sor2 and YlSdr was demonstrated (chapter 3.2.1). However, the growth and production performance behavior diverged strongly.

To obtain closer insights into the biochemistry of the sorbitol dehydrogenases Sor2 and YlSdr, their enzyme activity was measured in crude cell extracts from strains SiHY001 (*AnGATA, AnGAR1, HXT13* and *YlSDR*) and SiHY003 (*AnGATA, AnGAR1, HXT13* and *SOR2*). The total protein concentration in the crude cell extract was measured in a Bradford assay. In an enzymatic assay, the enzyme activity of sorbitol oxidation with $NAD^+$ or $NADP^+$ was measured as the change in the absorption of light of the wavelength 340 nm (Figure 3-6).

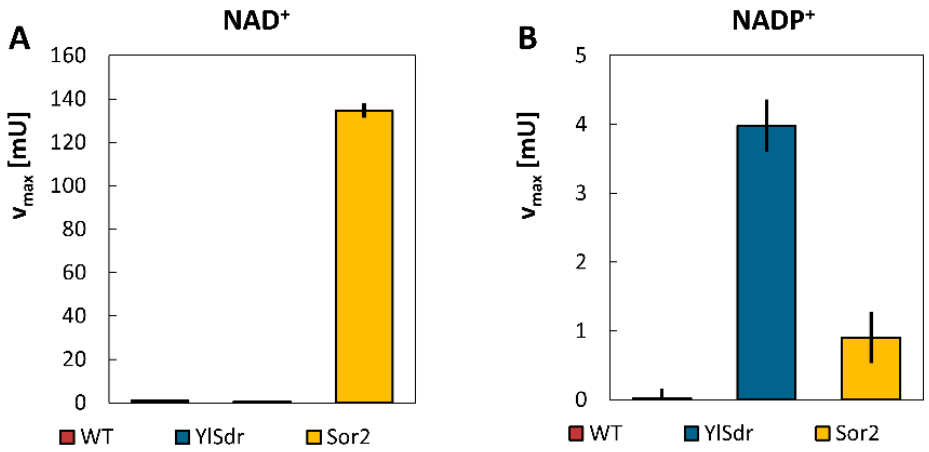


**Figure 3-6: Investigation of the employed sorbitol dehydrogenases Sor2 from *S. cerevisiae* and YlSdr from *Y. lipolytica*.**
The enzymes were expressed from genomic copies in the strain SiHY007 (*YlSDR*) and SiHY008 (*SOR2*). The background strain EBY.VW4000 was included as negative control, as it does not overexpress the sorbitol dehydrogenases. Protein extracts from disrupted cells were used to perform the enzyme assay. The enzyme activity was measured with supplementation of (**A**) $NAD^+$ and (**B**) $NADP^+$. The specific activity was calculated in milli units per mg protein, mU $mg^{-1}$. Mean values and error bars were calculated from technical triplicates.

The activity measurements confirmed the preferences of Sor2 and YlSdr for $NAD^+$ and $NADP^+$, respectively. The maximal velocity measured for the Sor2 was 134.66 mU using $NAD^+$, while YlSdr showed a maximal velocity of 3.98 mU using $NADP^+$. The activity of the endogenous enzyme Sor2 was, however, roughly 30 times higher compared to YlSdr. This difference may, at least partly explain the observed slow growth of the YlSdr expressing strains (Figure 3-6, A).
Overall, this enzyme assay demonstrates strong cofactor preference for both enzymes, however, the maximal velocities spread widely.

### 3.2.3 Investigating the Late Growth Start of the GalOA-Producing Strain on Sorbitol

In chapter 3.2.1, the production of GalOA was established on sorbitol by employing the heterologous sorbitol dehydrogenase YlSdr. However, strains expressing this enzyme showed a severe growth phenotype and a strongly delayed growth start of up to 3 days, which often points to adaptation issues during the cultivation.

To further investigate the growth defect in the fermentation based on sorbitol metabolism catalyzed by YlSdr, the carbon source in the preculture was varied. The sugars maltose, fructose and sorbitol were used. Sorbitol fluxes through fructose into the glycolysis, while the disaccharide maltose is cleaved into two molecules of glucose and therefore fluxes into glycolysis as well. Sorbitol

and fructose were used in the preculture to at least partially adapt the cells metabolism to sorbitol consumption. Maltose was used as carbon source, due to its independence to the sorbitol metabolism. Since the strains SiHY002 and SiHY004, which were used in the foregoing chapters 3.2.1 and 3.2.2, are descendants of the hxt0-strain EBY.VW4000, these were reconstructed in the analogue wildtype background CEN.PK2-1C to enable endogenous fructose transport. The resulting strains SiHY018 (*AnGATA, TrGAR1, HXT13* and *YlSDR*) and SiHY019 (*AnGATA, TrGAR1, HXT13* and *SOR2*), were grown in 20 g $L^{-1}$ maltose, fructose or sorbitol; main cultures were started in phosphate buffered SC-sorbitol medium supplemented with GalA from these precultures (Figure 3-7, A). The cell growth was continuously monitored using the Cell Growth Quantifier (Aquila Biolabs), the end point composition of the production medium was measured via HPLC (Figure 3-7).

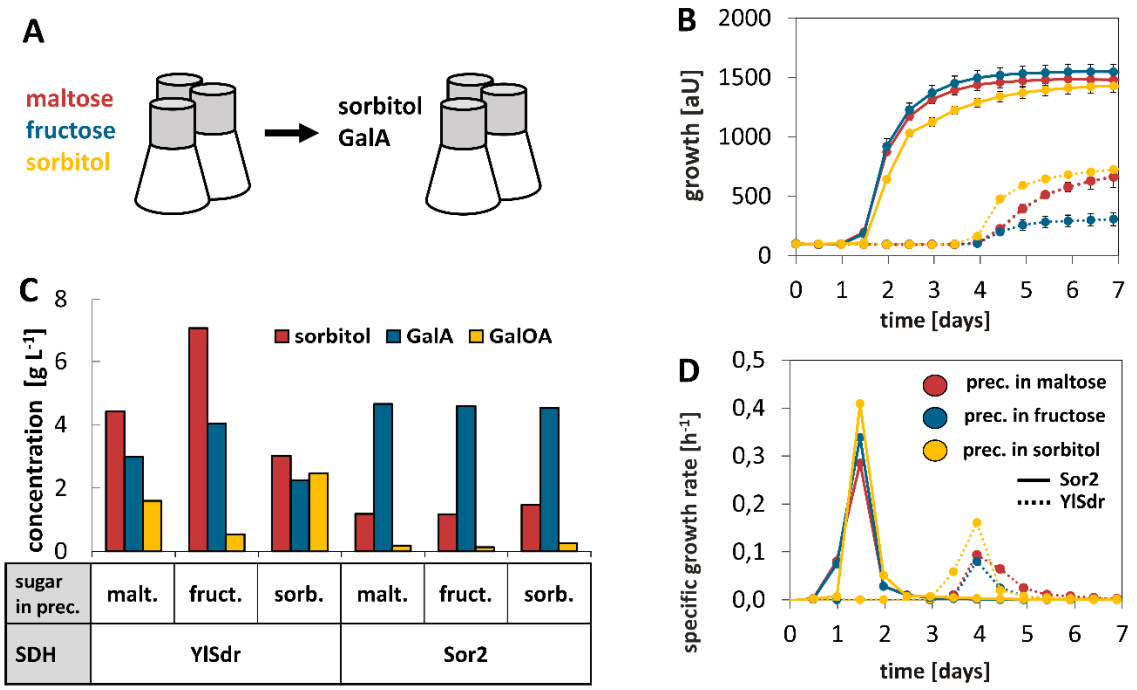


**Figure 3-7: Variation of the carbon source used in the preculture.**
The influence of the sugar used in the preculture on the growth behavior and production performance in a sorbitol-based production culture was investigated. (**A**) The sugars maltose, sorbitol and fructose were tested as carbon source in the preculture, after which the cells were transferred to sorbitol and GalA containing media. (**B**) The cell growth of biological duplicates was online monitored using the Cell Growth Quantifier (Aquila Biolabs). (**C**) The concentration of sorbitol, GalA and GalOA was measured via HPLC-analysis at the end of the cultivation after 7 days. (**D**) The growth rates of the strains expressing the sorbitol dehydrogenases (SDH), *SOR2* and *YlSDR*, were calculated for each recorded data point by the Cell Growth Quantifier software.

Independent of the preculture condition, the cultures of the strain SiHY019 expressing the *SOR2* showed strong growth and sorbitol consumption (Figure 3-7, B and C). Like the results from chapter 3.2.1, the GalOA-concentration of approximately 0.26 g $L^{-1}$ measured in the main cultures was low (Figure 3-7, C). Differently, the GalOA-production performance of strain SiHY018 expressing the *YlSDR* was substantially affected by the preculture conditions. Even though, the late growth start in

the main culture was reproduced for the strain SiHY018, the growth rates and final cell densities varied depending on the sugar used in the preculture (Figure 3-7, B). Noteworthy, the cell growth of the preculture of the strain expressing the *YlSDR* in sorbitol was very slow. The specific growth rates (Figure 3-7, D) were calculated using formula (2) from chapter 2.6.1. Generally higher growth rates were observed in the strain expressing the SOR2 than in the strain expressing the *YlSDR*. Furthermore, the main cultures started from a preculture performed in sorbitol showed highest growth rates regardless the expressed sorbitol dehydrogenase, indicating an adaptation to the carbon source.

Not only the growth behavior, but also the metabolism diverged as consequence to the variation of the carbon source in the preculture (Figure 3-7, C). At the end of the fermentation, the HPLC-analysis of the main culture started from a maltose preculture showed GalOA-production of 1.6 g $L^{-1}$ while 4.43 g $L^{-1}$ sorbitol remained in the medium. Further, the main culture started from a fructose preculture showed GalOA-production of 0.54 g $L^{-1}$ while 7.09 g $L^{-1}$ sorbitol remained in the medium. The culture of the YlSdr-strain which showed the best growth behavior, also resulted in the highest GalOA-production and sorbitol consumption, with 2.47 g $L^{-1}$ GalOA and 2.24 g $L^{-1}$ sorbitol measured in the culture at day 7.

Already in chapter 3.2.1 it was shown that growth of cells expressing *YlSDR* is hampered if no redox partner is provided. Providing GalA as redox partner for the accumulated NADPH already in the preculture might alleviate the phenotype of slow and late growth start in the main culture.

### 3.2.4 Adaptation of Strains to Sorbitol Metabolism Together with GalA Increases the GalOA-Production and Alleviates the Negative Growth Phenotype

So far, GalOA-production on sorbitol was established via heterologous expression of the *Y. lipolytica* gene *YlSDR*, whose gene product codes for a $NADP^+$-dependent sorbitol dehydrogenase. However, a severe growth phenotype was observed (chapter 3.2.1), presumably due to an open redox cycle of $NADP^+$/NADPH resulting in NADPH-accumulation. In the case of a Δ*pgi1*-strain, this phenotype was already described in literature and could be mitigated by providing a suitable partner to close the redox cycle (Boles et al., 1993).

To mitigate the growth phenotype observed in sorbitol cultivations based on *YlSDR* expression, GalA was provided in the preculture, so the strain could adapt to sorbitol metabolism and set up a functioning redox cycle already in the preculture. Therefore, the recombinant yeast strains from chapter 3.2.1, SiHY001 (*AnGATA, AnGAR1, HXT13* and *YlSDR*), SiHY002 (*AnGATA, TrGAR1, HXT13* and *YlSDR*),

SiHY003 (*AnGATA, AnGAR1, HXT13* and *SOR2*) and SiHY004 (*AnGATA, TrGAR1, HXT13* and *SOR2*) were grown for adaptation in phosphate buffered SC-sorbitol medium supplemented with GalA until the cell growth reached early stationary phase. The cell growth and the metabolism of the consecutive main culture were monitored by photometric measurement and HPLC-analysis over the time of the cultivation (Figure 3-8).

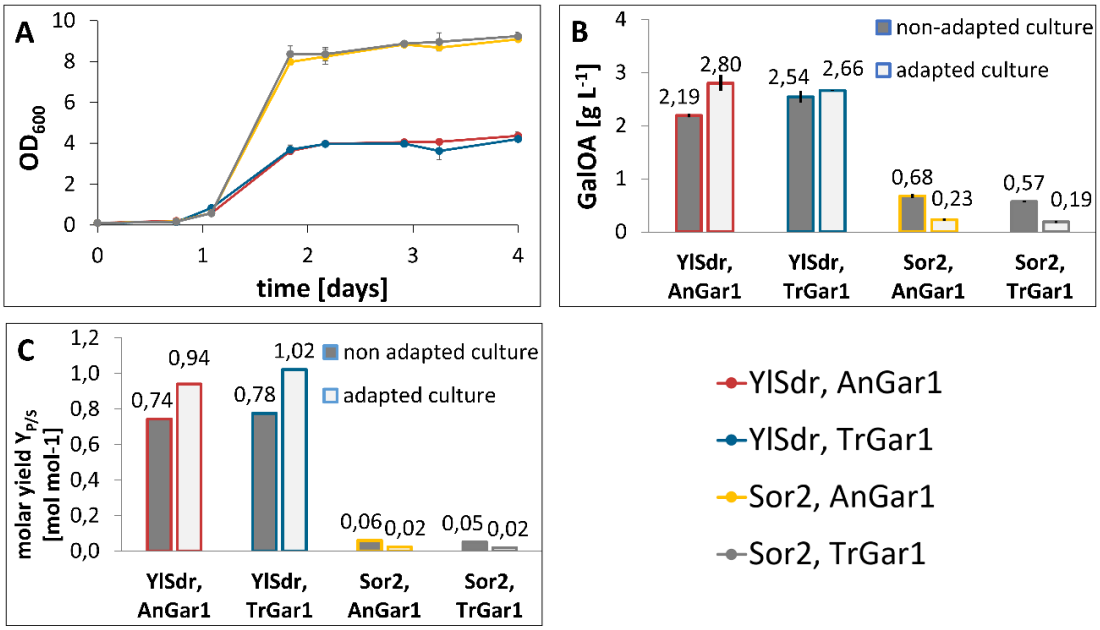


**Figure 3-8: The adaptation of yeast strains to the sorbitol metabolism supplemented with GalA mediates benefits in growth and GalOA-production.**
Recombinant yeast strains expressing the GalA-transporter *AnGATA* and the sorbitol transporter *HXT13* with a combination of the indicated GalA-reductases, *TrGAR1* or *AnGAR1,* and the sorbitol dehydrogenases, *SOR2* (NADH) or *YlSDR* (NADPH), from constitutive promoters were adapted to sorbitol metabolism supplemented with GalA. (**A**) The growth and (**B**) the GalOA-production of the consecutive main cultivation was monitored via photometric measurement and HPLC-analysis. (**C**) From the sorbitol consumption and the GalOA-production, the molar yields were calculated. For comparative reasons, the end titers of GalOA and the molar yields from chapter 3.2.1, Figure 3-5, are shown again. The mean value and the standard deviation of biological duplicates are depicted, error bars may be smaller than the symbols or bar borders.

The cell growth of the strains SiHY001 to SiHY004 was monitored after inoculation from a preculture performed under adaptive conditions. The simultaneous adaptation to sorbitol and GalA could alleviate the growth phenotype of the *YlSDR*-expressing strains (SiHY001 and SiHY002), as the growth of these yeast strains started at the same time as the stable growth enabled by constitutive *SOR2*-expression (SiHY003 and SiHY004). However, the final optical density of *YlSDR*-expressing strains was less than half of the growth conferred by *SOR2*-expression (Figure 3-8, A). Considering the GalOA-production, the effect of the modified preculture conditions behaved contrarily for the tested conditions (Figure 3-8, B). Using adapted cells not only had beneficial effect on growth, but

also boosted the GalOA-production in the *YlSDR*-expressing strains. However, this preculture conditions decreased the already low production of GalOA in the *SOR2*-expressing strains. Thus, the production of the GalA-reductases AnGar1 or TrGar1 in a *YlSDR*-expressing background strain, SiHY001 and SiHY004, resulted in final GalOA-titers of 2.8 g $L^{-1}$ and 2.66 g $L^{-1}$ after 100 h of cultivation. Here, the AnGar1 and TrGar1 converted roughly 60% of the supplemented GalA. In contrast, the same reductase only produced 0.23 g $L^{-1}$ and 0.16 g $L^{-1}$ GalOA in the *SOR2*-expressing background strains. The effect of adaptation even fostered efficient carbon source utilization in the YlSDR-expressing strains, as the molar yield $Y_{P/S}$ increased (Figure 3-8, C).
Further, investigation of the medium composition bears great potential to overcome certain metabolic limitations and to further boost the production performance.

### 3.2.5 Variation of the Sorbitol and GalA Concentration in the Production Medium

So far, a GalOA-producing strain was constructed by expressing suitable fungal GalA-reductases in combination with the expression of *YlSDR*, a NADPH generating sorbitol dehydrogenase. In the used production medium, this strain showed an extensive growth delay, which could be overcome by suitable preculture conditions. However, with GalA remaining in the cultivation broth the incomplete biotransformation to GalOA means vast room for optimization.
The enzyme activity is significantly determined by the concentration of the substrate it accepts, which, as well, applies to transporter proteins. In nature, two major groups of sugar transporters are known, the (passive) facilitators and the (active) symporters. The mechanism of facilitators is based on a conformation change, whose driving force is the gradient of the substrate itself. Differently, the sugar transport performed by symporters is driven by the gradient of a second compound, often protons. Two transporters, Hxt13 and AnGatA, were deployed in the so far constructed strains; while the former is a facilitator, the latter is a proton symporter. Especially the transport efficiency of facilitators slows down with decreasing substrate concentration in the medium. For the facilitator Hxt13 a $K_M$ of 20.4±2.4 mM was reported (Jordan et al., 2016). The concentration of 20.4 mM sorbitol equals a concentration of 3.72 g $L^{-1}$, once the medium concentration falls below this value, the transporter works under sub-saturating conditions.

To examine possible transport limitations, the effect of different GalA concentrations of 5 g $L^{-1}$ and 10 g $L^{-1}$ in combination with different sorbitol concentration of 10 g $L^{-1}$, 20 g $L^{-1}$ and 40 g $L^{-1}$ in the production medium was tested. The strain SiHY001 (*AnGATA, AnGAR1, HXT13* and *YlSDR*) was precultured in SC medium supplemented with 10 g $L^{-1}$ sorbitol and 5 g $L^{-1}$ GalA. Several production

cultures were started with different combinations of GalA and sorbitol concentrations. Cell growth was monitored photometrically and metabolite analysis was performed via HPLC (Figure 3-9).

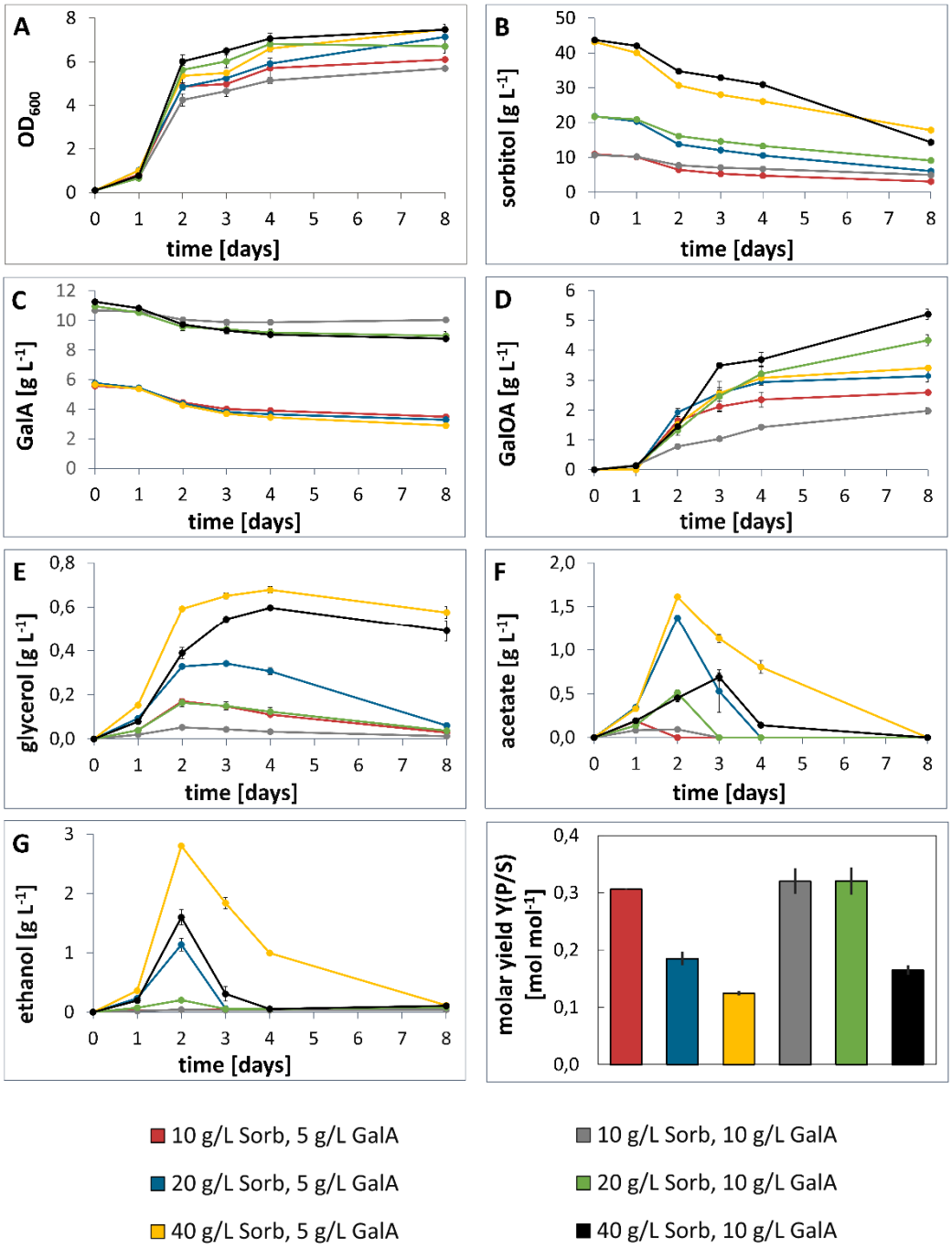


**Figure 3-9: Variation of the sorbitol- and GalA concentrations in the production medium of a sorbitol-based fermentation.**
The influence of the medium components GalA and sorbitol on the production performance of the strain SiHY001 (*AnGATA, AnGAR1, HXT13* and *YlSDR*) was investigated. Therefore, combinations of the different GalA concentrations 5 g $L^{-1}$ and 10 g $L^{-1}$, as well as sorbitol concentrations of 10 g $L^{-1}$, 20 g $L^{-1}$ and 40 g $L^{-1}$ supplemented to the medium. (**A**) The cell growth and the concentrations of (**B**) sorbitol, (**C**) GalA, (**D**) GalOA, (**E**) glycerol, (**F**) acetate and (**G**) ethanol were monitored over the time of cultivation. (**H**) Further, the molar yield $Y_{P/S}$ of the GalOA-production was calculated by the end of the cultivation. The mean value and the standard deviation of biological triplicates are depicted, error bars may be smaller than the symbols.

Considering cell growth, the variation of GalA and sorbitol in the medium did not affect the strains entry into the exponential growth phase, though the cell growth slightly diverged towards receding exponential and stationary growth phase to an optical density between 5 and 7 after 8 days cultivation time. Cultures cultivated in medium with high sorbitol concentrations of 20 g $L^{-1}$ and 40 g $L^{-1}$ reached slightly higher cell densities towards the end of the cultivation, compared to the culture started from only 10 g $L^{-1}$ sorbitol (Figure 3-9, A).

The HPLC-analysis revealed that half of the sorbitol was consumed in all cultivation setups, regardless the start concentration of sorbitol in the medium. Further, in all cultivations the sorbitol consumption slowed down towards the end of the exponential growth phase and almost came to a halt by day 8 of the cultivation (Figure 3-9, B). The different concentrations of the residual sorbitol demonstrate that this halt cannot be explained by the kinetics of the transporter. The metabolite analysis demonstrated high GalOA-titers of 4 g $L^{-1}$ and 5 g $L^{-1}$ in cultures supplemented with 10 g $L^{-1}$ GalA and 20 g $L^{-1}$ or 40 g $L^{-1}$ sorbitol, respectively. Consequently, cultivations supplemented with lower start concentrations of sorbitol and GalA tended to produce lower amounts of GalOA. However, not only the amount of sorbitol but especially the ratio of sorbitol to GalA was of great impact, as the GalOA-titers increased with greater excess of sorbitol over GalA. Thus, in the cultivations supplemented with 5 g $L^{-1}$ GalA the final titers of GalOA increased from 2.58 g $L^{-1}$ (red line) to 3.14 g $L^{-1}$ (blue line) and 3.41 g $L^{-1}$ (yellow line) in the cultivations supplemented with 10 g $L^{-1}$, 20 g $L^{-1}$ and 40 g $L^{-1}$ sorbitol, respectively. This finding reproduced in cultures supplemented with 10 g $L^{-1}$ GalA, as the final product titers increased from 1.97 g $L^{-1}$ (grey line) to 4.34 g $L^{-1}$ (green line) and 5.21 g $L^{-1}$ (black line) with increasing supplementation of sorbitol in the cultivations, 10 g $L^{-1}$, 20 g $L^{-1}$ and 40 g $L^{-1}$, respectively. This effect drastically visualized in the cultivation supplemented with equally 10 g $L^{-1}$ sorbitol and GalA (grey line), as the GalOA-production is even lower than in the cultivation of the same sorbitol but lower GalA-supplementation (Figure 3-9, C-D).

In this cultivation the formation of the typical yeast metabolites glycerol, acetate and ethanol over the cultivation time was HPLC-analyzed (Figure 3-9, E-G). The analysis showed that cultivations supplemented with sorbitol on a high level (20 g $L^{-1}$ and 40 g $L^{-1}$) tended to accumulate more acetate and ethanol, but especially glycerol, in the cultivation broth. However, the cultivation started with 20 g $L^{-1}$ sorbitol and 10 g $L^{-1}$ GalA does not align with this observation, which might relate to higher GalOA-production observed in this cultivation. While glycerol mainly accumulated in the cultivation broth, acetate and ethanol were fully consumed after its formation peaked on the second day of cultivation.

The molar yield $Y_{P/S}$ of GalOA-production on sorbitol was calculated after 8 days of cultivation (Figure 3-9, H). This calculation indicates more efficient sorbitol utilization when the ratio of supplemented sorbitol over GalA was not higher than 2. With sorbitol being the NADPH-source for the

GalA-reduction, the calculated molar yield also describes the efficiency of the cofactor utilization of the process.

Overall, high supplementation of sorbitol and GalA indeed led to a strong increase of GalOA-production, however the molar yield describing the ratio between GalOA produced per sorbitol consumed decreased with increasing supplementation of GalA and sorbitol. This finding refers to increased byproduct formation and thus the decline in efficiency due to inefficient valorization of the costly carbon source sorbitol. Despite relatively low GalOA-production, the cultivations started with sorbitol-GalA-ratio of not higher than 2, seemed to provide optimal conditions for the biotransformation if efficient sugar utilization is taken into account.

### 3.2.6 Establishing Basic Cultivation Techniques towards Continuous Production of GalOA on Sorbitol

Previous chapter demonstrated how concentration and ratio of sorbitol and GalA in the production medium affected the GalOA-production of the strain SiHY001 (*AnGATA, AnGAR1, HXT13* and *YlSDR*). The experiment found that higher substrate and sugar supplementation consecutively resulted in an increased production of GalOA, yet to the expense of unfavorably inefficient sugar utilization as the formation of typical fermentation byproducts like acetate, glycerol and ethanol increased steadily. Efforts of bioprocess engineering showed that suitable fermentation techniques could efficiently circumvent described effect by continuous or fed batch cultivations. This cultivation techniques keep the concentration of certain medium constituent in a beneficial range, which is a powerful tool to evade both limitations and overflow metabolism.

In continuous process set ups, producing cells remain in the cultivation vessel for many generations, therefore the genetic stability must be guaranteed. To assess the applicability of this process engineering strategies, the robustness of the GalOA-production of strain SiHY001 (*AnGATA, AnGAR1, HXT13* and *YlSDR*) was tested in a simulated fed batch and a continuous cultivation set up. For this purpose, a preculture of SiHY001 was performed in buffered SC-sorbitol medium supplemented with GalA for 5 days until the culture medium measured an $OD_{600}$ of 2-4. From this adapted preculture, a main culture was performed in buffered SC-sorbitol medium supplemented with GalA. After 4 days, the cells reached and remained in stationary phase for about one day, a new flask was inoculated ($OD_{600}$=0.1) from the previous culture and fermented for another 4 days. This procedure was repeated. Samples were taken before every medium switch and analyzed via HPLC-analysis. Cell growth was recorded via the *Cell Growth Quantifier* from *Aquila Biolabs* (Figure 3-10).

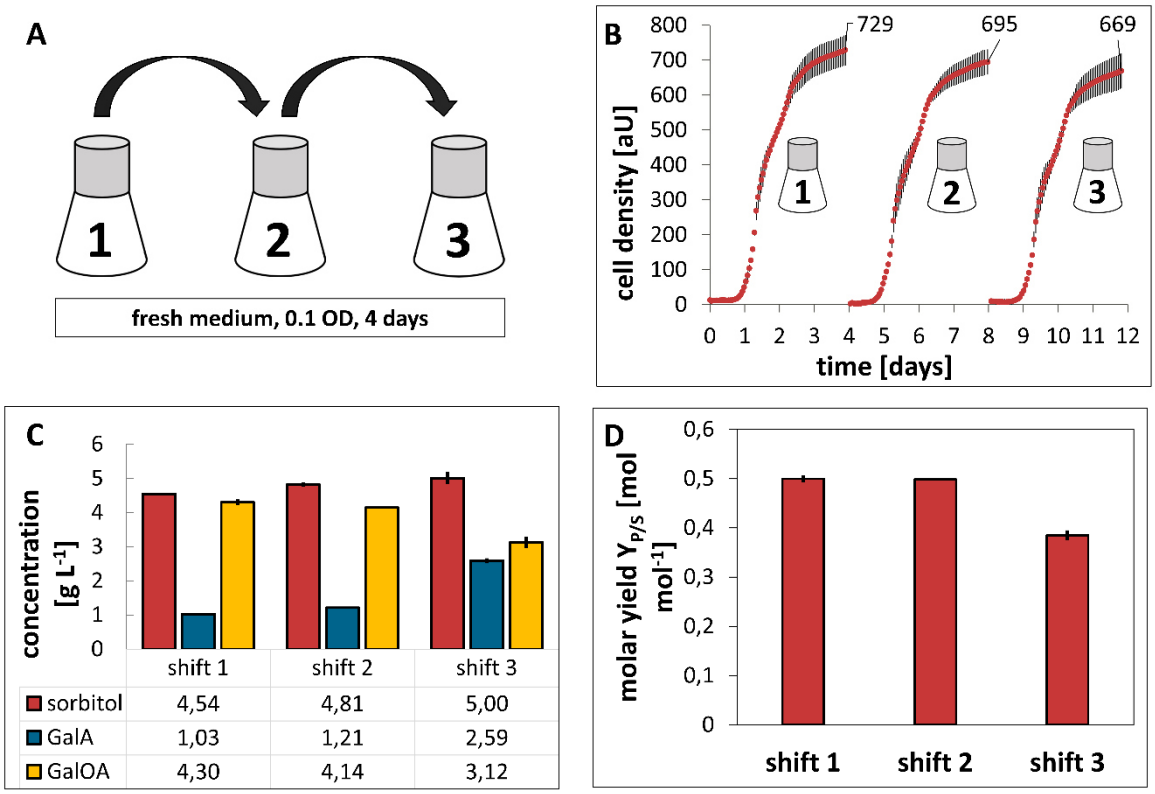


**Figure 3-10: Repeated reinoculation of the sorbitol-based fermentation.**
(**A**) Towards fed batch cultivation, the strain SiHY001 (*AnGATA, AnGAR1, HXT13* and *YlSDR*) was repeatedly shifted to fresh phosphate buffered SC medium supplemented with 10 g $L^{-1}$ sorbitol and 5 g $L^{-1}$ GalA. (**B**) The growth behavior was recorded using the *Cell Growth Quantifier (Aquila Biolabs)*. (**C**) The metabolite composition was analyzed via HPLC before every reinoculation and in the end of the fermentation. (**D**) The molar yield $Y_{P/S}$ of the GalOA-production was calculated. The measurements represent the results of biological triplicates, the calculated standard deviation might be smaller than the border of the bar charts.

After every medium switch, the cultures entered exponential growth phase within 20 h of cultivation. Considering the final cell density, a slight decrease in the shift 2 and 3 was observed compared with shift 1 (Figure 3-10, B). Furthermore, the sorbitol consumption slowed down towards latter shifts, as 4.54 g $L^{-1}$ sorbitol remained in shift 1, 4.81 g $L^{-1}$ sorbitol in shift 2 and 5.00 g $L^{-1}$ sorbitol in shift 3 (Figure 3-10, C). Also, the GalOA-production in the different shifts decreased from 4.30 g $L^{-1}$ in shift 1 to 4.14 g $L^{-1}$ and 3.12 g $L^{-1}$ in shifts 2 and 3, respectively. This means an overall loss of roughly 30% in the final GalOA-titer of the respective shift (Figure 3-10, C). Furthermore, the calculation of the molar yield revealed further room for optimization, as the produced molecules GalOA per consumed molecule sorbitol dropped in the third shift from 0.5 mol $mol^{-1}$ to 0.39 mol $mol^{-1}$ (Figure 3-10, D).

Overall, the GalOA-production declined, even though, only marginal decrease in cell fitness and sorbitol consumption towards later shifts was observed.

To further investigate the long cultivation robustness of the GalOA-production on sorbitol, the same cultivation setup was deployed with cells retained in the shake flask to achieve higher final cell

densities. For this, a main culture was performed in buffered SC-sorbitol medium supplemented with GalA. After 4 days, the cells reached and remained in stationary phase for about one day. The cultures were centrifuged and the supernatant was replaced with fresh medium. The cultivation was proceeded for another 4 days and a further medium exchange was performed, whereby the cultivation was split into three stages. The growth was recorded using the *Cell Growth Quantifier (Aquila Biolabs)* and the metabolite production was analyzed using the HPLC (Figure 3-11).

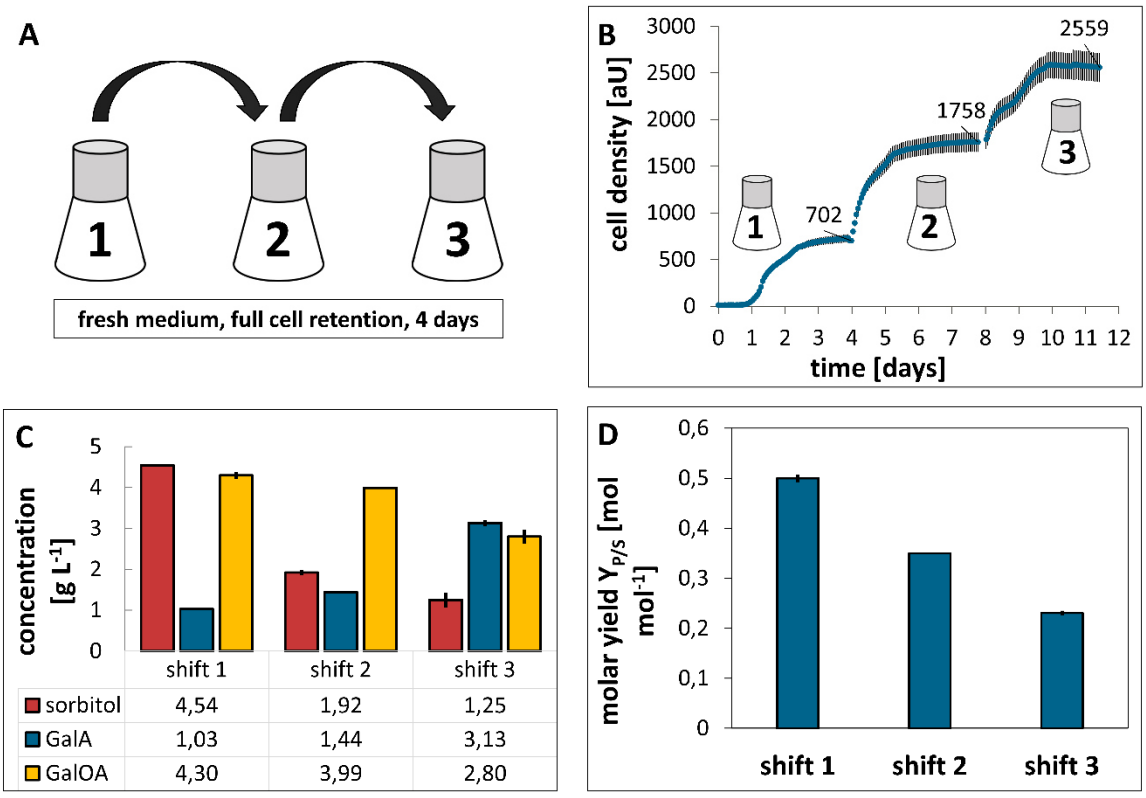


**Figure 3-11: Medium exchange study of sorbitol- based fermentations with cell retaining.**
(**A**) To further proof the production robustness of the strain SiHY001 expressing *AnGATA, AnGAR1, HXT13* and *YlSDR* for sorbitol based GalOA-production, the medium was repeatedly exchanged, but cells were retained. (**B**) The growth was recorded using the *Cell Growth Quantifier (Aquila Biolabs)* and (**C**) the biotransformation of GalA and the sorbitol consumption was measured via HPLC. (**D**) The molar yield of produced GalOA and consumed sorbitol was calculated. The measurements represent the results of biological triplicates, the calculated standard deviation might be smaller than the border of the bar charts.

Immediately after the medium exchange cells started to grow, no lag phase was observed (Figure 3-11, B). The HPLC-analysis showed that more sorbitol was consumed after the first and the second medium exchange, as 4.5 g $L^{-1}$ sorbitol remained after the first stage of cultivation, while only 1.9 g $L^{-1}$ and 1.2 g $L^{-1}$ sorbitol remained in the medium after the second and third stage, respectively. Thus, at later time points, when the cell density was higher, more sorbitol was consumed (Figure 3-11, C). Further analysis of the HPLC-data, showed that the GalOA-production is high in the first two stages of the cultivation, with 4.3 g $L^{-1}$ and 4.0 g $L^{-1}$ GalOA measured, but decreased in the last stage of the cultivation with only 2.8 g $L^{-1}$ produced (Figure 3-11, C). This finding indicates that the

sorbitol metabolism decoupled from the GalOA-production towards later growth stages, which was further illustrated by the molar yield $Y_{(P/S)}$ (Figure 3-11, D).

### 3.2.7 Investigation of the Interplay of AnGatA, TrGar1, Hxt13 and YlSdr

The sorbitol-based production of GalOA is based on the expression of the four genes *AnGATA, AnGAR1*, *HXT13* and *YlSDR*. The constitutive expression of these genes resulted in a considerable GalOA-production (chapter 3.2.1). Naturally, the endogenous catabolism of yeasts mainly generates the reducing equivalent NADH. In contrast, the sorbitol metabolism based on the activity of the heterologous enzyme YlSdr generates NADPH. Consecutively, the YlSdr reaction might shift the intracellular ratio between $NADP^+$ and NADPH more towards NADPH-excess. In *S. cerevisiae*, the reducing equivalent NADH can be used in the respiratory chain at the membrane of mitochondria, which fuels the energy metabolism of the cell. The cofactor NADPH, on the other hand, cannot be utilized in the respiratory chain and therefore excessively generated NADPH would accumulate in the cell. The crucial effect of NADPH-accumulation in the cell was well observed in Δ*pgi1*-mutants, which show a strong growth defect when grown on glucose. Due to the knockout of the *PGI1* gene, the major glycolytic path of the glucose metabolism is blocked resulting in the bypass through the pentose phosphate pathway, the natural source of NADPH, which then accumulates in the cell. The growth could only be restored by suitable NADPH consumption (Boles et al., 1993). This effect illustrates the great impact of a balanced $NADP^+$/NADPH-cycle on the global performance of a cell. This finding could apply to the sorbitol-based GalOA-production as well, as the enzymes used in this study affect the NADPH-level. Here even the sugar transporters could contribute to such effect, as they decisively determine the sugar levels inside the cell. Certain imbalance in the interplay of these proteins could negatively influence the cells fitness, similar to the NADPH-accumulation in the Δ*pgi1*-mutants.

So far, the four genes *AnGATA, TrGAR1*, *HXT13* and *YlSDR* were expressed from genomic integrations driven by strong constitutive promoters. To unveil bottlenecks and possibly imbalanced interplay between the transporters and enzymes AnGatA, TrGar1, Hxt13 and YlSdr, the expression strength of respective genes was varied individually by placing them under the control of the promoter *pRNR1,* which is of lower strength (Lee et al., 2015). This test required the construction of the novel plasmids SiHV090-093, which were used to construct the strains SiHY023 (*pRNR1-AnGATA*), SiHY024 (*pRNR1-TrGAR1*), SiHY025 (*pRNR1-HXT13*) and SiHY026 (*pRNR1-YlSDR*). Besides the

varied expression strength of the gene indicated, the other three genes were expressed from the strong promoters used in the construction of strain SiHY001 (Figure 3-12).

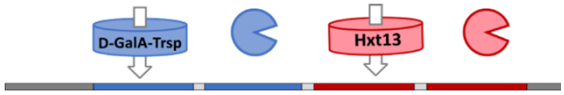


| | AnGATA | TrGAR1 | HXT13 | YlSDR |
|---|---|---|---|---|
| SiHY002 | +++ | +++ | +++ | +++ |
| SiHY023 | weak | +++ | +++ | +++ |
| SiHY024 | +++ | weak | +++ | +++ |
| SiHY025 | +++ | +++ | weak | +++ |
| SiHY026 | +++ | +++ | +++ | weak |

**Figure 3-12: Variation of the expression strength of the genes involved in the sorbitol-based GalOA-production.**
The production of GalOA based on sorbitol consumption is based on the expression of the four genes *AnGATA, TrGAR1*, *HXT13* and *YlSDR.* Successful GalOA-production was observed, if respective ORFs were cloned behind strong constitutive promoters (+++). Individually replacing the strong promoters with the weak *pRNR1* should reveal the limiting factor(s).

The production culture in phosphate buffered SC-sorbitol medium supplemented with GalA, was started from a SC-maltose preculture. The strain SiHY002 was cultivated for comparative reasons. The growth was monitored via $OD_{600}$-measurement and the GalOA-production was analyzed via HPLC (Figure 3-13).

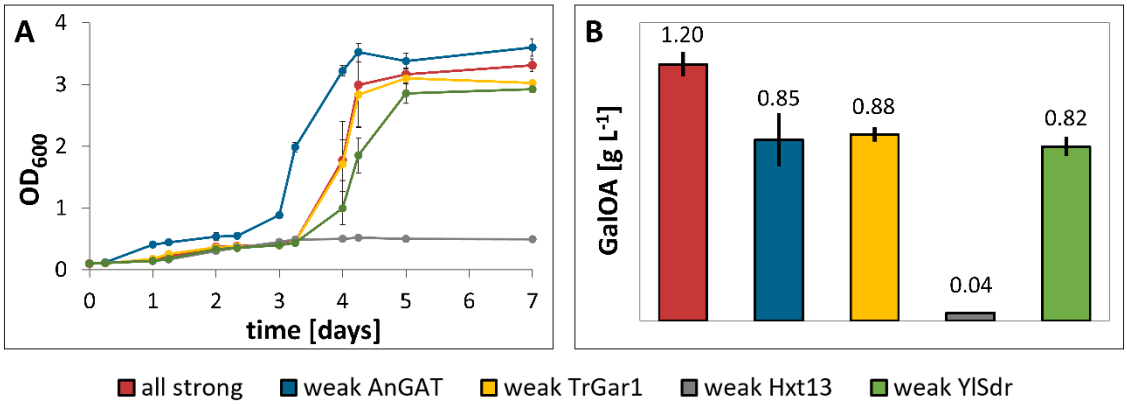


**Figure 3-13: Bottleneck investigation of the sorbitol-dependent GalOA-production via promoter variation of involved genes.**
The expression of four genes confers GalOA-production when sorbitol is used as a co-substrate. Through variation of the expression strength conducted by promoter exchange, the interplay between involved proteins AnGatA, TrGar1, Hxt13 and YlSdr was examined. (**A**) Growth performance and (**B**) final GalOA-titers after 7 days of cultivation were illustrated. The diagrams represent the results of biological triplicates, the calculated standard deviation might be smaller than the symbols or the border of the bar charts.

Slightly better growth of the strain SiHY023 (downregulation of *AnGATA*) and very poor growth of the strain SiHY025 (downregulation of *HXT13*) was observed for the respective cultures compared to the other strains of the experiment. The impact of downregulated *YlSDR* or *TrGAR1* expression seemed to only slightly affect the growth behavior of the strain compared to SiHY002 (Figure 3-13, A). Furthermore, the HPLC-measurement revealed highest GalA-conversion in the strain expressing

the pathway under the control of strong promoters, 1.2 g $L^{-1}$ after 7 days of cultivation, and decreased production of the strains expressing *AnGATA*, *TrGAR1* and *YlSDR* driven by the *pRNR1* promoter; in the respective cultures around 0.82 g $L^{-1}$ to 0.88 g $L^{-1}$ GalOA was measured after 7 days of cultivation (Figure 3-13, B). Barely any GalA-conversion was observed for the strain expressing the *HXT13* at a decreased level (0.04 g $L^{-1}$ GalOA was measured after 7 days of cultivation), which is probably due to only a marginal growth of this strain.

Overall, lower expression of all four investigated genes lowered the GalOA-production, which indicates the need for high expression level of all components. Especially the reduced expression of the sorbitol-transporter gene was fatal for the strain performance, demonstrating that sorbitol uptake imposes the strongest limitation to the system.

### 3.2.8 Genomic Overexpression of *AnGATA*, *AnGAR1*, *HXT13* and *YlSDR* from an Additional Genomic Copy

The foregoing chapter illustrated great impact of varied expression strengths of the involved ORFs, *AnGATA, AnGAR1, HXT13* and *YlSDR* on GalOA-production capability of yeast strains. The experimental set up unveiled bottlenecks, presumably due to limiting protein accessibility throughout the GalOA-production.

To overcome bottlenecks in the sorbitol-based production of GalOA, involved genes were expressed from an additional genomic copy under the control of the strong promoter *pTDH3* in the strain SiHY001. In SiHY001 *pCCW12* drives *AnGATA* expression, *pPGK1* drives *AnGAR1* expression, *pTDH3* drives *HXT13* expression and *pTEF2* drives *YlSDR* expression. The plasmids SiHV201-204 were constructed to introduce an additional copy of respective gene into the *LEU2*-locus under the control of the *TDH3*-promoter. The integration of these plasmids into SiHY001 (*pCCW12-AnGATA, pPGK1-AnGAR1, pTDH3-HXT13* and *pTEF2-YlSDR*) resulted in the novel strains SiHY081 (*pTDH3-AnGAR1*), SiHY082 (*pTDH3-HXT13*), SiHY083 (*pTDH3-YlSDR*) and SiHY084 (*pTDH3-AnGATA*). The preculture was conducted in phosphate buffered SC-sorbitol medium and GalA-supplementation to adapt the strains to the production medium, which was used in the production culture as well. During the cultivation of 8 days, the cell growth and metabolite production was monitored via $OD_{600}$-measurement and HPLC-analysis, respectively (Figure 3-14).

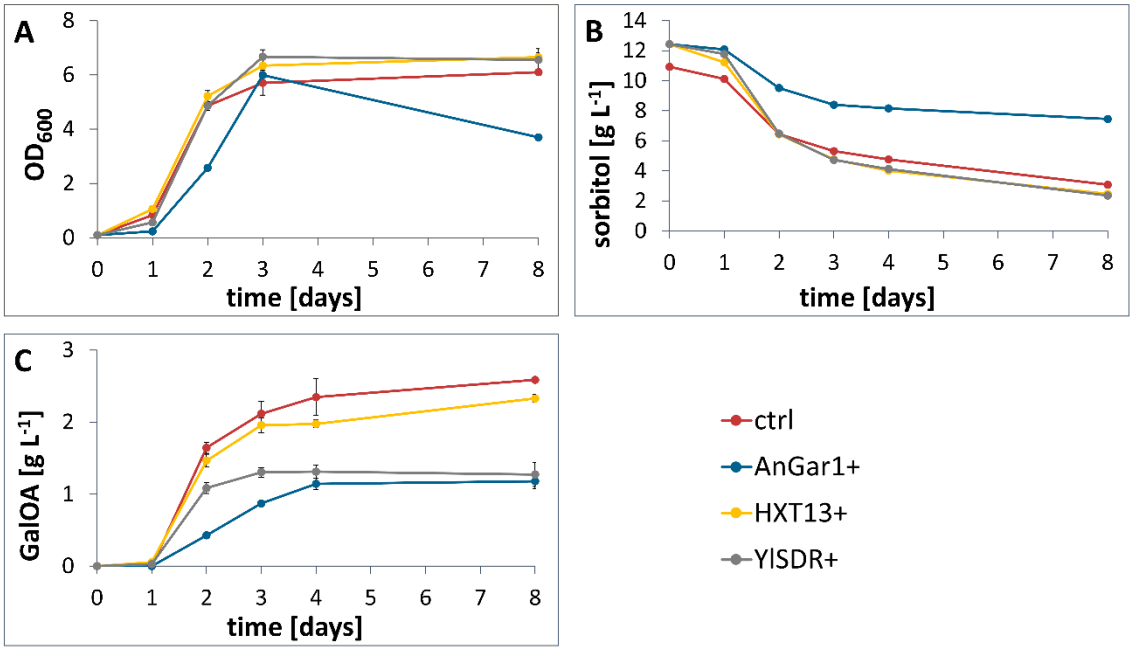


**Figure 3-14: Overexpression of *AnGAR1*, *HXT13* and *YlSDR* from an additional genomic copy under the control of the strong promoter *pTDH3*.**
Possible bottlenecks were investigated by individual overexpression of the genes *AnGAR1, HXT13* and *YlSDR* in the strain SiHY001 (*pCCW12-AnGATA, pPGK1-AnGAR1, pTDH3-HXT13* and *pTEF2-YlSDR*). The overexpression was achieved by integration of gene cassettes driven by the promoter *pTDH3* into the *LEU2*-locus. (**A**) Cell growth was monitored by $OD_{600}$-measurement and (**B**) sorbitol consumption and (**C**) GalOA-production were analyzed via HPLC. The diagrams represent the results of biological triplicates, the calculated standard deviation may be smaller than the symbols.

The preculture of the *AnGATA* overexpression did not show cell growth, so further production culture was not conducted. The control strain SiHY001 and the remaining overexpression strains showed similar growth behavior up to an $OD_{600}$ of 6 until day 3 of the cultivation. While the control strain and the strains overexpressing *HXT13* and *YlSDR* remained in stationary phase without notable change in $OD_{600}$ until the end of the cultivation, the cell growth of the strain overexpressing the GalA-reductase *AnGAR1* decreased drastically to an $OD_{600}$ of 4 by the end of the cultivation (Figure 3-14, A). Similar observation was made considering the sorbitol consumption over the time of the cultivation. The control strain SiHY001 and the strains overexpressing *HXT13* and *YlSDR* showed strong sorbitol consumption of approximately 10 g $L^{-1}$ over the time of cultivation, on the other hand, the strain expressing *AnGAR1* from an additional copy showed rather weak sorbitol consumption of only 4 g $L^{-1}$ (Figure 3-14, B). Further, only the cultivation of the strain overexpressing *HXT13* resulted in GalOA-production similar to the control strain, for these strains the final GalOA-titers were 2.33 g $L^{-1}$ and 2.59 g $L^{-1}$, respectively. In contrast, the cultivations of the strains overexpressing *YlSDR* and *AnGAR1* only resulted in GalOA-productions of around 1 g $L^{-1}$ (Figure 3-14, C).
Overall, the GalOA-production decreased as an effect of the overexpression of the additional copy driven by the *pTDH3*-promoter. Due to the use of the same promoter for the overexpression cassette and the *HXT13* in the parental strain, possible titration effect of the transcription machinery

might explain the effects observed in this study. The negligible effect of the additional *HXT13* overexpression cassette, which did not affect growth or GalOA-production by much compared to the control strain, supports this hypothesis. Further investigation using a different promotor for the overexpression cassette might mitigate the possible titration effect.

### 3.2.9 Bottleneck Investigation of Strain SiHY001 Performed by Plasmid-Based Overexpression of *AnGATA, AnGAR1, HXT13* and *YlSDR*

Autonomously replicating plasmids are a handy genetic tool to quickly overexpress certain genes in microbes. Due to the autonomous replication of plasmids, leading to a higher plasmid number per cell, a higher expression is expected (Broach and Hicks, 1980).

To investigate the impact of strong overexpression of the genes *AnGATA, AnGAR1, HXT13* and *YlSDR* in the sorbitol based GalOA-production strain SiHY001, overexpression plasmids were constructed and tested in a cultivation. Therefore, the 2µ (multicopy) plasmids SiHV112 (*pTEF1-AnGATA*), SiHV114 (*pTEF1-AnGAR1*), SiHV117 (*pTEF1-YlSDR)*, SiHV122 (*pTEF1-HXT13*) and SiHV123 (*pCCW12-AnGATA-pPGK1-AnGAR1-pTDH3-HXT13-pTEF2-YlSDR*) were cloned. The plasmids were transformed into the strain SiHY001 (*pCCW12-AnGATA, pPGK1-AnGAR1, pTDH3-HXT13* and *pTEF2-YlSDR*). Plasmids in yeasts tend to undergo recombination events when cultivated for a long time. Therefore, in favor of plasmid stability, the preculture was conducted in SC-maltose medium without uracil, which, however, does not adapt the cells to the production medium, but confers faster growth. The production culture was performed in phosphate SC-sorbitol medium lacking uracil and with GalA-supplementation. The cell growth was monitored via $OD_{600}$-measurement and the metabolite composition was analyzed via HPLC (Figure 3-15).

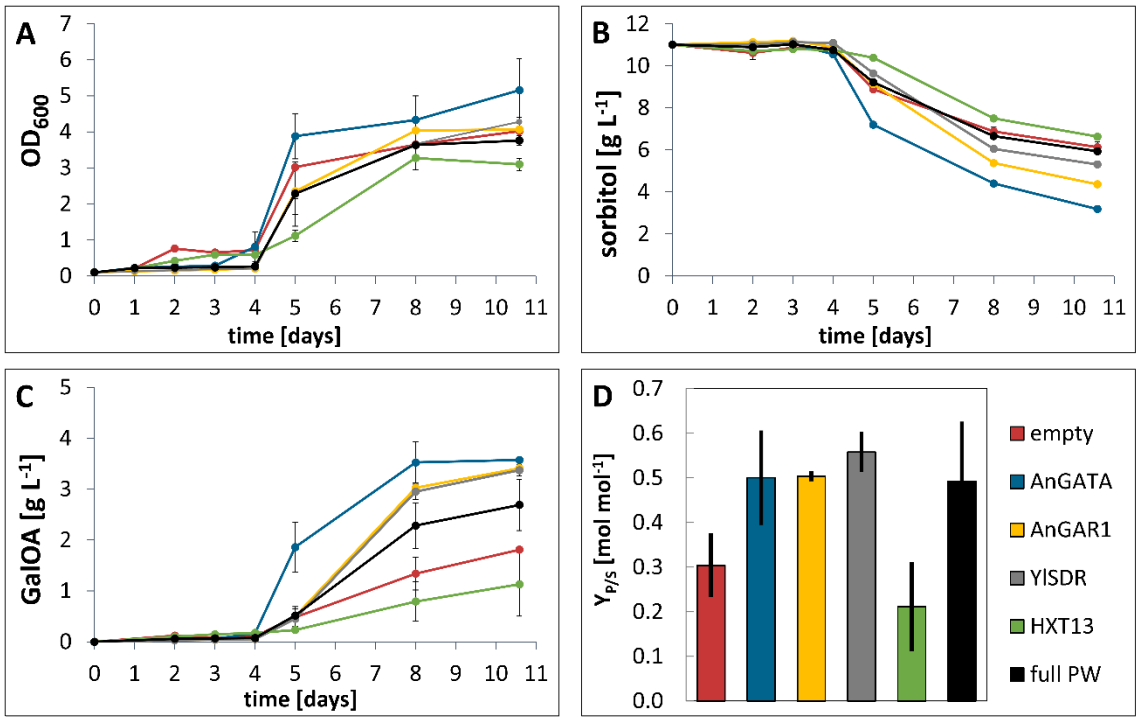


**Figure 3-15: Plasmid borne overexpression of *AnGATA, AnGAR1, HXT13* and *YlSDR*.**
The sorbitol based GalOA-production strain was transformed with plasmids for overexpression of the involved genes *AnGATA, AnGAR1, HXT13* and *YlSDR*, individually and in certain combinations. (**A**) Cell growth, (**B**) sorbitol consumption and (**C**) GalOA-production were monitored over the time of cultivation. (**D**) The molar yield was calculated from the samples taken after 8 days of cultivation. The diagrams represent the results of biological triplicates, the calculated standard deviation might be smaller than the symbols.

The plasmid-based overexpression of the genes *AnGAR1*, *YlSDR* and the full pathway (*AnGATA, AnGAR1, HXT13* and *YlSDR* in combination) resulted in growth behavior similar to the empty vector control, these strains resulted in final cell densities of around $OD_{600}$ of 4. Differently, the overexpression of the transporter genes affected the growth phenotype, resulting in slightly better growth of a final $OD_{600}$ of 5.2 for *AnGATA* overexpression and slightly worse growth for *HXT13* overexpression resulting in an $OD_{600}$ of 3.1 by the end of the fermentation (Figure 3-15, A). The sorbitol consumption mirrored the growth behavior throughout the fermentation, as stronger growth resulted in high sorbitol utilization and weaker growth in low sorbitol utilization, respectively (Figure 3-15, B). Further, certain connection between the growth phenotype and the GalOA-production could be observed, since the overexpression of the GalA-transporter *AnGATA* was beneficial and resulted in a highest final titer of 3.51 g $L^{-1}$ GalOA. In contrast, the overexpression of *HXT13* had a detrimental effect and resulted in a final GalOA-titer of only 1.13 g $L^{-1}$. However, the growth behavior is no absolute indicator for GalOA-production, as the empty vector control strain produced second lowest GalOA-titers of 1.81 g $L^{-1}$ despite good growth (GalOA-production machinery also in the genome). The strong overexpression of *YlSDR* and *AnGAR1* seemed beneficial as well, as regarding cultivations showed GalOA-titers of 3.37 g $L^{-1}$ and 3.41 g $L^{-1}$, respectively. Interestingly, the overexpression of the full pathway from a plasmid, seemed to combine the beneficial effects of *AnGATA*,

*AnGAR1* and *YlSDR* overexpression and the detrimental effect of the *HXT13* overexpression, as the GalOA-production of 2.89 g $L^{-1}$ ranked below the results of individually overexpressed *AnGATA*, *AnGAR1* and *YlSDR* but above the empty vector control, which expressed respective genes only from a single genomic integration (Figure 3-15, C). Considering the molar yields calculated from the data obtained after day 8 of the cultivation, overexpression of the genes *AnGATA*, *AnGAR1* and *YlSDR* enhanced the produced amount of GalOA per consumed sorbitol, which is beneficial for the cost efficiency of the global process (Figure 3-15, D).

This suggests the simultaneous overexpression of *AnGATA*, *AnGAR1* and *YlSDR* from one plasmid is a promising strategy for future studies, as it combines the overexpression of the beneficial genes, but omits *HXT13* overexpression which was found to be detrimental for the process.

## 3.3 Site Directed Mutagenesis of AnGar1 and TrGar1 towards Switched Cofactor Utilization from NADH to NADPH

In foregoing chapters, the GalOA-production based on the consumption of the highly reduced sugar alcohol sorbitol catalyzed by the heterologous enzyme YlSdr was successfully demonstrated and further boosted through medium optimization and suitable enzyme overexpression. Throughout the sorbitol fermentations, the importance of suitable cofactor supply became obvious. High conversion of GalA to GalOA only was possible in strains regenerating NADPH the major cofactor accepted by the employed GalA-reductases TrGar1 (Kuorelahti et al., 2005) and AnGar1 (Harth et al., 2020; Hilditch, 2010). However, sorbitol is a cost intensive carbon source and thus does not qualify for industrial processes. Unfortunately, the allocation of NADPH is limited in *S. cerevisiae* and only few reactions replenish the NADPH-pool (reviewed by van Dijken and Scheffers, 1986). An alternative strategy could be the expression of NADH-dependent GalA-reductases, but only low levels of GalOA were observed with TrGar1 and AnGar1 in combination with the NADH-yielding metabolism in chapter 3.2.1. In that chapter, NADH-supply catalyzed by the endogenous $NAD^+$-dependent sorbitol dehydrogenase Sor2 was tested. In literature, successful switches of enzyme cofactor specificities from NADPH to NADH have already been reported, e.g. imine reductases (Borlinghaus and Nestl, 2018), formate dehydrogenase (Seelbach et al., 1996) and phosphite dehydrogenase (Woodyer et al., 2003). Basis of such protein engineering approaches often are solved enzyme structures or structural homology models. Studying the cofactor binding pockets, especially the amino acid residues interacting with the phosphate group of NADPH are promising target for site directed mutagenesis.

### 3.3.1 Switching the Cofactor Preference of the GalA-Reductases AnGar1 and TrGar1 from NADPH to NADH

So far, the GalOA-production was established in combination with the NADPH-dependent enzyme YlSdr, which oxidizes sorbitol to funnel it into glycolysis. Since the core carbon metabolism of yeasts mainly is $NAD^+$/NADH-dependent and especially because sorbitol is a cost intensive sugar, the urge for NADH-dependent GalA-reductases is high. In the literature, the enzyme AnGaaA found in *A. niger* was described to, at least partially, accept NADH, however its catalytic efficiency is around 50-times lower with this cofactor in comparison with NADPH (Martens-Uzunova and Schaap, 2008).

To switch the cofactor specificity of the enzymes TrGar1 and AnGar1 toward NADH, variants with mutagenized cofactor binding pocket were constructed based on structure-guided mutagenesis. These were tested in a suitable sorbitol screening strains based on the expression of *SOR2* (NADH) (Figure 3-16).

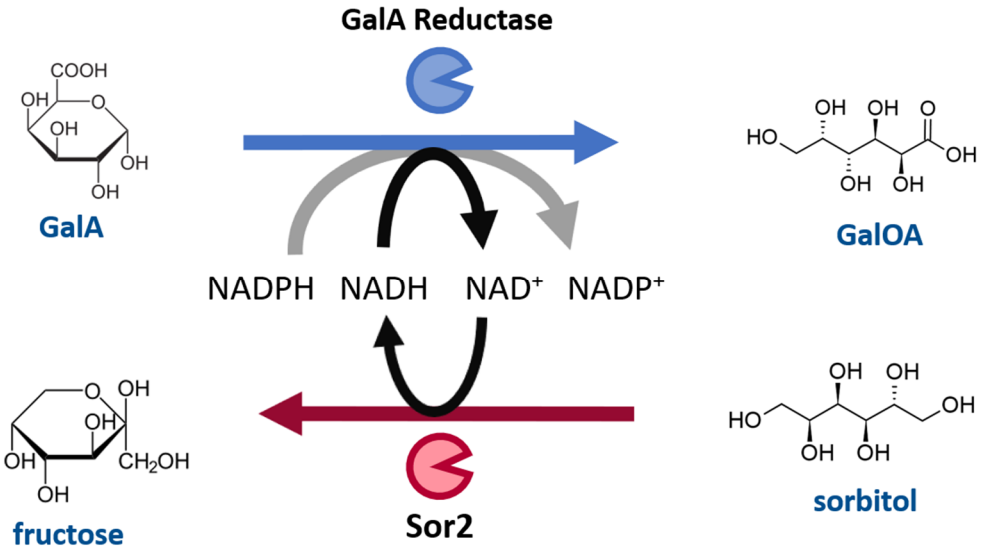


**Figure 3-16: Scheme depicting the benefit of switching the cofactor preference of the GalA-reductases from NADPH to NADH in the screening strain.**
GalA is reduced to GalOA by the GalA-reductases TrGar1 and AnGar1 by utilization of NADPH, naturally. Switching the cofactor specificity of the reductases could make NADH accessible as a cofactor, which, in *S. cerevisiae*, is generated to a higher extent in the core metabolism. To generate a NADH-excess in a screening strain, the endogenous sorbitol dehydrogenase Sor2 was overexpressed from a genomic gene copy together with the genes encoding the transporters AnGatA and Hxt13 for GalA and sorbitol uptake, respectively.

First, the amino acid residues responsible for NADPH binding had to be identified. Therefore, structural models of TrGar1 and AnGar1 were generated using the crystal structure of the NADPH-dependent aldehyde reductase AKR1A1 from *Sus scrofa* (PDB ID 1HQT) as template, which shared 37% sequence identity with the GalA-reductases. The software *Molecular Operating Environment* (MOE; Chemical computing Group) was used to build the homology structure. The resulting structural

models of TrGar1 and AnGar1 were similar, as the enzymes themselves showed 63% identity and 81% similarity. From studying the model, the amino acid residues of lysine and arginine were found in the cofactor binding pocket and thus were presumed to be involved in the cofactor binding. Their positive charge could stabilize the negatively charged phosphate group of the nicotinamide adenine dinucleotide cofactor NADPH. The lysine was found at positions 254 in TrGar1 and at 261 in AnGar1 and the arginine is located at position 260 in TrGar1 and at position 267 in AnGar1. Exchanging these two amino acids with non-charged amino acids of similar size could perturb the electrostatic interaction necessary for enzyme-cofactor-interplay and at the same time preserve the structural integrity of the protein. Therefore, replacing lysine with methionine and arginine with leucine seemed promising approach for cofactor switch (Figure 3-17).

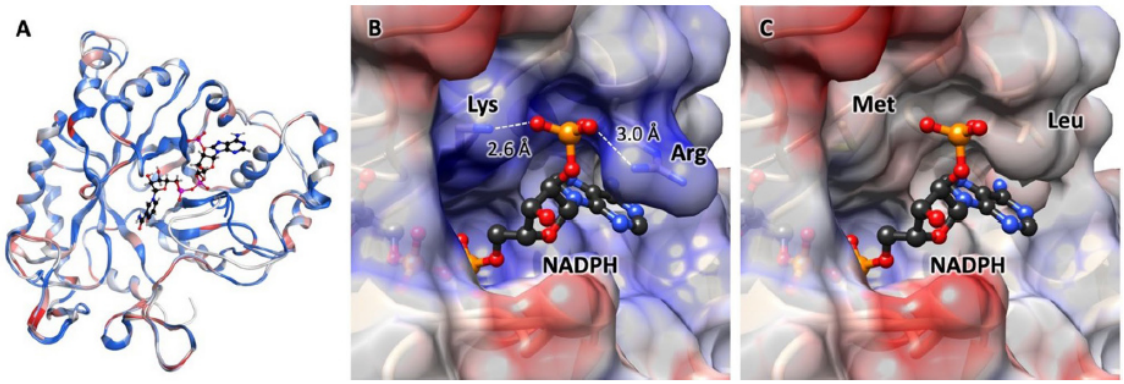


**Figure 3-17: Structure homology models of TrGar1 and AnGar1 and engineered cofactor binding pocket.** The homology structural models of the GalA-reductases TrGar1 and AnGar1 were derived from the crystal structure of the NADPH-dependent aldehyde reductase AKR1A1 from *Sus scrofa* (PDB ID 1HQT). (**A**) Direct comparison by overlay of the resulting models of TrGar1 and AnGar1 shows only little differences to each other. Blue coloration shows high amino acid similarity or even amino acid identity (dark blue), while red coloration refers to differences in the amino acid sequence. The cofactor NADPH is depicted as ball and stick model. (**B**) Close up of the cofactor binding pockets of the GalA-reductases. The amino acids involved in the stabilization of the phosphate group of the NADPH cofactor are illustrated. The electrostatic interaction is depicted in shades of blue (positive) and red (negative). The coulombic protein surface was calculated with the UCSF Chimera (www.rbvi.ucsf.edu/chimera). (**C**) Through amino acid exchange from lysine to methionine and arginine to leucine, the engineered cofactor binding pocket, does not show high capability to stabilize the highly negative charged phosphate moiety of the NADPH. The wildtype locus of the lysine is at position 254 in TrGar1 and at 261 in AnGar1, while the arginine is located at position 260 in TrGar1 and at position 267 in AnGar1. The protein structure was modelled and the mutations were predicted from comparative structure analysis by Jun-yong Choe from Rosalind-Franklin University of Medicine and Science. Figure was taken from Harth et al., 2020.

The suggested amino acid exchanges in TrGar1 and AnGar1 were constructed via site directed mutagenesis on DNA-level, resulting in the high copy (2µ) plasmids SiHV058 (*TrGAR1* [K254M]), SiHV059 (*TrGAR1* [R260L]), SiHV060 (*TrGAR1* [K254M, R260L]), SiHV100 (*AnGAR1* [K261M]), SiHV101 (*AnGAR1* [R267L]) and SiHV102 (*AnGAR1* [K261M, R267L]). Furthermore, the wildtype versions of *TrGAR1* and *AnGAR1*, as well as the *AnGAAA* were cloned on plasmids, SiHV074 (*TrGAR1*), SiHV079 (*AnGAR1*) and SiHV057 (*AnGAAA*). The GalA-reductase AnGaaA was described in literature

to naturally accept NADPH and NADH, although it accepts NADPH to a much higher extent (Martens-Uzunova and Schaap, 2008), was included for comparative reasons. The strains SiHY007 and SiHY008 were constructed to perform as platform strains for the screen, as these strains express respective genes of the GalA-transporter AnGatA, the sorbitol transporter Hxt13 and one of the sorbitol dehydrogenases YlSdr (NADPH) or Sor2 (NADH), respectively. The novel plasmids were transformed into these strains and test cultivations were conducted. The preculture was performed in SC-maltose medium without uracil and the screen was performed in phosphate buffered SC-sorbitol medium supplemented with GalA but no uracil. The cell growth was monitored via $OD_{600}$-measurement and the GalOA-production was measured via HPLC-analysis (Figure 3-18).

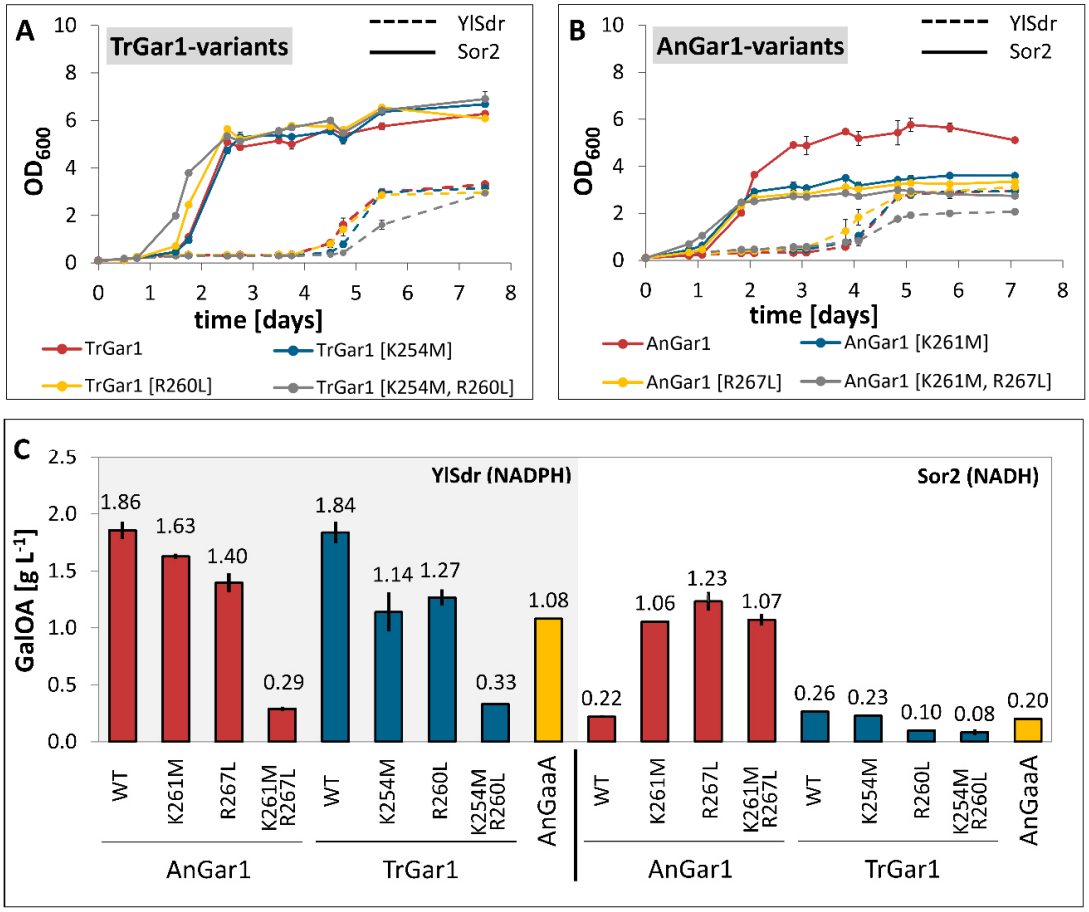


**Figure 3-18: Screening the TrGar1- and AnGar1-variants towards switch of the cofactor specificity.** Variants of the wildtype reductases TrGar1 and AnGar1 as well as the phylogenetically independent AnGaaA were tested in strains generating excess of NADH or NADPH from sorbitol metabolism. (**A, B**) The growth behavior of the screening strains expressing *TrGAR1* and *AnGAR1*-variants and the wildtype versions was monitored via optical density measurement ($OD_{600}$). Expression of the reductases in the strain generating excess NADH is depicted in solid lines and in the strain of excess NADPH in dotted lines, respectively. (**C**) The GalOA-production of the different reductase variants of TrGar1, AnGar1 and AnGaaA was analyzed via HPLC. The two strain backgrounds SiHY007 (NADPH) and SiHY008 (NADH) are indicated by the background color of the bar chart. The measurements represent the results of biological duplicates, the calculated standard deviation might be smaller than the symbols or the border of the bar charts. The figure was adapted from Harth et al., 2020.

The expression of *TrGAR1*-variants caused strong growth differences in strains generating excess NADH (Sor2) or NADPH (YlSdr). While the strain expressing *SOR2* (NADH) showed strong growth after the first day of cultivation up to an $OD_{600}$ of 7, the strains expressing the NADPH-dependent *YlSDR* only showed minor growth after 4 days of cultivation up to an $OD_{600}$ of 3. To a great extent, this growth observation was independent of the expressed *TrGAR1* variant, however slightly worse cell growth was observed when the double mutated *TrGAR1* [K254M, R260L] was expressed in the NADPH-strain (Figure 3-18, A). In contrast, the screen of AnGar1-variants in the NADH-strain resulted in a different growth phenotype, as the cell growth seemed to be affected by the expression of the mutated *AnGAR1*-variants K261M and R267L, separately and in combination. Regarding yeast strains only reached final cell densities of $OD_{600}$ around 3. The expression of the wildtype *AnGAR1* did not cause the same growth defect, as the growth performance resembled the screen of the *TrGAR1*-variants expressed in the Sor2-strain. Expression of the *AnGAR1*-variants in the NADPH-strain showed the same growth delay as observed in the TrGar1-screen. The growth only reached an $OD_{600}$ of around 3, even worse the growth of the NADPH-strain transformed with the double mutant *AnGAR1* [K261M, R267L], which only reached $OD_{600}$ of 2 by the end of the cultivation (Figure 3-18, B).

Following the expectation, the wildtype reductases TrGar1 and AnGar1 produced GalOA only in the strain expressing the YlSdr to a relevant extent of nearly 2 g $L^{-1}$ after more than 7 days of cultivation. In comparison, only half the GalOA was produced by AnGaaA under NADPH-supply by YlSdr expression, which resulted in a titer of 1.08 g $L^{-1}$. According to the hypothesis, decreased amounts of GalOA were measured based on the mutated variants of AnGar1 and TrGar1 on NADPH. Furthermore, only minor GalOA-production of below 0.3 g $L^{-1}$ was produced by the double mutants AnGar1 [K261M, R267L] and TrGar1 [K254M, R260L] in combination with YlSdr. Transformed into the NADH-strain, the TrGar1-variants produced amounts of GalOA even lower than the regarding wildtype enzyme in this strain background. In contrast to this finding, the variants of the AnGar1 produced considerable amounts of GalOA of 1-1.2 g $L^{-1}$ with NADH-supply, which is five times higher than with AnGaaA under the same conditions. However, the emerging NADH-dependent GalOA-production of the AnGar1 mutants seemed to affect the cells fitness, as the final $OD_{600}$ measured was 4 $OD_{600}$ lower compared with the growth performance of the strain expressing the wildtype reductase, which did not confer GalOA-production in the NADH-strain (Figure 3-18, C).

Overall, these results show the successful switch of the cofactor specificity of AnGar1, as the single mutations K261M and R267L conferred the usage of NADPH and NADH, while the double mutated version only accepted NADH. Since the metabolism of neutral sugars, e.g. glucose, mainly yields

NADH, these results pave the way for a more cost-efficient GalA-conversion based on glucose consumption. Further characterization of these AnGar1-variants might unveil the biochemical mechanism, which enabled NADH-utilization.

### 3.3.2 Characterization of the AnGar1-Variants in an Enzyme Assay

Foregoing chapter demonstrated the feasibility of the model-based mutagenesis of the GalA-reductase AnGar1. Based on the homology-model, it was presumed that the positively charged amino acids K261 and R267 could be involved in the NADPH stabilization. Stepwise substitution of these amino acids with the neutral amino acids methionine and leucine, showed that single mutants can use either NADH or NADPH and the double mutation even excluded the acceptance of NADPH.

To further investigate the AnGar1-variants and to analyze the molecular basis of these *in vivo* observations, *in vitro* assays were performed. For further analysis, the wildtype AnGar1, the superior single mutant AnGar1 [R267L] and the double mutant AnGar1 [K261M, R267L] were selected. The reductases were expressed from the same high copy plasmids already used in chapter 3.3.1 in the CEN.PK2-1C wildtype strain and the enzyme assay was performed with crude cell extracts; the same strain transformed with the empty vector was included as negative control. The activity of the GalA-reductases was tested with NADPH and NADH. Additionally, the influence of $NADP^+$ on the enzyme activity using NADH was tested. The decrease of the NAD(P)H-absorbance of the reaction mix at 340 nm was taken as a measure for the enzyme activity (Figure 3-19).

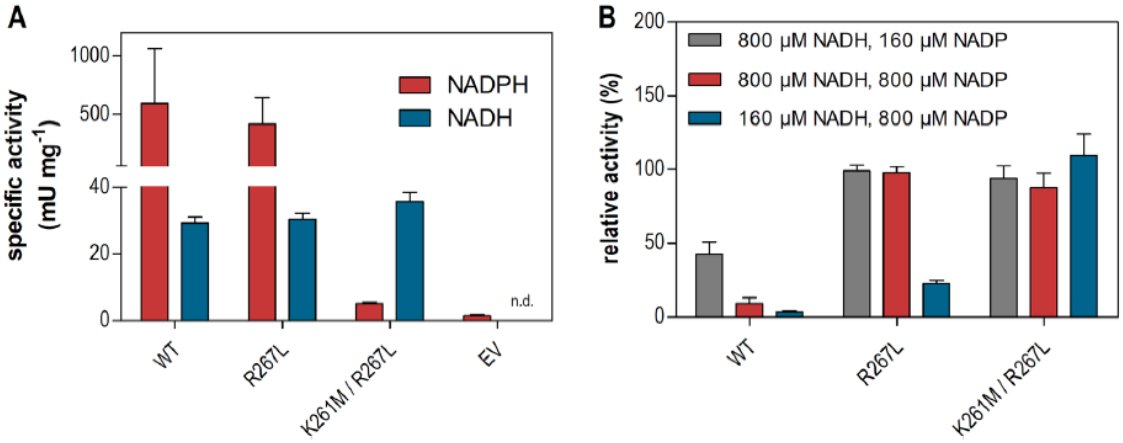


**Figure 3-19: Enzyme activity measurement of the AnGar1-variants.**
The AnGar1-variants were expressed from high copy plasmids in the wildtype strain CEN.PK2-1C, an empty vector (EV) was included as a control. Protein extracts from disrupted cells were used to perform the enzyme assay. (**A**) The enzyme activity was measured with NADPH and NADH. The specific activity was calculated in milli units per mg protein, mU $mg^{-1}$. For better visualization the y-axis was divided into two segments. (**B**) The competitive influence of the oxidized cofactor $NADP^+$ on the NADH-enzyme activity was investigated. Therefore, the indicated cofactor mixtures of stated concentrations were tested. Error bars represent standard deviations of technical triplicates. n.d. not detectable. Figure was taken from (Harth et al., 2020)

The results of the enzyme assay reflected the observations made *in vivo,* as the activity of the reductase on NADPH decreased with the number of mutations inserted. While the single mutant accepted NADPH and NADH, the double mutant only accepted NADH, almost exclusively. Although it was shown that *in vivo* the wildtype reductase functioned by far better with NADPH, interestingly, *in vitro* it also showed activity with only NADH on the same level as the engineered variants of AnGar1 (Fig 3-16, A). However, *in vivo,* only the mutated versions showed GalOA-production in combination with the NADH-yielding sorbitol dehydrogenase (Figure 3-18, chapter 3.3.1).

Further, adding $NADP^+$ to the reaction mix caused the collapse of the activity of the wildtype AnGar1, demonstrating the inhibitory effect of $NADP^+$ on the NADH-utilization. Differently, the single mutated AnGar1 [R267L] showed lower sensitivity to $NADP^+$ supplementation, as the activity only decreased after $NADP^+$ was added in excessive surplus. Furthermore, this effect consolidated in the case of the double mutant AnGar1 [K261M, R267L], which showed NADH-activity even if the amount of $NADP^+$ exceeded the NADH-concentration by far. This effect presented the double mutant insensitive to $NADP^+$.

Overall, it was shown that the AnGar1 wildtype reductase also accepted NADH naturally, however this ability was strongly impaired by $NADP^+$. Further, the inhibitory effect of $NADP^+$ could be mitigated by suitable mutagenesis targeting the amino acids, which stabilize the phosphate group of the cofactor in the binding pocket. Consequently, the engineered GalA-reductase variants showed activity using NADH as cofactor while $NADP^+$ was present. Therefore, the described success of the enzyme engineering is rather based on excluding $NADP^+$ from the cofactor binding pocket, than the

actual increase of NADH-affinity in the binding pocket itself. The presented results demonstrated the successful engineering of the AnGar1 to use NADH, and thereby expand the possibilities for metabolic engineering of GalA utilization.

## 3.4 Implementing the Engineered AnGar1-Variants in the NADH-Providing Glucose Metabolism of *Saccharomyces cerevisiae*

Glucose is a prominent and easily metabolized sugar in nature and is favored by most organisms, including yeasts. Whilst a small moiety branches off through the NADPH-dependent pentose phosphate pathway, most of the glucose fluxes down the glycolysis, which yields two moles of NADH per mol of glucose. In *Saccharomyces cerevisiae*, NADH-molecules are largely consumed for the ethanol formation on high glucose concentrations, even under aerobic conditions, which is called the Crabtree-effect (De Deken, 1966). Furthermore, as the central reducing equivalent in yeasts, NADH is used in many other metabolic branches of the core metabolism as well (Piškur et al., 2006; Pronk et al., 1996).

### 3.4.1 Testing the Engineered AnGar1-Variants on Glucose in an *Δadh1*-Strain under Aerobic and Micro-Aerobic Conditions

The reduction of GalA to GalOA requires efficient generation of reducing equivalents. After the mainly NADPH-dependent wildtype AnGar1 was engineered towards the use of NADH, the reducing equivalents can be sourced from the NADH-dependent core metabolism of *S. cerevisiae*. Furthermore, this enables to switch the carbon source in the fermentation from the cost intensive sorbitol to relatively cheap glucose. However, most of the NADH generated in the glucose-based metabolism is lost in the strictly aerobic respiration at the mitochondria and through the formation of ethanol, catalyzed by the major ethanol dehydrogenase Adh1. By switching the cultivation conditions from aerobic to micro-aerobic and by deleting the ORF of the *ADH1*, a higher accumulation of NADH is expected.

To establish and improve GalOA-production deploying the engineered reductases AnGar1 [R267L] and AnGar1 [K261M, R267L] on glucose, the effect of Δ*adh1* was investigated under aerobic and micro-aerobic conditions. Consequently, the accumulated NADH could be used by the GalA-reductases AnGar1 [R267L] and AnGar1 [K261M, R267L]. This experiment required the construction of

the novel plasmids SiHV136 (*AnGATA*, *AnGAR1 [R267L]*) and SiHV137 (*AnGATA*, *AnGAR1 [K261M, R267L]*), which were integrated into the wildtype strain CEN.PK2-1C and the novel constructed *Δadh1*-strain SiHY033. The resulting strains were SiHY036 (*Δadh1, AnGATA*, *AnGAR1 [R267L]*), SiHY037 (*Δadh1, AnGATA*, *AnGAR1 [K261M, R267L]*), SiHY040 (*AnGATA*, *AnGAR1 [R267L]*) and SiHY041 (*AnGATA*, *AnGAR1 [K261M, R267L]*). Instead of strictly anaerobic conditions, micro-aerobic conditions were created by an air-tight tube plug filled with water, which allowed occurring gas production to leave the experimental set up. The fermentation broth was agitated with a magnetic stirrer. While the preculture was performed in SC-medium supplemented with 20 g $L^{-1}$ glucose, the test cultivation was performed in phosphate buffered SC-medium supplemented with 20 g $L^{-1}$ glucose and 5 g $L^{-1}$ GalA and started with an $OD_{600}$ of 1. Samples were taken with a syringe without removing the plug from the shake flasks. The metabolic performance of the strain was analyzed via HPLC (Figure 3-20).

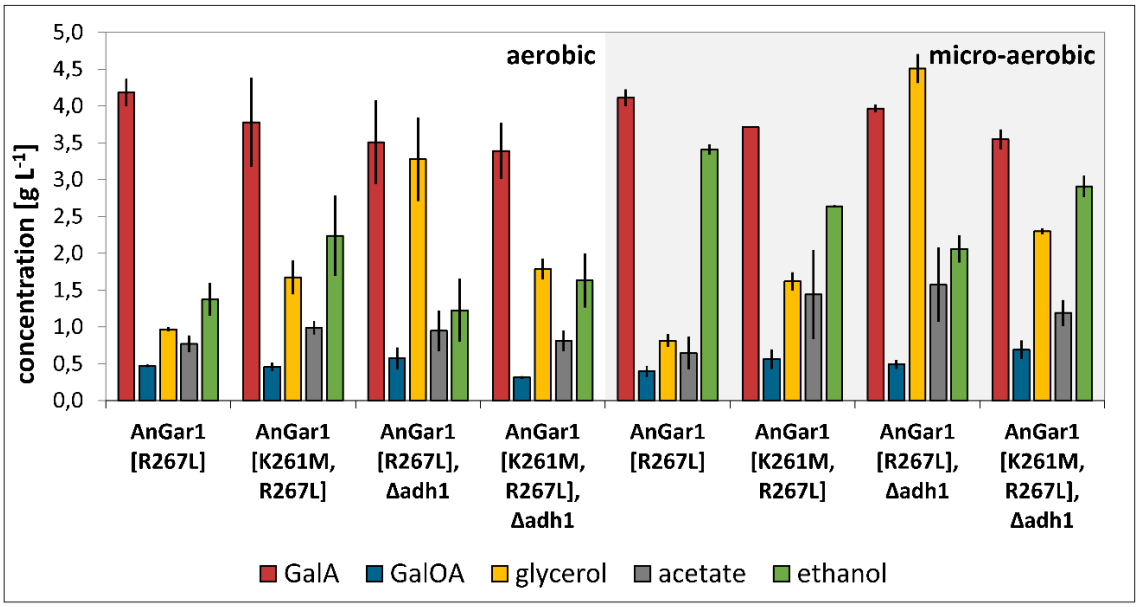


**Figure 3-20: Investigation of the GalOA-production under aerobic and micro-aerobic fermentation conditions in a wildtype or Δ*adh1*-strain on glucose deploying the engineered GalA-reductase variants AnGar1 [R267L] and AnGar1 [K261M, R267L].**
The GalOA-production of the NADH-dependent GalA-reductases AnGar1 [R267L] and AnGar1 [K261M, R267L] were tested on glucose. Furthermore, the experiment studied how deleting the ORF of the *ADH1* gene and micro-aerobic cultivation conditions affected the production performance. The metabolic data is derived from HPLC-analysis; values of GalA, GalOA, glycerol, acetate and ethanol are depicted. Error bars represent standard deviations of technical triplicates.

Already the expression of the genes *AnGAR1 [R267L]* and *AnGAR1 [K261M, R267L]* coding for the engineered GalA-reductases in the wildtype strain background resulted in comparable GalOA-production on glucose of 0.47 g $L^{-1}$ and 0.46 g $L^{-1}$, respectively. These titers improved according to the hypothesis of accumulated NADH, as highest GalOA-production was observed in the *Δadh1*-strain under micro-aerobic conditions deploying the strictly NADH-dependent reductase AnGar1 [K261M,

R267L] 0.69 g $L^{-1}$ GalOA were produced. In contrast, the same GalA-reductase produced 0.46 g $L^{-1}$ GalOA under aerobic conditions and under micro-aerobic conditions 0.56 g $L^{-1}$ GalOA in the wildtype strain background. However, under aerobic conditions, the GalOA-production of the AnGar1 [K261M, R267L] was hampered, when expressed in the *Δadh1*-strain compared to the wildtype strain background. Similar improving effect could not be observed, when the *AnGAR1 [R267L]* was expressed, whose more promiscuous gene product accepts NADH and NADPH (chapter 3.3). While the expression of the singly mutated GalA-reductase in the Δ*adh1*-strain was beneficial compared to the wildtype strain, this effect was vanished under micro-aerobic conditions; the GalOA-titer dropped from 0.57 g $L^{-1}$ GalOA to 0.49 g $L^{-1}$ GalOA. Furthermore, strongly increased glycerol values were measured in these fermentations, which increased from approx. 1 g $L^{-1}$ in the wildtype strain background up to 4.51 g $L^{-1}$ in the Δ*adh1*-strain under micro-aerobic conditions. This effect was observed in cultivations of the strain expressing the double mutated GalA-reductase variant as well, but the extent was lower. However, in these cultivations the ethanol values were slightly increased compared to cultures containing *AnGAR1 [R267L]* expressing strains. Regardless the GalA-reductase, the ethanol values increased under micro-aerobic conditions and in the Δ*adh1*-strains.

Overall, increased GalOA-production performance was observed in the *Δadh1*-strain expressing the AnGar1 [K261M, R267L] under micro-aerobic conditions. This effect is presumably due to NADH-accumulation and mitigation of cofactor competition of the AnGar1 [K261M, R267L] with the ethanol formation and the respiratory chain at the mitochondrial membrane. Further optimization targets must be investigated as the vast majority of the supplemented GalA remained unused in the fermentation broth after the end of cultivation.

### 3.4.2 Testing the GalA-Reductase Variants in a Strain Optimized for NADH-Supply from Genomic Expression

As the major reducing equivalent in *S. cerevisiae*, NADH is intertwined in various cellular processes like ethanol and glycerol production. Especially due to the Crabtree effect, a predominant fraction of the NADH generated in the GAPDH reaction of the glycolysis is oxidized during ethanol production (Piškur et al., 2006; Pronk et al., 1996). Wess et al. (2019) reported a beneficial effect on the NADH-dependent isobutanol production in *S. cerevisiae*, when, among other pathways, the ethanol (Δ*adh1*) and glycerol formation (Δ*gpd1*, Δ*gpd2*) were impaired. By deleting genes of involved enzymes that study also aimed to accumulate pyruvate inside the cell, a precursor for the isobutanol pathway. However, those deletions also fostered the NADH-regeneration of the cell. Possibly, this

finding can be transferred to GalOA-production based on NADH by installing the engineered variants of the GalA-reductases AnGar1 in this strain.

The engineered reductases AnGar1 [R267L] and AnGar1 [K261M, R267L] were tested in the strain JWY019 optimized for NADH-supply from Wess et al., 2019. To confer GalOA-production, the strain was transformed with the linearized plasmids SiHV136 (*AnGATA, AnGAR1 [R267L]*), SiHV137 (*AnGATA, AnGAR1 [K261M, R267L]*) and SiHV158 (*AnGATA, AnGAR1$^{WT}$),* resulting in the strains SiHY062, SiHY063 and SiHY072, respectively. The novel strains were tested in a cultivation conducted in phosphate buffered SC-medium supplemented with 20 g $L^{-1}$ glucose and 5 g $L^{-1}$ GalA. The preculture was performed in SC-glucose medium. During the cultivation, the cell growth was monitored photometrically and the medium composition and GalOA-formation was measured via HPLC-analysis (Figure 3-21).

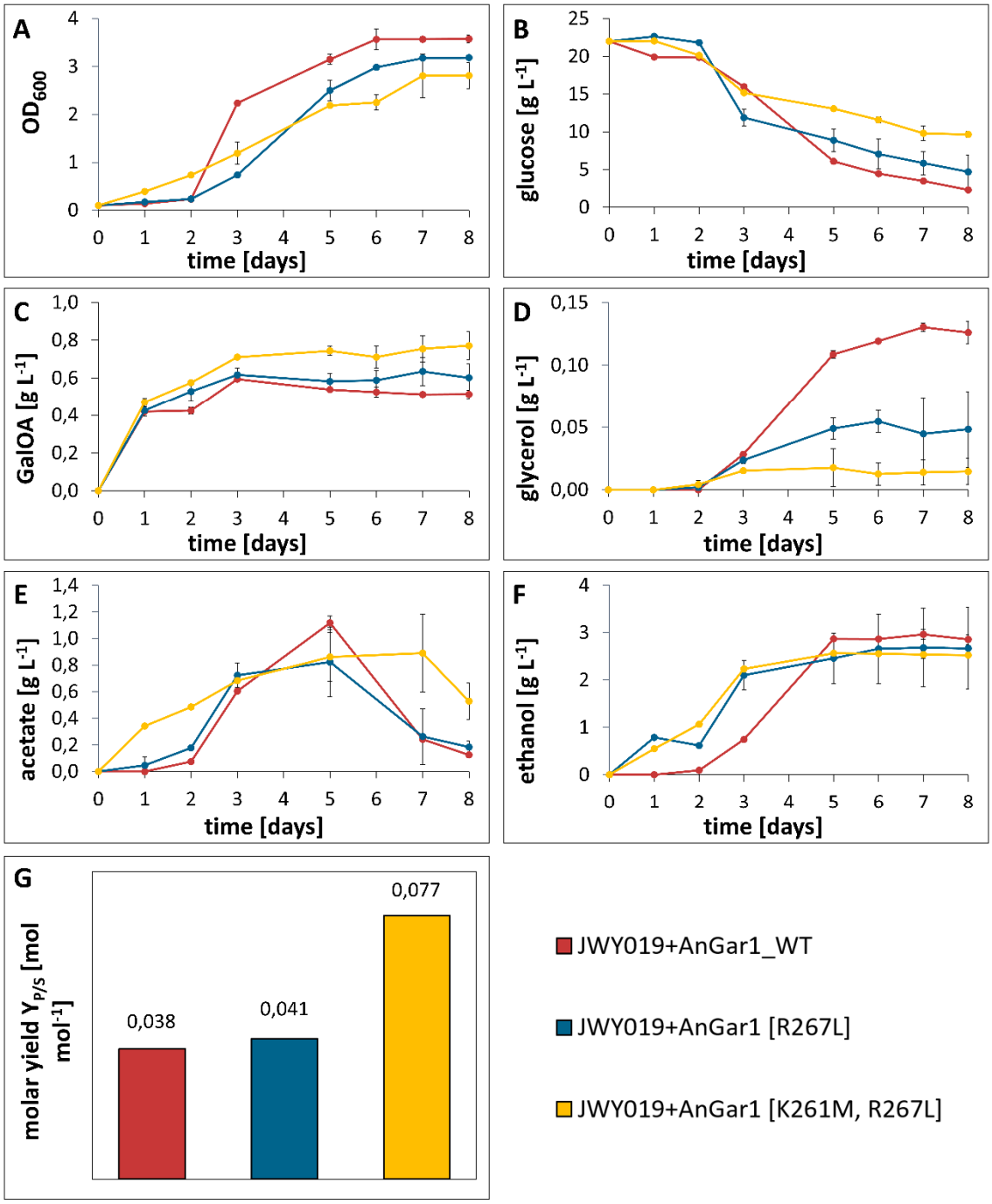


**Figure 3-21: GalOA-production by the engineered AnGar1 [R267L] and AnGar1 [K261M, R267L] in the yeast strain optimized for NADH-supply on glucose.**
The GalA-reductases AnGar1$^{WT}$ and its variants AnGar1 [R267L] and AnGar1 [K261M, R267L] together with the transporter AnGatA were tested in the strain JWY019 optimized for NADH-supply (Wess et al., 2019). The reductases and the transporter were expressed from a genomically integrated cassette. (**A**) The cell growth was monitored via $OD_{600}$-measurement and the metabolite production was measured via HPLC, (**B**) glucose, (**C**) GalOA, (**D**) glycerol, (**E**) acetate and (**F**) ethanol. (**G**) From the GalOA-production and the glucose consumption, the molar yield as mol GalOA-produced per mol glucose consumed was calculated. The measurements represent the results of biological duplicates, the calculated standard deviation might be smaller than symbol or border of bar charts. Figure adapted from Harth et al., 2020.

The strain expressing the wildtype *AnGAR1$^{WT}$* entered the exponential growth phase before the strains expressing the AnGar1-variants, which also reflected in the final $OD_{600}$. While the strain expressing *AnGAR1$^{WT}$* reached a final $OD_{600}$ of 3.58, the strains expressing *AnGAR1 [R267L]* and *AnGAR1 [K261M, R267L]* reached slightly decreased final cell densities of $OD_{600}$ 3.19 and 2.81, respectively. However, the differences in growth were only minor, which also applied for the glucose consumption (Figure 3-21, A-B). Considering the HPLC-analysis, with 0.84 g $L^{-1}$ and 0.61 g $L^{-1}$ the AnGar1 [R267L] and AnGar1 [K261M, R267L] produced more GalOA than the AnGar1$^{WT}$ with 0.51 g $L^{-1}$ (Figure 3-21, C). However, rather high amount of GalA remained in the fermentation broth.

Furthermore, the three strains produced similar amounts of 1 g $L^{-1}$ acetate and approximately 3 g $L^{-1}$ ethanol throughout the cultivation (Figure 3-21, E-F). The HPLC-analysis resulted in different glycerol formation of the three strains, as the strain expressing the *AnGAR1$^{WT}$* with 0.13 g $L^{-1}$ glycerol ranked higher than the strains expressing the variants *AnGAR1 [R267L]* and *AnGAR1 [K261M, R267L]* with 0.05 g $L^{-1}$ and 0.02 g $L^{-1}$ (Figure 3-21, D). This suggests that the production of GalOA via mutant reductases indeed acts as a redox sink for the accumulated NADH. All three strains produced around 2.5 g $L^{-1}$ ethanol throughout the cultivation. The molar yield of the process was calculated as the ratio between produced GalOA per consumed glucose in mol per mol after 8 days of cultivation (Figure 3-21, G). The strain expressing the double mutant *AnGAR1 [K261M, R267L]* showed the highest molar yield while it also showed only low byproduct formation (acetate, glycerol and ethanol).

Overall, employing the double mutant AnGar1 [K261M, R267L] in the NADH-optimized strain JWY019 for GalA-reduction resulted in the highest GalOA-titer compared with the AnGar1$^{WT}$ and the single mutant AnGar1 [R267L], simultaneously, the formation of glycerol was low in this strain. However, GalA was not converted completely, which leaves room for optimization.

### 3.4.3 Rewired Acetate Formation for Enhanced Generation of Reducing Equivalents

Rather high acetate formation was observed in foregoing productions employing the variants of the AnGar1. The fermentations were performed on glucose, which fluxes through glycolysis to generate NADH, while a certain moiety of the glucose flux branches off into the pentose phosphate pathway, the major source for NADPH. The carbon body of the glucose results in pyruvate, which is further converted to acetaldehyde. From acetaldehyde the flux bifurcates in the two prominent byproducts of glucose fermentations, ethanol and acetate. While the formation of ethanol consumes NADH,

the acetate formation catalyzed by Ald2 and Ald6 generates the reducing equivalents NADH or NADPH, respectively (chapter 1.3).

By deleting the *ALD6*, the resulting strain could produce acetate in the cytosol only via the Ald2 and thus might accumulate more NADH. Respective strain JWY023 was constructed by Wess et al. (2019). The increased supply of NADH should benefit the GalOA-production based on AnGar1 [R267L] and AnGar1 [K261M, R267L]. The ability to produce GalOA was conferred to JWY023 via transformation with the linearized plasmids SiHV136 (*AnGATA, AnGAR1 [R267L]*), SiHV137 (*AnGATA, AnGAR1 [K261M, R267L]*) and SiHV158 (*AnGATA, AnGAR1$^{WT}$)* for genome integration, resulting in the strains SiHY064, SiHY065 and SiHY073, respectively. The consecutive fermentation in phosphate buffered SC-glucose medium supplemented with 5 g $L^{-1}$ GalA was started from a preculture performed in SC-glucose medium. The cell growth was monitored via photometric measurement and the GalOA-production and metabolite formation was analyzed via HPLC (Figure 3-22).

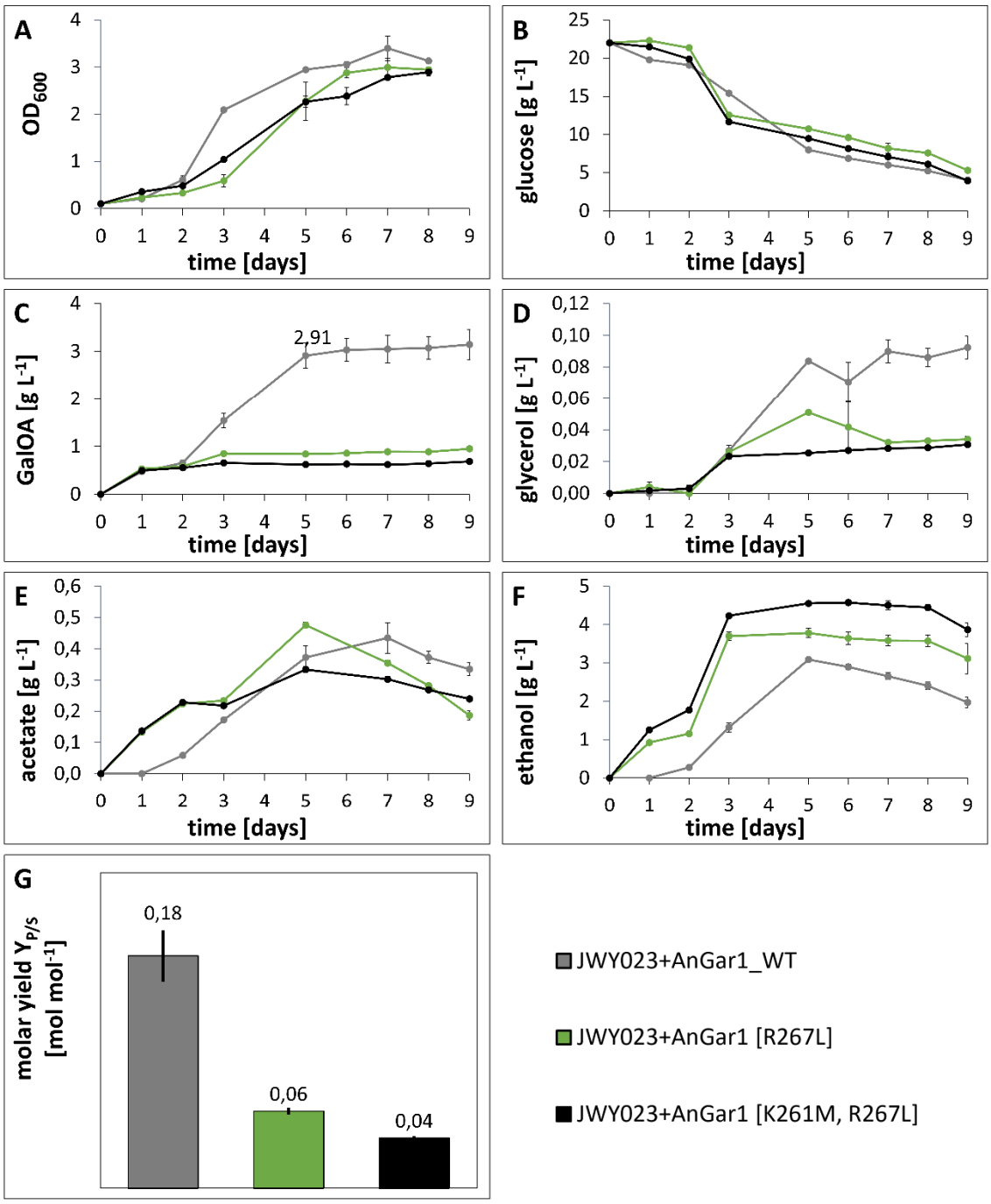


**Figure 3-22: The effect of the *ALD6* deletion on the GalOA-production.**
The GalA-reductase AnGar1$^{WT}$ and its NADH-dependent variants AnGar1 [R267L] and AnGar1 [K261M, R267L] were tested together with the transporter AnGatA in the strain JWY023, which is optimized for NADH-supply. Further, the acetate formation via the NADP$^+$-dependent Ald6 was blocked in JWY023 (Wess et al., 2019). (**A**) The cell growth was monitored via $OD_{600}$-measurement and the metabolite production was measured via HPLC, (**B**) glucose, (**C**) GalOA, (**D**) glycerol, (**E**) acetate and (**F**) ethanol. (**G**) From the GalOA-production and the glucose consumption, the molar yield as mol GalOA-produced per mol glucose consumed was calculated. Depicted are the mean values and standard deviations of biological triplicates of the respective measurements, the error bars may be smaller than the symbols.

The cells of the three strains expressing variants of the GalA-reductase from *A. niger* entered exponential growth phase after two days of cultivation. Even though half of the glucose still was present in the cultivation medium, the cell growth reached stationary phase after day 5 or 6 after inoculation. The cultivation resulted in a final cell density of $OD_{600}$=3 for all three strains, independent of the GalA-reductase expressed (Figure 3-22, A-B). Surprisingly, the mainly NADPH-dependent AnGar1$^{WT}$ produced much higher amounts of GalOA, than the engineered variants AnGar1 [R267L] and AnGar1 [K261M, R267L], which have a reduced or fully abolished capability of using NADPH (see chapter 3.3). AnGar1$^{WT}$ produced 2.91 g $L^{-1}$ GalOA by day 5 and 3.14 g $L^{-1}$ GalOA by the end of the cultivation (8 days), whereas the engineered enzymes AnGar1 [R267L] and AnGar1 [K261M, R267L] produced only 0.95 g $L^{-1}$ GalOA or 0.68 g $L^{-1}$ GalOA by the end of the cultivation (Figure 3-22, C). However, the comparison of the cell growth and the GalOA-production showed that 90% of the product formation already occurred within the first 5 days of the cultivation, the exponential growth phase, and nearly none during the stationary phase, notwithstanding ongoing glucose consumption. With values between 0.03 to 0.08 g $L^{-1}$, the production of glycerol was only low (Figure 3-22, D). Acetate formation was reduced compared to the strain harboring an intact *ALD6* gene (compare Figures 3-21, E and 3-22, E) and peaked in all three cultivations after 5 to 6 days with titers of 0.3 g $L^{-1}$ to 0.5 g $L^{-1}$ (Figure 3-22, E). In the cultures of the strains expressing the *AnGAR1 [R267L]* and *AnGAR1 [K261M, R267L]* higher ethanol formation of 3.5 to 4.5 g $L^{-1}$ was measured by day 9, whereas the ethanol production measured in the cultures of the strain expressing the *AnGAR1*$^{WT}$ peaked with 3 g $L^{-1}$ by day 5 and even decreased towards the end of the cultivation (Figure 3-22, F). From the produced GalOA and the consumed glucose, the molar yields of the fermentations were calculated. Compared to the mutated GalA-reductase variants, the molar yield indicated roughly 4 times higher process efficiency by deploying the AnGar1$^{WT}$ (Figure 3-22, G).

Overall, it was observed that the more the reductase preferred NADPH over NADH, the higher the measured titer of GalOA. Consequently, the AnGar1$^{WT}$ produced the outstanding GalOA-titer of approximately 3 g $L^{-1}$ after only 5 days of cultivation in the strain JWY023. Considering the AnGar1$^{WT}$ cofactor preference for NADPH, the question arises how the *ALD6* deletion boosted the NADPH accessibility. So far, this strain, called SiHY073, showed best production considering the process time and the GalOA-production in this study.

### 3.4.4 Characterization of Zwf1 and Pgi1 Enzyme Activity

The aldehyde dehydrogenase Ald6 generates NADPH by converting the glycolysis byproduct acetaldehyde to acetate and thereby is a major source for this cofactor. However, in foregoing chapter

the NADPH-dependent AnGar1$^{WT}$ showed strong increase in GalOA-production performance after the deletion of *ALD6* in the host strain. Consequently, in this strain, the oxidative pentose phosphate pathway might be upregulated as the only remaining NADPH-yielding pathway as a (over)compensatory mechanism to cope with the loss of the Ald6 activity. The flux through the pentose phosphate pathway is determined by the interplay of the enzymes Pgi1 and Zwf1. Both enzymes share the same substrate, glucose-6-phosphate, with the Pgi1 reaction favoring the glycolysis and the Zwf1 reaction providing entry into the pentose phosphate pathway (chapter 1.3.2).

To illuminate the effect of increased GalOA-production caused by a *ALD6* deletion, the enzyme activities of Pgi1 and Zwf1 were measured in an enzyme assay performed from crude cell extract. Therefore, the strains CEN.PK2-1C, SiHY072 *(Δadh1, Δgpd1, Δgpd2*, *AnGATA, AnGAR1$^{WT}$*) and SiHY073 (*Δald6, Δadh1, Δgpd1, Δgpd2 AnGATA, AnGAR1$^{WT}$*) were grown in YPD medium to an $OD_{600}$ between 1 and 2. The cells were disrupted and the crude cell extracts were used in the photometric enzyme assay as described in chapter 2.5.11. The measured enzyme velocities are illustrated in Figure 3-23.

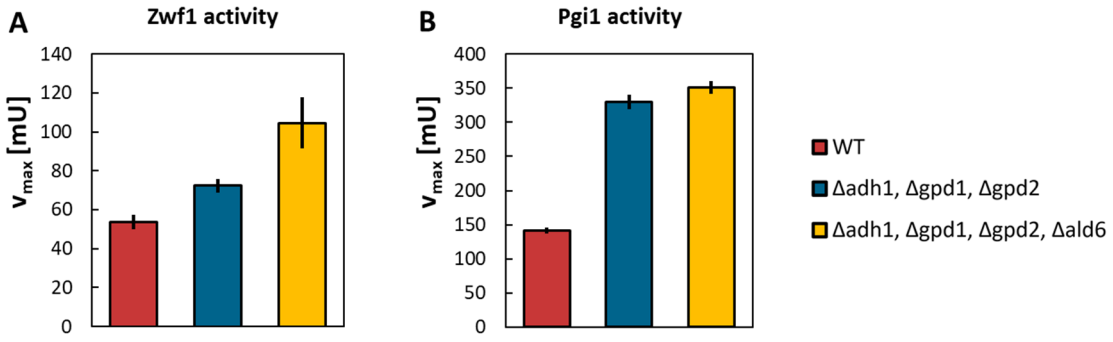


**Figure 3-23: Measurement of the Zwf1 and Pgi1 activity in strains with modulated metabolic branches of the glycolysis.**
To illuminate the effect of modulated metabolic branches of the glycolysis on the NADPH-generation through the pentose phosphate pathway, the enzyme activity of Zwf1 and Pgi1 were measured. The strains CEN.PK2-1C (WT), SiHY072 (*Δadh1, Δgpd1, Δgpd2*) and SiHY073 (*Δald6, Δadh1, Δgpd1, Δgpd2*) were tested. (**A**) The Zwf1 activity was measured directly by using glucose-6-phosphate and $NADP^+$. (**B**) The Pgi1 activity was measured indirectly. In a coupled enzyme assay fructose-6-phosphate was added as a substrate and the formation of glucose-6-phosphate was monitored by adding excessive glucose-6-phosphate dehydrogenase and $NADP^+$. Four technical replicates were measured per strain and enzyme. Depicted are the mean values and standard deviations of the respective measurements.

Compared to the WT strain background, the impairment of the glycolytic side branches for ethanol and glycerol formation (*Δadh1, Δgpd1, Δgpd2*) increased the activity of the Zwf1 to 135%. Interfering in the endogenous acetate formation by deleting *ALD6* further increased the Zwf1 activity, as the $v_{max}$ measured almost doubled compared to the WT (Figure 3-23, A). Furthermore, the Pgi1 activity was indirectly measured via its reversed reaction which is linked directly to the Zwf1. In case of the Pgi1, the enzyme activity increased to 230-250% compared to the WT by interfering in the

ethanol, glycerol and acetate formation. Thus, the additional impairment of the acetate formation had only a minor effect (Figure 3-23, B).

Overall, strong increase of the Zwf1 and Pgi1 activity was measured as a consequence of the performed genetic modifications. The increased activity of Zwf1 would be consistent with an enhanced production of NADPH via the oxidative pentose phosphate pathway. The elevated activity of Pgi1 does not necessarily contradict this scenario, as a bottleneck in the downstream glycolytic reactions (due to the abovementioned gene deletions) would also cause an accumulation of glucose-6-phosphate. The slow consumption of glucose (Fig. 3-22, B) supports this view.

### 3.4.5 Overexpression of the GalA-Reductase AnGar1 in the Strain SiHY073

Expressing heterologous genes in production hosts can be limited at various levels, such as transcription, translation or the stability and correct folding of the enzyme. All these obstacles influence the enzyme dose in the host cell and thereby affect the velocity of the favored heterologous enzymatic reaction, which can result in the limitation of the pathway efficiency. These bottlenecks often can be, at least partly, counterbalanced by a strong overexpression of the limiting enzyme. Thus, different approaches were tested to enhance the production of AnGar1 in yeast.

#### 3.4.5.1 *AnGAR1* Overexpression Based on the Backbone Vector SiHV005

To investigate the possible limitation of the AnGar1$^{WT}$ protein dose per cell, respective gene was overexpressed from a plasmid in the strain SiHY073, which was presented in foregoing chapter. Therefore, the plasmid SiHY079, carrying the *AnGAR1$^{WT}$* under the control of the *pPGK1* promoter, and its empty parent plasmid SiHV005 were transformed into the strain SiHY073 (*pCCW12-AnGATA-tPGK1, pPGK1-AnGAR1-tENO1*). The plasmids carried the endogenous *URA3*-expression cassette from *S. cerevisiae* for auxotrophic selection and plasmid maintenance. Consecutive plasmid strains were precultured in SC-glucose medium lacking uracil and shifted to phosphate buffered SC-glucose medium lacking uracil but supplemented with GalA. The cell growth was photometrically monitored and the sugar consumption and the metabolite production were analyzed via HPLC (Figure 3-24).

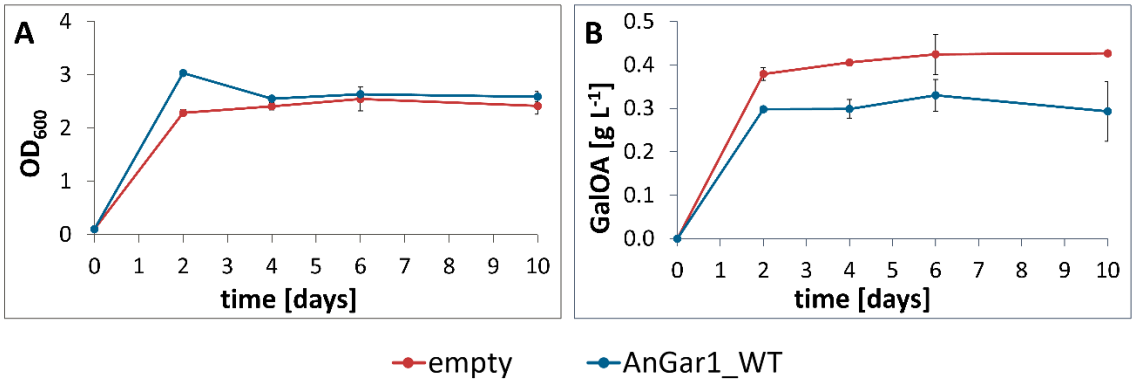


**Figure 3-24: Expression of *AnGAR1$^{WT}$* from the plasmid SiHV005 in SiHY073 causes a reduction of the GalOA-production.**
To investigate possible enzyme limitation in the strain SiHY073 (presented in chapter 3.4.3), the *AnGAR1$^{WT}$* was expressed from the plasmid SiHV005 carrying the endogenous *URA3* gene for plasmid maintenance. (**A**) The cell growth was monitored via $OD_{600}$-measurement and (**B**) the GalOA-production via HPLC. Depicted are the mean values and standard deviations of biological triplicates of the respective measurements; the error bars may be smaller than the symbols.

Over the time of cultivation, the yeast cells grew to an $OD_{600}$ of approximately 2.5 (Figure 3-24, A). Contrary to the hypothesis, the expression of the *AnGAR1$^{WT}$* from a multicopy plasmid did not result in GalOA-production higher than the empty vector control. In both fermentations the measured GalOA concentration was not higher than 0.4 g $L^{-1}$ (Figure 3-24, B), which was a strong decrease compared with the GalOA-production of SiHY073 without a plasmid of nearly 3 g $L^{-1}$ (presented in chapter 3.4.3).
Since the GalOA-production of SiHY073 collapsed due to plasmid transformation, the effect of the empty vector had to be further investigated.

### 3.4.5.2 Testing a Series of Empty Vector Controls

Foregoing chapter illustrated the serious effects of the plasmid transformation on the GalOA-production performance of the strain SiHY073.

To further investigate this effect, a series of empty vectors, carrying auxotrophic and dominant selection markers, were transformed into the strain SiHY073 and tested in a fermentation. The plasmids SiHV005, p426HXT7, p426MET25 and YEplac195, all with the *URA3*-marker, as well as the plasmids SiHV009 and pRS62 with the dominant ClonNAT-marker were transformed into the strain SiHY073, individually. The resulting plasmid strains were tested in a fermentation performed in phosphate buffered SC-glucose medium under consideration of the appropriate selection pressure

for plasmid maintenance. The cell growth was monitored via $OD_{600}$-measurements and the sugar consumption and the GalOA-production were analyzed via HPLC (Figure 3-25).

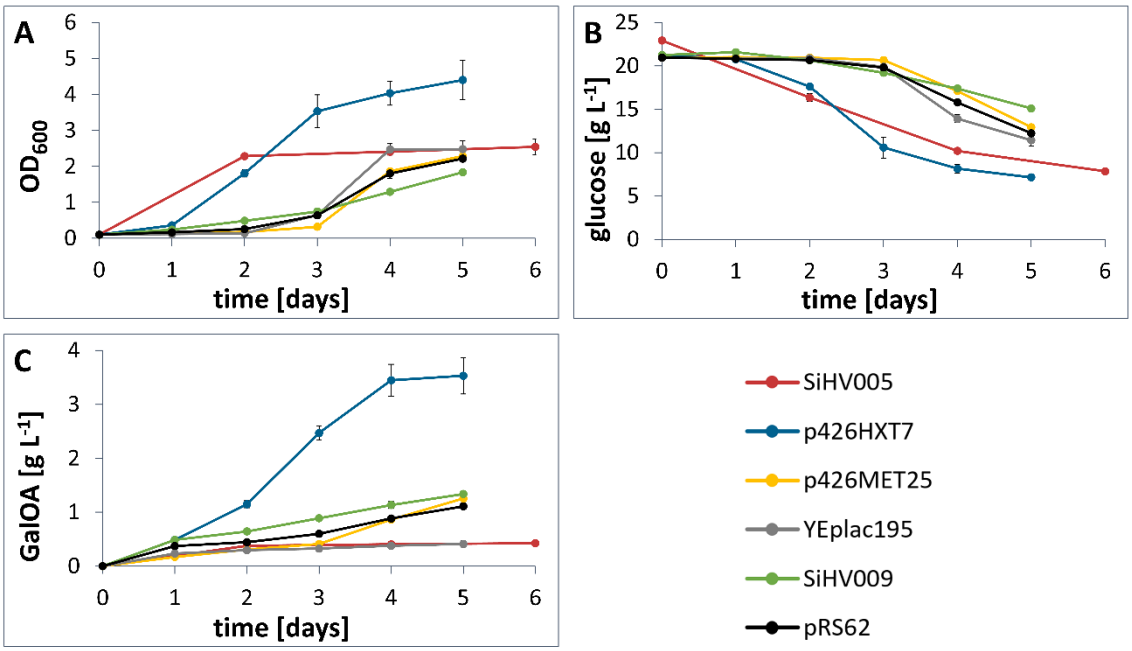


**Figure 3-25: GalOA-production in SiHY073 transformed with different empty vectors.**
The strain SiHY073 was transformed with a set of empty plasmids: SiHV005 (*URA3*), p426HXT7 (*URA3*), p426MET25 (*URA3*) and YEplac195 (*URA3*), as well as the plasmids SiHV009 (ClonNAT) and pRS62 (ClonNAT). The effect of these plasmids on the GalOA-production and the growth of the strain SiHY073 was studied in a fermentation. (**A**) The cell growth was monitored via $OD_{600}$-measurement and (**B**) the glucose consumption as well as (**C**) the GalOA-production was tracked via HPLC. Depicted are the mean values and standard deviations of biological triplicates of the respective measurements; the error bars may be smaller than the symbols.

The cell growth was monitored as general measure for the fitness of the yeast transformed with the plasmids tested. Cell growth of the plasmid strains SiHY073 transformed with SiHV005 or p426HXT7 started quickly after inoculation, while the same strain transformed with the plasmids p426MET25, YEplac195, SiHV009 and pRS62 entered the exponential growth phase only after 3 days of cultivation. Except the plasmid strain SiHY073 transformed with p426HXT7, which reached a final $OD_{600}$ of around 4, all other strains did not exceed an $OD_{600}$ of 2.5 after 5 or 6 days of cultivation (Figure 3-25, A). Glucose consumption was measured as soon as the growth started, so that the glucose consumption profile mirrored the growth profile of the strains. Thus, the strains showing strong growth also showed strong glucose consumption. In most of the fermentations roughly half of the glucose was consumed by the end of the fermentation (Figure 3-25, B). The HPLC-analysis showed that the titers of produced GalOA diverged for the different plasmid strains. The effect of the different empty plasmids on the GalOA-production performance of SiHY073 could be assigned to three groups of GalOA-productions of around 0.4 g $L^{-1}$ (SiHY005 and YEplac195), of around 1 g $L^{-1}$ (SiHY009, pRS62N and p426MET25) and 3.53 g $L^{-1}$ (p426HXT7) (Figure 3-25, C). Surprisingly, the production of the strain SiHY073 transformed with the plasmid p426HXT7 exceeded the production of

the same strain transformed with the p426MET25 plasmid, even though the plasmids differ only in the cloned promoter. The p426HXT7 carries the truncated *pHXT7* promoter (Hauf et al., 2000) and the p426MET25 carries the inducible *pMET25* promoter. On both empty plasmids, there is no ORF cloned between the promoter and the *tCYC1* terminator. Furthermore, compared to the GalOA-production performance of 2.91 g $L^{-1}$ of the strain SiHY073 without any plasmid transformed (chapter 3.4.3), the transformation of the strain SiHY073 with p426HXT7 caused an increase in GalOA-production of 20%.

Overall, great influence - positive or negative - of the transformed plasmid on the GalOA-production performance was observed.

### 3.4.5.3 Overexpression of *AnGAR1$^{WT}$* and Variants Based on p426HXT7

Foregoing chapter demonstrated that the drastic effect of the empty vector SiHV005 leading to a GalOA-production collapse in SiHY073 (presented in chapter 3.4.5.1) could be mitigated by using the empty plasmid p426HXT7.

Therefore, the plasmid p426HXT7 was subsequently used to overexpress the GalA-reductase gene in SiHY073. Furthermore, it was tested whether the AnGar1-variants, which predominantly use NADH for the GalA-reduction, can be harnessed to increase the GalOA-production titer. Hereby, it was aimed to distribute the burden of GalOA-production on the regeneration systems of both co-factors, NADH and NADPH. Therefore, the ORFs *AnGAR1$^{WT}$*, *AnGAR1 [R267L]* and *AnGAR1 [K261M, R267L]* were cloned on the parent plasmid p426HXT7. The consecutive plasmids SiHV221 (*pHXT7t-AnGAR1$^{WT}$-tCYC1*), SiHV222 (*pHXT7t-AnGAR1 [R267L]-tCYC1*) and SiHV223 (*pHXT7t-AnGAR1 [K261M, R267L]-tCYC1*) were transformed into SiHY073 and tested in a fermentation. The fermentation was performed in phosphate buffered SC-medium lacking uracil and supplemented with 5 g $L^{-1}$ GalA and 20 g $L^{-1}$ glucose. The preculture was performed in SC-glucose medium lacking uracil. During the cultivation, the cell growth was monitored photometrically by $OD_{600}$-measurements and the medium composition and GalOA-production was measured via HPLC-analysis (Figure 3-26).

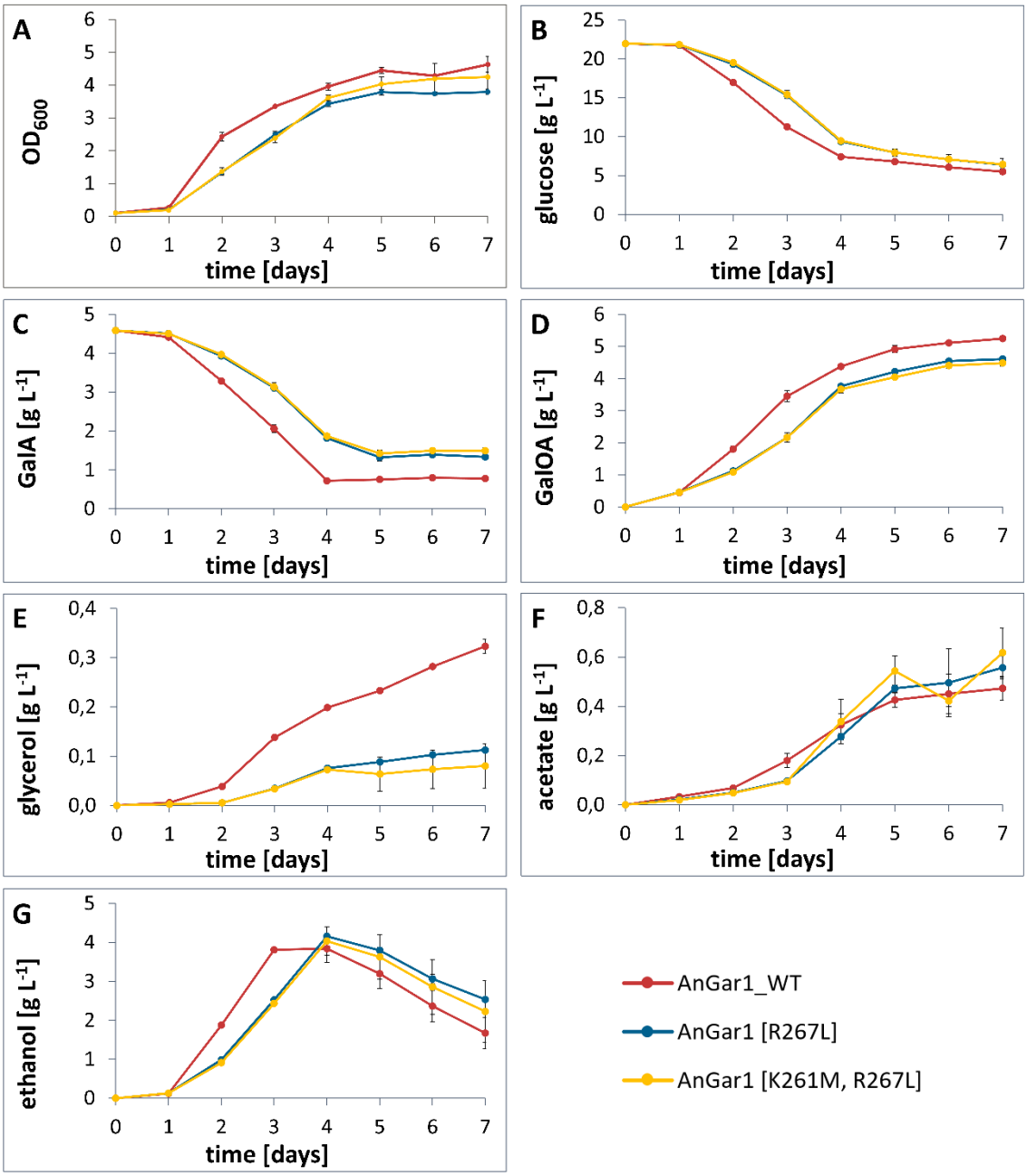


**Figure 3-26: Overexpression study of the genes of the GalA-reductase variants AnGar1$^{WT}$, AnGar1 [R267L] and AnGar1 [K261M, R267L] in SiHY073 using the p426HXT7 vector.**
To improve the GalOA-production in SiHY073, the AnGar1$^{WT}$, AnGar1 [R267L] and AnGar1 [K261M, R267L] coding genes were overexpressed from the parent plasmid p426HXT7. (**A**) The cell growth was monitored by photometrical measurement of the $OD_{600}$ and the metabolic performance was analyzed using HPLC, as the concentrations of (**B**) glucose, (**C**) GalA, (**D**) GalOA, (**E**) glycerol, (**F**) acetate and (**G**) ethanol were measured. The fermentation was conducted in phosphate buffered SC medium supplemented with 5 g $L^{-1}$ GalA and 20 g $L^{-1}$ glucose. Depicted are the mean values and standard deviations of biological triplicates of the respective measurements; the error bars may be smaller than the symbols.

Slightly better growth was observed in the culture of the SiHY073 with improved *AnGAR1$^{WT}$* expression, as it entered exponential phase before the cultures of the same strain with improved *AnGAR1 [R267L]* and *AnGAR1 [K261M, R267L]* expression. All cultivations reached a final $OD_{600}$ of around 4 (Figure 3-26, A) and showed sturdy glucose consumption until day 4 of the cultivation. However,

roughly 6 g $L^{-1}$ glucose remained in the cultures by the end of the fermentation (Figure 3-26, B). The HPLC-analysis revealed strong GalA-consumption in all three experimental setups, with only 1-1.5 g $L^{-1}$ GalA remaining unused after completion of the biotransformation (Figure 3-26, C). Concomitantly, the GalOA-values measured in the cultivations increased with the decrease in GalA. While the strain SiHY073 overexpressing the *AnGAR1 [R267L]* and *AnGAR1 [K261M, R267L]* already produced around 4 g $L^{-1}$ GalOA, the overexpression of the *AnGAR1$^{WT}$* in SiHY073 even led GalOA-production of 5.25 g $L^{-1}$. In all cultivations, the GalOA-production was strong until day 4 of the cultivation. However, GalOA amounts can be easily overestimated due to overlap with GalA peaks in the HPLC chromatograms (Figure 3-26, D). Furthermore, the metabolites acetate, glycerol and ethanol were monitored over the time of the cultivation. Within the experiment, the overexpression of the GalA-reductases had only slight influence on the formation of acetate and ethanol, which resulted in acetate values of around 0.5 g $L^{-1}$ after 7 days of cultivation and ethanol values of around 4 g $L^{-1}$ after 4 days of cultivation. The produced ethanol was steadily consumed after its values peaked on day 4 in all cultures (Figure 3-26, F-G). In contrast to the overexpressed mutants, the overexpression of the *AnGAR1$^{WT}$* caused in the strain 3 times higher glycerol production of 0.3 g $L^{-1}$ than the overexpression of the *AnGAR1*-variants (Figure 3-26, E).

Overall, the production of GalOA was strongly increased in SiHY073 by overexpressing the GalA-reductase variant genes compared with the results from SiHY073 without a plasmid (2.91 g $L^{-1}$, see chapter 3.4.3) and SiHY073 transformed with the parent plasmid p426HXT7 (3.53 g $L^{-1}$, see chapter 3.4.5.2). Unfortunately, roughly a quarter of the supplemented glucose remained in the fermentation broth, and therefore subsequent experiments targeted an improvement in the utilization of this substrate.

#### 3.4.5.4 Overexpression of *AnGAR1$^{WT}$* and variants Based on p426HXT7 in Medium of Decreased Glucose Supplementation

Foregoing chapter demonstrated the successful increase of the GalOA-production of the strain SiHY073 by overexpressing the *AnGAR1$^{WT}$* and variants. However, even by the end of the fermentation, a large proportion of the supplemented glucose remained unused in the fermentation broth. Excess glucose in the fermentation broth aggravates the cost efficiency of the entire process.

To improve the cost efficiency of the process, the GalOA-production performance of the strain SiHY073 overexpressing the *AnGAR1$^{WT}$* and variants was investigated in culture medium with decreased glucose supplementation. The plasmids SiHV221 (*pHXT7t-AnGAR1$^{WT}$-tCYC1*), SiHV222

(*pHXT7t-AnGAR1 [R267L]-tCYC1*) and SiHV223 (*pHXT7t-AnGAR1 [K261M, R267L]-tCYC1*) were transformed into SiHY073 and tested in a fermentation performed in phosphate buffered SC-medium lacking uracil and supplemented with 5 g $L^{-1}$ GalA and only 12.5 g $L^{-1}$ glucose. The preculture was performed in SC-glucose medium lacking uracil. The cell growth was monitored via $OD_{600}$-measurement and the GalOA-production was measured via HPLC-analysis (Figure 3-27).

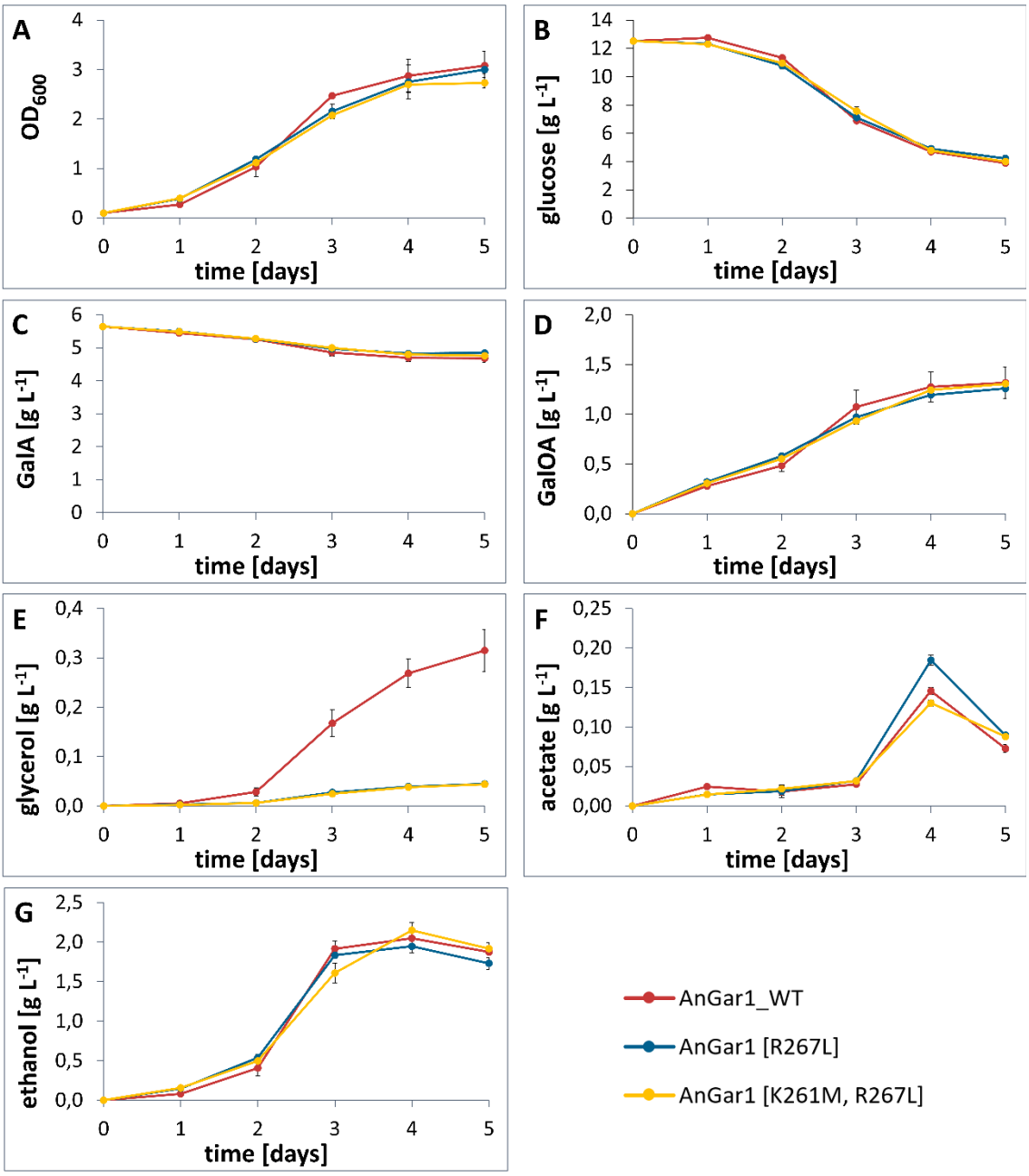


**Figure 3-27: Overexpression study of the genes of the GalA-reductases AnGar1$^{WT}$, AnGar1 [R267L] and AnGar1 [K261M, R267L] in SiHY073 using p426HXT7 as parent plasmid in SC medium with reduced glucose content.**

To improve the GalOA-production in SiHY073, the AnGar1$^{WT}$, AnGar1 [R267L] and AnGar1 [K261M, R267L] coding genes were overexpressed from the parent plasmid p426HXT7. (**A**) The cell growth was monitored by photometrical measurement of the $OD_{600}$ and the metabolic performance was analyzed using HPLC, as the concentrations of (**B**) glucose, (**C**) GalA, (**D**) GalOA, (**E**) glycerol, (**F**) acetate and (**G**) ethanol were measured. Since the glucose consumption was incomplete in previous fermentations, this fermentation was conducted in phosphate buffered SC medium supplemented with 5 g $L^{-1}$ GalA and only 12.5 g $L^{-1}$ glucose. Depicted are the mean values and standard deviations of biological triplicates of the respective measurements; the error bars may be smaller than the symbols.

The expression of the genes of the GalA-reductases AnGar1$^{WT}$, AnGar1 [R267L] and AnGar1 [K261M, R267L] in the strain SiHY073 resulted in a similar growth phenotype, the cultures reached a final $OD_{600}$ of approx. 3 (Figure 3-27, A). The cultures were supplemented with 12.5 g $L^{-1}$ glucose of which

around 4 g $L^{-1}$ remained in the fermentation broth by the end of the cultivation, which equals roughly a quarter of the start concentration (Figure 3-27, B). The HPLC-analysis showed only minor differences between the three strains in GalA-consumption, GalOA-production, acetate- and ethanol formation (Figure 3-27, C-D, F-G). Hereby, the production of roughly 1.3 g $L^{-1}$ GalOA was measured in all three strains. However, the overexpression of *AnGAR1$^{WT}$* in the strain SiHY073 caused increased glycerol production of 0.3 g $L^{-1}$ compared to the overexpression of *AnGAR1 [R267L]* and *AnGAR1 [K261M, R267L]* in the same strain, which meant an enhancement by a factor of 3 (Figure 3-27, E). This effect is consistent with the results shown in Figure 3-26, E.

Even though this experiment was performed in medium with reduced glucose content, roughly a quarter of the glucose remained in the fermentation broth by the end of the fermentation. This phenomenon was already shown when the glucose supplementation was twice as high. Combined with the results illustrated in foregoing chapter, the outstanding impact of the glucose supplementation was demonstrated, when halved glucose concentration in the cultivation medium caused the GalOA-titer to decrease by a factor of 4.

## 3.5 Further Investigation and Optimization of the Production Performance of the Strain SiHY073

In foregoing chapter, the NADH-utilizing GalA-reductase variants AnGar1 [R267L] and AnGar1 [K261M, R267L] from chapter 3.3 were successfully installed in the strain JWY019, which was streamlined for NADH-regeneration in glucose-containing media (Wess et al., 2019). Slow glucose metabolism and the concurrent knockout of the NADH-consuming reactions caused the production of 0.84 g $L^{-1}$ GalOA on glucose (chapter 3.4.2). To favor NADH-generation the gene of the $NADP^+$-dependent acetaldehyde dehydrogenase Ald6 was deleted. Surprisingly, this deletion substantially increased the GalOA-production performed by the reductase AnGar1$^{WT}$. Considering the NADPH-specificity of this enzyme demonstrated in chapter 3.3.2 this effect is presumably due to a vast boost in NADPH-generation.

Due to the great production performance of approximately 3 g $L^{-1}$ after only 5 days of cultivation (chapter 3.4.3), further engineering approaches and applications were tested in the strain SiHY073.

### 3.5.1 Biotransformation of GalA in a High Cell Density Fermentation

Great production performance was observed for the strain SiHY073, in which the glucose metabolism is slowed down and the gene encoding the acetaldehyde dehydrogenase Ald6 is knocked out. The process of biotransformations can be separated in two processes: i) generation of the biomass, ii) biotransformation of the substrate. Through the decoupled process strategy, the cells can be grown and then used in the respective process, whereby possible toxic effects can be evaded.

The production performance of the strain SiHY073 was tested in a high $OD_{600}$ approach, where cell growth and GalOA-production were decoupled. Therefore, the strain was cultivated in SC-glucose medium and shifted to a phosphate buffered SC-glucose culture supplemented with GalA with a starting cell density of $OD_{600}$ 5 and 10. Further cell growth and metabolite concentrations were recorded via photometric measurement and HPLC-analysis, respectively (Figure 3-28).

The cell density of the high $OD_{600}$-fermentations increased right after the medium was renewed, but the overall increase in cell density was low (Figure 3-28, A). Expectedly, the glucose consumption rate correlated with the cell density of the inoculum (Figure 3-28, B). A similar observation was made examining GalA-conversion to GalOA, which strongly increased with the cell density in the culture. Although the measured GalOA titers are overestimated due to overlapping peaks in the HPLC chromatogram, the experiment clearly shows that the productivity of the process can be increased with a higher inoculum of the fermentation. (Figure 3-28, C-D). Excluding acetate, the production of the typical fermentation byproducts of a yeast cultivation, glycerol and ethanol, increased with the total amount of cells in the fermentation broth. The acetate formation in both high cell density fermentations was similar and peaked around 0.5 g $L^{-1}$ on day 3 of the cultivation (Figure 3-28, E-G).
Overall, this study demonstrated the striking impact of the cell number in the fermentation broth on the cultivation parameters product titer and process time.

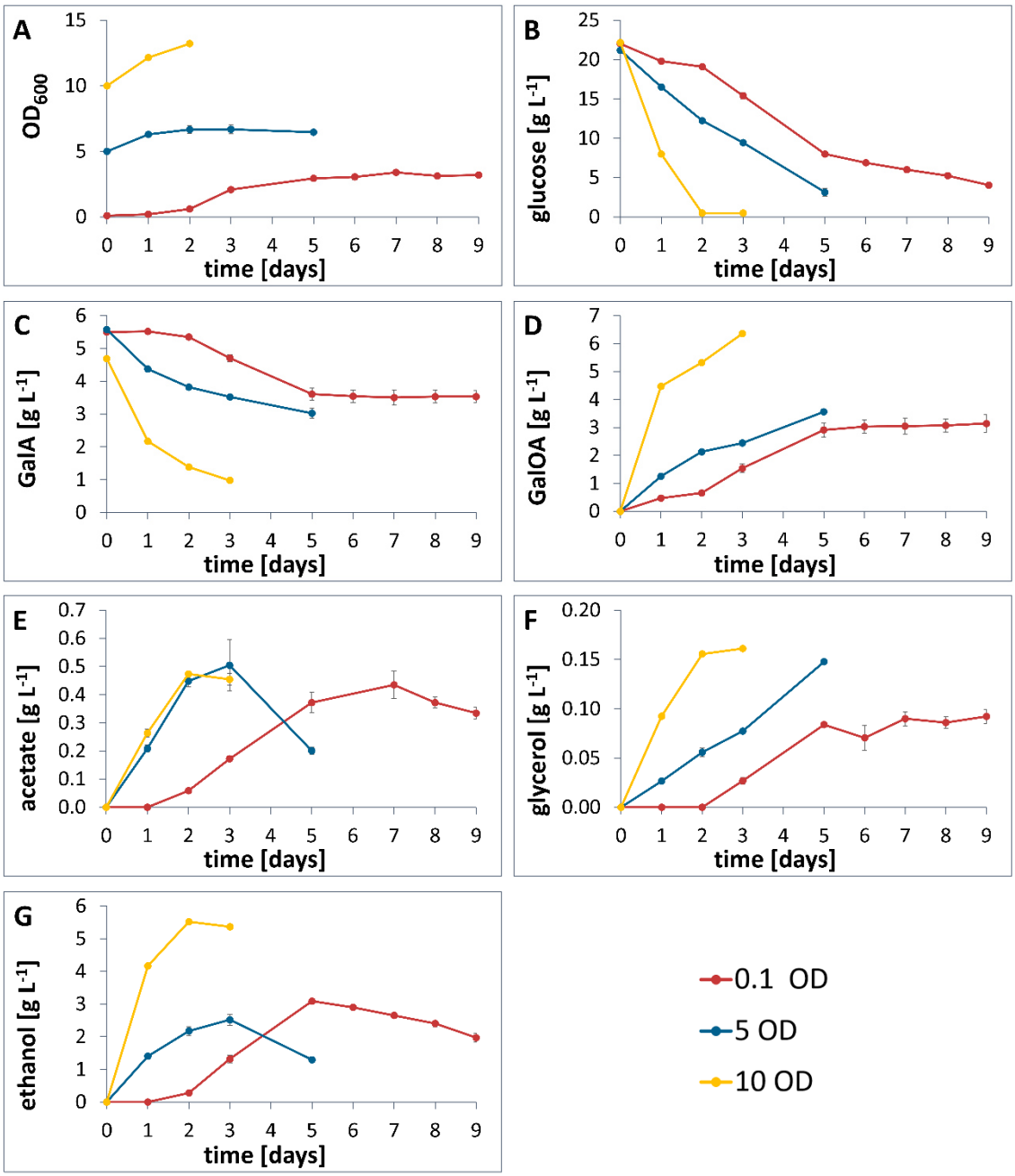


**Figure 3-28: High cell density fermentation and comparison with low cell density-fermentation of the strain SiHY073.**

The benefit of high cell density fermentations on the production performance of the strain SiHY073 was tested. The preculture of the strain was grown in SC-glucose medium and the main culture was started with an $OD_{600}$ of 0.1 (red), 5 (blue) and 10 (yellow) in phosphate buffered SC-glucose culture supplemented with GalA. (**A**) Further cell growth and the HPLC-analysis for (**B**) glucose, (**C**) GalA, (**D**) GalOA, (**E**) acetate, (**F**) glycerol and (**G**) ethanol was monitored. For comparative reasons the results from Figure 3-22 are shown again (red). Depicted are the mean values and standard deviations of biological triplicates of the respective measurements, the error bars may be smaller than the symbols.

### 3.5.2 Favoring GalA-Biotransformation by Slowing down Glucose Metabolism

Glucose is one of the most prominent sugars to be utilized by microbes, hence the glucose metabolism is highly energy efficient and fast compared to other fermentable sugars. In foregoing chapters, it was demonstrated that slow core metabolism often had beneficial effect on the GalOA-production, which was remarkably demonstrated with the strain SiHY001 on sorbitol (chapter 3.2.1), a slowly consumed carbon source, and with the strain SiHY073 on glucose (chapter 3.4.3). A probable reason is an extension of the phase, in which NAD(P)H can be derived from the metabolism of the co-substrate. The abovementioned SiHY073 is based on the strain JWY023, which contains multiple deletions to tailor its metabolism for isobutanol production. While some of these block competing pathways only specific for isobutanol production, others affect the recycling system of the redox cofactor pairs NAD(H) and NADP(H) and therefore are more likely to contribute to the success of SiHY073 to reduce GalA. Therefore, this chapter aims to investigate the underlying molecular mechanism by reverse engineering a strain, which excludes isobutanol specific modifications form the consideration. Instead, the focus lays on the genes *ALD6*, *GPD2*, *ADH1* and *ECM31.* Among these, *ALD6* in particular qualifies as a potential engineering target, as the corresponding deletion strain demonstrated vast production increase in chapter 3.4.3, Figure 3-22. Further investigations focus on the glycerol and ethanol formation, which are prominent branches of the core metabolism of *S. cerevisiae* and thus are strongly involved in the NAD(H)-metabolism. In the study of Wess et al. (2019), *ECM31* was deleted, because its gene product competes with the isobutanol production over an important intermediate to produce a precursor of pantothenate. However, one of the consecutive reactions downstream of the Ecm31 catalyzed step requires NADPH and therefore respective deletion might be of indirect effect on the NADP(H)-pool. Further isobutanol specific modifications from Wess et al. (2019), namely *Δilv1, Δilv2, Δbdh1, Δbdh2, Δleu4* and *Δleu9*, were considered of low relevance for the following reverse engineering approach.

To reverse engineer a redox cofactor recycling like that of JWY023 in a *S. cerevisiae* strain, the genes *ALD6*, *GPD2*, *ADH1* and *ECM31* were deleted in a stepwise manner as they partake to the redox cofactor recycling. Several new deletion strains were constructed for this study. The *ALD6* deletion was constructed using the CRISPR/Cas9-plasmid VSV111 and the DNA oligomers VSP390 and JWP092 as donor DNA for homologous recombination and the *GPD2* deletion was constructed using the CRISPR/Cas9-plasmid pRCCK_GD01 and the DNA oligomers JWP061 and JWP062 as donor DNA for homologous recombination. Consecutively, the *ADH1* and *ECM31* deletions were constructed using the CRISPR/Cas9-plasmids FWV100 and JWV03 and the DNA oligomer pairs SiHP370/SiHP371 and WGP518/JWP005 as donor DNA for homologous recombination, respec-

tively. The deletions were verified by running an analytical PCR. The consecutive strains were transformed with the linearized plasmid SiHV158, carrying expression cassettes for *AnGATA* and *AnGAR1*$^{WT}$. The GalOA-production of the novel strains SiHY080 (*Δald6*), SiHY095 (*Δald6, Δgpd2*), SiHY105 (*Δald6, Δgpd2, Δadh1*) and SiHY115 (*Δald6, Δgpd2, Δadh1, Δecm31*) were compared to the reference strain SiHY057 (CEN.PK2-1C background). The fermentations were performed in phosphate buffered SC-glucose medium supplemented with 5 g $L^{-1}$ GalA. The cell growth was monitored by $OD_{600}$-measurement and the chemical composition was analyzed via HPLC (Figure 3-29).

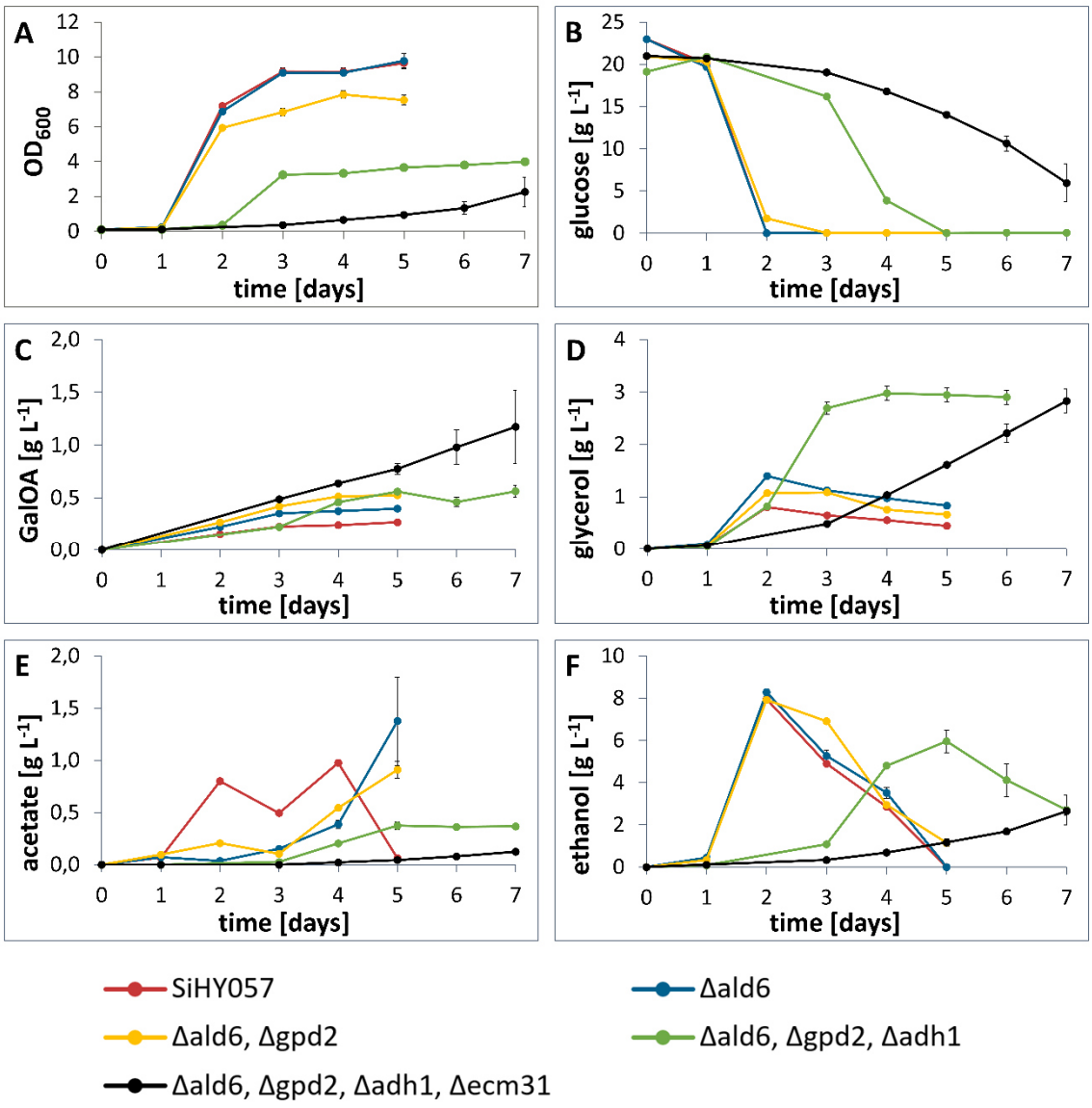


**Figure 3-29: Slowing down the glucose metabolism to favor GalOA-production on glucose.**
The genes of various enzymes involved in the core metabolism around glucose were deleted. The effect on NADPH-accessibility and thus GalOA-production was examined in these strains. (**A**) The increase in cell density was monitored via $OD_{600}$-measurement and the medium constituents (**B**) glucose, (**C**) GalOA, (**D**) glycerol, (**E**) acetate and (**F**) ethanol were analyzed via HPLC. Depicted are the mean values and standard deviations of biological triplicates of the respective measurements, the error bars may be smaller than the symbols.

The deletion of the *ALD6* did not affect the growth behavior nor the glucose consumption compared to the strain SiHY057, unfortunately also the production of GalOA was similar, as the product titer only increased slightly (Figure 3-29, C). The *Δald6*-strain showed minor increased glycerol production, which often is a cellular response to excess NADH in the cell (Figure 3-29, D). To further slow down the core metabolism of the cell, the glycerol formation was reduced by deleting *GPD2* the gene of one of the glycerol-3-phosphate dehydrogenases, which are the key enzymes of the glycerol formation. However, only the additional deletion of the alcohol dehydrogenase gene *ADH1* majorly slowed the glucose consumption (Figure 3-29, B), but concomitantly caused an increase in glycerol formation (Figure 3-29, D), most likely due to the NADH-excess that had just been triggered and the gene product of the remaining *GPD1*. Finally, the additional deletion of the *ECM31* showed a major effect on the consumption of glucose and the formation of glycerol, acetate and ethanol (Figure 3-29, B, D-F), which most likely is due to the overall low growth performance (Figure 3-29, A). Interestingly, this strain showed the highest GalOA-production of approx. 1 g $L^{-1}$ throughout the recorded fermentation time (Figure 3-29, C). Noteworthy, in this strain the biomass generation from glucose is very low, instead the glycerol formation was increased compared to the wildtype strain (Figure 3-29, A-B, D).

Overall, this study demonstrated that modifying the common branches of the glucose metabolism, the formation of acetate, glycerol and ethanol caused by the deletion *Δald6, Δgpd2* and *Δadh1* could enhance the GalOA-production on glucose. Additional increase of the GalOA-production was achieved by deleting the *ECM31*. However, the progressing steps of modification resulted in severely perturbed cell growth and vast glycerol production. Furthermore, the drastic effect of the *ALD6* deletion on the GalOA-production demonstrated in chapter 3.4.3, Figure 3-22 could only partially be reproduced especially only in combination with the other modifications tested.

# 4 Discussion

In Europe, the production of sugar for food industry is mainly based on sugar beet refineries, which produce large quantities of sugar waste streams rich in pectin. As one of the major compounds of these sugar waste streams, the potential of the abundant pectin-monomer GalA as second-generation feedstock is highly underused. So far, GalA is only used to feed cattle or is simply burnt. Establishing a value adding process on this waste sugar stream, especially on GalA, is of high interest for industry. The compound GalOA, which can be generated from GalA by one reducing step, is a potential product. Due to its high similarity to L-gluconate, which is already used as preservative, moisturizer, leavening agent, slow acidifier and pH-stabilizer, GalOA can possibly be used in similar applications (Faich and Strobos, 1999; Ishikawa et al., 2008; Sawyer, 1964).

*S. cerevisiae* qualifies as promising production host for this process since it is well-understood and already a common host for industrial processes. To pave the way for the biotransformation of GalA, certain obstacles must be overcome. Since GalA is no natural substrate for *S. cerevisiae*, its uptake and reduction have to be conferred to this yeast. However, as example for GalA metabolism in a yeast, it was found, that the basidiomycete yeast *Rhodosporidium toruloides* is capable to efficiently consume GalA (Protzko et al., 2019). Filamentous fungi as prominent decomposers in nature are known to degrade complex biomatter; thus, the GalA-transporter AnGatA (Benz et al., 2014; Sloothaak et al., 2014) and the GalA-reductases AnGar1 (Harth et al., 2020; Hilditch, 2010) and TrGar1 (Kuivanen et al., 2012) were found in *A. niger* and *H. jecorina* (formerly known as *Trichoderma reesei*), respectively. By heterologously expressing respective genes in *S. cerevisiae* and by streamlining its metabolism to meet the requirements of the GalA-reduction, in this work an attempt is made to develop a process for GalOA-production.

## 4.1 Establishing GalOA-Production in Yeast by Heterologous Expression of a GalA-Transporter and a GalA-Reductase

In general, sugars like glucose are relatively bulky hydrophilic molecules, which cannot pass the cell membrane simply by diffusion. Thus, for most living organisms and cells, *S. cerevisiae* included, sugar uptake is essential for growth and cell maintenance. Therefore, yeast evolved a versatile set of transporters for substrates it naturally consumes, especially for the hexose glucose (Gamo et al., 1995; Heredia et al., 1968). However, no GalA-specific transporter has been described in *S. cerevisae* to date. Even though GalA is no natural substrate for yeast, it was reported by Protzko et al. (2018) that GalA can be taken up in medium of low extracellular pH (below the $pK_a$=3.51 of GalA (Kohn and Kovác, 1978)). Since no saturation was observed, the authors suggested that GalA is

taken up in its protonated form by a channel-type system. Furthermore, it was suggested that the nearly pH-neutral cytoplasm of yeasts acts like a trap for the GalA, as the sugar acid would rapidly dissociate after entering the cell, thereby acidifying the cytosol. This effect is also known as weak acid stress (Piper et al., 2001). The dissociated GalA is negatively charged and thus hindered to leave the cell (Huisjes et al., 2012a; Souffriau et al., 2012). Since evidence was delivered that GalA enters the cell via the Gal2 permease in its protonated form and that this transport is competitively inhibited by glucose, this means an obstacle for later glucose based fermentations (Huisjes et al., 2012a; Protzko et al., 2018). However, Souffriau et al. in 2012 reported that a *Δgal2* strain still was capable to take up GalA sufficiently, suggesting the existence of an alternative transport mechanism. Furthermore, it was reported that at low pH the GalA severely affects the uptake of the hexose galactose and the pentoses xylose and arabinose, which are taken up by Gal2. Only glucose uptake, which is facilitated through other hexose transporters showed no transport inhibition (Huisjes et al., 2012a). Due to the inability to take up GalA in presence of glucose and the inhibiting effect of GalA on the uptake of galactose, xylose and arabinose, which are natural constituents of hydrolysates from pectin-rich feedstocks, facilitating Gal2 is unsuitable for the aimed application in this study. However, the specific GalA-transporters NcGat1 and AnGatA from the filamentous fungi *Neurospora crassa* and *A. niger*, respectively, are capable to transport GalA also in its dissociated form, enabling individual GalA-uptake and potentially its co-fermentation with other sugars. Previous studies showed that heterologous expressions of these transporters confer GalA-uptake in *S. cerevisiae* even in presence of glucose (Benz et al., 2014; Protzko et al., 2018). Once the GalA is taken up, it can be reduced to GalOA by a suitable reductase. In nature, the NADPH-dependent reductases AnGar1 (Harth et al., 2020; Hilditch, 2010) and TrGar1 (Kuivanen et al., 2012) were found in filamentous fungi.

In this work, the fungal genes *AnGATA* and *AnGAR1* were heterologously expressed in *S. cerevisiae* to confer GalOA-production resulting in a product titer of 0.27 g $L^{-1}$ after 5 days of cultivation. Given that in this experiment 5 g $L^{-1}$ of GalA were supplemented to the medium, this means vast room for optimization (chapter 3.1.2). To fuel cell growth and energy metabolism, the fermentation was performed in the presence of glucose. Since the glucose metabolism strongly relies on NADH-generation, this result can be explained by the strong NADPH-specificity of the GalA reductase. This experiment raises the presumption that not only expressing heterologous enzymes but also streamlining the hosts metabolism is necessary to meet the requirements of a high-scale production process. This observation is supported by the study of Matsubara et al., 2016, which presented first approaches to fermentatively produce GalOA in yeasts by deploying the NADPH-dependent GalA-reductase CdGar1 from *Cryptococcus diffluens* combined with the native capability of yeasts to take up GalA. The study of Matsubara drew the conclusion that a sturdy NADPH-regeneration system is

essential to produce higher amounts of GalOA from pectic wastes. Since also the AnGar1 utilizes the cofactor NADPH, efficient production of GalOA requires increased generation of this cofactor to replenish the consumed NADPH and to close the redox cycle within the yeast metabolism.

## 4.2 Boosting the GalOA-Production on Glucose by Strengthening the Pentose Phosphate Pathway on the Level of Transcription

The predominant source of NADPH in *S. cerevisiae* is the (oxidative) pentose phosphate pathway (PPP), which branches off from glycolysis at the glucose-6-phosphate (G6P) node and furthermore generates NADPH in the reactions of the glucose-6-phosphate dehydrogenase Zwf1 and the 6-phosphogluconate dehydrogenases Gnd1/2. Therefore, every glucose molecule fluxing through the PPP fuels the pool of NADPH rather than NADH, which is generated in the glycolysis. Certain studies showed the beneficial effect of a strengthened PPP on NADPH-dependent metabolic reactions. For instance, Zhao et al. in 2015 showed how the overexpression of *ZWF1* increased the production yield of β-carotene in yeasts, as the carotenoid pathway relays on NADPH as key cofactor in multiple reaction steps. By plasmid-based overexpression of the *ZWF1* in a β-carotene producing yeast, the final production yield was increased by roughly 20%. To indirectly strengthen Zwf1 activity, modulating *PGI1* expression became a prominent target for metabolic engineering, since its decreased activity accumulates G6P and therefore might affect the efficiency of the Zwf1 catalyzed reaction step. Hence, the modulation of the competitor reaction performed by *PGI1* deletion or down regulation of its gene was studied extensively. *Δpgi1* strains often showed increased NADPH-supply and therefore became a common tool to boost metabolite production in various organisms, e.g., in the industrially well used bacteria *Corynebacterium glutamicum* (Smith et al., 2010) and *E. coli* (Charusanti et al., 2010). However, in *S. cerevisiae* the deletion of the respective gene severely compromises the growth in high glucose medium and thus is not applicable in metabolic engineering (Aguilera, 1986). To alleviate the growth phenotype associated with the deletion *Δpgi1*, Yu et al. in 2018 presented a strategy which included only the down regulation instead of the deletion of the phosphoglucose isomerase gene. Therefore, they replaced the endogenous promoter *pPGI1* with the relatively weak promoter *pCOX9* to drive reduced *PGI1* expression. The promoter *pCOX9* was reported to show only 15% of the activity of the native *pPGI1* (Keren et al., 2013). Indeed, the promoter replacement decreased the Pgi1 activity, as measured by Wernig et al. (2021). According to the hypothesis of increased NADPH-supply, this strategy increased the production of free fatty acids in *S. cerevisiae* by roughly 25% in their study (Yu et al., 2018).

In this work, this strategy was transferred to the GalOA-production. Following the strategy of Yu et al., 2018, the relatively weak *pCOX9* was cloned in front of the *PGI1*. Moreover, replacing the endogenous *pZWF1* promoter with the constitutively active variant of the *pHXT7t* promoter (Hauf et al., 2000) resulted in increased Zwf1 activity as reported by Wernig et al. in 2021. Novel strains with modulated PPP-flux were tested in a fermentation (Figure 3-3). According to the expectation, the strain exhibiting decreased *PGI1* expression produced more GalOA in the fermentation, showing that the NADPH-supply was limiting. As already demonstrated by Wernig et al. (2021), the increased Zwf1 activity boosted the production of GalOA as well. Furthermore, the combination of *ZWF1* and *PGI1* modulation in one strain resulted in the highest titer among the tested strains. This indicates a combinatorial effect of accumulated G6P by decreased Pgi1 activity and therefore higher substrate supply for a thus more effective Zwf1.

Overall, the acetate formations peak in all modulated strains compared to the wildtype background strain. *S. cerevisiae* owns two aldehyde dehydrogenases, Ald6 and Ald2, which utilize $NADP^+$ or $NAD^+$, respectively. The *ALD6* is regulated by the transcription factor Stb5. In general, Stb5 is known to be involved in the regulation of NADPH-generation, however it does not recognize the *pZWF1* (Ouyang et al., 2018). This transcription factor is involved in the upregulation of the PPP genes *SOL3, GND1/2, RKI1* and *TAL1*, the gene *ALD6* and the gene *YEF1* coding for the cytosolic NADH-kinase *YEF1* (Bergman et al., 2019; Larochelle et al., 2006). Given that NADPH plays a crucial role in the oxidative defense mechanisms (Juhnke et al., 1996), it is plausible that Stb5 itself is induced by oxidative stress (Larochelle et al., 2006). While in laboratory experiments, oxidative stress can easily be imitated by adding chemicals, e.g., diamide and menadione to the cells. Here the production of GalOA might cause similar cell response, since the reduction of GalA is a massive sink for NADPH and therefore harshly decreases its intracellular level, the *STB5* expression possibly is induced. If this applies, this could serve as explanation for the increased acetate formation in the modulated strains, thus produced by the Ald6. Moreover, the increased glycerol formation also observed for the modulated strains could be an indicator for the oxidative stress of the cells, as glycerol formation is a common response to oxidative stress in yeasts (Påhlman et al., 2001).

Although the strategy to modulate the enzyme activities of Pgi1 and Zwf1 successfully increased the GalOA-titer, the produced amount of 0.38 g $L^{-1}$ GalOA still leaves vast room for optimization, since 5 g $L^{-1}$ GalA was supplemented to the fermentation medium.

## 4.3 GalOA-Production Based on the Highly Reduced Sugar Alcohol Sorbitol

### 4.3.1 Establishing GalOA-Production Based on the Highly Reduced Sugar Alcohol Sorbitol to Meet the Extensive Urge for Reducing Equivalents

The foregoing chapter discussed how the heterologous expression of *AnGATA* and *AnGAR1* from *A. niger* established the production of GalOA *S. cerevisiae*. However, the production was only low, presumably due to insufficient cofactor replenishment, which aligns with findings from the literature. Due to the high oxidative state of GalA, it was discussed that efficient NADPH replenishment is required and can be sourced from the metabolism of co-substrates like the hexoses glucose, galactose and fructose (Biz et al., 2016; Matsubara et al., 2016), the pentoses arabinose and xylose (Jeong et al., 2020) as well as glycerol (Perpelea et al., 2022). This work presents the potential of using sorbitol as carbon source to drive the biotransformation of GalA (Figure 3-4 and Figure 3-5). Compared to glucose, sorbitol is a more reduced sugar, which qualifies it as source to provide redox power to the GalA-reduction. Sorbitol is oxidized to fructose by one enzymatic step and then directed into the glycolysis. Catalyzed by sorbitol dehydrogenases (SDH), the oxidation of sorbitol generates either NADH or NADPH, depending on the enzyme used. *S. cerevisiae* owns transporters and the SDHs Sor1/2 to metabolize sorbitol (Jordan et al., 2016). While these enzymes rely on $NAD^+$ as cofactor, the SDH from *Y. lipolytica* (YlSdr) was reported to be dependent on $NADP^+$ (Napora et al., 2013). Utilizing sorbitol as co-substrate for GalA-reduction was tested in a fermentation. Constitutive expression of the sorbitol dehydrogenase *SOR2* and the sorbitol transporter *HXT13* resulted in strong growth on sorbitol, which was roughly delayed by one day when GalA was added to the medium. Differently to the GalA-toxicity test presented in chapter 3.1.1, Figure 3-1, where no negative effect of GalA on the growth of the strain was observed, in this fermentation the GalA was taken up into the cell. Thus, the growth delay most likely is due to weak acid stress caused by GalA itself (Piper et al., 2001). Weak acids quickly dissociate in the cytoplasm when taken up from the medium of low pH. With a $pK_a$ of 3.51 (Kohn and Kovác, 1978), GalA classifies as a weak acid. As common cell response to weak acid stress, the protons are transported out of the cell by the proton pump Pma1 (Cole and Keenan, 1986; Holyoak et al., 1996), which consumes ATP und thus burdens the metabolism and potentially affects the growth performance. Therefore, the delayed growth compared to the strain without GalA-supplementation could reflect the energetic cost of the proton export. Moreover, the transporter Hxt13 was found to be related to the Gal2 transporter (Jordan et al., 2016), which was reported to be inhibited by GalA (Huisjes et al., 2012a). Consequently, the sorbitol uptake could be inhibited by GalA. However, this does not appear likely since the rate of sorbitol consumption was not substantially affected in the presence of GalA.

Even though this strain produced twice as much GalOA (up to 0.68 g $L^{-1}$) than the wildtype strain on glucose (up to 0.27 g $L^{-1}$, chapter 3.1.2), the production was still inefficient, which most likely is due

to unsuitable cofactor supply for the reductase. The GalA-reductases AnGar1 and TrGar1 mainly use NADPH instead of the NADH (Harth et al., 2020), which is supplied by Sor2 (Jordan et al., 2016). This finding was strongly supported by the strong GalOA-production of up to 2.5 g $L^{-1}$ based on the NADPH generating YlSdr. Here, the crucial importance of aligning cofactor demand and supply of a metabolic reaction was demonstrated vividly (Figure 3-5).

Despite the great GalOA-production performance, the heterologous expression of *YlSDR* conferred only weak growth more than 3 days after inoculation. One possible reason could be the lower YlSdr activity compared to the Sor2 activity (Figure 3-6). An even more likely explanation could be the inability of the cell to reoxidize NADPH (Boles et al., 1993). Consistent with this hypothesis, the supplementation of GalA, whose reduction to GalOA acts as a NADPH sink, increased the overall growth performance (Figure 3-5). Moreover, the strong GalOA-production proves that the NADPH reoxidation by the GalA-reductases efficiently recycles the accumulated NADPH generated by the YlSdr. Furthermore, this experiment demonstrates the urge to couple the GalA-reduction performed by AnGar1 and TrGar1 with a metabolically engineered source of NADPH. The comparison of the molar yields $Y_{P/S}$ (calculated as mole GalOA produced per mole sorbitol consumed) further supports this phenomenon, as the yield based on the NADPH-dependent YlSdr is 12 times higher than the yield based on the NADH-dependent Sor2, regardless the reductase expressed. This finding aligns with the observation of increased GalOA-production due to a boosted PPP, a cellular source for NADPH, discussed in chapter 4.2.

Despite the high production titers, the poor growth performance observed for the YlSdr-based fermentation is unsuitable for an efficient industrial process.

### 4.3.2 Optimizing the Growth Performance of the GalOA-Producer Strain Based on Sorbitol Metabolism

The previous chapter discussed that the poor growth performance despite the efficient GalOA-production of a YlSdr-based strain utilizing sorbitol necessitates further optimization. So far, the preculture for the fermentation was performed in maltose medium, as the requirements of the parental strain demanded it (*hxt0*-strain). Since the preculture of a fermentation adapts the cells to the fermentation conditions, this is not optimal and might bear the reason for the late growth start. Reconstructed in the suitable parental strain CEN.PK2-1C, the variation of sugars metabolically related to sorbitol showed the necessity of a sorbitol-preculture. Compared to maltose and fructose, the final GalOA-production titer and the specific growth rate during the exponential phase was higher in the fermentation started from sorbitol-adapted cells, regardless the poor growth of the

sorbitol preculture itself (Figure 3-7). This strongly indicates the importance of cell adaptation to the fermentation medium. Cell adaptation means the induction of gene expression of necessary enzymes and global activation of the cell metabolism to efficiently utilize certain sugars. However, consecutive to the fructose preculture the fermentation showed only low GalOA-production and a low specific growth rate during the exponential growth phase (Figure 3-7). In contrast, the fermentations based on Sor2 expression showed sturdy growth quickly after the inoculation. As already seen in Figure 3-5, short delay was associated with weak acid stress caused by GalA (Piper et al., 2001). However, the major difference between the growth based on YlSdr- and Sor2-expression is the cofactor preference. In contrast to the YlSdr, the Sor2-conferred sorbitol metabolism rely on $NAD^+$. Contrarily to the pair $NADP^+$/NADPH, the cofactor pair $NAD^+$/NADH is abundantly used in glycolysis. More importantly, cytosolic NADH but not cytosolic NADPH can be reoxidized at the mitochondrial membrane under aerobic conditions. Considering the abundance of $NAD^+$/NADH in the cell, the levels of $NADP^+$/NADPH are low and thus the maximum velocity of the sorbitol consumption through the YlSdr might be limited. Therefore, the rate of the NADPH reoxidation could benefit from adaptation of the cell to this circumstance. This presumption was confirmed, as the growth rate was increased due to adding GalA to the sorbitol preculture of the YlSdr-strain (Figure 3-8). Providing a redox partner for the NADPH-dependent sorbitol degradation closes the cycle around the pair $NADP^+$/NADPH and thus defuses its threatening accumulation. Moreover, the closed redox cycle presumably induces a metabolic adaptation to the increased need for $NADP^+$/NADPH. The increased demand of the phosphorylated cofactor could be met by the induction of the cytoplasmatic NADH-kinases Yef1 and Utr1 (Kawai et al., 2001; Shi et al., 2005), as well as generally boosted synthesis of the nicotinamide dinucleotide cofactors. The beneficial effect of NADH-kinase overexpression was often discussed in the literature, reporting beneficial effect on various NADPH-dependent pathways like xylose utilization (Hou et al., 2009) as well as the production of carotenoids (Zhao et al., 2015) and of protopanaxadiol (Gao et al., 2018).

In addition to the increased growth behavior, higher GalOA titers and yields were measured in the YlSdr-fermentation started with cells simultaneously adapted to sorbitol and GalA (Figure 3-8, B). This strongly suggests, that the NADPH reoxidation is increased by enhancing the GalA reduction rather than by other possible redox sinks, which would be expected to decrease the GalOA yields. However, the exact adaptation mechanism remains obscured.

In contrast, the GalOA yields were decreased by pre-adaptation of cells expressing Sor2. This is possibly due to an increased oxidation rate of NADH as a consequence of the adaptation, for instance by the abovementioned mitochondrial system.

### 4.3.3 Approaches to Optimize the GalOA-Production by Variation of the Cultivation Conditions and Technique

The strong impact of suitable preculture conditions on GalOA-production and growth performance during the fermentation was discussed in the foregoing chapter. Notwithstanding, the effect of the optimized preculture conditions the biotransformation of GalA to GalOA is not complete, as roughly half of the GalA remains in the fermentation broth. Due to the ongoing process of the biotransformation the concentration of the medium constituents decreased towards the end of the fermentation, which can affect the fermentations efficiency. Thus, different ratios and concentrations of the medium constituents sorbitol and GalA demonstrated great impact on the production performance (Figure 3-9), while the growth was only minorly influenced by the increased sorbitol concentration in the medium. The Hxt13 transporter was well characterized in the study of Jordan et al. in 2016, the transport kinetics stating a $K_M$ value of 20.4±2.4 mM and a $v_{max}$ of 4.8±0.2 nmol $min^{-1}$ $mg^{-1}$. Compared to the tested sorbitol concentrations in this study which range from 10 g $L^{-1}$ to 40 g $L^{-1}$ corresponding to 55 mM to 220 mM the growth transport velocity was high at least at the beginning of the fermentations of the tested sorbitol concentrations (Figure 3-9, B). Additionally, the fermentation presented in Figure 3-5, B, clearly demonstrated that the complete consumption of sorbitol indeed is possible even though the transport velocity decreases towards the end of the fermentation when in the medium the sorbitol concentration is lower.

Furthermore, this study found high GalOA-production when the culture was highly supplemented with sorbitol and GalA. The kinetic parameters of the AnGatA transporter for GalA-uptake were reported in the literature as $K_M$ of 340 µM and a $v_{max}$ of 12.1 nmol $min^{-1}$ $mg^{-1}$ (Protzko et al., 2018). This qualifies AnGatA as a high-affinity and high-capacity transporter for GalA. Both GalA concentrations tested in this study (5 g $L^{-1}$ ≙ 26 mM, 10 g $L^{-1}$ ≙ 52 mM) exceeded the $K_M$ by far. Even though the transport itself most likely is not limiting, it is expectable that the intracellular concentrations of sorbitol and GalA are higher in cells cultured in highly supplemented medium. Higher intracellular concentrations entail higher educt and substrate turnover.

Sugars, here especially sorbitol, increase the osmolarity of the medium compared to the yeast cell. External osmolarity disturbs the osmotic gradient across the plasma membrane favoring water to leave the yeast cell, which, in extreme cases, causes cell shrinkage (Mager and Varela, 1993). Consequently, yeasts have evolved a mechanism to increase the intracellular osmolarity. In literature, it was demonstrated and discussed that yeast cells produce glycerol as response to hyperosmotic stresses (Attfield, 1998; Hirayama et al., 1995). High osmolarity stimulates an osmosensing signal transduction pathway called the HOG (high osmolarity glycerol response) pathway by induction of *HOG1* and *PBS2*, which code for a MAP (mitogen activated protein) kinase and a MAP kinase kinase, respectively (Boguslawski, 1992; Brewster et al., 1993). The HOG signal transduction induces the

upregulation of *GPD1*, which was described as response to osmotic stress (Attfield and Kletsas, 2000; Larsson et al., 1993). The upregulation of the *GPD1* strongly increases the demand of NADH in the cell. To meet the increased need of NADH for glycerol formation it was found that *ALD2* expression was induced. The *ALD2* codes for an aldehyde dehydrogenase, which generates acetate from acetaldehyde. As a consequence, the acetate formation is increased as well (Blomberg, 2000). The observations made in the metabolite analysis of these fermentations align with the described phenomenon from literature, as increased glycerol and acetate formation was detected with increasing sorbitol starting concentrations (Figure 3-9). Thereby a sorbitol concentration of around 20 g $L^{-1}$ seemed to trigger the HOG signal transduction. Presumably, the increased flux towards glycerol and acetate formation boosts the velocity of the glycolysis by extensive cofactor recycling, which finds proof in increased ethanol values in highly supplemented fermentations. The increased activity in the lower part of the glycolysis, indicated by the strong ethanol formation, might increase the overall flux through glycolysis und thereby benefit the sorbitol metabolism as well. However, the increased byproduct formation could be caused simply by higher substrate supplementation as well.

Moreover, the molar yield (mole product/ mole consumed substrate) was calculated for the different fermentation conditions after 8 days. This yield is a measure for efficient substrate utilization during the GalOA-production and was high in fermentations of a sorbitol over GalA-ratio not higher than 2 (10 g $L^{-1}$ sorbitol/ 5 g $L^{-1}$ GalA, 10 g $L^{-1}$ sorbitol/ 10 g $L^{-1}$ GalA and 20 g $L^{-1}$ sorbitol and 10 g $L^{-1}$ GalA). However, a high molar yield is not necessarily linked with high GalOA-production titer, as the fermentation supplemented with 10 g $L^{-1}$ sorbitol and 10 g $L^{-1}$ GalA showed a high molar yield yet the lowest GalOA-production. Furthermore, the cell growth under tested conditions indicates correlation between biomass production and higher sorbitol concentrations in the medium. Since the biomass generation is NADPH-dependent, this could be interpreted as the reason for the lower molar yields of the fermentations with a sorbitol over GalA-ratio higher than 2. However, to verify this assumption, a more accurate carbon balance of the entire process would be necessary.

Overall, the variation of the medium constituents led to the conclusion that both sorbitol and GalA concentrations are of great impact on the production efficiency of the GalA-biotransformation. Thereby the sorbitol-GalA-ratio should be around 2 since a lower ratio results in a low GalOA-titer. Given the relatively high price of sorbitol and its incomplete consumption in all fermentation conditions tested the recommended medium supplementation is 10 g $L^{-1}$ sorbitol and 5 g $L^{-1}$ GalA.

The so far facilitated batch fermentation leaves room for optimization and therefore may not be the cultivation technique of choice. Towards more efficient utilization of costly substrates, continuous and fed batch cultivations, which are characterized by a continuous feed or single feed pulses proved as valuable strategies to increase fermentation efficiencies. Following these approaches,

the substrate concentration can be modulated during the ongoing fermentation. Transferred to the GalA-biotransformation, the continuous feed of sorbitol to the fermentation medium holds promise to increase the efficiency by ongoing product formation while subverting the osmotic trigger point of the HOG pathway (Jacobus Albertyn et al., 1994; Schüller et al., 1994). These fermentation techniques require genetically stable production strains, as the fermentation processes standardly are run over a long time.

This work described two approaches to investigate the suitability of the engineered yeast strains for such a cultivation strategy: i) the strain was repeatedly inoculated to a low $OD_{600}$ in fresh medium and ii) the cells were retained in the shake flask while the medium was refreshed. In i), sturdy growth and production performance was demonstrated in the first and the second shift, and only a minor decrease in productivity and efficiency was observed after another shift (Figure 3-10). Differently in strategy ii), in which the sorbitol consumption enhanced and the GalOA-production diminished over the fermentation time causing a severe impact on the process efficiency (Figure 3-11). The increased capability to consume sorbitol most likely is due to the onset of *SOR1/2* expression. In *S. cerevisiae*, these endogenous sorbitol dehydrogenase genes are normally silenced. However, it was reported in the literature that after a long cultivation time, hexitol dehydrogenases indeed are derepressed (Quain and Boulton, 1987; Sarthy et al., 1993). Presumably, the endogenous Sor1/2 thus expressed compete with YlSdr for sorbitol and thus aggravate the crucial NADPH-supply for the GalA-biotransformation. Even more detrimental, at least Sor2 showed higher activity than YlSdr in an *in vitro* enzyme assay performed in this study (Figure 3-6). Therefore, adapted cells prevail over non adapted cells at the price of the overall process efficiency, which is observed in the molar yield (calculated as the moles GalOA produced per mole sorbitol consumed).

Due to the much higher retention time of yeast cells in approach ii), the effect of the upregulated endogenous *SOR1/2* might be higher, because the adapted cells accumulate in the fermentation, whereas in i) a vast moiety of the cells is excluded from further cultivation and thereby the number of already negatively adapted cells is kept low. To avoid the upregulation of *SOR1/2*, respective ORFs could be deleted. However, it is noteworthy that both ORFs are located in telomeric regions where deletions are often intricate. Even though each tested cultivation approach only imitates the fermentative conditions of a continuous or fed batch cultivation, they still indicate great potential to boost the process efficiency. The actual cultivation situation of a continuous fermentation in this case most likely combines aspects of both tested conditions, as the medium would be constantly refreshed and the cells would only partially be retained to a stable cell density.

Overall, the presented studies in this chapter demonstrated the burden on the efficiency of the process due to high medium supplementation of sorbitol and GalA. Furthermore, indications are

delivered on how suitable fermentation strategies could avoid the induction of side product formation, given the requirement of deleting the endogenous genes *SOR1/2.*

### 4.3.4 Optimizing the Interplay of AnGatA, Hxt13, AnGar1 and YlSdr during the GalA-Biotransformation by Testing Different Expression Strategies

The foregoing chapter discussed the great impact of the medium composition combined with a suitable cultivation strategy on the GalOA-production efficiency. The experiments suggested that at the beginning of the fermentations the transporters Hxt13 and AnGatA are saturated and facilitate the uptake of sorbitol and GalA, respectively, close to $v_{max}$. Once taken up, the compounds are substrates of the enzymes YlSdr and AnGar1, whose reaction velocities create their own dynamics driven by $NADP^+$ reduction and NADPH oxidation. The involved overexpressed genes, *HXT13*, *YlSDR*, *AnGATA* and *AnGAR1*, were individually downregulated by exchanging their strong constitutive promoters by the relatively weak promoter *pRNR1* (Lee et al., 2015) (Figure 3-12 and Figure 3-13). Of all downregulations, the lower *HXT13* expression caused a fatal effect, as growth and GalOA-production collapsed. This observation demonstrates the importance of a high number of Hxt13 transporters at the cell membrane to enable effective sorbitol permeability. Thus, the downregulation presumably causes starvation, which halts growth and GalOA-production. Furthermore, recalling the much higher transport efficiency of the AnGatA (Protzko et al., 2018) over Hxt13 (Jordan et al., 2016) discussed in chapter 4.3.3, the reduced number of Hxt13 at the membrane likely leads to a disbalanced uptake of sorbitol and GalA. These findings combined with the slow transport kinetics raise the assumption that additional overexpressions of *HXT13* could be beneficial for GalOA-production.

To investigate the effect of the overexpression of all involved genes, additional genomic copies were integrated into the genome under the control of the *pTDH3* promoter (Figure 3-14). Due to the essential role of the Tdh3 in the glycolysis, the *pTDH3* promoter is one of the strongest and constitutively expressed on substrates passing down the glycolysis (Apel et al., 2017; Lee et al., 2015). The Tdh3 is the glyceraldehyde-3-phosphate dehydrogenase a core enzyme of the glycolysis, which catalyzes the dehydrogenation of glyceraldehyde-3-phosphate and concomitant generation of NADH (McAlister and Holland, 1985). In addition to the endogenous *TDH3* expression, in this study, the *pTDH3* was used another two times for overexpression; first to express the *HXT13* gene within the cassette comprising all genes for GalA/sorbitol co-utilization and secondly to individually overexpress *HXT13*, *YlSDR*, *AnGATA* and *AnGAR1* from a second genomic integration (Figure 4-1).

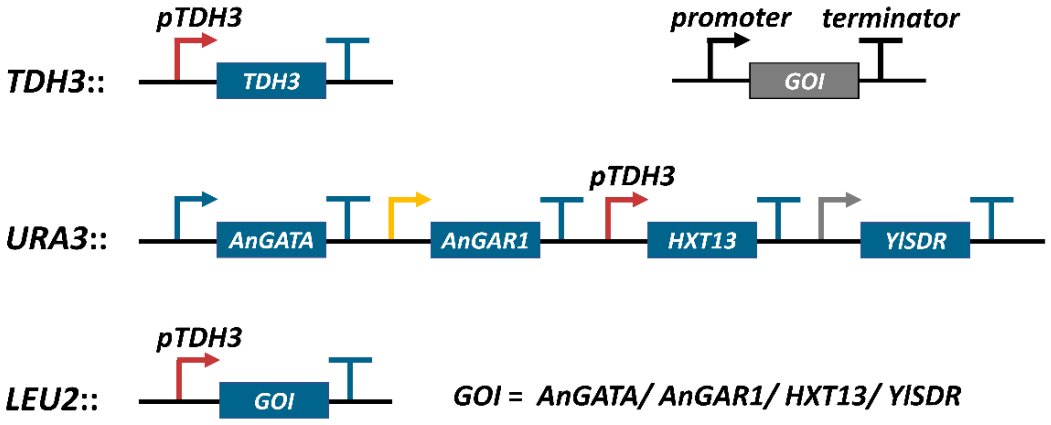


**Figure 4-1: Scheme of the multiple use of the *pTDH3*.**
The genes *AnGATA*, *AnGAR1*, *HXT13* and *YlSDR* were overexpressed in SiHY001 from an additional genomic copy driven by the promoter *pTDH3* (indicated in red). The genomic loci *TDH3*, *URA3* and *LEU2* are illustrated. Respective *ORFs* (bar) their promoter (arrow) and terminator (T) are indicated. Different promoters are represented by different arrows. The *GOI* (gene of interest) can represent any mentioned *ORF*.

The additional genomic integration of *AnGATA* resulted in a severe growth defect on medium supplemented with GalA and sorbitol. Moreover, the GalOA-production of the strains additionally expressing *AnGAR1* and *YlSDR* from the *pTDH3* decreased vastly. These observations seem to be related to a potential cross-interference of the *pTDH3* driving multiple genes. In eucaryotes the gene expression is majorly regulated by transcription factors, which activate and repress the expression of genes by binding to certain motifs in the promoter region and thus recruit the transcription machinery. However, it was reported that excess copies of a promoter can decoy the expression of its endogenous gene by sequestering the transcription machinery and therefore attenuate the dose of certain enzymes per cell (Görgens et al., 2001; Irani et al., 1987; Lee and Maheshri, 2012). Moreover, it was discussed in the literature that the expression of *TDH3* or its paralog *TDH2* is essential for viability of the cells (McAlister and Holland, 1985). The negative effect on growth of a second cassette driven by *pTDH3* appears to be specific for *AnGATA*. Therefore, the growth defect cannot be explained simply by a reduced expression of the *TDH3* gene (Figure 3-14). Only the strain overexpressing the *pTDH3-AnGATA* turned out to be severely troubled in growth, which must be based on a different aspect of this strain. Considering further targets of titrated expression and their effects, brings the Hxt13 into the center of discussion. The first integration of *HXT13* (*URA3*-locus) is as well driven be the *pTDH3* and therefore potential target of the titration effect as well (Figure 4-1). Recalling the importance of the sorbitol-GalA-ratio in the fermentation medium (chapter 4.3.3) and the fatal effect of the *HXT13* downregulation on the fitness of the cell (earlier this chapter), the efficient expression of *HXT13* seems to be a crucial factor affecting the GalOA-production performance. This observation is supported by the outcome of this overexpression study, since the growth of the additionally overexpressed *HXT13*, *AnGAR1* and *YlSDR* did not affect the growth, but

the process productivity in case of the *pTDH3-AnGAR1* and *pTDH3-YlSDR.* However, the overexpression of the *pTDH3-HXT13* seemed to complement the defect in productivity, since it only produced as much GalOA as the control strain without additional expression. This observation most likely is due to the transcription machinery distributing over two copies of the same expression cassette, which on the one hand negatively affect each other, but on the other hand might sum up to the expression strength of only one copy. This effect also explains the reduced efficiency of the strains expressing the *pTDH3-AnGAR1* and *pTDH3-YlSDR*, since the hampered sorbitol uptake could not be compensated by additional overexpression of *AnGAR1* or *YlSDR*. Furthermore, the inability of the strain overexpressing *pTDH3-AnGATA* to grow indicates that the phenotype of this strain most likely is determined by a very unfavorable intracellular ratio between sorbitol and GalA. In this case, the overexpression of the *pTDH3-AnGATA* presumably increases the intracellular GalA concentration, while the concomitantly reduced *HXT13* expression further impairs the intracellular sorbitol-GalA-ratio by limited sorbitol uptake. However, other deleterious effects, such as applied stress to the endoplasmic reticulum due to the overexpression of a heterologous membrane protein, cannot be excluded.

A further overexpression study was conducted, which was based on the transient overexpression of respective genes from a plasmid. This demonstrated the beneficial effect of individual overexpression of *AnGATA*, *AnGAR1* and *YlSDR* or of the full pathway. In this approach, the multiple use of *pTDH3* was avoided, as the strong promoter *pTEF1* was used to drive the overexpression. Here the empty vector showed decreased GalOA-production, compared to the wildtype strain itself, one possible explanation might be the plasmid, which was reported to aggravate the cells fitness. Growth rates in general were found to be affected in cells carrying plasmids, which was associated with additional DNA synthesis and expression pressure on the selection markers (Karim et al., 2013). The increased GalOA-production due to the transformation with the *AnGATA-/AnGAR1-/ YlSDR*-plasmids, revealed certain limitation of the GalA- and NADPH-supply in the untransformed strain (Figure 3-15). The overexpression of the full pathway did not lead to an additive effect, possibly due to the presence of an additional *HXT13* copy, which, when overexpressed individually, had a detrimental effect on GalOA-production. Thereby, a possible positive effect of a combined overexpression of *AnGATA, AnGAR1* and *YlSDR* might be masked. In the light of the findings discussed above, it appears that the expression of *HXT13* must be subtly balanced, possibly due to trade-offs between the need for efficient sorbitol uptake and the membrane over load caused by the overexpression of the transporter. For instance, addressing AnGatA to the plasma membrane (and thereby the GalA-uptake) might be negatively affected by the saturation of the secretory pathway with Hxt13. Negative effects on the uptake of glucose in yeast have been observed when the membrane

was saturated with a mutant transporter, which appeared to compete with the endogenous glucose transporters (Tamayo Rojas et al., 2021).

Thus, a promising strategy could be the expression of a sorbitol transporter, which has a superior transport capacity compared to Hxt13 and thereby would require a less strong expression. Unfortunately, such a (heterologous) transporter, which is at the same time active in yeast, is not available at present. Not only is the sorbitol transport into the cell challenging, but also is the utilization of sorbitol a costly burden for the overall process. Despite the easy deployment to generate an excess of reductive equivalents, sorbitol is a rarely used sugar and rather expensive compared to glucose. Henceforth, strategies are conducted to establish a sorbitol-independent process.

## 4.4 Site Directed Mutagenesis of the GalA-Reductases to Switch Cofactor Preference from NADPH to NADH

In foregoing chapters, the GalA-biotransformation was established on the highly reduced sugar sorbitol, which can be deployed as source for reductive equivalents when combined with Sor2 (NADH) and YlSdr (NADPH). Notwithstanding the success of biotransforming roughly 60% of the supplemented GalA and the production of up to 3.5 g $L^{-1}$ GalOA, sorbitol is costly and has to be replaced by a more accessible sugar to meet industrial requirements. In contrast, glucose is commonly used to serve as carbon source for industrial processes and is also part of the pectin rich waste material mix obtained from sugar refinery. Unfortunately, the core glucose metabolism generates NADH, which is only rarely accepted by the GalA-reductases AnGar1 (Harth et al., 2020; Hilditch, 2010) and TrGar1 (Kuorelahti et al., 2005) (compare Figure 3-16). First optimization approaches by boosting the PPP, one of the major sources of NADPH in yeast, showed only limited success (chapter 4.2). Therefore, switching the cofactor specificity of the GalA-reductases appears to be a more promising target for further engineering approaches.

The expression of *SOR2* (NADH) and *YlSDR* (NADPH) created suitable yeast strains to deploy as screening platform based on sorbitol utilization. In these strains GalA-reductases were tested, which were constructed from site directed mutagenesis based on a structural homology model created by Jun-yong Choe from the Rosalind Franklin University of Medicine and Science, North Chicago (Figure 3-17). The positively charged amino acid residues lysine (K) and arginine (R) located in the cofactor binding pocket were suggested to be involved in stabilizing the phosphate group of the NADPH by electrostatic interaction. To facilitate the cofactor switch, these amino acid residues were replaced with the uncharged amino acid residues of comparable size methionine (M) and leucine (L). The variants K261M and R267L in AnGar1 as well as K254M and R260L in TrGar1 were

tested individually and in combination. Due to the high sequence identity of the GalA-reductases AnGar1 and TrGar1, regarding amino acid residues were found at similar loci, which indicate similarly located cofactor binding pockets in the reductases.

Both wildtype enzymes, as expected, produced GalOA only in the screening strain supplying NADPH, while only minor amounts of GalOA were produced using NADH (Figure 3-18). This observation aligns with the findings in Figure 3-5, in which *AnGAR1* and *TrGAR1* were expressed under the same conditions but from genomic copies. The stepwise decrease of the GalOA-productivity with every mutation inserted is in accordance with the prediction that the positively charged amino acids lysine and arginine are involved in cofactor stabilization. Furthermore, it indicates that for stable cofactor binding mainly only one of the two amino acid residues is necessary. At the same time, the single mutations already enable the AnGar1-variants K261M and R267L to accept NADH, while respective TrGar1-variants barely showed any GalOA-production with NADH. The combination of both mutations in one enzyme fully excludes NADPH from the reaction in variants of both enzymes. However, only the double mutations of the AnGar1 were able to accept NADH. Moreover, these novel NADH-dependent GalA-reductases exceeded the productivity of the AnGaaA, which was used for comparison and was described to naturally accept NADH and NADPH (Biz et al., 2016). Surprisingly, the only moderate differences in the protein sequence (63% sequence identity and 81% sequence similarity) determined the success of the AnGar1-variants in contrast to TrGar1-variants (Harth et al., 2020). In the literature, the necessity to switch the cofactor specificity of reductases and other enzymes was often discussed; for instance, it was demonstrated that the cofactor specificity of an imine reductase (Borlinghaus and Nestl, 2018) and a xylose reductase (Khoury et al., 2009) can be switched from NADPH to NADH. Both strategies predicted mutations based on structural models as well. Interestingly, these studies also reported lysine residues in the binding pockets of the imine and the xylose reductases indicating its central role involved in NADPH stabilization.

The successful cofactor switch was mainly determined by HPLC-measurement, however the strains expressing the NADH-accepting variants of the *AnGAR1* showed a growth phenotype similar to the growth defect of the GalOA-production based on the YlSdr-dependent NADPH-generation on sorbitol. The growth defect on NADPH-dependent sorbitol metabolism characterized by a prolonged adaptation phase of around 4 days and weak growth of up to an $OD_{600}$ of only 3 occurred in several experiments during this work whenever the GalOA-production exceeded 1 g $L^{-1}$ (Figure 3-5, Figure 3-8 and Figure 3-18). The late growth start was shown to be associated with the adaptation to increased utilization of the reductive equivalent pair $NADP^+$/NADPH (compare chapter 4.3.2). Since the AnGar1-variants were engineered to utilize NADH, which this yeast notoriously relies on, no such adaptation phase was observed, as the cells entered exponential growth phase quickly after

the fermentation started. This observation delivers further evidence that in chapter 3.2.1, Figure 3-5, the late growth start indeed is due to adapting to extensive $NADP^+$/NADPH utilization. However, that producing strains did not exceed an $OD_{600}$ of 3 regardless the utilized cofactor indicates an effect of the produced GalOA itself. Possibly, this effect could be connected to the property of GalOA to sequester essential metal ions like $Fe^{2+}$, $Cu^{2+}$, $Zn^{2+}$, which was shown for its structurally close related L-gluconate (Sawyer, 1964). For example, iron ions are incorporated in heme and iron-sulfur-clusters and thus part of the prosthetic group in some enzymes. However, this is only an assumption and was not further investigated in this study.

The molecular mechanism of the engineered AnGar1 reductases was further investigated in an enzyme assay from crude cell extracts (Figure 3-19). The enzyme assay showed strong NADPH utilization for the wildtype and the single mutated version, whereas the double mutated variant showed only marginal NADPH utilization. Surprisingly, when performing the enzyme assay on NADH, it was revealed that all tested variants, the wildtype AnGar1 included, utilized NADH on a comparable level. This finding stands in contrast with the results collected *in vivo*, where the wildtype GalA-reductase showed much lower GalOA-production than the engineered variants. The insight into the molecular mechanism behind the cofactor switch was further deepened when $NADP^+$ was added to reaction mix with NADH. Thereby, the inhibitory effect of $NADP^+$ was observed, which the wildtype AnGar1 was most sensitive for, while the single mutated variant (AnGar1 [K261M]) was not affected up to an equimolar supplementation of $NADP^+$ and NADH and the double mutant (AnGar1 [K261M, R267L]) overall resulted insensitive to $NADP^+$ in the tested concentration range. Thus, the molecular mechanism was unraveled, as the tested mutations did not only destabilize the NADPH-binding, but also excluded $NADP^+$ from the cofactor binding pocket, which unveiled the intrinsic capability of the AnGar1 to utilize NADH (as well). Consecutively, the sensitivity of the wildtype AnGar1 towards $NADP^+$ delivers evidence that the extensive utilization of NADPH during GalOA producing conditions switched the ratio of NADPH/$NADP^+$, which usually is higher than 1 (VanLinden et al., 2015), towards more $NADP^+$ than NADPH compared to normal conditions. Showing the impact of the NADPH/$NADP^+$-ratio as driving force for metabolic reactions, a sensor system was described in literature. This sensor system measures the ratio between the two cofactors NADPH and $NADP^+$ by implementing the heterologous shikimate dehydrogenase into the *S. cerevisiae* metabolism. The shikimate dehydrogenase interconverts shikimate and dehydroshikimate by utilizing $NADP^+$ or NADPH, respectively. Due to the direct coupling of the respective metabolite production and the accessibility of the respective cofactor, the NADPH/$NADP^+$ ratio can be estimated by measuring the metabolic products (Zhang et al., 2015).

## 4.5 Implementing the Engineered GalA-Reductases into the Glycolytic Metabolism of *Saccharomyces* cerevisiae

Hitherto, the GalOA-production was based on the reducing equivalent NADPH, whose generation system, however, is limited. In contrast, the engineered AnGar1-variants AnGar1 [K261M] (in the following referred to as AnGar1 [R267L]) and AnGar1 [K261M, R267L] (in the following referred to as AnGar1 [K261M, R267L]) showed activity with NADH. Since the core glucose metabolism of *S. cerevisiae* strongly relies on the generation of NADH, the engineered GalA-reductase holds great potential to establish a process independent of sorbitol. However, the vast majority of the NADH generated during glycolysis and the consecutive TCA-cycle, is utilized during ethanol production or reoxidized at the mitochondrial membranes, which provides energy for the cell.

### 4.5.1 Streamlining the NADH-Supply of the GalOA-Production by Micro-Aerobic Fermentation in an *Δadh1* Strain

Since the majority of the generated NADH in yeast is reoxidized at the mitochondrial membrane or during the ethanol formation the GalA-reductases compete for this cofactor with these pathways. To alleviate the NADH-competition and to favor the AnGar1 [R267L]/ [K261M, R267L] reaction, the yeast metabolism was tailored accordingly.

The reoxidation of NADH at the mitochondrial membrane is a complex pathway, which includes a series of enzymatic steps and results in ATP, which enforces the energy supply of the cell (Boumans et al., 1998; Johnston and Davis, 1984). Already the deletion of single genes, whose gene products are involved in the electron transport chain, stunts the functionality of the mitochondria. Consequently, the loss of function causes the NADH to accumulate and severely slows down the cell growth. Regarding cells do only form small colonies, therefore they are commonly described as the *petite* (French “small”, “little”) phenotype (Bernardi, 1979). The accumulated NADH could be utilized by the engineered GalA-reductases. However, *petite* mutants are only tediously handled in laboratory, so, in this study, the essential need for elemental oxygen of the respiratory chain was targeted to decrease the respiratory activity. Therefore, the cells were cultivated under micro-aerobic conditions, which severely compromises the NADH-reoxidation via the respiratory chain. Moreover, as the major moiety of the generated NADH is used for alcohol formation in yeast even under aerobic conditions, due to the so-called Crabtree effect (Piškur et al., 2006; Pronk et al., 1996). Its perturbation by deleting the major alcohol dehydrogenase *ADH1* could further improve the NADH-supply of the GalA-biotransformation (compare chapter 3.4.1, Figure 3-20).

Both, the AnGar1 [R267L] (0.47 g $L^{-1}$) and the AnGar1 [K261M, R267L] (0.46 g $L^{-1}$), already produced more GalOA than the wildtype GalA-reductase in the wildtype strain (0.27 g $L^{-1}$, chapter 3.1.2). This indicates and further suggests the great potential of NADH-dependent GalA-reductases for GalOA-production in yeasts, which thoroughly was discussed to better align with the yeast metabolism (Biz et al., 2016; Jeong et al., 2020; Matsubara et al., 2016). Due to the abundance of NADH in yeasts, henceforth, the extensive need for reductive equivalents of a bulk GalOA-production could be based on this cofactor.

In an *Δadh1* strain the production of the AnGar1 [R267L] was increased, indicating that the cofactor supply was enhanced due to alleviated NADH-competition of the ethanol formation. Since the AnGar1 is ambiguous in its cofactor utilization, the increased GalOA-production could be based on the reduced ethanol formation and therefore potentially higher NADH-supply. However, this effect was not observed for the rather strictly NADH-dependent AnGar1 [K261M, R267L], indicating that the deletion of *ADH1* could cause a secondary effect. The Adh1 produces ethanol from the reduction of acetaldehyde, which, however, is substrate to the acetate formation as well. The acetate formation was found increased in the fermentation of the AnGar1 [R267L] strain associated with the *Δadh1.* In yeast, the acetate formation is catalyzed by the Ald2 and the Ald6, which generate NADH or NADPH, respectively. While the additional NADH could be utilized by the AnGar1 [K261M, R267L] as well, the additional NADPH from acetate formation could further fuel the GalOA-production of the AnGar1 [R267L]. Due to excessive NADPH utilization, the devouring character of the NADPH-utilization of the AnGar1 [R267L] could cause oxidative stress to the cell, which usually boosts glycerol formation (Påhlman et al., 2001). Given the glycerol production which was only increased associated to the AnGar1 [R267L], this delivers a considerable body of evidence for this being a secondary effect of the impaired ethanol formation. Furthermore, the effect of increased glycerol formation was observed earlier in this study (compare chapter 4.2), when the expression of the genes *PGI1* and *ZWF1* were modulated to boost the NADPH-generation via the pentose phosphate pathway. That chapter hypothesized that the extensive NADPH consumption of the wildtype AnGar1 could cause oxidative stress due to the lack of NADPH and therefore trigger glycerol production as common response to this condition (Påhlman et al., 2001). However, this hypothesis requires further investigation.

Both engineered reductases were tested in a wildtype strain under micro-aerobic (not strictly anaerobic) conditions, to avoid ergosterol auxotrophy. Micro-aerobic fermentation conditions increased the production of the AnGar1 [K261M, R267L] by 20%, which was found further increased in the *Δadh1* strain background under micro-aerobic fermentation by 50% compared to the wildtype strain background fermented aerobically. This increase in GalOA-production presumably

demonstrates the beneficial effect of an alleviated NADH-competition. However, the ethanol production remained similar throughout the tested conditions, which most likely is due to upregulation of the other alcohol dehydrogenase genes (*ADH2-6*). Moreover, regarding effect did not appear in case of the AnGar1 [R267L] under micro-aerobic conditions, also in the *Δadh1* strain. This could indicate strong accumulation of $NADP^+$, which was found to hamper only the AnGar1 [R267L] but not the AnGar1 [K261M, R267L] *in vitro* (chapter 3.3.2). However, the vast interventions in the yeast metabolism, especially under micro-aerobic conditions, indicate a severely stressed yeast cell. Furthermore, the scarce production of GalOA indicates limitation of the process. The GalA-transport via the AnGatA, requires ATP, whose generation, however, is perturbed under micro-aerobic conditions. This presumably hampered the GalA-transport and concomitantly severely worsened the energy supply for essential processes in the cell resulting in a highly burdened metabolism, which cannot function efficiently.

Overall, this chapter demonstrated how the alleviation of NADH-competition increased the production of GalOA successfully. However, glycerol and ethanol formation increased because of metabolic alterations. Hence, intervening into the glycerol formation could further boost the GalOA-productivity of yeast strains.

### 4.5.2 Optimizing the Core Metabolism of *Saccharomyces cerevisiae* Results in High GalOA Titers and Yields

The foregoing chapter showed the implementation of the engineered NADH-dependent GalA-reductases and furthermore revealed the potential of a tailored core metabolism to meet the requirements of the bulk production of GalOA based on the co-fermentation with glucose in the yeast *S. cerevisiae*.

Further increase of the GalOA-production was observed, when the *AnGATA* and the *AnGAR1* were expressed in the strain JWY019, which was described to show improved isobutanol production. The isobutanol production consumes NADH as well (Wess et al., 2019). Besides modifications designed to improve the isobutanol formation, this strain contains *Δadh1*, which proved beneficial as discussed in the foregoing chapter (4.5.1), and furthermore *Δgpd1/2* to impede the glycerol formation. The glycerol formation consumes NADH and therefore competes with the AnGar1 [R267L] and AnGar1 [K261M, R267L] for the cofactor. Impeding the glycerol formation showed great impact on the GalOA-production, as the AnGar1 [K261M, R267L] produced 80% more GalOA in JWY019 (0.84 g $L^{-1}$, Figure 3-21) than in the wildtype strain (0.46 g $L^{-1}$, Figure 3-20). Overall, the measured glycerol values vastly decreased in fermentations of the strain JWY019, which phenotypically verifies the

*Δgpd1/2* genotype. The minor glycerol formation could be caused by less selective dehydrogenases present in the cell, presumably alcohol dehydrogenases, which would accept glycerone-phosphate as well. However, the glycerol formation varied dependent on the GalA-reductase present in the cell. Given the decreasing glycerol formation with increasing preference for NADH of the GalA-reductase in this strain, demonstrated the ability of the NADH-dependent AnGar1 [K261M, R267L] to further scavenge NADH from the glycerol formation. That the AnGar1 [K261M, R267L] scavenges NADH from the glycerol formation results in lower byproduct formation and therefore in a more efficient utilization of the substrate glucose. This finding reflects in the molar yield of the process, which was calculated as the moles of GalOA produced per mole of glucose consumed, which was twice as high for the variant AnGar1 [K261M, R267L] than for the also NADPH-accepting AnGar1$^{WT}$/[R267L].

Rather high acetate values of around 1 g $L^{-1}$ were measured in all cultures, which in yeast predominantly is produced by Ald2 and Ald6. These aldehyde dehydrogenases generate NADH (Ald2) or NADPH (Ald6) from the oxidation of acetaldehyde to acetate. The deletion of the *ALD6* was assumed to further favor the NADH-generation and therefore boost the GalOA-formation by the mutant GalA-reductases. However, contrary to the expectation, the productivity of the AnGar1$^{WT}$ expressing strain was boosted up to almost 3 g $L^{-1}$ after 5 days of cultivation. This result exceeded the so far best production of the adapted SiHY001 strain on sorbitol of 2.80 g $L^{-1}$ after 4 days (Figure 3-5). Considering that the AnGar1$^{WT}$ only accepts NADPH and despite the excluded Ald6 being a major source for cytosolic NADPH, the deletion of the *ALD6* must cause a strong increment in NADPH-regeneration in the resulting strain JWL023. Under these circumstances, the AnGar1$^{WT}$ reaction quickly consumes the NADPH of the cell, which causes NADPH-depletion. The NADPH-depletion most likely triggers the cell to react, as the cofactor is required to maintain essential processes within the cell. A possible effect could be the upregulation of the PPP, which is another prominent source of NADPH. In fact, the expression of *ALD6* and certain genes of the PPP is coupled by the transcription factor *STB5* (Bergman et al., 2019). The Stb5 mediates the expression by binding to the promoter region of certain genes and thereby recruits the transcription machinery. However, in case of the JWY023, the promoter region of the *ALD6* is deleted and thus the Stb5 might trigger the expression of its other target genes more effectively. Further genes activated by Stb5 are the PPP genes *SOL3, GND1/2, RKI1* and *TAL1* as well as the cytosolic NADH-kinase *YEF1* (Bergman et al., 2019; Larochelle et al., 2006), all involved in reactions favoring NADPH-generation. However, the Stb5 does not affect the expression of the *ZWF1* itself (Ouyang et al., 2018), but it does repress the *PGI1* expression. Since Pgi1 is a direct competitor of Zwf1 for glucose-6-phosphate, their shared substrate, the glucose flux through the oxidative branch of the PPP is indirectly increased, thereby

boosting the NADPH-generation. Complementary to this study, Kim et al. in 2018 found an increased NADPH/$NADP^+$ ratio in a *Δzwf1* strain, which overexpressed the *ALD6*. Thereby, the production of a NADPH-dependent heterologous compound was increased. Either way, the deletion of one of the major sources for NADPH, seems to induce an over-compensatory mechanism for NADPH-regeneration.

The correlation between the deleted *Δald6* and a strengthened PPP was further investigated in an *in vitro* assay measuring the enzyme activity of Pgi1 and Zwf1 in the strains JWY019 (relevant genotype: *Δadh1; Δgpd1; Δgpd2*), JWY023 (relevant genotype: *Δadh1; Δgpd1; Δgpd2; Δald6*) and the wildtype strain CEN.PK2-1C. The assay, in fact, showed that the Zwf1 activity was increased in both tested strains compared to the wildtype strain CEN.PK2-1C, even two-fold in case of the JWY023. This finding supports the hypothesis of an increased flux through the PPP mediated by increased *ZWF1* expression in an *Δald6* strain. However, the activity of Pgi1 was found two-fold increased in both strains, the JWY019 and JWY023 compared to the wildtype strain CEN.PK2-1C. This could indicate the presence of a transcription activator, which surpasses the presumed repression of the *PGI1* gene by Stb5. Moreover, this could further be caused by accumulation of intermediates of the glycolysis due to the intervention into the glycerol, acetate and ethanol formation. These side product pathways usually ease the overall flux through glycolysis by distributing intermediates over multiple pathway routes but more importantly they contribute by closing redox cycles.

After unveiling the mechanism behind the strong productivity of the $AnGar1^{WT}$ in the JWY023 strain due to a boosted NADPH-generation via the PPP, the rather low productivity of the AnGar1 [R267L] enzyme variant raises questions compared to the wildtype enzyme. The results from the *in vitro* assay of the AnGar1-variants dependent on different cofactor supply (depicted in Figure 3-19 and discussed in chapter 4.4.) showed strong activity of the AnGar1 [R267L] with NADPH as well. However, the $v_{max}$ was measured by adding the cofactors in excess, which does not elucidate further kinetic properties of the enzyme. Since the mutagenesis was successful in regard of the cofactor switch, it certainly decreased the affinity of the enzyme for NADPH. Since the concentrations of the regarding cofactor is far lower *in vivo* than in the enzyme assay, the effect of the enzyme affinity is more pronounced in the living cell.

Overall, this chapter discussed the benefit of decoupling the metabolic branches of the glycolysis in favor of the NADH-supply for the GalOA-production performed by the engineered NADH-dependent AnGar1 [K261M, R267L]. Moreover, the molecular basis for how the deletion of *ALD6* could surpass the discussed effect by far, as the deletion of the acetaldehyde dehydrogenase gene strongly favored the production of GalOA by the NADPH-dependent wildtype enzyme. Henceforth, the potential of the resulting strain JWY023 expressing *AnGATA* and *AnGAR1*, from now on called SiHY073, was further investigated.

## 4.6 Optimization of the Producer Strain SiHY073 for Improved GalOA-Production and Pursued Applications

The wildtype AnGar1 was found very productive in the strain JWY023 (*Δadh1; Δgpd1; Δgpd2; Δald6*). In this strain certain branches of the core metabolism are detained to attenuate ethanol, glycerol and acetate formation. Due to these modulations, the PPP is highly upregulated by boosting *ZWF1* expression. The resulting producer strain bears great potential to establish an efficient process for GalA-biotransformation.

### 4.6.1 Improving the GalOA-Production in SiHY073 by Overexpressing the GalA-Reductase Gene *AnGAR1*

Already in the strain SiHY001, the best producer strain on sorbitol, the expression of the *AnGAR1*$^{WT}$ was found limiting (discussed in chapter 4.3.4). Hence, *AnGAR1* overexpression from a plasmid was assumed to bear great potential to further enhance the GalOA-production performance in SiHY073 as well. However, introducing *AnGAR1* plasmids or even the respective empty plasmid into SiHY073 caused the GalOA-production to collapse (Figure 3-24). This suggests that this effect is independent of the *AnGAR1*$^{WT}$ gene and its regulatory elements, as no difference was observed for the empty vector SiHV005.

To further test whether this effect is specific to the empty plasmid SiHV005 and its descendants, a set of different empty plasmids was screened. These plasmids carry different selection markers for plasmid maintenance and regulatory elements for recombinant gene expression. The screen revealed the vast influence of empty plasmids on the production performance of the host, as the GalOA-production ranged from 0.41 g $L^{-1}$ to 3.53 g $L^{-1}$ (Figure 3-25). Thereby, the plasmid p426HXT7 (*URA3*-marker) not only complemented the observed production collapse, but even improved the GalOA-production and the cell growth compared to SiHY073 fermented without a plasmid (compare Figure 3-22). This finding aligns with the literature, as it was shown that in auxotrophic cells the uptake of essential nutrients often causes growth limitations and therefore weighs heavier than the effort, which prototrophic cells put into the production of these nutrients. Hence, the growth and production performance of prototrophic strains often is improved compared to auxotrophic strains, which are dependent on externally supplied nutrients (Landi et al., 2011). However, this conflicts with the poor performance of the SiHV005, p426MET25 and YEplac195, which also carry *URA3*-marker genes. This conflict could be caused by either the cloned *URA3*-gene, which might show sequence variations, or the cloned promoter, which differ in p426HXT7, p426MET25 or none. However, due to the success of the p426HXT7 plasmid the molecular mechanism behind was not further investigated.

Besides auxotrophic markers, two plasmids carrying the dominant marker ClonNAT, were tested as well. Dominant markers confer the expression of a resistance gene, whose gene product neutralizes an antibiotic added to the medium, here nourseothricin. Nourseothricin targets the protein biosynthesis in many eucaryotes blocking the translation. The resistance gene codes for a nourseothricin-acetyltransferase, which transfers acetyl groups to the nourseothricin and therefore defuse the antibiotic properties. However, this resistance mechanism requires acetyl-CoA, which is generated from acetate. Since the acetate formation in the *Δald6* strain SiHY073 is decreased, sufficient supply of acetate might be limiting for the resistance marker to be fully functional. In fact, the transformation of both plasmids resulted in weak growth and low GalOA-production, indicating troubled cell proliferation due to slowed down protein biosynthesis.

Overall, the exact molecular mechanism for the vast effect of the plasmid transformation on the GalOA-production performance remains obscure. However, the superior performance of prototrophic cells over auxotrophic cells was discussed and is to be considered in future fermentation experiments.

Finally, GalA-reductase genes were overexpressed from the strong constitutive promoter *pHXT7t* from the p426HXT7 plasmid, which was described to be about three-fold stronger than the *pPGK1* promoter, which was cloned in front of the genomic copy of the *AnGAR1*$^{WT}$ in SiHY073 (Hauf et al., 2000). The genes for the NADH-dependent AnGar1 [R267L] and AnGar1 [K261M, R267L], were included in this study as well, to source reductive equivalents not only from the NADPH-pool but also the NADH-pool (Figure 3-26). Strong increase in GalOA-productivity resulted from this overexpression, especially for the *AnGAR1*$^{WT}$. The GalOA-production exceeded the production of the empty vector control, which unveils the expression of the GalA-reductase as limiting factor for the biotransformation. Even though, the overexpression of the *AnGAR1*$^{WT}$ was most effective towards almost complete conversion of the used GalA, it was shown that the variants AnGar1 [R267L]/ [K261M, R267L] indeed contributed to the overall production, even if only to a limited extent. Especially the reduced glycerol values in these fermentations substantiate this interpretation (Figure 3-26, E), as the NADH necessary for glycerol formation via the Gpd1 might be scavenged by the NADH-dependent AnGar1-variants. Additionally, the ethanol formation profile was found slightly delayed, probably also caused by NADH-consumption of the engineered AnGar1-variants. However, in the three strains overexpressing different *AnGAR1*-variants, the glucose was not completely consumed, as roughly a quarter of the start concentration remained in the fermentation broth, even after 7 days of fermentation when the biotransformation came to a halt. Towards a more cost-efficient process, the same experimental set up was repeated with only half of the initial glucose concentration (Figure 3-27). However, this approach resulted in vastly decreased productivities for all three tested strains. None of the overexpression strains exceeded a GalOA-production of

1.5 g $L^{-1}$, indicating the crucial role of high glucose concentration for efficient GalOA-production in the previously constructed strains. This indicates that the accumulation of redox cofactors requires a saturation of the glycolysis in the engineered strain.

Overall, in a yeast strain bearing a highly streamlined glycolysis, causing the accumulation of glycolytic intermediates, the expression especially of the *AnGAR1$^{WT}$* unveiled limiting. The overexpression of the genes coding for the engineered NADH-dependent GalA-reductases AnGar1 [R267L]/ [K261M, R267L] enabled to source the intracellular NADH-pool for GalOA-production as well. All three overexpressions shown resulted in nearly complete conversion of GalA to GalOA, Thereby, the titer was highest, when *AnGAR1$^{WT}$* was overexpressed. However, the high glucose level was found necessary for efficient GalOA-production.

### 4.6.2 High Cell Density Fermentation Increases GalOA-Production

Further improvement of the GalOA-production was found in a high $OD_{600}$ fermentation. Starting a GalA-biotransformation from a higher $OD_{600}$ shortened the fermentation due to a shifted production profile (Figure 3-28). Overall, the cultivations started from higher $OD_{600}$ showed faster consumption of glucose and GalA, whereas the titers of GalOA, glycerol, acetate and ethanol increased strongly and earlier during the fermentation. This indicates that the increased number of cells reduces the burden of the production process on individual cells and thereby improves the overall rate of the biotransformation. The fermentations started with an $OD_{600}$ of 10 showed a more stable and faster process performance than fermentations started from $OD_{600}$ of 5 or 0.1. High $OD_{600}$-fermentations completely consumed glucose. Furthermore, the GalA-supplemented to the fermentation was almost completely converted to GalOA, which as well could be due to the high number of cells, whereby the burden of the biotransformation is distributed through a larger cell population. Similar effect occurs for fermentative byproduct formation of glycerol, acetate and ethanol, which are quickly produced in densely inoculated cultures.

Overall, the high-$OD_{600}$-fermentation proved to be a promising approach to alleviate the burden of the GalOA-production on the cell and achieve a highly efficient biotransformation on glucose. The effect of higher GalA-feed and even higher cell numbers is to be investigated, as it bears a potential to further increase the process efficiency.

## 4.7 The Powerful Cofactor-Recycling of the Strain SiHY073 Was Caused by Perturbation of Glycolytic Side-Branches

The powerful application of the strain SiHY073 was discussed in previous chapters and the outstanding potential of this yeast strain for industrial utilization of GalA was demonstrated. By exploiting this strain, efficient production of GalOA was demonstrated (chapter 4.5.2), which was further boosted by overexpressing the GalA-reductase (chapter 4.6.1). Additionally, the improved bioprocess performance was investigated in high cell density cultivation (chapter 4.6.2). Despite the versatile set of applications of this strain, the molecular mechanism behind the splendid production performance remains obscure. However, accumulation of glycolytic intermediates and exclusion of competitive pathways was hypothesized to be the reason. These aspects were investigated in a consecutive deletion series of the genes *ALD6, GPD2, ADH1* and *ECM31*. These modifications in SiHY073 were associated with slowed down glucose metabolism and in case of Ecm31 with mitigated cofactor competition. In this study the modifications were tested in following order: *Δald6, Δgpd2*, *Δadh1* and *Δecm31*. Thereby, the gene *ALD6* of the aldehyde dehydrogenase which is involved in NADPH-generating acetate formation was deleted first, since it showed outstanding effect in Figure 3-22, discussed in chapter 4.5.2. Furthermore, the genes *GPD2* and *ADH1* were deleted since their gene products are involved in glycerol and ethanol formation, respectively. In SiHY073, the slowed down glucose consumption by weakening glycolytic branches was interpreted as crucial condition for the strain's performance. The accumulation of the glycolytic intermediates supposedly supports the PPP derived NADPH-generation by the Zwf1 catalyzed reaction. Finally, the NADPH-consuming cytosolic pantothenate production was perturbed by deleting *ECM31*. SiHY073 also bears the deletions *Δilv1/2*, which block the NADPH-dependent production of the branched amino acids isoleucine, valine and leucine. However, these amino acids are built in the mitochondria and thus regarding pathways source from a different NADPH-pool than the AnGar1$^{WT}$. Since the mitochondrial membrane is a diffusion barrier for NADPH in both directions, mitochondrial NADPH is produced by the NADH-kinase Pos5 (Shi et al., 2005).

Indeed, slowed down glucose consumption and concomitantly increased GalOA-production (roughly 400% increase) was stepwise observed in strains with increasing number of metabolic modifications (this order: *Δald6, Δgpd2*, *Δadh1* and *Δecm31*) (Figure 3-29), despite the poor growth phenotype of the final strain. These observations support the hypothesized beneficial effect of the accumulation of glycolytic intermediates. However, the final GalOA-titer of the best producer strain in this deletion series study (*Δald6, Δgpd2*, *Δadh1* and *Δecm31*) roughly produced only half of the GalOA compared to strain SiHY073. Interestingly, the strains in this experiment depict much higher glycerol formation of up to 3 g $L^{-1}$ (Figure 3-29), whereas in the fermentation of SiHY073 not more than 0.1 g $L^{-1}$ glycerol formation was measured (Figure 3-22). Especially in the last two strains of

this deletion series (*Δald6, Δgpd2*, *Δadh1* (*Δecm31*, respectively*)*) the glycerol production was high, which indicates a strong cellular response to the strongly accumulated glycolytic compounds. In contrast to the SiHY073, in these two strains the glycerol dehydrogenase gene *GPD1* still is present. It seems like the expression of *GPD1* might be strongly triggered in these strains. Thereby, the glycerol formation catalyzed by the Gpd1 is the only option left to reoxidize the NADH, which is produced in the glycolysis, given the absence of Adh1 and Gpd2 and the downregulated respiratory system due to high glucose content (Crabtree-effect) (De Deken, 1966). Therefore, *Δgpd1* most likely bears great potential to avoid the leakage of glycolytic intermediates via glycerol formation. In case, the *Δgpd1* causes great boost in GalOA-production, even in the strain with the wildtype *ECM31*, the poor phenotype associated with the *Δecm31* could be circumvented. Especially for industrial application strong growth is of high importance due to time and cost restrictions in latter processes.

Overall, the hypothesis of accumulated glycolytic intermediates causing increased NADPH-generation in the strain SiHY073 was supported to a major extent. However, a deletion of the *GPD1* has to be considered to deliver final proof.

# 5 Summary in English Language

In Europe, the sugar refinery is largely based on sugar beets. This route for obtaining household sugar results in a large amount of biomass waste, consisting mainly of the insoluble beet residues, e.g., cell wall fragments. To a vast moiety this debris consists of the polymer pectin (up to 20% in the dry total solids). The structure of pectin is based on a backbone of D-galacturonic acid units (GalA), but also contains various other sugar monomers, predominantly L-arabinose, D-galactose, L-rhamnose and D-xylose. The amount of GalA adds up to a moiety of up to 70% within this sugar cocktail. So far, this debris is only fed to cattle or simply burnt. In nature, pectin is a common substrate for various organisms. The degradation of pectin-rich biomass is often performed by filamentous fungi like *Hypocrea jecorina* (also known as *Trichoderma reesei*) and *Aspergillus niger*, which evolved pectinases to degrade the pectin backbone and pathways to consume the monomer GalA as a sole carbon source. The fungal catabolism of pectin residues starts with the reduction of GalA to L-galactonate (GalOA) by a GalA-reductase. Even though filamentous fungi are native hosts of the GalA-catabolism and certain engineering approaches have already been demonstrated, this class of organisms remains challenging with regard to bioreactor cultivation and tedious genetic accessibility. In contrast, the yeast *S. cerevisiae* is well known in fermentation processes and easily modified by a versatile set of genetic tools. So far, first approaches have already been conducted to transfer the GalA utilization pathways into *S. cerevisiae*, but these approaches indicated limitations regarding GalA-uptake and redox cofactor replenishment due to the relatively high oxidative state of GalA compared to other sugars like glucose and galactose. Furthermore, the generally strongly increased demand for redox cofactors must be met by GalA reduction by finding new cofactor sources or redirecting reactions of the core metabolism.

This work aimed at the production of GalOA, which is the first intermediate of the fungal GalA catabolism. This compound shows an interesting range of potential applications, for instance as a food and cosmetic additive. To overcome the oxidized character of GalA, the presence of a more reduced co-substrate as a redox donor and as a carbon and energy source was required. To further enhance the reduction of GalA, modulation of the redox-cofactor supply and enzyme engineering were performed.

At the beginning of this work, the influence of the educt and the desired product on the vitality of *S. cerevisiae* was investigated in a growth-based assay. This assay showed no effect of GalA or GalOA on the growth behavior of the yeast, when added to the growth medium. This finding was an important prerequisite for an efficient biotechnological process.

To initially establish the production of GalOA, the GalA-transporter *AnGATA* and the GalA-reductase *AnGAR1* ORFs (both from *A. niger*) were overexpressed under the control of strong yeast promoters from genomically integrated copies. These genetic modifications conferred the production of

0.27 g $L^{-1}$ GalOA after 5 days of cultivation, when glucose, the preferred carbon source of *S. cerevisiae*, was used as a co-substrate. However, the major part of the supplied 5 g $L^{-1}$ GalA remained unused in the fermentation broth, which showed the inefficiency of the process. The GalA-reductase, AnGar1, requires NADPH to perform the reaction, but this cofactor is not abundant in *S. cerevisiae*, which usually shows strong NADH-regeneration instead. In *S. cerevisiae*, the oxidative pentose phosphate pathway (oxPPP) is a major source of NADPH, which is produced in two consecutive reactions catalyzed by the glucose-6-phosphate dehydrogenase (Zwf1) and 6-phosphogluconate dehydrogenase (Gnd1/2), respectively. To favor the entrance of glucose-6-phosphate into oxPPP instead of glycolysis and thereby boost the supply of NADPH, the expression of the *ZWF1* gene was enhanced, whereas the gene encoding the phosphoglucose isomerase (*PGI1*) was downregulated. The expression strength of both genes was modulated by suitable promoter exchanges. The success of this approach was demonstrated by fermentation experiments, where both modifications individually and synergistically showed increased GalOA-production. Nevertheless, the GalOA titers remained relatively low.

Therefore, sorbitol, a polyol exhibiting a more reduced character compared to glucose, was used as a co-substrate in the following experiments. The utilization of sorbitol as a carbon source by *S. cerevisiae* requires the overexpression of at least one polyol transporter (such as the endogenous Hxt13) and a sorbitol dehydrogenase, which oxidizes sorbitol to fructose, a substrate of the glycolysis. Dependent on the employed sorbitol dehydrogenase, either NADH or NADPH can be produced in this reaction. For this purpose, either the endogenous enzyme Sor2 or YlSdr from *Yarrowia lipolytica* were overexpressed, respectively. Thereby, it could be shown that YlSdr is a powerful source of NADPH for two different GalA-reductases (from *A. niger* and *H. jecorina*). Even though the respective strain showed a severely delayed growth phenotype, its productivity was high, yielding around 2.5 g $L^{-1}$ GalOA. On the other hand, only a low amount of GalOA was produced when the NADH-yielding Sor2 was used instead. This confirmed the strong cofactor preference of the GalA-reductases for NADPH and demonstrated the importance of the supply of appropriate cofactors for the GalA-catalyzed reaction.

The growth phenotype observed in the strain expressing YlSdr was further investigated by studying the carbon source supply in the preculture and testing cells adapted to sorbitol metabolism. These studies demonstrated, that a functional redox cycle already in the preculture is of great benefit for the performance of the later cultivation, as late growth start vanished and the GalOA-productivity increased.

After assessing the appropriate preculture conditions, the suitable medium composition of the main culture was investigated by varying sorbitol and GalA concentrations. The concentration of the compounds can have great impact on the kinetics of their uptake and metabolism and thus on

the process itself. Here, it was shown, that higher supplementation of sorbitol and GalA indeed had a beneficial effect on the GalOA-titers. However, the advantage came at the expense of efficiency, as the molar yield (calculated as the produced mole of GalOA per consumed mole of sorbitol) decreased.

In order to limit the loss in efficiency but keep the concentration of the media components optimal, different cultivation techniques were tested. It was investigated how the efficiency of the process was affected by repeated inoculation of the yeast cells into fresh medium with and without cell retention.

The sorbitol-based fermentations were shown to be very productive and efficient, as long as the NADPH-dependent YlSdr was provided for sorbitol utilization. However, sorbitol is an expensive sugar and therefore uneconomic for use in industrial processes. The sparse NADPH-pool in *S. cerevisiae* suggested that connecting the GalA-reduction to the more abundant NADH-pool could be beneficial for GalOA-production. Since no NADH-preferring GalA-reductases have been described to date, their specificity must be shifted towards NADH by enzyme engineering. Thus, supported by comparative protein structure analysis, a mutagenesis study of the cofactor binding pocket was performed. The focus here was on amino acids, which stabilize the phosphate residue of NADPH through their electrostatic interaction. The resulting enzyme variants were tested in sorbitol-based fermentations, since an excess of NADH or NADPH could easily be generated by using the Sor2 (NADH-dependent) or the YlSdr (NADPH-dependent). This mutagenesis study led to NADH-accepting variants of the AnGar1 bearing the mutations K261M and R267L. Individually the mutations allowed the parallel use of NADH and NADPH, and in combination, the exclusive use of NADH. Compared to AnGaaA, a GalA reductase, which was described in literature to be more promiscuous in cofactor use, these new variants showed more efficient NADH-utilization. The molecular mechanism could be further illuminated in an enzyme assay. This assay showed that the enzyme can already naturally accept NADH, which, however, is inhibited by the presence of the oxidized cofactor $NADP^+$. Since in a living cell both cofactors, NADH and NADPH, are present in reduced and oxidized form, the presence of $NADP^+$ so far has obscured the NADH-dependent function of the GalA reductase in previous fermentations. Consequently, the mutagenesis successfully caused the destabilization of NADP(H) by a missing partner for electrostatic interaction (here, lysine or arginine) in the binding pocket of the enzyme. This prevented the inhibitory effect of $NADP^+$ on NADH-dependent GalA-reduction. These novel enzyme variants enabled the coupling of the GalA-reduction to the NADH-yielding glycolysis.

The novel variants of AnGar1 were tested in fermentations supplemented with glucose as carbon source. To further increase the accessibility of NADH for the GalA-reduction the gene of the predominant alcohol dehydrogenase Adh1 was deleted and the fermentation was performed under

microaerobic conditions. These approaches should prevent the reoxidation of NADH through ethanol production and respiration at the mitochondria, respectively. Indeed, the productivity of the AnGar1 [K261M, R267L] was increased, supporting the hypothesis. Still, with highest titers of 0.69 g $L^{-1}$ GalOA, these modifications remained inferior to the results of sorbitol fermentations, which range between 2 and 4 g $L^{-1}$ GalOA.

Further increase of the GalOA-titer could be achieved by expressing *AnGAR1* [R267L] and *AnGAR1* [K261M, R267L] in the yeast strain JWY019, which has an increased pool of NADH due to the deletion of the glycerol-3-phosphate dehydrogenase genes *GPD1* and *GPD2* in addition to the *ADH1* deletion. By these modifications, the production of glycerol and ethanol as major NADH sinks in yeast are minimized. In this strain background, the production increased to 0.84 g $L^{-1}$ GalOA. To further improve this yeast strain, the effect of a rerouted acetate pathway was investigated. Acetate as a common metabolite of the yeast metabolism is formed in the cytosol by the NADH-generating Ald2 or the NADPH-generating Ald6. It was assumed that the deletion of the *ALD6* gene would lead to an increased NADH supply, since the Ald2 reaction would remain the sole source of acetate, the precursor of the essential cytosolic acetyl-CoA. Contrary to the hypothesis, the deletion of *ALD6* caused a strong increase in GalOA-production for the AnGar1$^{WT}$, while the GalOA-titer of the AnGar1 [R267L] and AnGar1 [K261M, R267L] increased only slightly. Since the AnGar1$^{WT}$ mainly uses NADPH, this experiment posed the question regarding the molecular mechanism behind the increased level of NADPH as a consequence of the *ALD6* deletion. This question was answered by investigating the enzyme activity of the Pgi1 and the Zwf1 in the strain SiHY073 and its parent strain in comparison to their wildtype strain. Indeed, the activity of the Zwf1 was increased indicating a higher flux through the PPP due to the deleted aldehyde dehydrogenase gene (*Δald6*).

Further improvement of the SiHY073 regarding the production performance could be achieved by transiently overexpressing the three GalA-reductase variants. This demonstrated that on the one hand, the expression of the AnGar1$^{WT}$ was limiting and on the other hand it was possible to source the redox cofactors from the NADH- and the NADPH-pool. Throughout this overexpression study, it was found that the choice of the plasmid backbone has crucial impact on the success of the GalA-reductase gene expression. By reducing the glucose supplementation, it was discovered that the amount of glucose in the medium has a great impact on the complete biotransformation of the supplemented 5 g $L^{-1}$ GalA. Not only the glucose supplementation, but also the number of cells used for the biotransformation had a big effect on the velocity and the efficiency of the process, as both increased with the cell density in the fermentation.

Finally, the success of the strain SiHY073 was further investigated. The parental strain of SiHY073 was generated for increased isobutanol production and thus contains some modifications that are

not important for GalA reduction. Accordingly, the essential metabolic modifications of this precursor strain were reconstructed in a wild-type yeast strain to investigate in particular the effects of acetate, ethanol and glycerol metabolism on the efficiency of the GalA-reduction. It was found that only a combination of all modifications was particularly effective.

Overall, in this study the successful construction of *S. cerevisiae* strains which are capable to efficiently biotransform GalA to GalOA was demonstrated. Combined with the efforts made on pectin degradation from waste streams, the success of this work paves the way towards a value adding process based on the waste sugar streams obtained from the sugar refinery industry.

# 6 Summary in German Language

In Europa basiert die Zuckerraffination weitgehend auf Zuckerrüben. Dieser Weg zur Gewinnung von Haushaltszucker resultiert in einer großen Menge an Biomasseabfällen, die hauptsächlich aus den unlöslichen Rübenrückständen, z.B. Zellwandbruchstücken, bestehen. Diese Abfälle bestehen hauptsächlich aus dem Polymer Pektin (bis zu 20 % der Gesamttrockensubstanz). Das Grundgerüst von Pektin besteht aus D-Galakturonsäureeinheiten (GalA), enthält aber auch verschiedene andere Zuckermonomere, wie L-Arabinose, D-Galaktose, L-Rhamnose und D-Xylose. In diesem Zuckercocktail beträgt der Anteil von GalA bis zu 70%. Bisher werden die Reste der Zuckerraffinerie hauptsächlich in der Landwirtschaft verfüttert oder zur Entsorgung verbrannt. In der Natur jedoch ist Pektin ein häufiges Substrat für verschiedene Organismen. Die Ascomyceten *Hypocrea jecorina* (auch bekannt als *Trichoderma reesei*) und *Aspergillus niger* können die pektinreiche Biomasse nutzen, da sie Pektinasen zum Abbau des Pektingerüsts und Stoffwechselwege zum Verbrauch des Monomers GalA als Kohlenstoffquelle entwickelt haben. Der pilzliche Katabolismus von Pektinresten beginnt mit der Reduktion von GalA zu L-Galaktonat (GalOA) durch GalA-Reduktasen. Obwohl filamentöse Pilze native Wirte für den GalA-Katabolismus sind und vereinzelt schon Anwendungen für den Einsatz dieser Pilze zur Verwertung von pektinreicher Biomasse gezeigt wurden, bleibt diese Klasse von Organismen eine Herausforderung im Hinblick auf ihre Kultivierung in Bioreaktoren und ihrer schwer zugänglichen Genetik. Im Gegensatz dazu ist die Hefe *S. cerevisiae* in Fermentationsprozessen gut bekannt und lässt sich mit einer Vielzahl von genetischen Methoden leicht modifizieren. Bisher wurden bereits erste Versuche unternommen, die Fähigkeit zur GalA-Verwertung in *S. cerevisiae* zu übertragen. Diese Ansätze stießen jedoch oft auf Einschränkungen hinsichtlich des Transports von GalA in die Zelle und der Bereitstellung von Redox-Cofaktoren, da GalA im Vergleich zu anderen Zuckern wie Glucose und Galaktose einen relativ hohen oxidativen Zustand vorweist. Weiter muss der generell stark erhöhte Bedarf an Redox-Cofaktoren durch die GalA-Reduktion gedeckt werden indem neue Cofaktor-Quellen gefunden oder Reaktionen des Zentralmetabolismus umgeleitet werden.

Diese Arbeit hatte die Herstellung von GalOA zum Ziel. GalOA ist das erste Zwischenprodukt des nativen GalA-Abbaus und könnte in verschiedenen interessanten Anwendungen eingesetzt werden, so z. B. als Lebensmittel- und Kosmetikzusatzstoff. Die hohe Oxidationsstufe von GalA stellt eine Herausforderung für den Metabolismus dar, um dies zu umgehen ist ein stärker reduziertes Co-Substrats als Redox-Donor und als Kohlenstoff- und Energiequelle erforderlich. Um die Reduktion von GalA weiter zu verbessern, mussten Recyclingsysteme und die Versorgung der Reaktion mit Redox-Cofaktoren verbessert werden, darüber hinaus wurde das zentrale Enzym, die GalA-Reduktase, in ihrer Cofaktor-Präferenz optimiert. Dafür wurden gezielt Aminosäuren in der Cofaktorbindetasche des nativen Enzyms mutiert.

Zu Beginn dieser Arbeit wurde getestet, ob das Edukt (GalA) oder das gewünschte Produkt (GalOA) Einfluss auf das Wachstumsverhalten und damit auf die Fitness der Hefezellen hat. Dieser wachstumsbasierte Assay zeigte keinen Einfluss von GalA oder GalOA auf das Wachstumsverhalten von *S. cerevisiae*, wenn es direkt dem Wachstumsmedium zugesetzt wird. Dies ist eine wichtige Voraussetzung für einen effizienten biotechnologischen Prozess.

Um die Produktion von GalOA in *S. cerevisiae* zu etablieren, wurden die offenen Leserahmen des GalA-Transporters *AnGATA* und der GalA-Reduktase *AnGAR1* (beide aus *A. niger*) unter der Kontrolle starker konstitutiver Hefepromotoren von genomisch integrierten Kopien exprimiert. In entsprechenden Hefekulturen führte dies zur Produktion von 0,27 g $L^{-1}$ GalOA nach 5-tägiger Kultivierung, wenn Glucose, die bevorzugte Kohlenstoffquelle von *S. cerevisiae*, als Co-Substrat verwendet wurde. Der größte Teil der dem Medium zugegebenen 5 g $L^{-1}$ GalA verblieb jedoch ungenutzt in der Fermentationsbrühe, was die Ineffizienz des Prozesses illustriert. Die GalA-Reduktase, AnGar1, benötigt NADPH zur Katalyse dieser Reaktion, allerdings ist dieser Cofaktor in *S. cerevisiae* seltener verfügbar als das häufiger genutzte NADH, das verstärkt durch Glykolyse und Citratzyklus generiert wird. In *S. cerevisiae* ist der oxidative Pentosephosphatweg (oxPPP) eine wichtige Quelle für NADPH, das in zwei aufeinanderfolgenden Reaktionen erzeugt wird, die von der Glucose-6-Phosphat-Dehydrogenase (Zwf1) bzw. der 6-Phosphogluconat-Dehydrogenase (Gnd1/2) katalysiert werden. Um Glucose-6-Phosphat vermehrt in den oxPPP statt in die Glykolyse zu schleusen und dadurch die Versorgung mit NADPH zu erhöhen, wurde die Expression des *ZWF1*-Gens verstärkt, während das Gen, das für die Phospho-Glucose-Isomerase (*PGI1*) kodiert, herunterreguliert wurde. Die Expressionsstärke beider Gene wurde durch einen geeigneten Austausch der jeweiligen nativen Promotoren erreicht. Der Erfolg dieses Ansatzes wurde durch Fermentationsversuche nachgewiesen, bei denen beide Modifikationen einzeln und synergistisch eine erhöhte GalOA-Produktion zeigten. Trotzdem blieben die nach der Fermentation gemessenen GalOA-Titer niedrig.

Folglich wurde in anschließenden Experimenten Sorbitol, ein Polyol, dass im Vergleich zur Glucose stärker reduziert vorliegt, als Co-Substrat verwendet. Die Nutzung von Sorbitol als Kohlenstoffquelle durch *S. cerevisiae* erfordert die Überexpression von mindestens einem Polyol-Transporter (wie dem endogenen Hxt13) und einer Sorbitol-Dehydrogenase, die Sorbitol zu Fructose, einem Substrat der Glykolyse, oxidiert. Je nach eingesetzter Sorbitol-Dehydrogenase kann bei dieser Reaktion entweder verstärkt NADH oder NADPH generiert werden. Zu diesem Zweck wurde entweder das endogene Enzym Sor2 oder YlSdr aus *Yarrowia lipolytica* genutzt. Dies konnte zeigen, dass YlSdr eine starke NADPH-Quelle für zwei verschiedene GalA-Reduktasen (aus *A. niger* und *H. jecorina*) darstellen kann. Obwohl der Stamm einen stark verzögerten Wachstumsphänotyp zeigte, war seine Produktivität mit etwa 2,5 g $L^{-1}$ GalOA hoch. Vergleichend dazu wurde nur eine geringe Menge GalOA produziert, wenn stattdessen das NADH-produzierende Sor2 verwendet wurde. Dies bestätigte

die starke Präferenz der GalA-Reduktasen für NADPH und zeigte, wie wichtig es ist die Cofaktor-Präferenz eines Enzyms hinsichtlich eines effizienten Prozesses zu berücksichtigen.

Indem die Kohlenstoffquellen in den Vorkulturen variiert wurden, wurde der Wachstumsphänotyp, der bei dem YlSdr-exprimierenden Stamm beobachtet wurde, weiter untersucht. So konnten sich die Zellen in den verschiedenen Vorkulturen an den jeweiligen Zucker adaptieren. Die Zellen, die sich an den Sorbitol-Stoffwechsel angepasst hatten, zeigten in der Produktionskultur keinen Wachstumsphänotyp und zusätzlich erhöhte GalOA-Produktion. So zeigte diese Studie, dass ein funktioneller Redoxzyklus bereits in der Vorkultur von großem Nutzen für die Leistungsfähigkeit der Zellen in der Biotransformation ist.

Nach Untersuchung der geeigneten Vorkulturbedingungen wurde die Zusammensetzung des Mediums für die Hauptkultur durch Variation der Sorbitol- und GalA-Konzentrationen untersucht. Die Konzentration dieser Stoffe im Medium kann einen großen Einfluss auf die Kinetik ihrer Aufnahme und ihres Stoffwechsels und damit auf den gesamten Prozess haben. Tatsächlich konnte gezeigt werden, dass eine höhere Zugabe von Sorbitol und GalA tatsächlich eine positive Wirkung auf die GalOA-Titer der verschiedenen Kulturen hatte. Dabei ging der Vorteil jedoch auf Kosten der Effizienz, da die molare Ausbeute (berechnet als produziertes Mol GalOA pro verbrauchtem Mol Sorbitol) abnahm.

Um den Verlust in der Effizienz einzuschränken, aber die Konzentration der Medienkomponenten optimal zu halten, wurden verschiedene Kultivierungstechniken getestet. Hierbei wurde untersucht, wie die Effizienz des Prozesses durch wiederholtes inokulieren der Zellen in frisches Medium mit und ohne Zellrückhaltung beeinflusst wurde. Dabei wurde vermutet, dass die Expression der endogenen *SOR1* und *SOR2* die Effizienz der ansonsten auf die Expression der *YlSDR* basierte GalOA-Produktion verringerte.

Sorbitol-basierte Fermentationen erwiesen sich bisher als sehr produktiv und effizient, solange die NADPH-abhängige YlSdr für die Sorbitolverwertung eingesetzt wurde. Da Sorbitol jedoch ein im Einkauf teurer Zucker ist, ist dieser im späteren Einsatz in industriellen Prozessen aus wirtschaftlichen Gründen zu vermeiden. Das geringe NADPH-Level in *S. cerevisiae* legt nahe, dass eine Kopplung der GalA-Reduktion mit dem reichlich vorhandenen NADH-Level für die GalOA-Produktion von Vorteil sein könnte. Da bisher noch keine NADH-präferierenden GalA-Reduktasen beschrieben wurden, muss ihre Spezifität durch Enzymoptimierung in Richtung von NADH verschoben werden. Daher wurde, unterstützt durch eine vergleichende Proteinstrukturanalyse, eine Mutagenesestudie der Cofaktor-Bindungstasche durchgeführt. Im Fokus standen hier die Aminosäuren, die durch ihre elektrostatische Wechselwirkung den Phosphatrest des NADPH stabilisieren. Die daraus resultierenden Enzymvarianten wurden in Fermentationen basierend auf Sorbitol getestet, da durch die Verwendung von Sor2 (NADH-abhängig) oder YlSdr (NADPH-abhängig) ein Überschuss an NADH

oder NADPH erzeugt werden konnte. Diese Mutagenese-Studie führte zu NADH-akzeptierenden Varianten der AnGar1, die die Mutationen K261M und R267L vorwiesen. Im Einzelnen getestet führten diese Mutationen zur parallelen Nutzung von NADH und NADPH, in Kombination jedoch wurde ausschließlich NADH genutzt. Diese neuen Varianten zeigten eine effizientere NADH-Nutzung im Vergleich zu AnGaaA, einer GalA-Reduktase, die bezogen auf ihre Cofaktor-Nutzung in der Literatur eher als promiskuitiv beschrieben wurde, jedoch klar NADPH bevorzugt. Der molekulare Mechanismus hinter dieser Beobachtung konnte durch einen Enzymtest weiter untersucht werden. Dieser Assay zeigte, dass die GalA-Reduktase, AnGar1, bereits auf natürliche Weise NADH nutzen kann, was jedoch durch die Anwesenheit des oxidierten Cofaktors $NADP^+$ stark gehemmt wird. Da in einer lebenden Zelle beide Cofaktoren, NADH und NADPH, sowohl in reduzierter als auch in oxidierter Form vorliegen, hat die Anwesenheit von $NADP^+$ die NADH-abhängige Funktion der GalA-Reduktase in bisherigen Fermentationen verschleiert. Durch die Mutagenese wurde folglich die Destabilisierung des NADP(H) durch einen fehlenden Partner zur elektrostatischen Wechselwirkung (hier, Lysin oder Arginin) in der Bindetasche des Enzymes erfolgreich erwirkt. Hierdurch wurde die hemmende Wirkung des $NADP^+$ auf die NADH-abhängige GalA Reduktion unterbunden. Diese neuen Enzymvarianten ermöglichten die Kopplung der GalA-Reduktion an die NADH-produzierende Glykolyse.

Diese neuen Varianten der AnGar1 wurden in Fermentationen getestet, die mit Glucose als Kohlenstoffquelle durchgeführt wurden. Um die Verfügbarkeit von NADH für die GalA-Reduktion zu erhöhen, wurde das Gen der vorherrschenden Alkoholdehydrogenase Adh1 deletiert und die Fermentation unter mikroaeroben Bedingungen durchgeführt. Diese Ansätze sollten die Reoxidation von NADH durch die Ethanolproduktion bzw. die respiratorische Atmung an den Mitochondrien verringern. In der Tat war die Produktivität der AnGar1 [K261M, R267L] erhöht, was diese Hypothese unterstützt. Mit einem maximalen Titer von 0,69 g $L^{-1}$ GalOA blieben diese Modifikationen jedoch hinter den Ergebnissen der Sorbitol-Fermentationen zurück in denen zwischen 2 und 4 g $L^{-1}$ GalOA produziert wurden.

Eine weitere Steigerung des GalOA-Titers konnte durch die Expression von *AnGAR1* [R267L] und *AnGAR1* [K261M, R267L] im Hefestamm JWY019 erreicht werden, der aufgrund der Deletionen der Glycerin-3-Phosphat-Dehydrogenase-Gene *GPD1* und *GPD2* zusätzlich zur *ADH1*-Deletion einen erhöhten NADH-Pool aufweist. Durch diese Veränderungen wird die Produktion von Glycerin und Ethanol als Hauptkonkurrenten um den Cofaktor NADH in der Hefe minimiert. Bei diesem Stamm konnte die Produktion auf 0,84 g $L^{-1}$ GalOA gesteigert werden. Um diesen Hefestamm noch weiter zu verbessern, wurde untersucht, welche Wirkung ein umgeleiteter metabolischer Fluss von Acetat hat. Acetat als üblicher Metabolit des Hefestoffwechsels wird im Cytosol durch das NADH-bildende Ald2 oder das NADPH-bildende Ald6 produziert. Es wurde vermutet, dass die Deletion des *ALD6*-

Gens zu einer erhöhten NADH-Versorgung führen würde, da die Ald2-Reaktion als einzige Quelle für Acetat verbliebe. Acetat kann als Vorstufe für das essentielle Acetyl-CoA fungieren, das in vielen zellulären Prozessen Anwendung findet. Entgegen der aufgestellten Hypothese führte die Deletion von *ALD6* jedoch zu einer stark gesteigerten GalOA-Produktion der AnGar1$^{WT}$, während der GalOA-Titer von AnGar1 [R267L] und AnGar1 [K261M, R267L] nur geringfügig anstieg. Da die AnGar1$^{WT}$ hauptsächlich NADPH verwendet, kam die Frage nach dem molekularen Mechanismus auf, der hinter dem erhöhten NADPH-Gehalt als Folge der *ALD6*-Deletion steht. Zur Beantwortung dieser Frage wurde die Enzymaktivität von Pgi1 und Zwf1 im Stamm SiHY073 und seinem Elternstamm im Vergleich zu ihrem Wildtyp-Stamm untersucht. Tatsächlich war die Aktivität von Zwf1 erhöht, was auf einen höheren Fluss durch den PPP hinweist. Somit hat die Deletion des Aldehyddehydrogenase-Gens (Δald6) offenbar einen Einfluss auf die Regulation des *ZWF1*.

Weitere Verbesserung des SiHY073 hinsichtlich der Produktionsleistung konnte durch transiente Überexpression der GalA-Reduktase-Varianten (*AnGAR1$^{WT}$*, *AnGAR1* [R267L] und *AnGAR1* [K261M, R267L]) erreicht werden. Dies zeigte, dass zum einen die Expression der *AnGAR1$^{WT}$* limitierend war und zum anderen, dass die Redox-Cofaktoren aus sowohl dem NADH- als auch dem NADPH-Pool bezogen werden konnten. Im Laufe dieser Überexpressionsstudie wurde festgestellt, dass die Wahl des Plasmidrückgrats einen entscheidenden Einfluss auf den Erfolg der Expression der GalA-Reduktase-Gene hat. Weiterhin wurde festgestellt, dass die Verringerung der Startkonzentration der Glucose im Medium einen großen Einfluss auf die vollständige Biotransformation des zugesetzten 5 g $L^{-1}$ GalA hat. Nicht nur die Menge an Glucose, sondern auch die Anzahl der für die Biotransformation verwendeten Zellen hatte einen großen Einfluss auf die Geschwindigkeit und die Effizienz des Prozesses, da gezeigt wurde, dass sowohl der Titer als auch die Prozesszeit mit der Zelldichte in der Fermentation zunahm.

Abschließend wurde der Erfolg des Stammes SiHY073 weiter untersucht. Der Vorläuferstamm zu SiHY073 wurde für erhöhte Isobutanol-Produktion generiert und enthält damit einige Modifikationen, die für die GalA-Reduktion nicht von Bedeutung sind. Demnach wurden die essenziellen Stoffwechselmodifikationen dieses Vorläufer-Stammes in einem wildtyp Hefe-Stamm rekonstruiert, um insbesondere die Effekte des Acetat-, Ethanol- und Glycerin Stoffwechsels auf die Effizienz der GalA-Reduktion zu untersuchen. Es resultierte, dass erst eine Kombination aus allen Modifikationen besonders effektiv war.

Insgesamt wurde in dieser Studie die erfolgreiche Konstruktion von *S. cerevisiae*-Stämmen gezeigt, die in der Lage sind, GalA in einer Biotransformation effizient zu GalOA umzusetzen. Zusammen mit den Ansätzen um den Pektinabbau, vorwiegend mit filamentösen Pilzen durchgeführt, leistet der Erfolg dieser Arbeit einen Beitrag für zukünftige Wertschöpfungsprozesse basierend auf den Zuckerabfallströmen aus der Zuckerraffinerie.

# 7 References

Abbott, D.A., Zelle, R.M., Pronk, J.T., Van Maris, A.J.A., 2009. Metabolic engineering of Saccharomyces cerevisiae for production of carboxylic acids: Current status and challenges. FEMS Yeast Res. 9, 1123–1136. https://doi.org/10.1111/j.1567-1364.2009.00537.x

Aguilera, A., 1986. Deletion of the phosphoglucose isomerase structural gene makes growth and sporulation glucose dependent in Saccharomyces cerevisiae. MGG Mol. Gen. Genet. 204, 310–316. https://doi.org/10.1007/BF00425515

Alazi, E., Khosravi, C., Homan, T.G., du Pré, S., Arentshorst, M., Di Falco, M., Pham, T.T.M., Peng, M., Aguilar-Pontes, M.V., Visser, J., Tsang, A., de Vries, R.P., Ram, A.F.J., 2017. The pathway intermediate 2-keto-3-deoxy-L-galactonate mediates the induction of genes involved in D-galacturonic acid utilization in Aspergillus niger. FEBS Lett. 591, 1408–1418. https://doi.org/10.1002/1873-3468.12654

Albertyn, Jacobus, Hohmann, S., Prior, B.A., 1994. Characterization of the osmotic-stress response in Saccharomyces cerevisiae: osmotic stress and glucose repression regulate glycerol-3-phosphate dehydrogenase independently. Curr. Genet. 25, 12–18. https://doi.org/10.1007/BF00712960

Albertyn, J, Hohmann, S., Thevelein, J.M., Prior, B.A., 1994. GPD1, which encodes glycerol-3-phosphate dehydrogenase, is essential for growth under osmotic stress in Saccharomyces cerevisiae, and its expression is regulated by the high-osmolarity glycerol response pathway. Mol. Cell. Biol. 14, 4135–4144. https://doi.org/10.1128/mcb.14.6.4135-4144.1994

Anderlund, M., Nissen, T.L., Nielsen, J., Villadsen, J., Rydström, J., Hahn-Hägerdal, B., Kielland-Brandt, M.C., 1999. Expression of the Escherichia coli pntA and pntB genes, encoding nicotinamide nucleotide transhydrogenase, in Saccharomyces cerevisiae and its effect on product formation during anaerobic glucose fermentation. Appl. Environ. Microbiol. 65, 2333–2340. https://doi.org/10.1128/aem.65.6.2333-2340.1999

Andrianantoandro, E., Basu, S., Karig, D., Weiss, R., 2006. Synthetic biology: new engineering rules for an emerging discipline. Mol. Syst. Biol. 2, 1–14. https://doi.org/https://doi.org/10.1038/msb4100073

Apel, A.R., D'Espaux, L., Wehrs, M., Sachs, D., Li, R.A., Tong, G.J., Garber, M., Nnadi, O., Zhuang, W., Hillson, N.J., Keasling, J.D., Mukhopadhyay, A., 2017. A Cas9-based toolkit to program gene expression in Saccharomyces cerevisiae. Nucleic Acids Res. 45, 496–508. https://doi.org/https://doi.org/10.1093/nar/gkw1023

Attfield, P. V., 1998. Physiological and molecular aspects of hyperosmotic stress tolerance in yeast. Recent res Devel Microbiol. 2.

Attfield, P. V., Kletsas, S., 2000. Hyperosmotic stress response by strains of bakers' yeasts in high sugar concentration medium. Lett. Appl. Microbiol. 31, 323–327. https://doi.org/10.1046/j.1472-765X.2000.00825.x

Baeshen, N., Beashen, M., Sheikh, A., Bora, R., Ahmed, M., Ramadan, H., Saini, K., Redwan, E., 2014. Cell factories for insulin production. Microb. Cell Fact. 13, 2749–2763. https://doi.org/10.1016/S0065-7743(08)60586-2

Bakker, B.M., Overkamp, K.M., Van Maris, A.J.A., Kötter, P., Luttik, M.A.H., Van Dijken, J.P., Pronk, J.T., 2001. Stoichiometry and compartmentation of NADH metabolism in Saccharomyces cerevisiae. FEMS Microbiol. Rev. 25, 15–37. https://doi.org/10.1016/S0168-6445(00)00039-5

Becker, J., Boles, E., 2003. A modified Saccharomyces cerevisiae strain that consumes L-arabinose and produces ethanol. Appl. Environ. Microbiol. 69, 4144–4150. https://doi.org/10.1128/AEM.69.7.4144-4150.2003

Beier, A., Bordewick, S., Genz, M., Schmidt, S., van den Bergh, T., Peters, C., Joosten, H.J., Bornscheuer, U.T., 2016. Switch in cofactor specificity of a Baeyer–Villiger monooxygenase. ChemBioChem 17, 2312–2315. https://doi.org/10.1002/cbic.201600484

Bennis, S., Chami, F., Chami, N., Bouchikhi, T., Remmal, A., 2004. Surface alteration of Saccharomyces cerevisiae induced by thymol and eugenol. Lett. Appl. Microbiol. 38, 454–458. https://doi.org/10.1111/j.1472-765X.2004.01511.x

Benz, J.P., Protzko, R.J., Andrich, J.M., Bauer, S., Dueber, J.E., Somerville, C.R., 2014. Identification and characterization of a galacturonic acid transporter from Neurospora crassa and its application for Saccharomyces cerevisiae fermentation processes. Biotechnol. Biofuels 7, 20. https://doi.org/10.1186/1754-6834-7-20

Bergman, A., Vitay, D., Hellgren, J., Chen, Y., Nielsen, J., Siewers, V., 2019. Effects of overexpression of STB5 in Saccharomyces cerevisiae on fatty acid biosynthesis, physiology and transcriptome. FEMS Yeast Res. 19, 1–16. https://doi.org/10.1093/femsyr/foz027

Bernardi, G., 1979. The petite mutation in yeast. Trends Biochem. Sci. 4, 197–201. https://doi.org/https://doi.org/10.1016/0968-0004(79)90079-3

Biz, A., Sugai-Guérios, M.H., Kuivanen, J., Maaheimo, H., Krieger, N., Mitchell, D.A., Richard, P., 2016. The introduction of the fungal D-galacturonate pathway enables the consumption of D-galacturonic acid by Saccharomyces cerevisiae. Microb. Cell Fact. 15, 1–11. https://doi.org/10.1186/s12934-016-0544-1

Blank, L.M., Kuepfer, L., Sauer, U., 2005. Large-scale 13C-flux analysis reveals mechanistic principles of metabolic network robustness to null mutations in yeast. Genome Biol. 6, 1–16. https://doi.org/10.1186/gb-2005-6-6-r49

Blomberg, A., 2000. Metabolic surprises in Saccharomyces cerevisiae during adaptation to saline conditions: Questions, some answers and a model. FEMS Microbiol. Lett. 182, 1–8. https://doi.org/10.1016/S0378-1097(99)00531-5

Boer, H., Maaheimo, H., Koivula, A., Penttilä, M., Richard, P., 2010. Identification in Agrobacterium tumefaciens of the D-galacturonic acid dehydrogenase gene. Appl. Microbiol. Biotechnol. 86, 901–909. https://doi.org/10.1007/s00253-009-2333-9

Boguslawski, G., 1992. PBS2 , a yeast gene encoding a putative protein kinase , interacts with the RAS2 pathway and affects osmotic sensitivity of Saccharomyces cerevisiae. J. Gen. Microbiol. 138, 2425–2432. https://doi.org/https://doi.org/10.1099/00221287-138-11-2425

Boles, E., Lehnert, W., Zimmermann, F.K., 1993. The role of the NAD-dependent glutamate dehydrogenase in restoring growth on glucose of a Saccharomyces cerevisiae phosphoglucose isomerase mutant. Eur. J. Biochem. 217, 469–477. https://doi.org/10.1111/j.1432-1033.1993.tb18266.x

Borlinghaus, N., Nestl, B.M., 2018. Switching the cofactor specificity of an imine reductase. ChemCatChem 10, 183–187. https://doi.org/10.1002/cctc.201701194

Boumans, H., Grivell, L.A., Berden, J.A., 1998. The respiratory chain in yeast behaves as a single functional unit. J. Biol. Chem. 273, 4872–4877. https://doi.org/10.1074/jbc.273.9.4872

Brewster, J.L., Valoir, T. De, Dwyer, N.D., Winter, E., Gustin, M.C., 1993. An osmosensing signal transduction pathway in yeast. Science. 259, 1760–1763. https://doi.org/https://doi.org/10.1126/science.7681220

Broach, J.R., Hicks, J.B., 1980. Replication and recombination functions associated with the yeast plasmid, 2μ circle. Cell 21, 501–508. https://doi.org/10.1016/0092-8674(80)90487-0

Bruinenberg, P.M., Van Dijken, J.P., Scheffers, W.A., 1983. A theoretical analysis of NADPH production and consumption in yeasts. J. Gen. Microbiol. 129, 953–964. https://doi.org/10.1099/00221287-129-4-953

Canelas, A.B., Van Gulik, W.M., Heijnen, J.J., 2008. Determination of the cytosolic free NAD/NADH ratio in Saccharomyces cerevisiae under steady-state and highly dynamic conditions. Biotechnol. Bioeng. 100, 734–743. https://doi.org/10.1002/bit.21813

Cazzulo, J., Stoppani, O., 1968. Effects of adenosine phosphate and nicotinamide nucleotides on pyruvate carboxylase from baker's yeast. Biochem. J 112, 755–762. https://doi.org/https://doi.org/10.1042/bj1120755

Chang, Y.F., Feingold, D.S., 1970. D-glucaric acid and galactaric acid catabolism by Agrobacterium tumefaciens. J. Bacteriol. 102, 85–96. https://doi.org/10.1128/jb.102.1.85-96.1970

Chang, Y.F., Feingold, D.S., 1969. Hexuronic acid dehydrogenase of Agrobacterium tumefaciens. J. Bacteriol. 99, 667–673. https://doi.org/https://doi.org/10.1128/jb.99.3.667-673.1969

Charusanti, P., Conrad, T.M., Knight, E.M., Venkataraman, K., Fong, N.L., Xie, B., Gao, Y., Palsson, B., 2010. Genetic basis of growth adaptation of Escherichia coli after deletion of pgi, a major metabolic gene. PLoS Genet. 6. https://doi.org/10.1371/journal.pgen.1001186

Cohen, S.N., Chang, A.C.Y., Boyer, H.W., Helling, R.B., 1973. Construction of biologically functional bacterial plasmids in vitro. Proc. Natl. Acad. Sci. U. S. A. 70, 3240–3244. https://doi.org/10.1073/pnas.70.11.3240

Cole, M., Keenan, M., 1986. Synergistic effects of weak-acid preservatives and pH on the growth of Zygosaccharomyces bailii. Yeast 2, 93–100. https://doi.org/https://doi.org/10.1002/yea.320020204

Csiba, M., Cleophax, J., Petit, S., Gero, S., 1993. An expedient and practical three-step synthesis of vitamin C from a byproduct of the sugar industry: the galactono-1,4-lactone pathway. J. Org. Chem. 58, 7281–7282.

De Deken, R.H., 1966. The Crabtree effect: a regulatory system in yeast. J. Gen. Microbiol. 44, 149–156. https://doi.org/10.1099/00221287-44-2-149

De Jong, E., Dam, M.A., Sipos, L., Gruter, G.J.M., 2012. Furandicarboxylic acid (FDCA), A versatile building block for a very interesting class of polyesters. Am. Chem. Soc. 1–13. https://doi.org/10.1021/bk-2012-1105.ch001

Dicarlo, J.E., Norville, J.E., Mali, P., Rios, X., Aach, J., Church, G.M., 2013. Genome engineering in Saccharomyces cerevisiae using CRISPR-Cas systems. Nucleic Acids Res. 41, 4336–4343. https://doi.org/10.1093/nar/gkt135

Dudáš, A., Chovanec, M., 2004. DNA double-strand break repair by homologous recombination. Mutat. Res. 566, 131–167. https://doi.org/10.1016/j.mrrev.2003.07.001

Edwards, M.C., Doran-Peterson, J., 2012. Pectin-rich biomass as feedstock for fuel ethanol production. Appl. Microbiol. Biotechnol. 95, 565–575. https://doi.org/10.1007/s00253-012-

4173-2

Enquist-Newman, M., Faust, A.M.E., Bravo, D.D., Santos, C.N.S., Raisner, R.M., Hanel, A., Sarvabhowman, P., Le, C., Regitsky, D.D., Cooper, S.R., Peereboom, L., Clark, A., Martinez, Y., Goldsmith, J., Cho, M.Y., Donohoue, P.D., Luo, L., Lamberson, B., Tamrakar, P., Kim, E.J., Villari, J.L., Gill, A., Tripathi, S.A., Karamchedu, P., Paredes, C.J., Rajgarhia, V., Kotlar, H.K., Bailey, R.B., Miller, D.J., Ohler, N.L., Swimmer, C., Yoshikuni, Y., 2014. Efficient ethanol production from brown macroalgae sugars by a synthetic yeast platform. Nature 505, 239–243. https://doi.org/10.1038/nature12771

Eriksson, P., Andre, L., Ansell, R., Blomberg, A., Adler, L., 1995. Cloning and characterization of GPD2, a second gene encoding sn-glycerol 3-phosphate dehydrogenase (NAD+) in Saccharomyces cerevisiae, and its comparison with GPD1. Mol. Microbiol. 17, 95–107. https://doi.org/https://doi.org/10.1111/j.1365-2958.1995.mmi_17010095.x

Faich, G., Strobos, J., 1999. Sodium ferric gluconate complex in sucrose: Safer intravenous iron therapy than iron dextrans. Am. J. Kidney Dis. 33, 464–470. https://doi.org/Faich, G., Strobos, J., 1999. Sodium ferric gluconate complex in sucrose: Safer intravenous iron therapy than iron dextrans.

Fiaux, J., Çakar, Z.P., Sonderegger, M., Wüthrich, K., Szyperski, T., Sauer, U., 2003. Metabolic-flux profiling of the yeasts Saccharomyces cerevisiae and Pichia stipitis. Eukaryot. Cell 2, 170–180. https://doi.org/10.1128/EC.2.1.170-180.2003

Gamo, F.J., Moreno, E., Lagunas, R., 1995. The low-affinity component of the glucose transport system in Saccharomyces cerevisiae is not due to passive diffusion. Yeast 11, 1393–1398. https://doi.org/10.1002/yea.320111407

Gao, X., Caiyin, Q., Zhao, F., Wu, Y., Lu, W., 2018. Engineering Saccharomyces cerevisiae for enhanced production of protopanaxadiol with cofermentation of glucose and xylose, Journal of Agricultural and Food Chemistry. https://doi.org/10.1021/acs.jafc.8b04916

Generoso, W.C., Gottardi, M., Oreb, M., Boles, E., 2016. Simplified CRISPR-Cas genome editing for Saccharomyces cerevisiae. J. Microbiol. Methods 127, 203–205. https://doi.org/10.1016/j.mimet.2016.06.020

Görgens, J.F., Van Zyl, W.H., Knoetze, J.H., Hahn-Hägerdal, B., 2001. The metabolic burden of the PGK1 and ADH2 promoter systems for heterologous xylanase production by saccharomyces cerevisiae in defined medium. Biotechnol. Bioeng. 73, 238–245. https://doi.org/10.1002/bit.1056

Grohmann, K., Baldwin, E.A., Buslig, B.S., 1994. Production of ethanol from enzymatically hydrolyzed orange peel by the yeast Saccharomyces cerevisiae. Appl. Biochem. Biotechnol. 45–46, 315–327. https://doi.org/10.1007/BF02941808

Grohmann, K., Bothast, R., 1994. Pectin-rich residues generated by processing of citrus fruits, apples, and sugar beets. https://doi.org/DOI: 10.1021/bk-1994-0566.ch019

Grote, A., Hiller, K., Scheer, M., Münch, R., Nörtemann, B., Hempel, D.C., Jahn, D., 2005. JCat: A novel tool to adapt codon usage of a target gene to its potential expression host. Nucleic Acids Res. 33, 526–531. https://doi.org/10.1093/nar/gki376

Harholt, J., Suttangkakul, A., Scheller, H.V., 2010. Biosynthesis of pectin. Plant Physiol. 153, 384–395. https://doi.org/10.1104/pp.110.156588

Harth, S., Wagner, J., Sens, T., Choe, J. yong, Benz, J.P., Weuster-Botz, D., Oreb, M., 2020.

Engineering cofactor supply and NADH-dependent D-galacturonic acid reductases for redox-balanced production of L-galactonate in Saccharomyces cerevisiae. Sci. Rep. 10, 1–12. https://doi.org/10.1038/s41598-020-75926-5

Hauf, J., Zimmermann, F.K., Müller, S., 2000. Simultaneous genomic overexpression of seven glycolytic enzymes in the yeast Saccharomyces cerevisiae. Enzyme Microb. Technol. 26, 688–698. https://doi.org/10.1016/S0141-0229(00)00160-5

Heredia, C.F., Sols, A., Fuente, G. Dela, 1968. Specificity of the constitutive hexose transport in yeast. Eur. J. Biochem. 5, 321–329. https://doi.org/10.1111/j.1432-1033.1968.tb00373.x

Hilditch, S., 2010. Identification of the fungal catabolic D-galacturonate pathway, VTT Publications. https://doi.org/http://urn.fi/URN:ISBN:978-951-38-7399-8

Hilditch, S., Berghäll, S., Kalkkinen, N., Penttilä, M., Richard, P., 2007. The missing link in the fungal D-galacturonate pathway: Identification of the L-threo-3-deoxy-hexulosonate aldolase. J. Biol. Chem. 282, 26195–26201. https://doi.org/10.1074/jbc.M704401200

Hirayama, T., Maeda, T., Saito, H., Shinozaki, K., 1995. Cloning and characterization of seven cDNAs for hyperosmolarity-responsive (HOR) genes of Saccharomyces cerevisiae. Mgg Mol. Gen. Genet. 249, 127–138. https://doi.org/10.1007/BF00290358

Holyoak, C.D., Stratford, M., Mullin, Z.M.C., Cole, M.B., Crimmins, K., Brown, A.J.P., Coote, P.J., 1996. Activity of the plasma membrane H(+)-ATPase and optimal glycolytic flux are required for rapid adaptation and growth of Saccharomyces cerevisiae in the presence of the weak-acid preservative sorbic acid 62, 3158–3164. https://doi.org/https://doi.org/10.1128/aem.62.9.3158-3164.1996

Hou, J., Vemuri, G.N., Bao, X., Olsson, L., 2009. Impact of overexpressing NADH kinase on glucose and xylose metabolism in recombinant xylose-utilizing Saccharomyces cerevisiae. Appl. Microbiol. Biotechnol. 82, 909–919. https://doi.org/10.1007/s00253-009-1900-4

Hubbard, B.K., Koch, M., Palmer, D.R.J., Babbitt, P.C., Gerlt, J.A., 1998. Evolution of enzymatic activities in the enolase superfamily: Characterization of the (D)-glucarate/galactarate catabolic pathway in Escherichia coli. Biochemistry 37, 14369–14375. https://doi.org/10.1021/bi981124f

Huisjes, E.H., de Hulster, E., van Dam, J.C., Pronk, J.T., van Maris, A.J.A., 2012a. Galacturonic acid inhibits the growth of Saccharomyces cerevisiae on galactose, xylose, and arabinose. Appl. Environ. Microbiol. 78, 5052–5059. https://doi.org/10.1128/AEM.07617-11

Huisjes, E.H., Luttik, M.A.H., Almering, M.J.H., Bisschops, M.M.M., Dang, D.H.N., Kleerebezem, M., Siezen, R., van Maris, A.J.A., Pronk, J.T., 2012b. Toward pectin fermentation by Saccharomyces cerevisiae: Expression of the first two steps of a bacterial pathway for D-galacturonate metabolism. J. Biotechnol. 162, 303–310. https://doi.org/10.1016/j.jbiotec.2012.10.003

Irani, M., Taylor, W.E., Young, E.T., 1987. Transcription of the ADH2 gene in Saccharomyces cerevisiae is limited by positive factors that bind competitively to its intact promoter region on multicopy plasmids. Mol. Cell. Biol. 7, 1233–1241. https://doi.org/10.1128/mcb.7.3.1233

Ishikawa, T., Nishikawa, H., Gao, Y., Sawa, Y., Shibata, H., Yabuta, Y., Maruta, T., Shigeoka, S., 2008. The pathway via D-galacturonate/L-galactonate is significant for ascorbate biosynthesis in Euglena gracilis: Identification and functional characterization of aldonolactonase. J. Biol. Chem. 283, 31133–31141. https://doi.org/10.1074/jbc.M803930200

Jeffcoat, R., 1975. Studies on the subunit structure of 4 deoxy 5 oxoglucarate hydro lyase

(decarboxylating) from Pseudomonas acidovorans. Biochem. J. 145, 305–309. https://doi.org/10.1042/bj1450305

Jeong, D., Ye, S., Park, H., Kim, S.R., 2020. Simultaneous fermentation of galacturonic acid and five-carbon sugars by engineered Saccharomyces cerevisiae. Bioresour. Technol. 295, 122259. https://doi.org/10.1016/j.biortech.2019.122259

Jinek, M., Chylinski, K., Fonfara, I., Hauer, M., Doudna, J.A., Charpentier, E., 2012. A programmable dual-RNA – guided DNA endonuclease in adaptive bacterial immunity. Science. 337, 816–821. https://doi.org/https://doi.org/10.1126/science.1225829

Johnston, M., Davis, R.W., 1984. Sequences that regulate the divergent GAL1-GAL10 promoter in Saccharomyces cerevisiae. Mol. Cell. Biol. 4, 1440–1448. https://doi.org/10.1128/MCB.4.8.1440

Jordan, P., Choe, J.-Y., Boles, E., Oreb, M., 2016. Hxt13, Hxt15, Hxt16 and Hxt17 from Saccharomyces cerevisiae represent a novel type of polyol transporters. Sci. Rep. 6, 1–10. https://doi.org/10.1038/srep23502

Juhnke, H., Krems, B., Kftter, P., Entian, K., 1996. Mutants that show increased sensitivity to hydrogen peroxide reveal an important role for the pentose phosphate pathway in protection of yeast against oxidative stress. Mol Gen Genet 252, 456–464.

Karim, A.S., Curran, K.A., Alper, H.S., 2013. Characterization of plasmid burden and copy number in Saccharomyces cerevisiae for optimization of metabolic engineering applications. FEMS Yeast Res. 13, 107–116. https://doi.org/10.1111/1567-1364.12016

Katz, S., Maytag, F., 1991. Brewing and ancient beer. Archaeology 44, 24–27.

Kavšček, M., Stražar, M., Curk, T., Natter, K., Petrovič, U., 2015. Yeast as a cell factory: current state and perspectives. Microb. Cell Fact. 1–10. https://doi.org/10.1186/s12934-015-0281-x

Kawai, S., Suzuki, S., Mori, S., Murata, K., 2001. Molecular cloning and identification of UTR1 of a yeast Saccharomyces cerevisiae as a gene encoding an NAD kinase. FEMS Microbiol. Lett. 200, 181–184. https://doi.org/https://doi.org/10.1111/j.1574-6968.2001.tb10712.x

Keasling, J.D., 2010. Manufacturing molecules through metabolic engineering. Science. 330, 1355–1359. https://doi.org/https://doi.org/10.1126/science.1193990

Keasling, J.D., 2008. Synthetic biology for synthetic chemistry. ACS Chem. Biol. 3, 64–76. https://doi.org/10.1021/cb7002434

Keren, L., Zackay, O., Lotan-Pompan, M., Barenholz, U., Dekel, E., Sasson, V., Aidelberg, G., Bren, A., Zeevi, D., Weinberger, A., Alon, U., Milo, R., Segal, E., 2013. Promoters maintain their relative activity levels under different growth conditions. Mol. Syst. Biol. 9, 1–17. https://doi.org/10.1038/msb.2013.59

Khoury, G.A., Fazelinia, H., Chin, J.W., Pantazes, R.J., Cirino, P.C., Maranas, C.D., 2009. Computational design of Candida boidinii xylose reductase for altered cofactor specificity. Protein Sci. 18, 2125–2138. https://doi.org/10.1002/pro.227

Kim, J., Jang, I., Sung, B.H., Kim, S.C., Lee, J.Y., 2018. Rerouting of NADPH synthetic pathways for increased protopanaxadiol production in Saccharomyces cerevisiae. Sci. Rep. 8, 1–11. https://doi.org/10.1038/s41598-018-34210-3

Kohn, R., Kovác, P., 1978. Dissociation constants of D-galacturonic and D-glucuronic acid and their O-methyl derivatives. Chem. Zvesti 32, 478–485.

Kresze, G., Ronft, H., 1981a. Pyruvate dehydrogenase complex from baker's yeast: 2. Molecular structure, dissociation, and implications for the origin of mitochondria. Eur. J. Biochem. 119, 573–579.

Kresze, G., Ronft, H., 1981b. Pyruvate dehydrogenase complex from baker's Yeast: 1. Purification and some kinetic and regulatory properites. Eur. J. Biochem. 119, 573–579. https://doi.org/10.1111/j.1432-1033.1981.tb05646.x

Kuivanen, J., Dantas, H., Mojzita, D., Mallmann, E., Biz, A., Krieger, N., Mitchell, D., Richard, P., 2014. Conversion of orange peel to L-galactonic acid in a consolidated process using engineered strains of Aspergillus niger. AMB Express 4, 1–8. https://doi.org/https://doi.org/10.1186/s13568-014-0033-z

Kuivanen, J., Mojzita, D., Wang, Y., Hilditch, S., Penttilä, M., Richard, P., Wiebe, M.G., 2012. Engineering filamentous fungi for conversion of d-galacturonic acid to L-galactonic acid. Appl. Environ. Microbiol. 78, 8676–8683. https://doi.org/10.1128/AEM.02171-12

Kuivanen, J., Wang, Y.M.J., Richard, P., 2016. Engineering Aspergillus niger for galactaric acid production: Elimination of galactaric acid catabolism by using RNA sequencing and CRISPR/Cas9. Microb. Cell Fact. 15, 1–9. https://doi.org/10.1186/s12934-016-0613-5

Kuorelahti, S., Jouhten, P., Maaheimo, H., Penttilä, M., Richard, P., 2006. L-Galactonate dehydratase is part D-galacturonic acid catabolism of the fungal path for D-galacturonic acid catabolism. Mol. Microbiol. 61, 1060–1068. https://doi.org/10.1111/j.1365-2958.2006.05294.x

Kuorelahti, S., Kalkkinen, N., Penttilä, M., Londesborough, J., Richard, P., 2005. Identification in the mold Hypocrea jecorina of the first fungal D-galacturonic acid reductase. Biochemistry 44, 11234–11240. https://doi.org/10.1021/bi050792f

Landi, C., Paciello, L., de Alteriis, E., Brambilla, L., Parascandola, P., 2011. Effect of auxotrophies on yeast performance in aerated fed-batch reactor. Biochem. Biophys. Res. Commun. 414, 604–611. https://doi.org/10.1016/j.bbrc.2011.09.129

Larochelle, M., Drouin, S., Turcotte, B., Room, H., Hospital, R.V., Ave, P., 2006. Oxidative stress-activated zinc cluster protein Stb5 has dual activator/ repressor functions required for pentose phosphate pathway regulation and NADPH production 26, 6690–6701. https://doi.org/10.1128/MCB.02450-05

Larsson, K., Ansell, R., Eriksson, P., Adler, L., 1993. A gene encoding sn-glycerol 3-phosphate dehydrogenase (NAD+) complements an osmosensitive mutant of Saccharomyces cerevisiae. Mol. Microbiol. 10, 1101–1111. https://doi.org/10.1111/j.1365-2958.1993.tb00980.x

Lee, M.E., DeLoache, W.C., Cervantes, B., Dueber, J.E., 2015. A highly characterized yeast toolkit for modular, multipart assembly. ACS Synth. Biol. 4, 975–986. https://doi.org/https://doi.org/10.1021/sb500366v

Lee, T.H., Maheshri, N., 2012. A regulatory role for repeated decoy transcription factor binding sites in target gene expression. Mol. Syst. Biol. 8, 1–11. https://doi.org/10.1038/msb.2012.7

Lewkowski, J., 2001. Convenient synthesis of furan-2,5-dicarboxylic acid and its derivatives. Pol. J. Chem. 75, 1943–1946.

Li, X., Wu, D., Lu, T., Yi, G., Su, H., Zhang, Y., 2014. Highly efficient chemical process to convert mucic acid into adipic acid and DFT studies of the mechanism of the rhenium-catalyzed deoxydehydration. Angew. Chemie 126, 4284–4288. https://doi.org/https://doi.org/10.1002/ange.201310991

Liepins, J., Kuorelahti, S., Penttila, M., Richard, P., 2006. Enzymes for the NADPH-dependent reduction of dihydroxyacetone and D -glyceraldehyde and L -glyceraldehyde in the mould Hypocrea jecorina. FEBS J. 273, 4229–4235. https://doi.org/10.1111/j.1742-4658.2006.05423.x

Loeschner, W., Everard, J., 2000. Regulation of sugar alcohol biosynthesis. Photosynthesis 9, 275–299.

Lõoke, M., Kristjuhan, K., Kristjuhan, A., 2011. Extraction of genomic DNA from yeasts for PCR-based applications. Biotechniques 50, 325–328. https://doi.org/10.2144/000113672

Luo, X., Reiter, M.A., d'Espaux, L., Wong, J., Denby, C.M., Lechner, A., Zhang, Y., Grzybowski, A.T., Harth, S., Lin, W., Lee, H., Yu, C., Shin, J., Deng, K., Benites, V.T., Wang, G., Baidoo, E.E.K., Chen, Y., Dev, I., Petzold, C.J., Keasling, J.D., 2019. Complete biosynthesis of cannabinoids and their unnatural analogues in yeast. Nature 567, 123–126. https://doi.org/10.1038/s41586-019-0978-9

Mager, W.H., Varela, J.C.S., 1993. Osmostress response of the yeast Saccharomyces. Mol. Microbiol. 10, 253–258. https://doi.org/10.1111/j.1365-2958.1993.tb01951.x

Martens-Uzunova, E.S., Schaap, P.J., 2008. An evolutionary conserved d-galacturonic acid metabolic pathway operates across filamentous fungi capable of pectin degradation. Fungal Genet. Biol. 45, 1449–1457. https://doi.org/10.1016/j.fgb.2008.08.002

Matsubara, T., Hamada, S., Wakabayashi, A., Kishida, M., 2016. Fermentative production of L-galactonate by using recombinant Saccharomyces cerevisiae containing the endogenous galacturonate reductase gene from Cryptococcus diffluens. J. Biosci. Bioeng. 122, 639–644. https://doi.org/10.1016/j.jbiosc.2016.05.002

McAlister, L., Holland, M.J., 1985. Isolation and characterization of yeast strains carrying mutations in the glyceraldehyde-3-phosphate dehydrogenase genes. J. Biol. Chem. 260, 15013–15018. https://doi.org/10.1016/s0021-9258(18)95695-4

McCaskill, D., Croteau, R., 1997. Prospects for the bioengineering of isoprenoid biosynthesis, Biotechnology of Aroma Compounds. https://doi.org/DOI: 10.1007/BFb0102064

Meaden, P.G., Dickinson, F.M., Mifsud, A., Tessier, W., Westwater, J., Bussey, H., Midgley, M., 1997. The ALD6 gene of saccharomyces cerevisiae encodes a cytosolic, Mg2+-activated acetaldehyde dehydrogenase. Yeast 13, 1319–1327. https://doi.org/10.1002/(SICI)1097-0061(199711)13:14<1319::AID-YEA183>3.0.CO;2-T

Mohnen, D., 2008. Pectin structure and biosynthesis. Curr. Opin. Plant Biol. 11, 266–277. https://doi.org/10.1016/j.pbi.2008.03.006

Murray, D.B., Haynes, K., Tomita, M., 2011. Redox regulation in respiring Saccharomyces cerevisiae. Biochim. Biophys. Acta 1810, 945–958. https://doi.org/10.1016/j.bbagen.2011.04.005

Napora, K., Wrodnigg, T.M., Kosmus, P., Thonhofer, M., Robins, K., Winkler, M., 2013. Yarrowia lipolytica dehydrogenase/reductase: An enzyme tolerant for lipophilic compounds and carbohydrate substrates. Bioorganic Med. Chem. Lett. 23, 3393–3395. https://doi.org/10.1016/j.bmcl.2013.03.064

Navarro-Aviño, J.P., Prasad, R., Miralles, V.J., Benito, R.M., Serrano, R., 1999. A proposal for nomenclature of aldehyde dehydrogenases in Saccharomyces cerevisiae and characterization of the stress-inducible ALD2 and ALD3 genes. Yeast 15, 829–842. https://doi.org/10.1002/(SICI)1097-0061(199907)15:10A<829::AID-YEA423>3.0.CO;2-9

Nevoigt, E., 2008. Progress in metabolic engineering of Saccharomyces cerevisiae. Microbiol. Mol. Biol. Rev. 72, 379–412. https://doi.org/10.1128/MMBR.00025-07

Norbeck, J., Påhlman, A.K., Akhtar, N., Blomberg, A., Adler, L., 1996. Purification and characterization of two isoenzymes of DL-glycerol-3-phosphatase from Saccharomyces cerevisiae: Identification of the corresponding GPP1 and GPP2 genes and evidence for osmotic regulation of Gpp2p expression by the osmosensing mitogen-acti. J. Biol. Chem. 271, 13875–13881. https://doi.org/10.1074/jbc.271.23.13875

Onofri, S., Poerio, E., Serangeli, P., Tosi, S., Garuccio, I., Arrigoni, O., 1997. Influence of L-galactonic acid -lactone on ascorbate production in some yeasts. Antonie Van Leeuwenhoek 71, 277–280. https://doi.org/https://doi.org/10.1023/A:1000161921389

Ouyang, L., Holland, P., Lu, H., Bergenholm, D., Nielsen, J., 2018. Integrated analysis of the yeast NADPH-regulator Stb5 reveals distinct differences in NADPH requirements and regulation in different states of yeast metabolism. FEMS Yeast Res. 18, 1–12. https://doi.org/10.1093/femsyr/foy091

Overkamp, K., Bakker, B., Kötter, P., Luttik, M., van Dijken, J., Pronk, J., 2002. Metabolic engineering of glycerol production in Saccharomyces cerevisiae. Appl. Environ. Microbiol. 68, 2814–2821. https://doi.org/DOI: 10.1128/AEM.68.6.2814–2821.2002

Paasikallio, T., Huuskonen, A., Wiebe, M.G., 2017. Scaling up and scaling down the production of galactaric acid from pectin using Trichoderma reesei. Microb. Cell Fact. 16, 1–11. https://doi.org/10.1186/s12934-017-0736-3

Paddon, C.J., Westfall, P.J., Pitera, D.J., Benjamin, K., Fisher, K., McPhee, D., Leavell, M.D., Tai, A., Main, A., Eng, D., Polichuk, D.R., Teoh, K.H., Reed, D.W., Treynor, T., Lenihan, J., Jiang, H., Fleck, M., Bajad, S., Dang, G., Dengrove, D., Diola, D., Dorin, G., Ellens, K.W., Fickes, S., Galazzo, J., Gaucher, S.P., Geistlinger, T., Henry, R., Hepp, M., Horning, T., Iqbal, T., Kizer, L., Lieu, B., Melis, D., Moss, N., Regentin, R., Secrest, S., Tsuruta, H., Vazquez, R., Westblade, L.F., Xu, L., Yu, M., Zhang, Y., Zhao, L., Lievense, J., Covello, P.S., Keasling, J.D., Reiling, K.K., Renninger, N.S., Newman, J.D., 2013. High-level semi-synthetic production of the potent antimalarial artemisinin. Nature 496, 528–532. https://doi.org/10.1038/nature12051

Påhlman, A., Granath, K., Ansell, R., Hohmann, S., Adler, L., 2001. The Yeast Glycerol 3-Phosphatases Gpp1p and Gpp2p are required for glycerol biosynthesis and differentially involved in the cellular responses to osmotic , anaerobic, and oxidative stress. J. Biol. Chem. 276, 3555–3563. https://doi.org/10.1074/jbc.M007164200

Perpelea, A., Wiranata, A., Martins, L.C., Rippert, D., Klein, M., Angelov, A., Peltonen, K., Teleki, A., Liebl, W., Richard, P., Thevelein, J.M., Takors, R., Isabel, S., Nevoigt, E., 2022. Towards valorization of pectin-rich agro-industrial residues: Engineering of Saccharomyces cerevisiae for co-fermentation of D-galacturonic acid and glycerol. Metab. Eng. 69, 1–14. https://doi.org/10.1016/j.ymben.2021.10.001

Pfeifer, B., Khosla, C., 2001. Biosynthesis of polyketides in heterologous hosts. Microbiol. Mol. Biol. Rev. 65, 106–118. https://doi.org/10.1128/MMBR.65.1.106

Piper, P., Calderon, C.O., Hatzixanthis, K., 2001. Weak acid adaptation : the stress response that confers yeasts with resistance to organic acid food preservatives. Microbiology 147, 2635–2642. https://doi.org/https://doi.org/10.1099/00221287-147-10-2635

Piškur, J., Rozpedowska, E., Polakova, S., Merico, A., Compagno, C., 2006. How did Saccharomyces evolve to become a good brewer? Trends Genet. 22, 183–186. https://doi.org/10.1016/j.tig.2006.02.002

Pollak, N., Dölle, C., Ziegler, M., 2007. The power to reduce: Pyridine nucleotides - Small molecules with a multitude of functions. Biochem. J. 402, 205–218. https://doi.org/10.1042/BJ20061638

Pronk, J.T., Steensma, H.Y., Van Dijken, J.P., 1996. Pyruvate metabolism in Saccharomyces cerevisiae. Yeast 12, 1607–1633. https://doi.org/10.1002/(SICI)1097-0061(199612)12:16<1607::AID-YEA70>3.0.CO;2-4

Protzko, R.J., Hach, C.A., Coradetti, S.T., Hackhofer, M.A., Magosch, S., Thieme, N., Geiselman, G.M., Arkin, A.P., Skerker, J.M., Dueber, J.E., Benz, J.P., 2019. Genomewide and enzymatic analysis reveals efficient D-galacturonic acid metabolism in the Basidiomycete yeast Rhodosporidium toruloides. mSystems 4, 1–16. https://doi.org/10.1128/msystems.00389-19

Protzko, R.J., Latimer, L.N., Martinho, Z., Reus, E. De, Seibert, T., Benz, J.P., Dueber, J.E., 2018. Engineering Saccharomyces cerevisiae for co-utilization of D-galacturonic acid and D-glucose from citrus peel waste. Nat. Commun. 9, 5059. https://doi.org/10.1038/s41467-018-07589-w

Quain, D.E., Boulton, C.A., 1987. Growth and metabolism of mannitol by strains of Saccharomyces cerevisiae. J. Gen. Microbiol. 133, 1675–1684. https://doi.org/10.1099/00221287-133-7-1675

Reed, L., Yeaman, S., 1987. Pyruvate dehydrogenase. Acad. Press 18, 77–95. https://doi.org/https://doi.org/10.1016/S1874-6047(08)60254-1

Reshamwala, S.M.S., Lali, A.M., 2020. Exploiting the NADPH pool for xylitol production using recombinant Saccharomyces cerevisiae. Biotechnol. Prog. 36, 1–7. https://doi.org/10.1002/btpr.2972

Richard, P., Hilditch, S., 2009. D-Galacturonic acid catabolism in microorganisms and its biotechnological relevance. Appl. Microbiol. Biotechnol. 82, 597–604. https://doi.org/10.1007/s00253-009-1870-6

Roland, J., Cayle, T., Dinwoodie, R., Mehnert, D., 1986. Fermentation production of ascorbic acid from L-galactonic substrate.

San Francisco, M.J.D., Keenan, R.W., 1993. Uptake of galacturonic acid in Erwinia chrysanthemi EC16. J. Bacteriol. 175, 4263–4265. https://doi.org/10.1128/jb.175.13.4263-4265.1993

Sarthy, A., Schopp, C., Idler, K., 1993. Cloning and sequencing determination of the gene encoding sorbitol dehydrogenase from Saccharomyces cerevisiae. Mol. Biol. 140, 121–126. https://doi.org/https://doi.org/10.1016/0378-1119(94)90741-2

Sawyer, D.T., 1964. Metal-gluconate complexes. Chem. Rev. 64, 633–643.

Schmitz, K., Protzko, R., Zhang, L., Benz, J.P., 2019. Spotlight on fungal pectin utilization—from phytopathogenicity to molecular recognition and industrial applications. Appl. Microbiol. Biotechnol. 103, 2507–2524. https://doi.org/10.1007/s00253-019-09622-4

Schüller, C., Brewster, J.L., Alexander, M.R., Gustin, M.C., Ruis, H., 1994. The HOG pathway controls osmotic regulation of transcription via the stress response element (STRE) of the Saccharomyces cerevisiae CTT1 gene. EMBO J. 13, 4382–4389. https://doi.org/10.1002/j.1460-2075.1994.tb06758.x

Seelbach, K., Riebel, B., Hummel, W., Kula, M.R., Tishkov, V.I., Egorov, A.M., Wandrey, C., Kragl, U., 1996. A novel, efficient regenerating method of NADPH using a new formate dehydrogenase. Tetrahedron Lett. 37, 1377–1380. https://doi.org/10.1016/0040-4039(96)00010-X

Sharma, N., Rathore, M., Sharma, M., 2013. Microbial pectinase: Sources, characterization and applications. Rev. Environ. Sci. Biotechnol. 12, 45–60. https://doi.org/10.1007/s11157-012-

9276-9

Shi, F., Kawai, S., Mori, S., Kono, E., Murata, K., 2005. Identification of ATP-NADH kinase isozymes and their contribution to supply of NADP(H) in Saccharomyces cerevisiae. FEBS J. 272, 3337–3349. https://doi.org/10.1111/j.1742-4658.2005.04749.x

Sloothaak, J., Schilders, M., Schaap, P.J., de Graaff, L.H., 2014. Overexpression of the Aspergillus niger GatA transporter leads to preferential use of D-galacturonic acid over D-xylose. AMB Express 4, 66. https://doi.org/10.1186/s13568-014-0066-3

Smith, K.M., Cho, K.M., Liao, J.C., 2010. Engineering Corynebacterium glutamicum for isobutanol production. Appl. Microbiol. Biotechnol. 87, 1045–1055. https://doi.org/10.1007/s00253-010-2522-6

Souffriau, B., Den Abt, T., Thevelein, J.M., 2012. Evidence for rapid uptake of d-galacturonic acid in the yeast Saccharomyces cerevisiae by a channel-type transport system. FEBS Lett. 586, 2494–2499. https://doi.org/10.1016/j.febslet.2012.06.012

Tamayo Rojas, S.A., Schadeweg, V., Kirchner, F., Boles, E., 2021. Identification of a glucose - insensitive variant of Gal2 from Saccharomyces cerevisiae exhibiting a high pentose transport capacity. Sci. Rep. 11, 1–10. https://doi.org/10.1038/s41598-021-03822-7

Tilmann, D., Socolow, R., Foley, J., Hill, J., Larson, E., Lynd, L., Pacala, S., Reilly, J., Searchinger, T., Somerville, C., Williams, R., 2009. Beneficial biofuels—The food, energy, and environment trilemma. Science. 5938, 270–271. https://doi.org/https://doi.org/10.1126/science.1177970

van Dijken, J.., Bauer, J., Brambilla, L., Duboc, P., Francois, J.., Gancedo, C., Giuseppin, M.L.., Heijnen, J.., Hoare, M., Lange, H.., Madden, E.., Niederberger, P., Nielsen, J., Parrou, J.., Petit, T., Porro, D., Reuss, M., van Riel, N., Rizzi, M., Steensma, H.., Verrips, C.., Vindeløv, J., Pronk, J.., 2000. An interlaboratory comparison of physiological and genetic properties of four Saccharomyces cerevisiae strains. Enzyme Microb. Technol. 26, 706–714. https://doi.org/https://doi.org/10.1016/S0141-0229(00)00162-9

van Dijken, J.P., Scheffers, W.A., 1986. Redox balances in the metabolism of sugars by yeasts. FEMS Microbiol. Lett. 32, 199–224. https://doi.org/10.1016/0378-1097(86)90291-0

van Urk, H., Schipper, D., Breedveld, G.J., Mak, P.R., Alexander Scheffers, W., van Dijken, J.P., 1989. Localization and kinetics of pyruvate-metabolizing enzymes in relation to aerobic alcoholic fermentation in Saccharomyces cerevisiae CBS 8066 and Candida utilis CBS 621. BBA - Gen. Subj. 992, 78–86. https://doi.org/10.1016/0304-4165(89)90053-6

VanLinden, M.R., Skoge, R.H., Ziegler, M., 2015. Discovery, metabolism and functions of NAD and NADP. Biochem. (Lond). 37, 9–13. https://doi.org/10.1042/bio03701009

Wargacki, A.J., Leonard, E., Win, M.N., Regitsky, D.D., Santos, C.N.S., Kim, P.B., Cooper, S.R., Raisner, R.M., Herman, A., Sivitz, A.B., Lakshmanaswamy, A., Kashiyama, Y., Baker, D., Yoshikuni, Y., 2012. An engineered microbial platform for direct biofuel production from brown macroalgae. Science. 335, 308–313. https://doi.org/10.1126/science.1214547

Wernig, F., Baumann, L., Boles, E., Oreb, M., 2021. Production of octanoic acid in Saccharomyces cerevisiae: Investigation of new precursor supply engineering strategies and intrinsic limitations. Biotechnol. Bioeng. 118, 3046–3057. https://doi.org/10.1002/bit.27814

Wess, J., Brinek, M., Boles, E., 2019. Improving isobutanol production with the yeast Saccharomyces cerevisiae by successively blocking competing metabolic pathways as well as ethanol and glycerol formation. Biotechnol. Biofuels 12, 1–15. https://doi.org/10.1186/s13068-019-1486-

8

Wieczorke, R., Krampe, S., Weierstall, T., Freidel, K., Hollenberg, C.P., Boles, E., 1999. Concurrent knock-out of at least 20 transporter genes is required to block uptake of hexoses in Saccharomyces cerevisiae. FEBS Lett. 464, 123–128. https://doi.org/10.1016/S0014-5793(99)01698-1

Woodyer, R., Van der Donk, W.A., Zhao, H., 2003. Relaxing the nicotinamide cofactor specificity of phosphite dehydrogenase by rational design. Biochemistry 42, 11604–11614. https://doi.org/10.1021/bi035018b

Ying, W., 2008. NAD+/NADH and NADP+/NADPH in cellular functions and cell death: Regulation and biological consequences. Antioxidants Redox Signal. 10, 179–206. https://doi.org/10.1089/ars.2007.1672

Yoichi, T., Akihiro, O., Hiroshi, I., 2008. One-step synthesis of dibutyl furandicarboxylates from galactaric acid. Chemístry Lett. 37, 50–51. https://doi.org/https://doi.org/10.1246/cl.2008.50

Yu, T., Zhou, Y.J., Huang, M., Liu, Q., Pereira, R., David, F., Nielsen, J., 2018. Reprogramming yeast metabolism from alcoholic fermentation to lipogenesis. Cell 174, 1549-1558.e14. https://doi.org/10.1016/j.cell.2018.07.013

Zhang, H., Li, X., Su, X., Ang, E., Zhang, Y., Zhao, H., 2016. Production of adipic acid from sugar beet residue by combined biological and chemical catalysis. ChemCatChem 8, 1500–1506. https://doi.org/https://doi.org/10.1002/cctc.201600069

Zhang, J., Pierick, A. Ten, Van Rossum, H.M., Maleki Seifar, R., Ras, C., Daran, J.M., Heijnen, J.J., Aljoscha Wahl, S., 2015. Determination of the cytosolic NADPH/NADP Ratio in Saccharomyces cerevisiae using shikimate dehydrogenase as sensor reaction. Sci. Rep. 5, 1–12. https://doi.org/10.1038/srep12846

Zhao, X., Shi, F., Zhan, W., 2015. Overexpression of ZWF1 and POS5 improves carotenoid biosynthesis in recombinant Saccharomyces cerevisiae. Lett. Appl. Microbiol. 61, 354–360. https://doi.org/10.1111/lam.12463

# 8 Register of Abbreviations

| | |
|---|---|
| % | percent |
| Δ (gene) | deletion |
| °C | degrees Celsius |
| µL | micro liter |
| µM | micro molar |
| µm | micro meter |
| A (DNA) | adenine |
| AD | *anno domini*, Latin |
| ADP | adenosine diphosphate |
| AmpR | β-lactamase gene |
| ATP | adenosine triphosphate |
| bp | base pair |
| C (DNA) | cytosine |
| CamR | chloramphenicol acetyltransferase gene |
| ClonNAT | nourseothricin N-acetyltransferase gene |
| $CO_2$ | carbon dioxide |
| CoA | coenzyme A |
| D-Api | D-apiose |
| $ddH_2O$ | double distilled water |
| D-Dha | 3-deoxy-D-lyxo-2-heptulosaric acid |
| D-Gal | D-galactose |
| D-GlcA | D-glucuronic acid |
| DH | dehydrogenase |
| DHAP | dihydroxyacetone phosphate |
| DNA | desoxyribonucleic acid |
| D-Xyl | D-xylose |
| et al. | *et alii*, Latin |
| F6P | fructose-6-phosphate |
| FBP | fructose-1-6-bisphosphate |
| fw | forward prime |
| g | centrifugal force |
| G (DNA) | guanine |
| g (weight) | gram |
| G3P | glycerol-3-phosphate |
| G418 | geneticin |
| GalA | D-galacturonic acid |
| GalOA | L-galactonate |
| GAP | D-glyceraldehyde-3-phosphate |
| GRAS | generally regarded as safe |
| HPLC | high performance liquid chromatography |
| hygR | hygromycin B phosphotransferase gene |
| K (amino acid) | lysine |
| KanMX | aminoglycoside phosphotransferase gene |
| KanR | neomycin phosphotransferase II gene |
| kb | kilo base |
| KDG | 2-keto-3-deoxy-D-gluconate |

| | |
|---|---|
| KDGP | 2-keto-3-deoxy-6-phosphogluconate |
| Kdo | 3-deoxy-D-manno-2-octulosonic acid |
| L | liter |
| L (amino acid) | leucine |
| L-Ara | L-arabinose |
| L-Fuc | L-fucose |
| L-Rha | L-rhamnose |
| M | molar |
| M (amino acid) | methionine |
| mg | milli gram |
| min | minute |
| mM | milli molar |
| mol | mole |
| mU | milli units (enzyme activity) |
| $NAD^+$ | nicotinamide adenine dinucleotide, oxidized |
| NADH | nicotinamide adenine dinucleotide, reduced |
| $NADP^+$ | nicotinamide adenine dinucleotide phosphate, oxidized |
| NADPH | nicotinamide adenine dinucleotide phosphate, reduced |
| ng | nano gram |
| NHEJ | non-homologous end joining |
| nm | nano meters |
| $OD_{600}$ | optical density measured at wavelength 600nm |
| ORF | open reading frame |
| oxPPP | oxidative pentose phosphate pathway |
| PCR | polymerase chain reaction |
| pH | potential of hydrogen |
| PPP | pentose phosphate pathway |
| R (amino acid) | arginine |
| RNA | ribonucleic acid |
| rpm | rounds per minute |
| rRNA | ribosomal RNA |
| rv (primer) | Reverse prime |
| s | second |
| SC | synthetic complete |
| SDH | sorbitol dehydrogenase |
| T | thymine |
| TCA-cycle | tricarboxylic acid cycle, citric acid cycle |
| U | unit (enzyme activity) |
| U (DNA) | uracil |
| $v_{max}$ | maximal enzyme velocity |
| WT | wild type |
| w/v | weight per volume |

# 9 Acknowledgements

Ich danke **Herrn Dr. Mislav Oreb** dafür, dass ich an dem spannenden Thema meiner Doktorarbeit arbeiten durfte und so mehr über den Metabolismus der Hefe *Saccharomyces cerevisiae* lernen durfte. Vielen Dank für die Betreuung und wissenschaftlichen Diskussionen über die Zeit. Es war sehr wertvoll von deiner Erfahrung zu lernen.

Mein Dank geht auch an **Herrn Prof. Dr. Jörg Soppa** für die Arbeit als Zweitprüfer und die Arbeitsgruppen übergreifende Unterstützung, nicht zuletzt auch humorvollen wissenschaftlichen Unterhaltungen.

Ebenso geht mein Dank an **Herrn Prof. Dr. Eckhard Boles**, der für mich eine große Hilfe bei allen Hefefragen war und mich mit seinem immensen Wissenspool unterstützt hat. Deiner Unterstützung ist man in deinem Arbeitskreis immer gewiss! Damit geht mein ausdrücklicher Dank auch an den gesamten **AK Boles** mit dem ich immer gern zusammengearbeitet habe, um mich den Tücken unserer Hefe zu stellen.

Ich freue mich entlang des Weges auch mit einigen Studierenden zusammengearbeitet haben zu dürfen. So danke ich **Elena Bierwirth, Leonie Harth, Fabian Haitz, Tamina Sens** und **Jade Martin** für die gemeinsame Zeit im Labor. Die Zusammenarbeit hat mich immer motiviert, außerdem habe ich mit und von euch mindestens genauso viel gelernt wie ihr in euren Praktika und Abschlussarbeiten: Danke!

Der besondere Reiz dieses Themas ging von der Struktur des Projektes aus, denn als PRO-SUGAR-Team haben wir uns gemeinsam verschiedenen Teilaspekten des Projektes gewidmet und in fruchtbaren Diskussionen jeweils darüber ausgetauscht wohin die nächsten Schritte gehen sollen. Somit danke ich **Prof. Dr. Phillipp Benz, Prof. Dr.-Ing. Dirk Weuster-Botz, Dr. Jacqueline Wagner, Kevin Schmitz** und **Dominik Schäfer**. Vielen Dank für diese Erfahrung!

Der wohl größte Dank geht an **Familie** und **Freunde**, die mich immer unterstütz haben, wenn es mal nicht ganz so lief, wie geplant. Besonders gemeint sind hier **meine Eltern**, **meine Schwester Juliane** und **meine Emotionsstütze Leni**, auf deren Mitgefühl, Unterstützung und Grundvertrauen ich immer zählen konnte. Nicht zuletzt ein besonderer Dank an **Anna Zahn** und **Christoph Berg** die mich mit sprachlichen Tipps und *Word*-Hilfestellungen, zum Teil seit dem Bachelor-Studium, unterstützt haben.

Dankend sei erwähnt, dass mir die **Deutsche Nationalbibliothek Frankfurt am Main, die Stadtbücherei Frankfurt am Main** und die **Universitätsbibliothek J.C. Senckenberg** trotz pandemischer Zustände oft ein schönes Plätzchen zum Schreiben bereitgestellt haben an denen mir **Johannes Reuther** oft motivierend zur Seite saß.